Study on the Verification Method of Pointing Performance of Submillimeter Wavelength Antenna through the ALMA

Ayumu Matsuzawa

Doctor of Philosophy

Department of Astronomical Science
School of Physical Sciences
SOKENDAI (The Graduate University for Advanced Studies)

Study on the Verification Method of Pointing Performance of Submillimeter Wavelength Antenna through the ALMA

Ayumu Matsuzawa

Abstract

The Atacama Large Millimeter/Submillimeter Array (ALMA) is a gigantic radio interferometer array for millimeter to submillimeter wavelengths (10 to 0.3 mm), which is located at Chajnantor Plateau in Chile (an altitude of about 5000 m). The ALMA array includes fifty 12-m antennas (12-m Array), the Atacama Compact Array (ACA; a.k.a., Morita Array), comprising a 7-m antenna array and a total power array with four 12-m antennas. To obtain an observed image with high reliability, all ALMA antennas require high referencing pointing performance, which is the accuracy needed to determine the relative positions of the target star and the reference position (first measured position of the star) during an observation. In ALMA, it is necessary for the referencing pointing performance of the antenna not to exceed 0.6 arcsecs under the primary operating conditions, corresponding to 1/19 and 1/11 of the Half-Power Beam Width (HPBW) of the ALMA 7-m and 12-m antennas, respectively, at the highest observing frequency (950 GHz). All ALMA antennas had been assembled and their scientific and system performances were verified at Operations Support Facility (OSF) of ALMA site (an altitude of about 3000 m) before transporting to high site. This study includes a detailed description of the accuracy verification of various components, including the referencing pointing performance of the ALMA ACA antennas and a physical interpretation of the referencing pointing performance. The referencing pointing performance of an ACA antenna is verified by measurering the Root Mean Square (RMS) of the distance between the centroid positions of the reference positions (the first measured centroid position) and of the target star, in images produced by the Optical Pointing Telescope (OPT) that is mounted in the backup structure of all ACA antennas. It is important to estimate the optical seeing component at the OSF with high accuracy when determining the referencing pointing performance because the optical seeing component accounts for a large portion of the measured value of the referencing pointing measurement. The contribution of optical seeing to the centroid positons of the OPT images is significant when the integration time of the OPT is short, so that in the measurement of the optical seeing with the OPT, an integration time should be one second shorter than that of the referencing pointing measurement (five seconds). In previous research, the time-dependence of the optical seeing was corrected from a Kolmogorov Power Spectrum Density (PSD) [Saito et al. (2012)]. However, it is known that this correction method tends to overestimate the required correction for optical seeing at an integration time of five seconds. In fact, according to earlier studies, the

134 in 458 datasets indicate that the residual between the measured value and the fluctuating components, which randomly change with the measurement date (for example, the optical seeing), becomes negative. These negative residuals may provide to underestimate the referencing pointing performance of the ACA antenna, decreasing the reliability of the verification result for referencing pointing performance. From the PSD, the time-dependence of the optical seeing with some weather parameters (wind velocity, wind attacking angle, ambient temperature, and opacity) had been in detail investigated using multiple regression analysis. From the results of the multiple regression analysis, it was newly found that there is a stronger correlation between a wind velocity and an index of integration time (t), and the relation was finally measured as $t^{-(0.16\pm0.05)-(0.06\pm0.02)\times V_{\mathrm{wind}}}$ when t is an integration time and V_{wind} is a wind velocity. On the other hand, in this study, the new relation between the optical seeing and wind velocity, $t^{-0.17}$, was derived in theory with the Kolmogorov model of turbulence under the observation scale of the OPT is smaller than the outer scale of eddy in the turbulence. When a wind velocity is too small, the measured relation can be represented by $t^{-(0.16\pm0.05)}$. This good matching between the theory and measurement results indicates that the new optical seeing correction method was valid for verifying the referencing pointing performance of the ACA antennas. It is therefore proposed in this study that the relation between the power law index and wind velocity is implemented into a new correction method for optical seeing. Using the new correction method, it was confirmed that the negative residuals of 134 in 458 datasets is successfully improved to be 63, suggesting that the new optical seeing correction method is valid for verifying the referencing pointing performance of the ACA antennas. Furthermore, the negative residuals may be caused by uncertainty in determining the reference position (the first measured centroid position). In order to estimate the referencing pointing performance of the ACA, random fluctuation components must be subtracted from the measured pointing results. The reference position will have an effect from the true average of the random fluctuation components. The random fluctuation components for any time is unknown and is not easy to be derived. The uncertainty was assumed in previous research to be comparable to the standard deviation of the random fluctuation components. However, the uncertainty of the reference position may be overestimated under this assumption. In this study, a new estimation method is proposed that uses the average of all measured centroid positions instead of the offset of the reference position. In addition, this method is applied to ACA antennas No. 1 to 4. With new correction method for optical seeing, the number of negative residuals decreases from 24 to 11 in 99 datasets of the four ACA antennas.

Then, with new estimation method of the reference position, the number of negative residuals furthermore decreases from 11 to 2 in 99 datasets. This indicates that most of the negative residuals are resolved by the two new methods that were proposed newly here. In this study, the Az and El dependencies of the optical seeing of the OSF were also verified independently. It was assumed that the optical seeing does not depend on the azimuth (Az) angle; rather, it depends only on the elevation (El) angle as $\sin(El)^{-0.5}$ is derived from the Kolmogorov model of turbulence. Verification tests confirmed that the optical seeing of the OSF does not depend on the Az angle; instead, it depends on the El angle, with the dependence derived from the Kolmogorov model of turbulence. The OPT cannot verify a component that changes on a shorter time scale than the integration time of the OPT (five seconds). In this study, the key component on such a short time scale was also verified by measuring the servo error. The servo error is caused by the antenna servo system that controls the antenna. It was measured by the difference between the readout angle measured by the angular resolver connected to the antenna control unit (ACU) and the angle commanded by the antenna bus master. In order to investigate the contribution of the RMS of servo errors to the referencing pointing performance, the servo errors were measured at various rotational velocities on the azimuth (Az) and elevation (El) axes, ranging the azimuth from 2 to 0.000002 deg/s and an the elevation from 0.2 to 0.000002 deg/s for 210 seconds. Verification tests confirmed that the RMS of servo errors is less than 0.1 arcsecs and enough small to contribute the RMS of servo errors to the referencing pointing performance (0.6 arcsecs). Also of importance, the ALMA antenna must stabilize more quickly to shorten the dead time after fast switching, to enable the observation of a target source and calibrator source to be as near to simultaneously as possible. In this study, the pointing performance during the settling time after fast switching was further verified. Verification tests with the ACA 7-m antenna No. 12 confirmed that the pointing performance during the settling time after fast switching meets the technical specification of the ALMA without directional biases. In conclusion, the referencing pointing performance of the ACA antenna was verified to have higher reliability than that shown in earlier studies.

Index

1 Introduction

Atacama Large Millimeter/Submillimeter Array (ALMA) is a gigantic radio interferometer array operated at Array Operation Site (AOS) (an altitude of 5000 m) on the Chajnantor plateau in northern Chile [1]. The ALMA is a synthesis telescope and consists of 66 antennas; fifty-four 12-m antennas and twelve 7-m antennas [2]. To obtain an astronomical image with high reliability, the ALMA has the array composed of fifty 12-m antenna (12-m Array) and the Atacama Compact Array (ACA, a.k.a. Morita Array) which are composed of the 7-m antennas array and the total power array with four 12-m antennas (Figure 1-2) [3]. All ALMA antennas were assembled and verified at Operations Support Facility (OSF) (an altitude of 2900 m) because hard works at AOS are danger and inefficient for people. The ALMA covers the observations of a millimeter to submillimeter wavelengths (10 to 0.3 mm) and achieves high angular resolution of 0.01 arc-second (hereinafter arcsec) and high sensitivity of 10 micro-Jy in 1 hour at 1mm wavelength in the continuous radiation observation [4].

The output power of an antenna has a gain loss due to the pointing error given by the angular deviation of the peaks of the antenna response from the actual target locations [5]. The requirement of the pointing error depends on the half-power beam width (HPBW) of the antenna. The output power of the antenna has a gain loss of only 0.7% when the pointing error is 1/20 of the HPBW of the antenna assuming that the antenna reception pattern is Gaussian [6]. If a pointing error is large, the output power of the antenna has a large gain loss (e.g. gain loss is 50% when 1/2 of HPBW), and, the image fidelity is declined by an increase of the pointing error. Tsutsumi et al. (2004) have reported the simulation results of the ALMA ACA 7-m antenna observations at 230GHz and 850GHz for various types of radio sources with a pointing error of 0.6 and 1.2 arcsecs [7]. The pointing errors of 0.6 and 1.2 arcsecs correspond respectively to about 1/19 and 1/11 of the HPBW of the ACA 7-m antenna at 950 GHz. According to Tsutsumi et al. (2004), the image fidelity of the ACA 7-m antenna with a pointing error of 0.6 arcsecs is twice that with a pointing error of 1.2 arcsecs in the best case.

In actual radio observations, the antenna switches between a target and a nearby pointing reference, with respect to which the pointing error is measured and corrected with the five-point method (see Section 2). After correcting the pointing error, the antenna switches back to the target source and begins tracking it. This observation process requires the following two conditions:

i) To carry out the five-point method, the pointing reference must come into the field of view (FOV) of the antenna after switching from any direction, and across any angular distance in all sky. This performance is called the absolute pointing performance. The ALMA requires that the absolute pointing error of the antenna shall not exceed 2.0 arcsecs across all sky under the primary operating conditions, a value that is the root sum square (RSS) of average values and standard deviations of the measurement results of the absolute pointing. 2.0 arcsecs is one-third of the FOV of the 12-m antenna at the highest observing frequency (950 GHz). If the absolute pointing performance is within an RSS of 2.0 arcsecs (1σ) after switching from any direction and any angular distance, the star will enter the FOV with a probability of 99.7% (3σ).

ii) To improve the quality of the observed image, the antenna must track the target source and calibration source without a significant pointing error due to the reference source position during the observation. This performance is called the referencing pointing performance (see Figure 1-3). In general, the referencing pointing performance is required to be within 1/20 of the HPBW of the antenna, as mentioned above. In ALMA, it is required that the referencing pointing performance of the antenna shall not exceed 0.6 arcsecs under the primary operating conditions (Table 1-1) [2], [3], [8]. At the highest observing frequency (950GHz), this corresponds to 1/20 and 1/10 of the HPBW of the ALMA 7-m and 12-m antennas, respectively. Although the output power of the antenna has a gain loss with 2.7% when 1/10 of the HPBW, it is not reasonable to specify pointing performance smaller than 0.6 arcsecs in ALMA 12-m antenna, because pointing jitter of about 0.4 arcsecs exists by water vapor content in the troposphere with anomalous refraction at the AOS even under the best conditions [9].

The pointing performance of the ALMA antenna was measured and verified at OSF. The pointing measurement result includes several factors, such as variability in the troposphere, ionosphere, wind, solar radiation, temperature gradient, etc. In order to derive the actual referencing pointing performance of the ALMA antenna, the undesirable effects (troposphere and ionosphere) must be removed from the referencing pointing measurement.

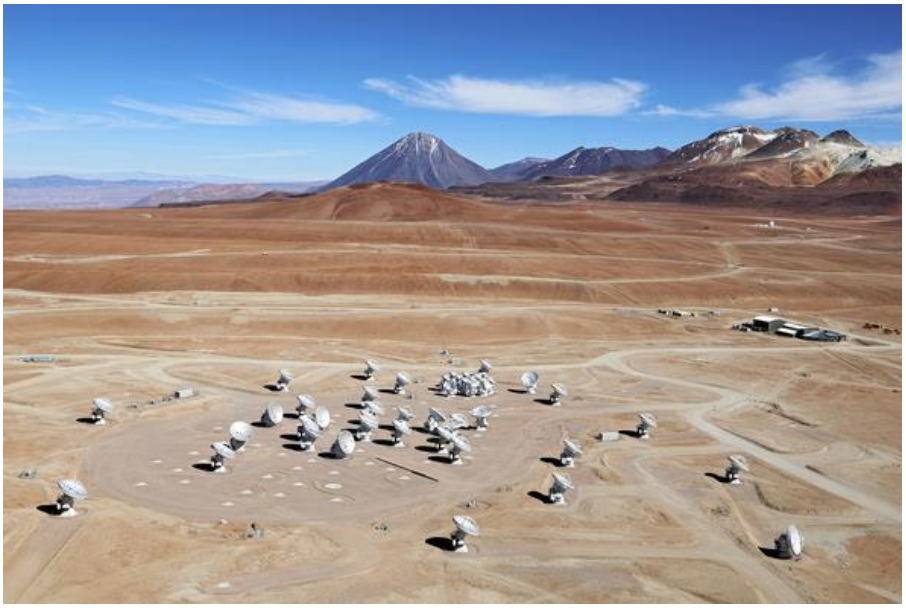

Figure 1-1 Picture of the ALMA at AOS Credit: Clem & Adri Bacri-Normier (wingsforscience.com)/ESO.

Figure 1-2 Pictures of ACA 12-m antenna (left) and ACA 7-m antenna (right).

Table 1-1 Primary operating conditions of the ALMA [8]

Primary Operation Conditions	Daytime	Nighttime
Ambient temperature [°C]	-20 to +20	-20 to +20
Altitude [m]	5050	5050
Pressure [hPa]	550	550
Precipitation	None	None
Wind velocity (average) [m/s]	6.0	9.0
Wind velocity (average + gust) [m/s]	6.4	9.5
Solar flux [W/m^2]	1290	None
Temperature change in ambient air temperature [°C/10 min]	0.6	None

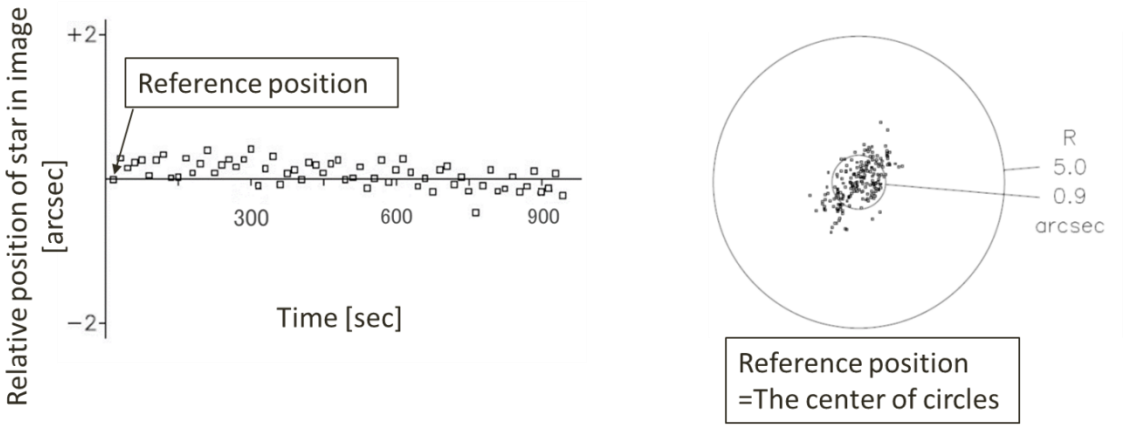

Figure 1-3 Example of the measurement result of the referencing pointing. The fluctuation of relative positions of the star from the reference position on the Azimuth axis in time (left) and in space (right).

The details of measurement verification and the physical interpretation of the referencing pointing performance of the ACA antennas are presented below. More stringent requirements apply to the pointing performance of a submillimeter antenna than those for centimeter wavelengths, assuming the same aperture size for both wavelengths. In order to achieve high pointing performance, it is essential to design and manufacture a high precision antenna. The verification method also requires high accuracy at every point, including the instrument itself, the measurement method, and the analysis of the variables. In this study, first, the verification method used by Saito et al. (2012) in the previous investigation of the referencing pointing performance of the ACA antenna, is checked. The typical verification method for referencing pointing performance and the verification method for OPT according to Saito et al. (2012) are described in Section 2. In this study, the fluctuation of the troposphere at optical wavelengths (called optical seeing) is an important factor in the referencing pointing measurement. In Saito et al. (2012), the optical seeing included in the referencing pointing measurement is measured with the OPT using an integration time of one second shorter than the measurement (five seconds), and the optical seeing is corrected with the time-dependence via the Kolmogorov power spectrum density (PSD) derived from Ukita et al. (2008). However, the correction method using the time-dependence from Kolmogorov PSD may overestimate the correction of optical seeing using an integration time of five seconds. Section 3 presents an investigation of the relation between the power law index of optical seeing for integration times of 1 to 5 seconds and weather parameters (wind velocity, wind attack angle, ambient temperature, and opacity), and the derivation of a new relation between the optical seeing and the wind velocity. Section 4 presents the verification results for the servo error, which is the portion of the pointing error of the antenna that originates in the antenna control of the ACA antenna. Section 5 describes the verification result of the azimuth dependence and the elevation dependence of the optical seeing due to the atmospheric path length at the OSF. Section 6 describes the verification result of the pointing performance during the settling time after fast switching. Section 7 deals with the verification result of the referencing pointing performance of the ACA antenna, together with the time-dependence of the optical seeing derived from this investigation and the physical interpretation of the new relation between the optical seeing and the wind velocity. Finally, Section 8 summarizes the conclusions reached and the future works planned.

2 Measurement of Referencing Pointing Performance

For a general radio telescope antenna, there are two major pointing measurement methods: the five-point method with the receiver that is used an actual observation and the method with an optical pointing telescope (OPT).

In the five-point method, the five output powers are measured at the position of a star and the additional four positions in the directions of positive and negative of an azimuth (hereinafter Az) and an elevation (hereinafter El) from the star separated by a half of the HPBW of the antenna. In general, a bright point source is observed on the five-point method. Assuming that the antenna reception pattern is Gaussian, the pointing error is estimated by fitting two-dimensional Gaussian to the measured output powers at the five positions [10]. The total time required for estimating the pointing error includes a measuring time and a settling time at each position, and a slew antenna time between the positions, that is typically the minute time scale [11].

The OPT is mounted on the back-up structure of the main reflector of the antenna to be aligned with the radio axis. The OPT obtains images in time series of a star with the Charge Coupled Device (CCD) camera. Since the star in each image is blurred and extended due to a fluctuation of the troposphere, however, the centroid position of the star must be in each image for an Az axis and an El axis respectively to determine the position of the star in the image [11]. The pointing error is estimated by determining the root mean square (RMS) of the measured time-variable positions of the star. A typical timescale of obtaining the image is a few seconds, depending on the CCD camera implemented in the OPT ant an image acquiring system [12]. A typical aperture size of the OPT is about 100 to 300 mm [12], [13], [14].

For the pointing measurements of a radio telescope antenna, the OPT method is utilized to verify the pointing performance because the OPT method has three advantages as compared with the five-point method. First, the spatial resolution of the OPT is better than a single radio telescope antenna [11], [13]. For instance, the special resolution of the 12-m diameter radio telescope antenna is about 6.6 arcsecs in a wavelength of 0.32 mm; while the special resolution of 100 mm diameter OPTS is 1.6 to 2.5 arcsecs in wavelengths of 640 to 1000 nm. Second, there are many stars to detect with OPT as compared with the single radio telescope antenna [11]. Third, the OPT can measure the non-repeatable component such as a pointing jitter due to the troposphere by obtaining images in a few seconds, which is faster than a cycle of the estimation of the pointing error with the time-dependence method [16].

Figure 2-1 The ALMA ACA 7-m antenna and optical pointing telescope. Optical pointing telescope is mounted on buck up structure of the main reflector antenna which position indicates as circle.

It is well known that a measured pointing value made using the OPT includes several undesirable effects of the troposphere and the environmental conditions around the antenna [8]. The first undesirable effect is the pointing jitter due to the troposphere at optical wavelengths. This is called the optical seeing, and is caused by variable refraction due to the random motion of turbulent eddies with different refractive indices, which are mainly caused by differences in temperature, pressure, or moisture content [15], [16]. In general, the optical seeing in optical astronomy is quantified by the full width at half-maximum (FWHM) of a point source (star) whose image is broadened and erratically displaced by the refraction of its light as it passes through the atmosphere. In contrast, optical seeing in this study refers to the RMS of the motion of the centroid of the image of a point source (star) that is distorted and displaced by refracted light passing through the atmosphere (hereinafter RMS of centroid positions). The difference between these size measurements of star images is described in Appendix A. The optical seeing may be influenced mainly by wind turbulence in the surface layer and just above the antenna [15]. The second undesirable effect is pointing jitter due to the deformation or the motion of the antenna due to wind load during OPT data acquisition. The pointing jitter due to wind load should be verified at the maximum wind velocity of the primary operating conditions (see Table 1-1) in order to verify the referencing pointing performance under those conditions. However, the wind velocity and pointing jitter due to wind load vary randomly with time. It is difficult to measure the pointing jitter at the maximum wind velocity. Therefore, the pointing jitter due to wind load in the measurement should be subtracted from the measured pointing values. Incidentally, the measured pointing value may include pointing error due to the OPT (For example, the unrepeatable gravitational deformation and the mechanical flexing and slack of the OPT and the joint between the OPT and the ACA antenna. However, any pointing error due to the OPT is considered to be negligible compared to the optical seeing and the pointing jitter due to wind load in the measurement.

On the other hand, the measured pointing value with the OPT does not include pointing components due to the sub reflector, the thermal metrology system of the main reflector, the environmental condition around the antenna, and the antenna servo system. The first missing component is the pointing error due to the vibration and non-repeatable components of gravitational deformation of the sub reflector of the antenna. The second missing component is the performance of the thermal metrology system that actively corrects the pointing errors due to the deformation of the main reflector by thermal load [17]. As mentioned above, the OPT is mounted on the back-up

structure of the main reflector of the antenna (see Figure 2-1). However, the OPT cannot directly measure the components due to the main and sub reflectors because it does not ray trace of the radio axis of the ALMA antenna perfectly. The third missing component is mainly the jitter due to the deformation of the antenna by wind load at the maximum wind velocity that is defined as one of the primary operating conditions (see Table 1-1 in the ALMA). As mentioned above, since the wind velocity and pointing jitter due to wind load change randomly with the date of the measurements, the pointing jitter due to wind load at AOS (9.5 m/s) should be estimated from an finite element analysis by the antenna vendor. The fourth missing component is the inherent error in the antenna servo system that controls the antenna in order to equalize the measured angle and the commanded angle. This is called servo error [18]. The servo error is the measured difference between an input value and an output value, determined by the angle measuring instrument. The servo error includes high-frequency pointing errors due to antenna vibration, etc. on a short time scale of 0.1 seconds, which are smoothed out over the integration time of the OPT.

In order to derive and verify the referencing pointing performance of the antenna, the undesirable components due to the optical seeing and wind load at the average wind velocity during OPT data acquisition must be estimated and removed from the measured pointing value with the OPT. Also, the components due to sub reflector, the main reflector metrology system, the wind load at the maximum wind velocity under primary operating conditions and the servo error must all be estimated and added in the measurement result [8].

The verification method of the referencing pointing performance of the ALMA ACA antenna from Saito et al. (2012) is described. The parameters of the referencing pointing in Saito et al. (2012) are summarized in Table 2-1. The work flow of the verification of the referencing pointing performance in Saito et al. (2012) is shown in Figure 2-2. The measurement of the referencing pointing performance reproduces a typical observation of the ALMA. In the measurement, three to five stars within 4 degrees on the sky are selected, and the antenna switches between these stars every 15 seconds during 900 seconds (Figure 2-3) [8]. The OPT can obtain an image with the integration time of five seconds in the cycle of 15 seconds to achieve a high signal-to-noise ratio. The measured pointing value with the OPT is estimated by the RMS of all relative positions between the reference position (the first measured centroid position) and the centroid positions of the star in 60 images with the integration time of five seconds during 900 seconds (see Figure 2-4). While the referencing pointing performance is measured with the OPT, the weather parameters are obtained with an

anemometer and a thermometer.

The measured pointing value include the pointing error due to the ACA antenna such as the systematic component due to a tracking during 900 seconds, the pointing error due to optical seeing, and pointing jitter due to wind load at the OSF. In Saito et al. (2012), the referencing pointing performance ($d\theta_{\mathrm{main}}$) is, from workflow shown in Figure 2-2, represented by

$$d\theta_{\mathrm{main}} = sqrt[d\theta_0{}^2 - 2 \times d\theta_{\mathrm{s}}{}^2 - 2 \times d\theta_{\mathrm{tw}}(OSF)^2 + d\theta_{\mathrm{tw}}(AOS)^2 + d\theta_{\mathrm{mr}}{}^2 + d\theta_{\mathrm{sr}}{}^2 + d\theta_{\mathrm{se}}{}^2], \quad (2\text{-}1)$$

where $d\theta_0$ is the measured pointing value from the OPT, $d\theta_{\mathrm{s}}$ is the pointing error due to optical seeing, $d\theta_{\mathrm{tw}}$ *(OSF)* is the pointing jitter due to wind load at the OSF, $d\theta_{\mathrm{tw}}$ *(AOS)* is the pointing jitter due to wind load at the AOS, $\mathrm{d}\theta_{\mathrm{mr}}$ is the pointing error due to the main reflector thermal metrology system, $d\theta_{\mathrm{sr}}$ is the pointing error due to the sub reflector, and $d\theta_{\mathrm{se}}$ is the RMS of servo error. The pointing jitter due to wind load at the AOS, the pointing error due to the main reflector thermal metrology system, and the pointing error due to the sub reflector are estimated from the simulation by the antenna vendor. The fluctuating component, which changes randomly day by day [$d\theta_{\mathrm{s}}$ and $d\theta_{\mathrm{tw}}$ *(OSF)*] (hereinafter random fluctuating components), must be subtracted twice from the measured pointing value. The measured pointing value from the OPT is estimated by the RMS of deviations of all observed relative positions from the reference position (the first measured centroid position) in both Az and El axes. The reference position has an offset from the true average value of the random fluctuating components, and this offset must be subtracted from the measured pointing value (see Figure 2-5). However, this true average value is an unknowable value. Saito et al. (2012) adopt the standard deviation of the random fluctuating components [$d\theta_{\mathrm{s}}$ and $d\theta_{\mathrm{tw}}$ *(OSF)*] for the offset between the reference position and the true average value. Consequently, the random fluctuating components must be subtracted twice from the measured pointing value.

The pointing jitter due to wind load at the OSF is estimated by using the ratio of wind force at the AOS and the OSF as follows [19].

$$d\theta_{\mathrm{tw}}(OSF) = d\theta_{\mathrm{tw}}(AOS) \times [V(measure)/V(AOS)]^2/[\mathrm{P(AOS)/P(OSF)}] \quad (2\text{-}2)$$

where *V (measure)* is the average wind velocity during the measurement of the pointing performance at the OSF, *V(AOS)* is the maximum wind velocity, 9.5 m/s, for nighttime

Table 2-1 Summary of parameters of pointing performance of the ALMA ACA antenna

(1) Parameters	(2)Parameters (variables)	(3) Description	(4) Method
Referencing pointing performance	$d\theta_{main}$	Expected referencing pointing performance of the ALMA antenna. This pointing performance is verified at radio wavelength.	Estimate from equation (2-1)
Measured pointing value	$d\theta_{o}$	Pointing result measured with OPT. This also includes the components of the atmosphere at optical wavelength, of environmental condition around the antenna (e.g. wind), and of OPT vibration and deformation.	Measure by OPT with low sampling time
Pointing error due to optical seeing	$d\theta_{s}$	Pointing error due to troposphere at an optical wavelength. This is measured by using OPT that can estimate by RMS of centroid position of a star in image with OPT	Measure by OPT with high sampling time
Pointing jitter due to wind load at the OSF	$d\theta_{tw}$*(OSF)*	Pointing jitter due to wind load at the averaged wind velocity during OPT data acquisition. This is measured at Operations Support Facility (OSF, the altitude of 2900m).	Estimate from equation (2-2) with wind velocity at measurement
Pointing jitter due to wind load at the AOS	$d\theta_{tw}$*(AOS)*	Pointing jitter due to wind load at the wind velocity of 9.5 m/s that is the maximum wind velocity at Array Operations Site (AOS, the altitude of 5000m) under primary operating conditions.	Estimated from a simulation.
Pointing error due to main reflector metrology system	$d\theta_{mr}$	Pointing error due to the thermal metrology system of the main reflector.	Estimated from a simulation.
Pointing error due to sub reflector	$d\theta_{sr}$	Pointing error due to vibrations and non-repeatable components of gravitational deformation of sub reflector and quadrupled.	Estimated from a simulation.
RMS of servo error	$d\theta_{se}$	RMS of the differences between the readout of angle and the commanded angle. The measured servo error with the angular resolvers in antenna control unit also includes a torque error and an encoders error	Measured by the angle encoders

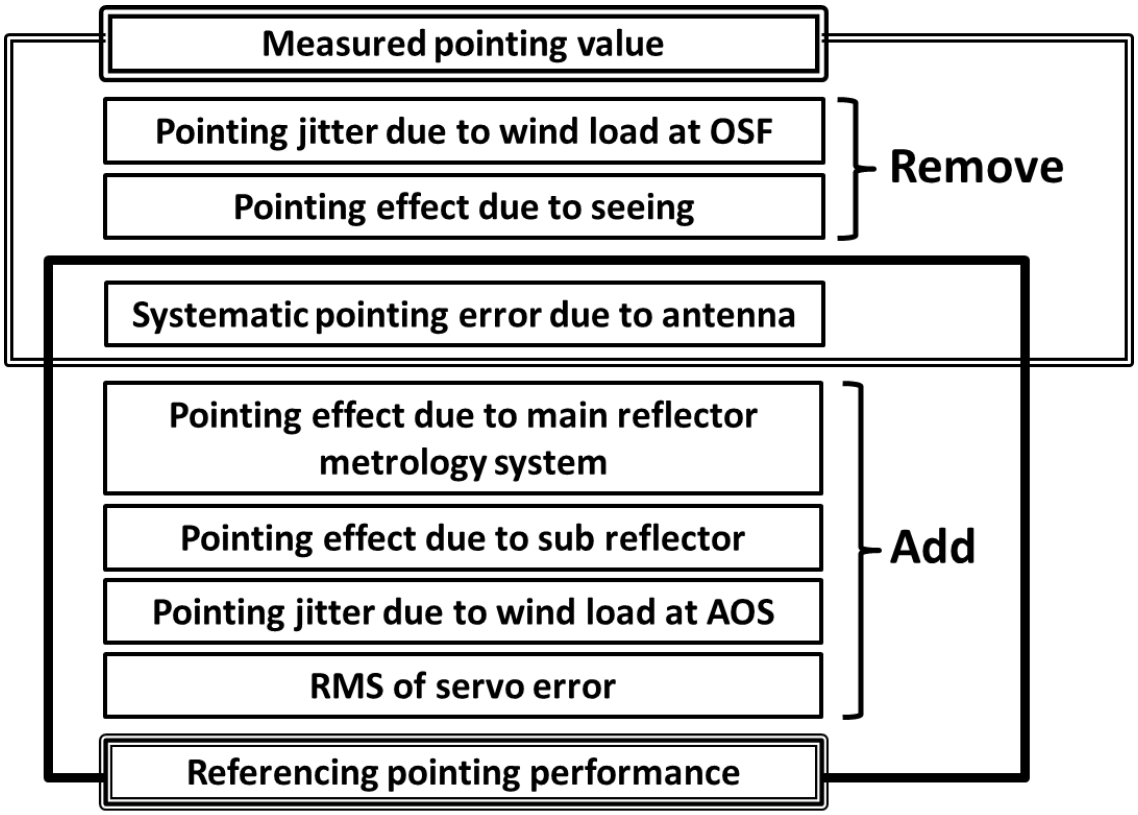

Figure 2-2 Work flow of verification of the referencing pointing performance.

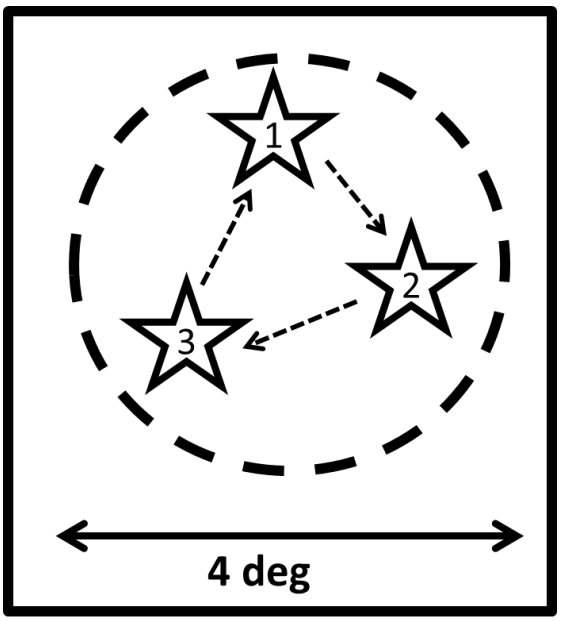

Figure 2-3 Observing stars of the measurement of the referencing pointing performance.

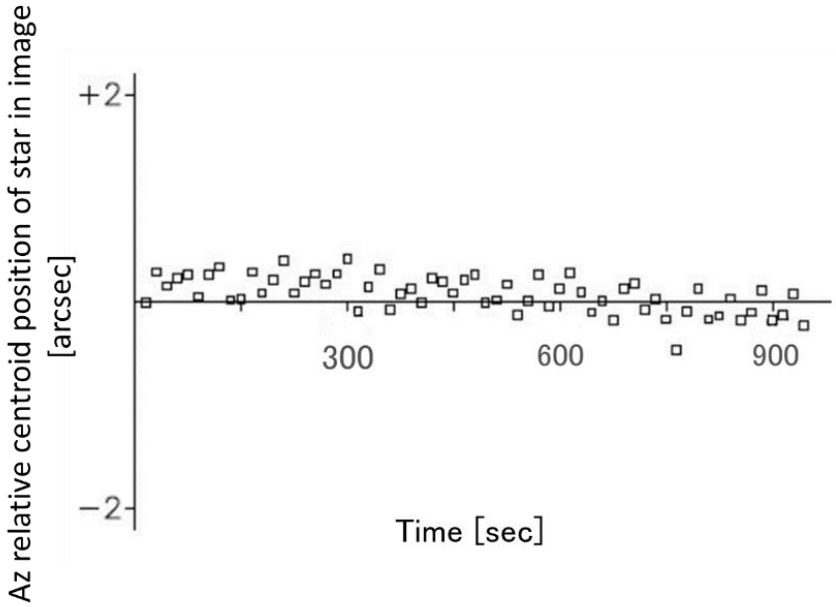

(a) The relative centroid positions of a star in image in Az axis.

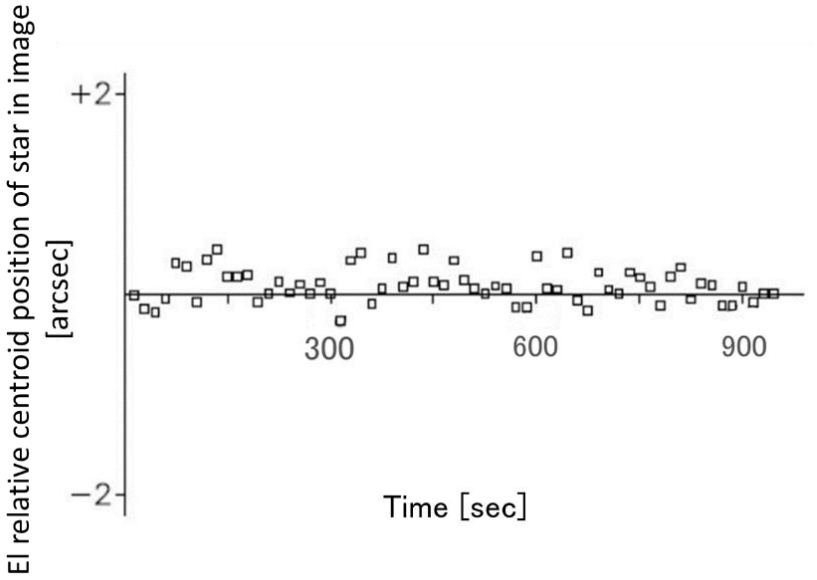

(b) Then relative centroid positions of a star in the image on El axis.

Figure 2-4 Example of the referencing pointing measurement which is RMS of centroid positions of a star in the image.

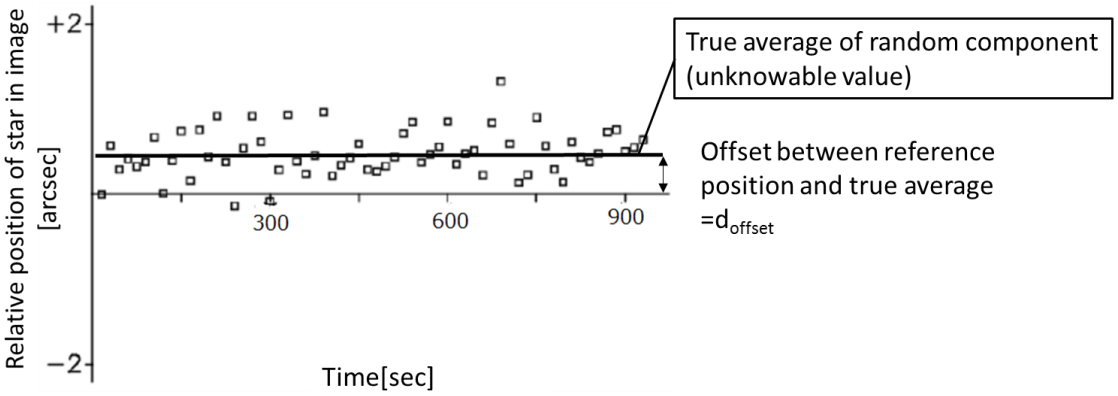

Figure 2-5 Offset between reference position (the first measured centroid position) and a true average of random fluctuating components.

Table 2-2 Difference between the two measurements of the referencing pointing performance and the optical seeing

	Referencing pointing performance	Optical seeing
The number of stars	3 - 5	1
The integration time of the OPT	5 [sec]	1 [sec]
The time to determinate the RMS of centroid positions of a star in image with OPT	900 [sec]	10 [sec]
The number of RMS to measure the result	1	12

under the primary operating condition at the AOS (see Table 1-1), and P (AOS)/ P(OSF) = 0.75 is the atmospheric pressure ratio at the AOS to the OSF.

In Saito et al. (2012), the optical seeing is measured using the OPT before/after the measurement of the referencing pointing performance (see Figure 2-6). To measure the optical seeing, the OPT takes 120 images with an integration time of one second while tracking a star for 120 seconds, and the 120 images are divided into 10-second groups. The RMS of centroid positions is estimated from the ten images obtained in each 10-second interval. The optical seeing is then estimated from the average of the twelve RMSs of centroid positions (see Figure 2-6). The measurement of optical seeing differs from that of the referencing pointing in the following three ways: i) the integration time of the measurement of optical seeing (one second) is shorter than the measurement for the referencing pointing (five seconds), to increase the contribution of the optical seeing. The difference in the integration times of the two measurements is corrected using the time-dependence of the optical seeing from Kolmogorov power spectrum density (PSD) according to Ukita et al. (2008). The verification of this correction method in this study is described in Section 3. ii) The direction of the star between two measurements is different. The measurements of the referencing pointing are performed towards the differing directions at each measurement to verify performance in various directions across the entire sky. In contrast, the optical seeing measurement is performed using pre-selected stars. Since the integration time of the optical seeing is 1/5 that of the measurement for referencing pointing, the star used in the optical seeing is $\sqrt{5}$ times (star of magnitude +1) brighter than the star used in the referencing pointing. Therefore, the direction of the star between two measurements is often different by several tens of degrees. The optical seeing contributions between the two different directions are different because the optical seeing is related to the atmospheric path length. The difference in direction between the two measurements is corrected by the Az and El dependence of the optical seeing due to the atmospheric path

length. The verification of this correction method in this study is described in Section 5.
iii) The RMS of centroid positions is calculated from the centroid position of images obtained within 10 seconds of each other to avoid the effect of pointing error due to lengthy tracking. These differences between two measurements are listed in Table 2-2.

The RMS of servo error is measured as the RMS of time-variable differences between readout angles measured by the angular resolver connected to the antenna control unit (ACU) and the angles commanded by the antenna bus master (see Appendix B) [21]. The ACU outputs the angles every 0.048 seconds. However, the angle measured with the angular resolver is affected by the antenna control, and the servo error includes a torque error due to incomplete suppression of external disturbances and detection error in the angle resolvers and resolvers-to-digital converter, in addition to error due to the antenna control by the ACU. If the instruments of the ACA antenna and the antenna control by the ACU have a problem, the servo error of the angular resolver may become large. Therefore, to check the ACU by measuring the servo error is important. The investigation of the servo error in this study is described in Section 4.

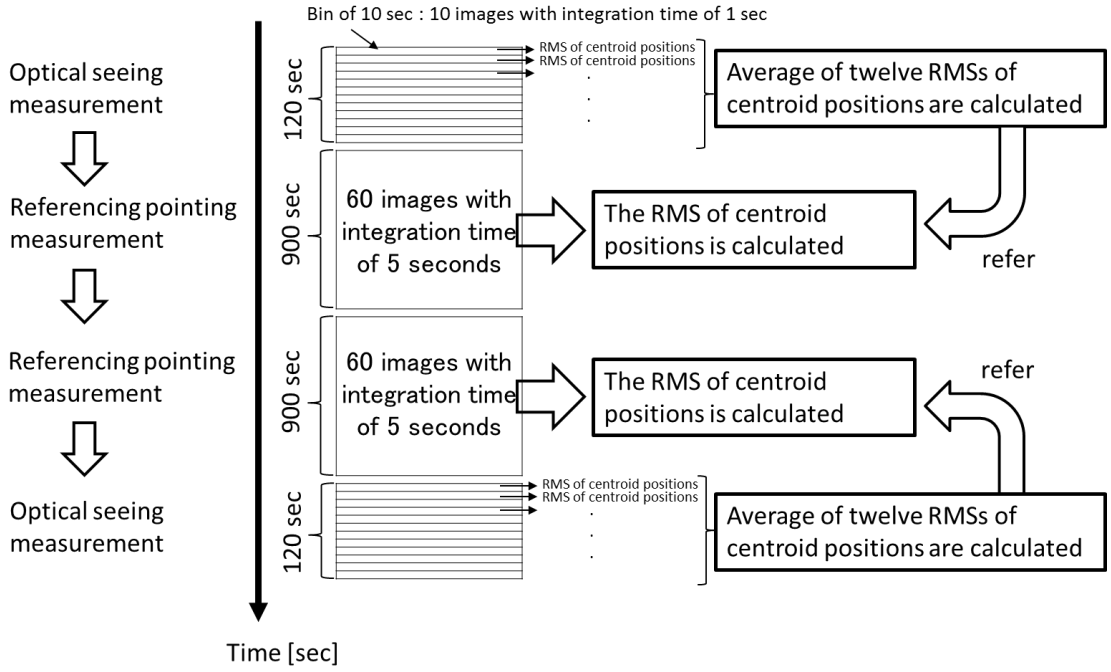

Figure 2-6 Typical measurement process of the referencing pointing and the optical seeing in Saito et al. (2012). The nearest optical seeing measurement result is referred to verify the referencing pointing performance.

3 Development of New Correction Method for Optical Seeing in Referencing Pointing Performance

As described in Section 2, the measured pointing value includes the referencing pointing performance of the ACA antenna, the pointing error due to optical seeing conditions (hereinafter: optical seeing), and the pointing jitter due to wind load during measurement at the OSF. In order to estimate the referencing pointing performance of the ACA antenna, the optical seeing and the pointing jitter due to wind load must be properly subtracted from the measured pointing value. Since the optical seeing accounts for a large portion of the measured pointing value, it is important to estimate the components of the optical seeing with high accuracy. Note that this optical seeing is different from the full width at half-maximum (FWHM) of a star image. In general, the optical seeing at the telescope site is investigated by a differential image motion monitor (DIMM) set at ground level [24], [25]. However, the DIMM set at ground level cannot measure the optical seeing at the height of the antenna (about 10 m above ground level). Moreover, the DIMM cannot measure low-frequency fluctuations (fluctuations on a scale larger than the aperture size), and may underestimate the optical seeing compared to a single aperture OPT [24]. Therefore, the single aperture OPT mounted on the ACA antenna is more appropriate for estimating the optical pointing components included in the measured pointing value.

The integration time of the referencing pointing measurement is longer than the optical seeing measurement to reduce the contribution of the optical seeing and as a result, the referencing pointing performance of the ACA antenna becomes more dominant. Therefore, the integration time is five seconds (with a sampling rate of 0.2 Hz) typically for the measurement of the referencing pointing [8]. On the other hand, for measuring the optical seeing, a short integration time of one second is more reasonable, to increase the contribution of the optical seeing and to obtain a solely optical seeing component. In Saito et al. (2012), the integration time for the optical seeing measurement was one second [8]. The difference in the integration times of the two measurements is corrected using the time-dependence of the optical seeing ($d\theta_s$) from Kolmogorov power spectrum density (PSD) according to Ukita et al. (2008) as follows,

$$d\theta_s \propto t^{-0.2}, \qquad (3\text{-}1)$$

where t is the integration time. However, in Ukita et al. (2008), the measured optical seeing from an integration time longer than one second indicates a different relationship

with the time-dependence from Kolmogorov PSD [20]. Therefore, the corrected optical seeing with an integration time of five seconds may be overestimated by the correction method for the time-dependence from Kolmogorov PSD (see Figure 3-1) [23]. In Saito et al. (2012), the residuals of the reference pointing measurement after subtracting the optical seeing became negative values for one-third of all the measurement results, which may have been caused by the overestimation of optical seeing. However, the difference between the measured optical seeing and the time-dependence from Kolmogorov PSD for integration times longer than one second has not been investigated.

In this study, RMSs of centroid positions with various integration times (1/20, 1/10, 1/5, 1/2, 1, 2, 5, 10, 20, and 50 seconds) were measured in order to investigate the difference between the measured optical seeing (RMS of centroid positions) and the power law relationship from Kolmogorov PSD. The power law index of the RMS of centroid positions with integration times of 1 to 5 seconds was calculated. Optical seeing may be affected by weather conditions, such as wind velocity, wind attack angle, ambient temperature, and opacity. The relationship between the power law index and the quantitatively expressed weather parameters was investigated by multiple regression analysis, which confirmed that the average wind velocity during measurement is strongly correlated with the power law index. In contrast, the scatter of the corrected power law indices with the wind velocity became small, indicating that only the average wind velocity determines the power law indices, so they can be well corrected using the average wind velocity. Finally, a new correction method for optical seeing, including the wind velocity, was derived in this study.

The derivation of the time-dependence from Kolmogorov PSD is described in Section 3.1. The result of multiple regression analysis between the power law indices as criterion variables and the four weather parameters as explanatory variables and the derivation of the new relation between the power law index and wind velocity are described in Section 3.2. The relation between the corrected power law index and the wind velocity and the four weather parameters (the wind velocity, the wind attacking angle, an ambient temperature, and opacity), and the derivation of the new correction method of the optical seeing are described in Section 3.3.

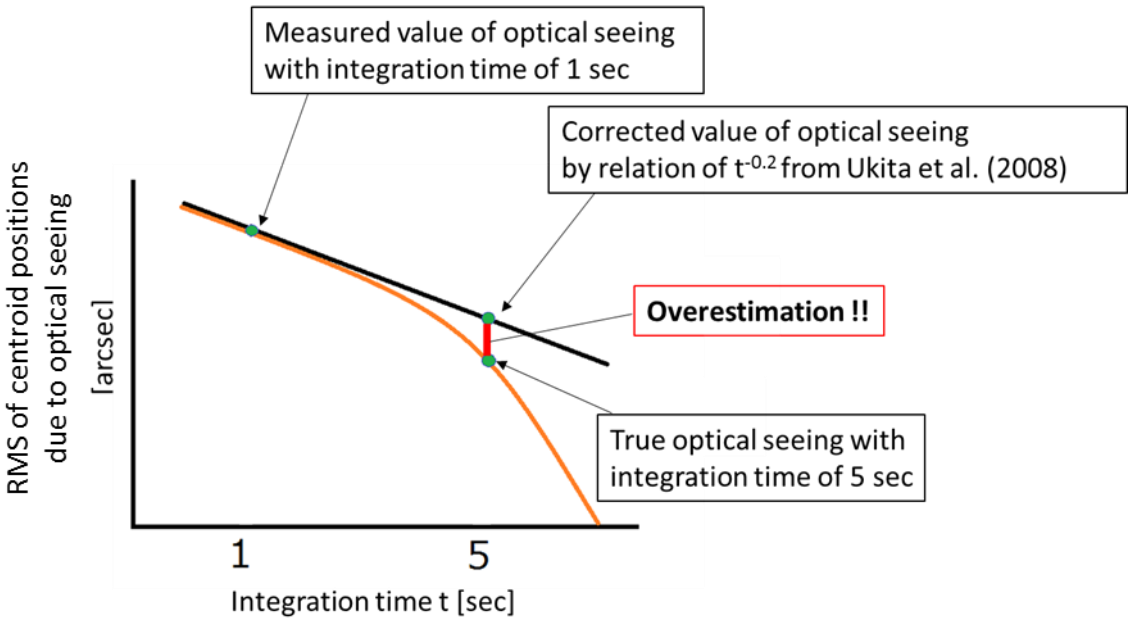

Figure 3-1 Conceptual diagram of the overestimation of the optical seeing at the integration time of five seconds with the correction by the time-dependence according to Ukita et al. (2008).

3.1 Time-Dependence of Optical Seeing with Kolmogorov PSD

Ukita et al. (2004) first provided the relation of the time-dependence of optical seeing from a Kolmogorov power spectrum density (PSD) but did not derive it in theory. In this section, the time-dependence of optical seeing with the Kolmogorov model of turbulence is derived in theory.

Atmospheric turbulence is well described with Kolmogorov model of turbulence, which shows the turbulence of incompressible fluids. Since the Reynolds number of the atmosphere is large (about 10^7 to 10^8), the atmosphere is considered to be turbulent [26] under the condition caused when a wind shear generates an eddy between two wind currents of different velocities (see Figure 3-2). In the Kolmogorov model of turbulence, the kinetic energy associated with large-scale eddies' motions is transferred to smaller and smaller size eddies until it is finally dissipated into heat by viscous friction (see Figure 3-3). The size of the smallest eddy generated from an eddy of the outer (largest) scale is called inner scale. Since the Kolmogorov model of turbulence has self-similarity in general, the rate of dissipation from the outer to the inner scale will become constant (see Figure 3-4). From Figure 3-4, the Kolmogorov model of turbulence in energy decreases according to a power law in the progression from the outer to the inner scale (inertial scale) [27]. The phase structure function [$D_\varphi(r)$] of the Kolmogorov model of turbulence is

$$D_\phi(r) = 6.88\left(\frac{r}{r_0}\right)^{\frac{5}{3}} \ (L > r > l), \qquad (3\text{-}2)$$

where r is the scale of eddy in turbulence, L is the outer scale, l is the inner scale, and r_0 is the Fried parameter [28]. The surface layer that extends to about one km above the ground dominates most of the optical path fluctuation [15]. In addition, the optical seeing may depend mainly on the optical path fluctuations in the surface layer, and some turbulence will occur near the antenna from the direct interaction of wind and antenna. The velocity of such turbulence is represented by the wind velocity at the height of the antenna (or the OPT mounted on the antenna), assuming frozen flow [29]. The RMS of centroid positions in the OPT images is given approximately by the RMS of the wave-front tilt error in observation scale of the telescope (d_{obs}) (Figure 3-5). Assuming that the path fluctuations on the near field, the observing scale of the telescope can correspond to the aperture size of the telescope d_{apeture} ($d_{\mathrm{obs}} = d_{\mathrm{apeture}}$). The RMS wave-front tilt error (σ) in the observation scale of the telescope is represented by

(see Appendix A) [24],

$$\sigma \cong \frac{\lambda}{2\pi}\frac{[D_\phi(d_{\rm obs})]^{\frac{1}{2}}}{d} \propto {d_{\rm obs}}^{-\frac{1}{6}}, \quad (3\text{-}3)$$

where λ is the wavelength.

A consideration of the wave-front tilt in any observation scales is derived as follows. A wave-front tilt along *x* and *y* directions are defined as

$$\alpha(x,y) \equiv \frac{\partial}{\partial x} l(x,y) = \frac{\lambda}{2\pi}\frac{\partial}{\partial x}\phi(x,y) \quad (3\text{-}4)$$

$$\beta(x,y) \equiv \frac{\partial}{\partial y} l(x,y) = \frac{\lambda}{2\pi}\frac{\partial}{\partial y}\phi(x,y) \quad (3\text{-}5)$$

where $l(x,y)$ is the optical path length, $\varphi(x, y)$ is the phase of optical wave (see Appendix A). The power spectra of the wave-front title along *x* and *y* directions [$\Phi_{\rm x}(\vec{\kappa})$ and $\Phi_{\rm y}(\vec{\kappa})$] are related to the power spectrum of the phase [$\Phi_\phi(\vec{\kappa})$] by

$$\Phi_\alpha(\vec{\kappa}) = \lambda^2 \kappa_{\rm x}^2 \Phi_\phi(\vec{\kappa}) \quad (3\text{-}6)$$

$$\Phi_\beta(\vec{\kappa}) = \lambda^2 \kappa_{\rm y}^2 \Phi_\phi(\vec{\kappa}) \quad (3\text{-}7)$$

where $\kappa_{\rm x}$ and $\kappa_{\rm y}$ are the components of the spatial frequency κ. The variance of the wave-front tilt along say x direction is

$$\sigma_\alpha^2 = \lambda^2 \int \kappa_{\rm x}^2 \Phi_\phi(\vec{\kappa})\, d\vec{\kappa}, \quad (3\text{-}8)$$

and the total variance of x and y direction is

$$\sigma_{\alpha\beta}^2 = \lambda^2 \int |\kappa|^2 \Phi_\phi(\vec{\kappa})\, d\vec{\kappa}, \quad (3\text{-}9)$$

A rigorous analysis of this problem was carried out by Fried, D. L (1965) [15], [28], [30] as

$$\sigma_{\alpha\beta}^2 = 0.36\,\lambda^2\, {d_{\rm obs}}^{-\frac{1}{3}}\, {r_0}^{-\frac{5}{3}}, \quad (3\text{-}10)$$

$$\sigma_{\alpha\beta} \propto {d_{\rm obs}}^{-\frac{1}{6}}. \quad (3\text{-}11)$$

Finally, equation (3-11) shows the same relation with equation (3-3), giving us the relation at any observation scales in the aperture.

Assuming the frozen flow according to Taylor (1938) [29], so that a perturbed wave-front is swept across the aperture, the observation scale (d_{obs}) becomes $V_{\mathrm{wind}} \times t + d_{\mathrm{apeture}}$ where V_{wind} is a wind velocity and t is an integration time. When $V_{\mathrm{wind}} \times t$ is larger than d_{apeture} or d_{apeture} is smaller than the outer scale, the observation scale is only dominated by the product of the wind velocity and the integration time, $d_{\mathrm{obs}} = V_{\mathrm{wind}} \times t$. Thus, the RMS wave-front tilt error (σ) is represented by

$$\sigma \cong \frac{\lambda}{2\pi} \frac{\left[D_{\phi}(V_{\mathrm{wind}} \times t)\right]^{\frac{1}{2}}}{V_{\mathrm{wind}} \times t} \propto {V_{\mathrm{wind}}}^{-\frac{1}{6}} \cdot t^{-\frac{1}{6}} \propto t^{-0.166\ldots\ldots} \propto t^{-0.17}. \quad (3\text{-}12)$$

The optical seeing ($d\theta_{\mathrm{s}}$) corresponds to the RMS wave-front tilt error (σ). The newly estimated index of the time-dependence of optical seeing, -0.17, is a little bit smaller than an amount of -0.2 that was empirically proposed in Ukita et al. (2004) [see equation (3-1)]. In this study, the time-dependence of optical seeing with Kolmogorov PSD, equation (3-12), is newly derived in theory.

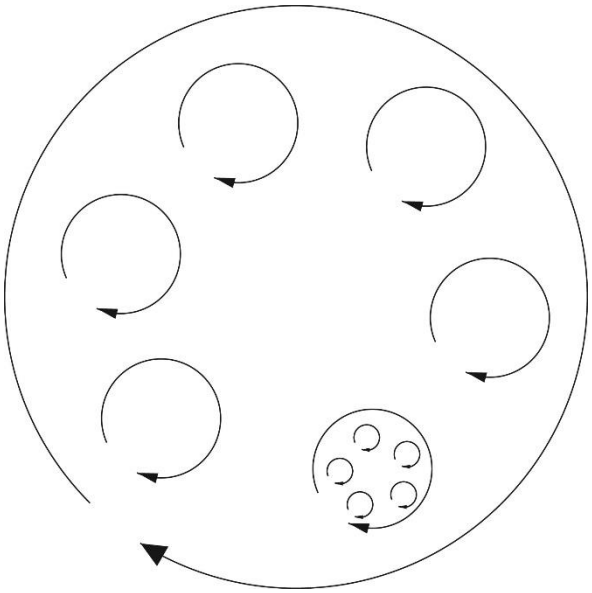

Figure 3-2 Conceptual diagram of eddies in the turbulence. Small eddies occur around large eddies secondary.

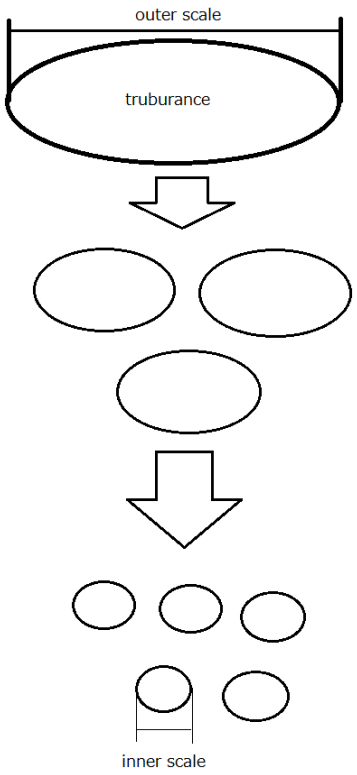

Figure 3-3 Conceptual diagram of the energy flow in the inertial scale of the Kolmogorov model of turbulence.

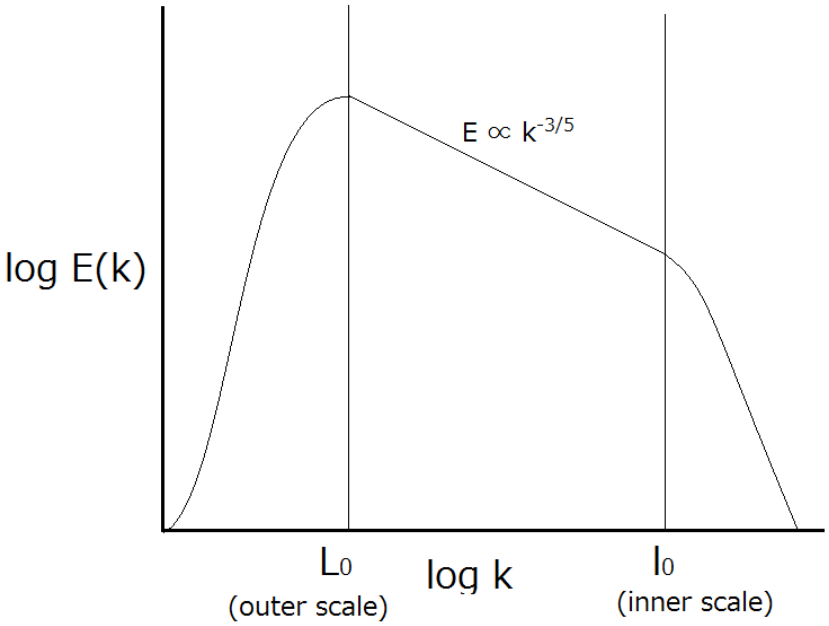

Figure 3-4 Kolmogorov energy spectrum of the Kolmogorov model of turbulence. κ is the wave number, L_0 is the outer scale, and l_0 is the inner scale.

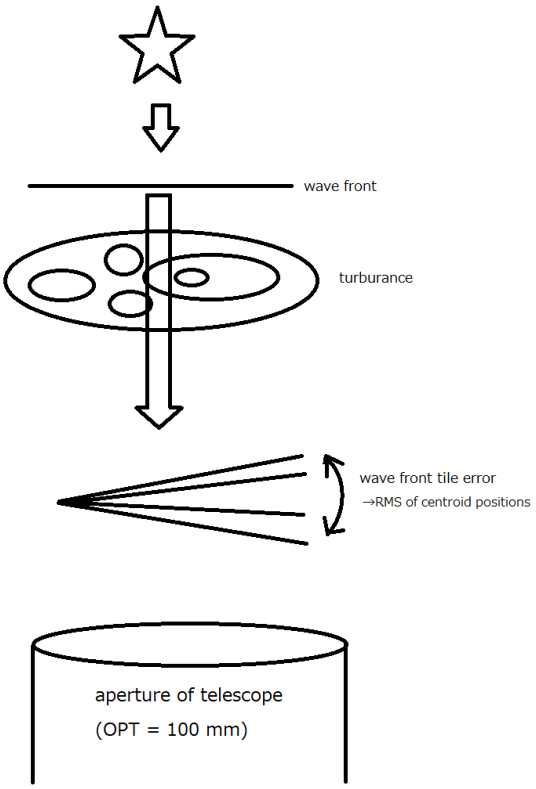

Figure 3-5 Conceptual diagram of the generation of the wavefront tilts error in the scale of the observation of the telescope (aperture size is 100 mm).

3.2 Relating Optical Seeing to Environmental Parameters

In this study, the RMSs of centroid positions at various integration times were measured using the OPT mounted on the ALMA ACA 7-m antenna No. 12, to investigate the time-dependence of optical seeing. The specifications of the OPT, the detail of the anemometer and the thermometer, the estimation of the RMS of centroid positions with the OPT, and the quality of the RMS of centroid positions are given in Appendix C, Appendix D, Appendix E, Appendix F, respectively. Results indicate that the measured RMS of centroid positions can be attributed entirely to the optical seeing (see Appendix G).

The measurement results of the RMSs of centroid positions with integration times of 1, 2, and 5 seconds and the power law indices from integration times of 1 to 5 seconds with linear fitting are listed in Table 3-1 and Table 3-2. The plots of the RMSs of centroid positions and the results of linear fitting are shown in Figure 3-7, Figure 3-8, Figure 3-9, and Figure 3-10. The dashed line is the time-dependence from Kolmogorov PSD [see equation (3-12)]. The OPT obtains the image with an integration time of 1/30 seconds while tracking the star for 900 seconds. The RMS of centroid positions is measured by the RMS of the centroid positions relative to the reference positions of the star in the image with an integration time of 1/30 seconds. The reference positions are determined by the average of centroid positions within one second from the start time of the measurement (see Figure 3-6). The RMSs of centroid positions with integration times of 1/20, 1/10, 1/5, 1/2, 1, 2, 5, 10, 20, and 50 seconds are measured by the RMS of the integrated relative centroid positions. From these Figures, RMSs of centroid positions with integration times longer than one second indicate a different time-dependence from Kolmogorov PSD, which is similar to the tendency reported in Ukita et al. (2008).

The power law indices are estimated by the RMSs of positions of the star in images with integration times of 1, 2, and 5 seconds, made every 300 seconds. These images, with an exposure time of 1/30 seconds were obtained by OPT during 900 seconds. However, RMSs are estimated every 300 seconds in order to consider the average wind velocity as well as the wind attack angle, which changes on a short time scale [21]. The power law indices of the RMS of centroid positions with integration times of 1, 2, and 5 seconds may be affected by the weather parameters (wind velocity, wind attack angle, ambient temperature, and opacity). In this study, multiple regression analysis was performed with the power law indices as criterion variables and the four weather parameters as explanatory variables.

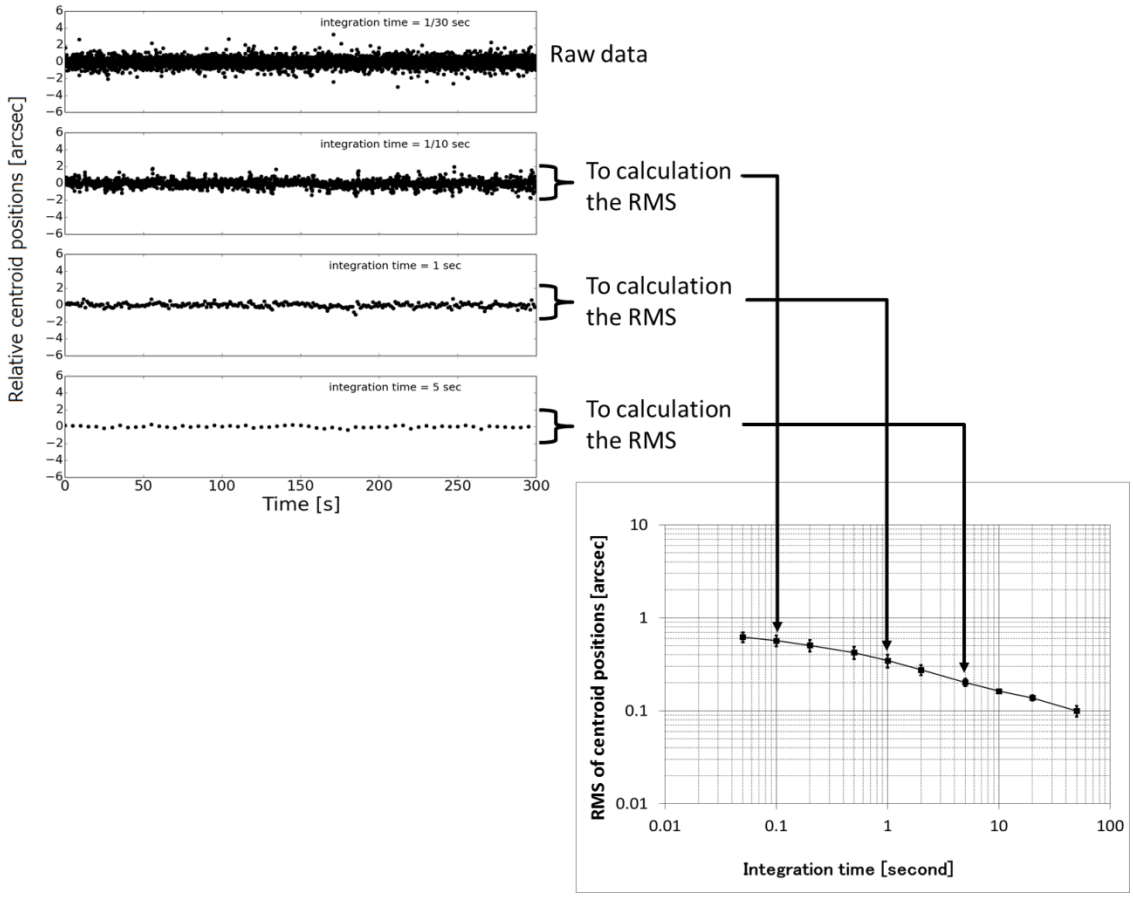

Figure 3-6 Example of integrated relative centroid positions with the various integration times and the calculation of RMSs of centroid positions. The relative positions with the integration time of 1/30 seconds are raw data. Other RMSs of centroid positions are obtained by similar calculation.

Table 3-1 Summary of measurement results of RMSs of centroid positions in the integration time of 1, 2, and 5 seconds and power law indices between integration time of 1 to 5 seconds.

(1) Date	(2) Start (UT) [hh:mm]	(3) End (UT) [hh:mm]		(4) RMS of centroid positions Integration time 1 second [arcsec]	2 second [arcsec]	5 second [arcsec]	(5) Power law index in 1 to 5 seconds
2012/6/11	3:43	3:58	1st 300 seconds	0.90	0.69	0.44	-0.44
			2nd 300 seconds	0.89	0.67	0.45	-0.41
			3rd 300 seconds	1.08	0.79	0.54	-0.44
2012/6/11	5:06	5:21	1st 300 seconds	0.34	0.26	0.20	-0.32
			2nd 300 seconds	0.30	0.25	0.18	-0.3
			3rd 300 seconds	0.41	0.31	0.22	-0.38
2012/6/11	5:43	5:58	1st 300 seconds	0.54	0.43	0.30	-0.35
			2nd 300 seconds	0.64	0.52	0.33	-0.39
			3rd 300 seconds	0.65	0.54	0.38	-0.33
2012/6/15	2:29	2:44	1st 300 seconds	0.37	0.32	0.27	-0.21
			2nd 300 seconds	0.37	0.31	0.24	-0.27
			3rd 300 seconds	0.34	0.29	0.21	-0.29
2012/6/15	4:05	4:20	1st 300 seconds	1.06	0.86	0.60	-0.34
			2nd 300 seconds	1.09	0.80	0.59	-0.39
			3rd 300 seconds	1.06	0.86	0.63	-0.32
2012/6/16	2:16	2:31	1st 300 seconds	0.74	0.64	0.49	-0.25
			2nd 300 seconds	0.79	0.68	0.55	-0.22
			3rd 300 seconds	0.48	0.41	0.33	-0.22
2012/6/16	2:51	3:06	1st 300 seconds	0.31	0.26	0.20	-0.26
			2nd 300 seconds	0.41	0.32	0.23	-0.36
			3rd 300 seconds	0.57	0.45	0.35	-0.32
2012/6/16	3:33	3:48	1st 300 seconds	1.04	0.86	0.63	-0.31
			2nd 300 seconds	1.01	0.78	0.60	-0.32
			3rd 300 seconds	1.02	0.75	0.51	-0.42

Table 3-2 Summary of averages and standard deviations of the RMSs of centroid positions in the integration time of 1, 2, and 5 seconds, and the average of power law index between integration time of 1 to 5 seconds.

(1) Date	(2) Start (UT) [hh:mm]	(3) End (UT) [hh:mm]	(4) Average of RMSs of centroid positions 1 second [arcsec]	2 second [arcsec]	5 second [arcsec]	(5) Standard deviation of RMSs of centroid positions 1 second [arcsec]	2 second [arcsec]	5 second [arcsec]	(6) Average of power law indices in 1 to 5 seconds
2012/6/11	3:43	3:58	0.96	0.72	0.47	0.11	0.06	0.05	-0.43
2012/6/11	5:06	5:21	0.35	0.28	0.20	0.06	0.03	0.02	-0.33
2012/6/11	5:43	5:58	0.61	0.49	0.34	0.06	0.06	0.04	-0.36
2012/6/15	2:29	2:44	0.36	0.31	0.24	0.02	0.02	0.03	-0.26
2012/6/15	4:05	4:20	1.07	0.84	0.61	0.02	0.04	0.02	-0.35
2012/6/16	2:16	2:31	0.67	0.58	0.46	0.17	0.14	0.11	-0.23
2012/6/16	2:51	3:06	0.43	0.34	0.26	0.13	0.10	0.07	-0.31
2012/6/16	3:33	3:48	1.02	0.80	0.58	0.02	0.05	0.06	-0.35

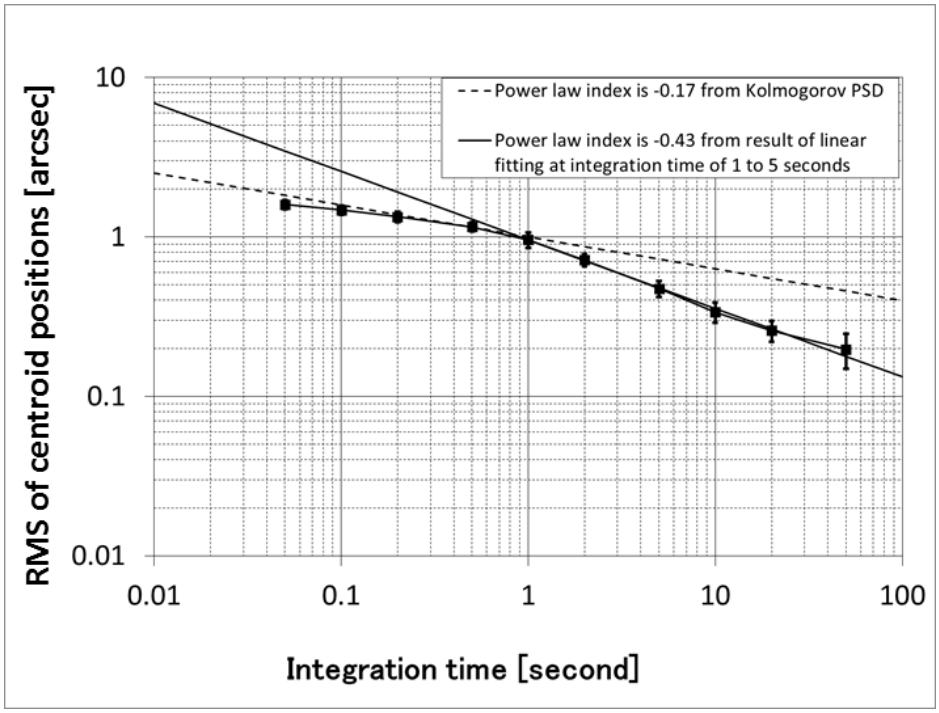

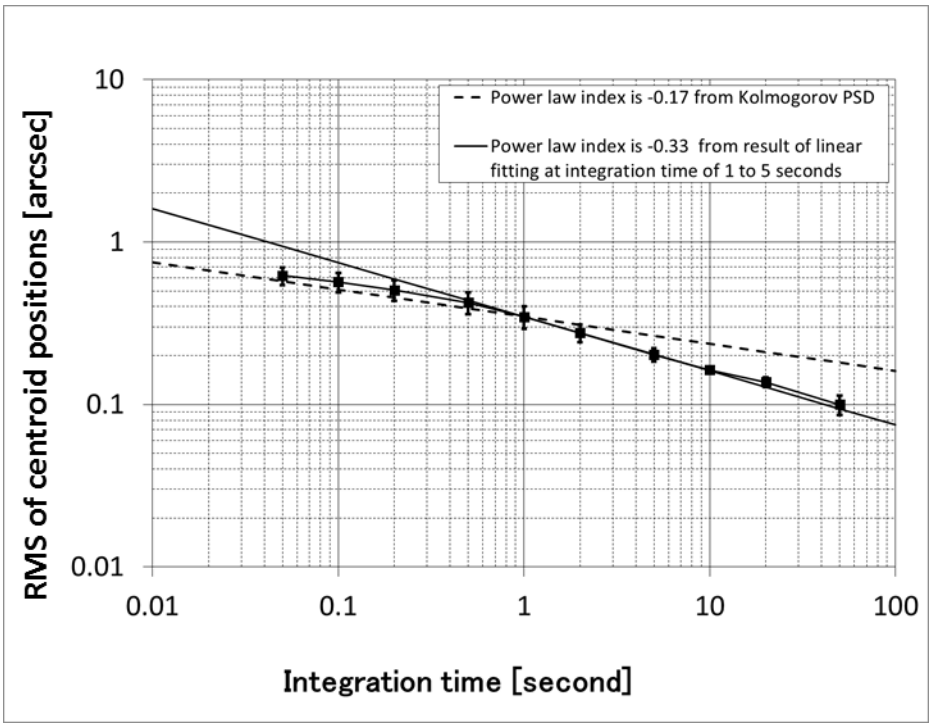

Figure 3-7 RMS of centroid positions with integration times taken at UT3:43 - 3:48, June 11, 2012 (upper) and UT5:06 - 5:21, June 11, 2012. The averaged wind velocities are 3.16 m/s (upper) and 2.90 m/s (lower). A dashed line is the time dependencies from Kolmogorov PSD. The solid lien is the result of linear fitting of the RMS of centroid positions in integration time of 1 to 5 seconds [see column (5) in Table 3-2].

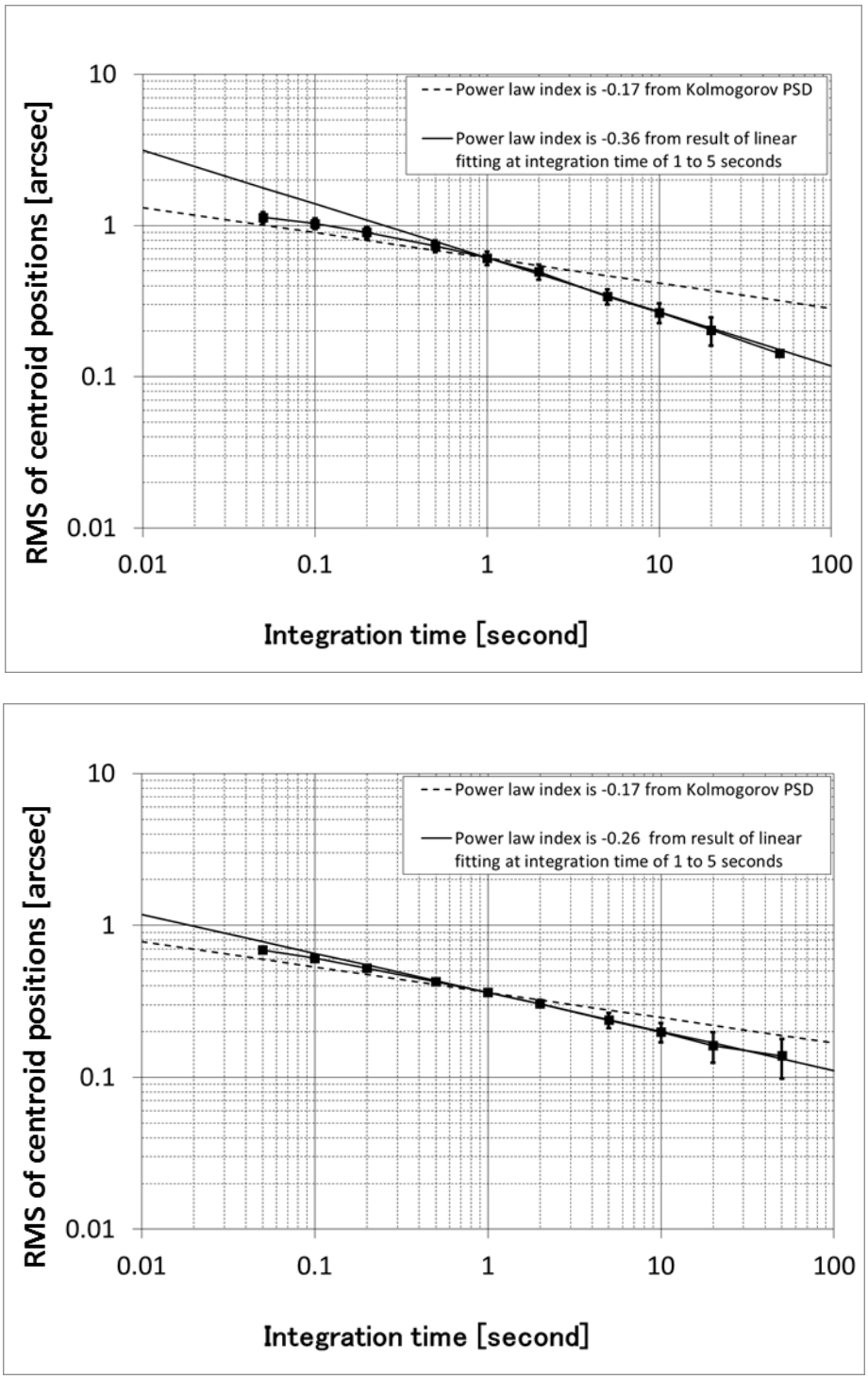

Figure 3-8 RMS of centroid positions with integration times taken at UT5:43 - 5:58, June 11, 2012 (upper) and UT2:29 - 2:34, June 15, 2012. The averaged wind velocities are 3.39 m/s (upper) and 1.30 m/s (lower). A dashed line is the time dependencies from Kolmogorov PSD. The solid lien is the result of linear fitting of the RMS of centroid positions in integration time of 1 to 5 seconds [see column (5) in Table 3-2].

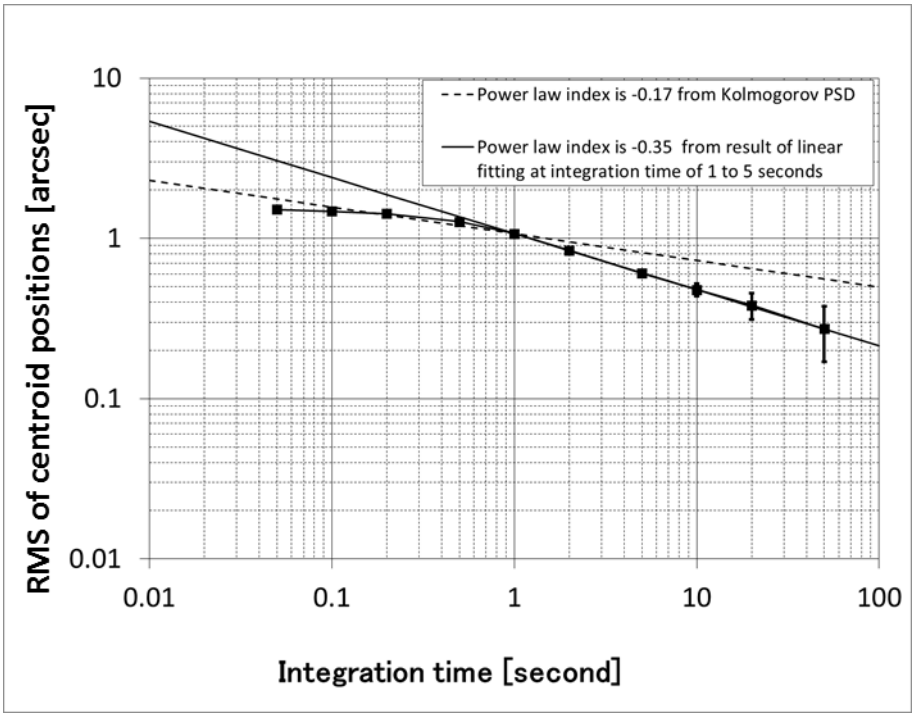

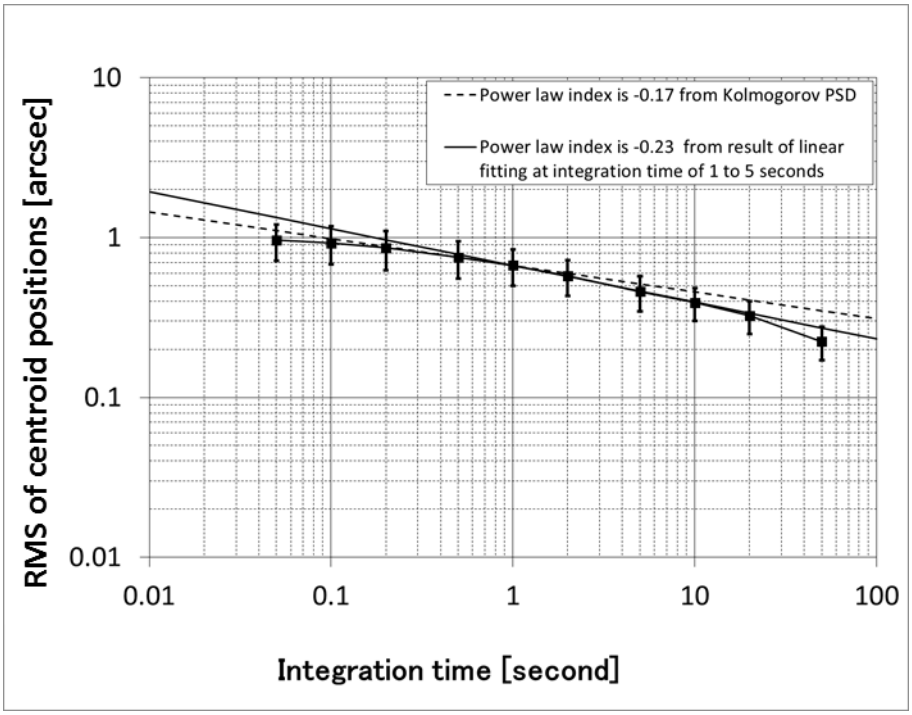

Figure 3-9 RMS of centroid positions with integration times taken at UT4:05 - 4:20, June 15, 2012 (upper) and UT2:16 - 2:31, June 16, 2012. The averaged wind velocities are 3.23 m/s (upper) and 1.52 m/s (lower). A dashed line is the time dependencies from Kolmogorov PSD. The solid lien is the result of linear fitting of the RMS of centroid positions in integration time of 1 to 5 seconds [see column (5) in Table 3-2].

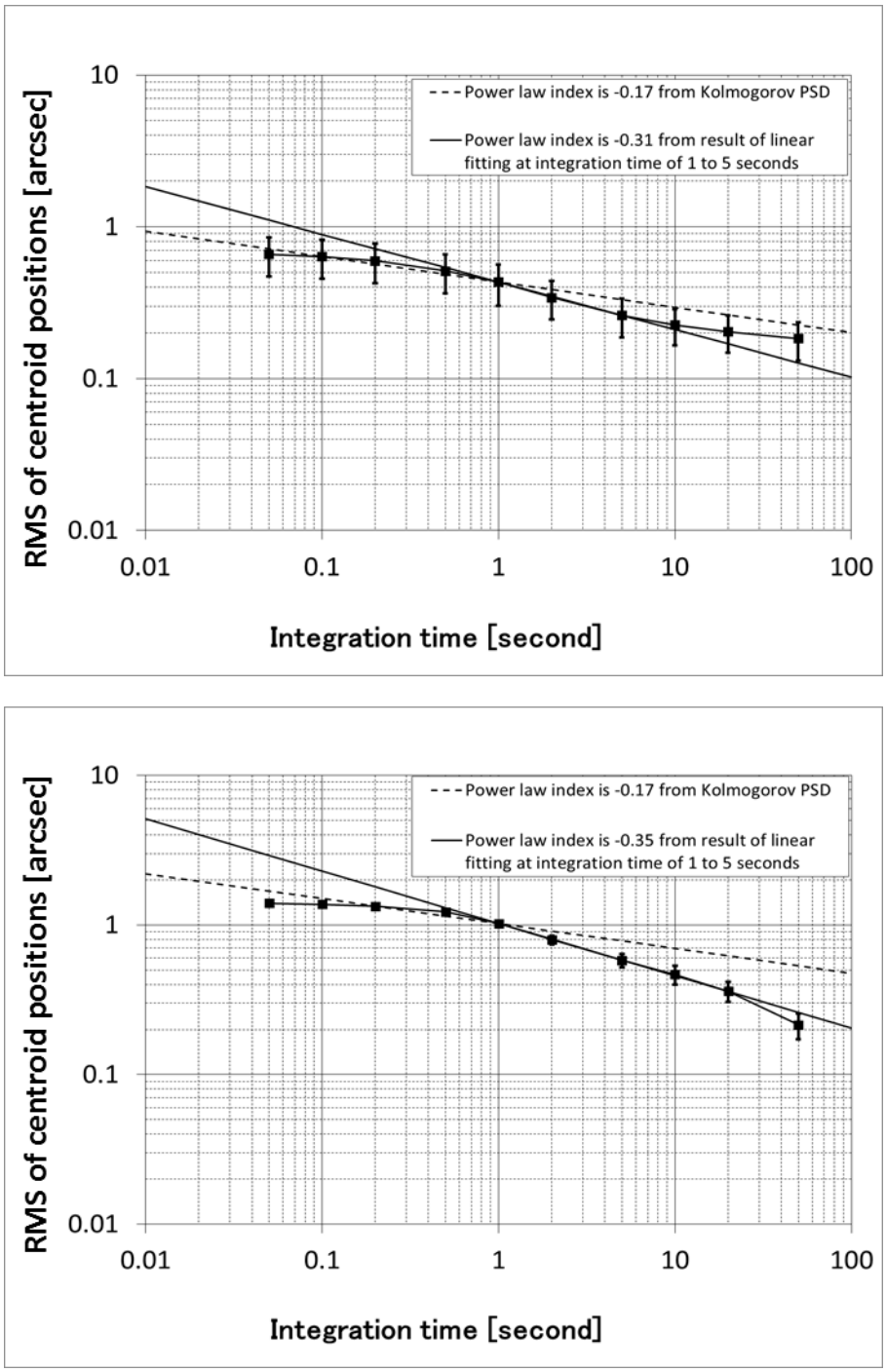

Figure 3-10 RMS of centroid positions with integration times taken at UT2:51 - 3:06, June 16, 2012 (upper) and UT3:33 - 3:48, June 16, 2012. The averaged wind velocities are 2.28 m/s (upper) and 3.29 m/s (lower). A dashed line is the time dependencies from Kolmogorov PSD. The solid lien is the result of linear fitting of the RMS of centroid positions in integration time of 1 to 5 seconds [see column (5) in Table 3-2].

Table 3-3 Summary of measurement results of power law index and weather parameters.

(1) Date	(2) Start (UT)	(3) End (UT)		(4) Estimated power law index in 1 to 5 seconds	(5) Measured average wind velocity	(6) Measured Wind attacking angle	(7) Deviation of measured ambient temperature	(8) Measured elevation angle
	[hh:mm]	[hh:mm]			[m/s]	[deg]	[°C]	[deg]
2012/06/11	03:43	03:58	1st 300 seconds	-0.44	3.16	91.36	0.06	33.21
			2nd 300 seconds	-0.41	3.02	89.27	0.05	32.63
			3rd 300 seconds	-0.44	3.33	82.91	0.12	32.04
2012/06/11	05:06	05:21	1st 300 seconds	-0.32	2.95	82.24	0.06	81.31
			2nd 300 seconds	-0.30	2.87	82.13	0.07	81.95
			3rd 300 seconds	-0.38	2.92	76.80	0.12	82.47
2012/06/11	05:43	05:58	1st 300 seconds	-0.35	3.14	66.25	0.22	41.27
			2nd 300 seconds	-0.39	3.64	66.68	0.03	41.03
			3rd 300 seconds	-0.33	3.40	67.13	0.03	40.77
2012/06/15	02:29	02:44	1st 300 seconds	-0.21	1.42	80.59	0.07	66.50
			2nd 300 seconds	-0.27	1.23	82.49	0.11	65.61
			3rd 300 seconds	-0.29	1.26	103.89	0.07	64.70
2012/06/15	04:05	04:20	1st 300 seconds	-0.34	3.16	90.20	0.09	28.44
			2nd 300 seconds	-0.39	3.27	88.70	0.05	27.72
			3rd 300 seconds	-0.32	3.22	83.94	0.10	27.00
2012/06/16	02:16	02:31	1st 300 seconds	-0.25	1.44	49.52	0.43	38.77
			2nd 300 seconds	-0.22	1.46	94.90	0.32	38.52
			3rd 300 seconds	-0.22	1.60	91.37	0.11	38.24
2012/06/16	02:51	03:06	1st 300 seconds	-0.26	2.01	77.49	0.08	61.80
			2nd 300 seconds	-0.36	2.27	74.05	0.08	60.85
			3rd 300 seconds	-0.32	2.60	68.83	0.22	59.90
2012/06/16	03:33	03:48	1st 300 seconds	-0.31	3.40	65.18	0.00	26.64
			2nd 300 seconds	-0.32	3.08	69.15	0.06	27.62
			3rd 300 seconds	-0.42	3.34	63.30	0.03	28.61

Table 3-4 Result of a multiple regression analysis of the power law indices.

Explanatory variables	Coefficient	Standard deviation	t-statics
Intercept	-0.17	0.07	-2.35
Average wind velocity	-0.07	0.02	-3.89
Deviation of ambient temperature	-0.00	0.12	-0.03
Cosine of wind attacking angle	0.04	0.06	0.59
Sine of El angle	0.01	0.06	0.92

By multiple regression analysis between the power law indices as criterion variables and four weather parameters (the average wind velocity in 300 second, the cosine of wind attacking angle, the deviation of ambient temperature, and the sine of elevation) as explanatory variables, the absolute value of the t-statistic of the average wind velocity, 3.89, is higher than that of the cosine of wind attack angle, 0.59, of the deviation of ambient temperature, 0.03, and of the sine of elevation, 0.92 (see Table 3-4). It was confirmed that the average wind velocity is more strongly correlated with the power law index than the cosine of the wind attack angle, the fluctuation of ambient temperature, and the sine of elevation. On the other hand, the other three relationships show no strong correlation. The regression equation is

$$d\theta_s \propto t^{-(0.07\pm0.02)\times V_{\mathrm{wind}}+(0.04\pm0.06)\times cos(\theta_a)-(0.00\pm0.12)\times dT+(0.01\pm0.06)\times sin(El)^{-0.5}-(0.17\pm0.07)}, \quad (3\text{-}13)$$

where $d\theta_s$ is the RMS of centroid positions that are attributed only to the optical seeing conditions, V_{wind} is the average wind velocity, θ_a is the wind attack angle, T is the ambient temperature, and El is the angle of elevation. The RMSs of centroid positions are affected by the wind attack angle relative to the telescope as reported in Martin (1986) [24]. In this study, the effect of the wind attack angle on the power law index was investigated by using different values of cos (θ_a). Furthermore, since optical seeing is strongly influenced by fluctuation of air temperature, the effect of the ambient temperature on the power law index was investigated by using the standard deviation of the ambient temperature at measurement time.

Plots of the RMSs of centroid positions versus average wind velocity, wind attack angle, fluctuation of ambient temperature, and the sine of the elevation angle are shown in Figure 3-11, Figure 3-12, Figure 3-13, and Figure 3-14. From a linear fitting between the power law index and the average wind velocity (see Figure 3-11), a new relation between the optical seeing ($d\theta_s$) and integration time (t) including average wind velocity (V_{wind}) was developed as follows,

$$d\theta_s \propto t^{-(0.16\pm0.05)-(0.06\pm0.02)\times V_{\mathrm{wind}}} \quad (3\text{-}14)$$

This agrees with the relation with the Kolmogorov model of turbulence [see equation (3-12)] in the case of a calm (V_{wind} = 0 m/s).

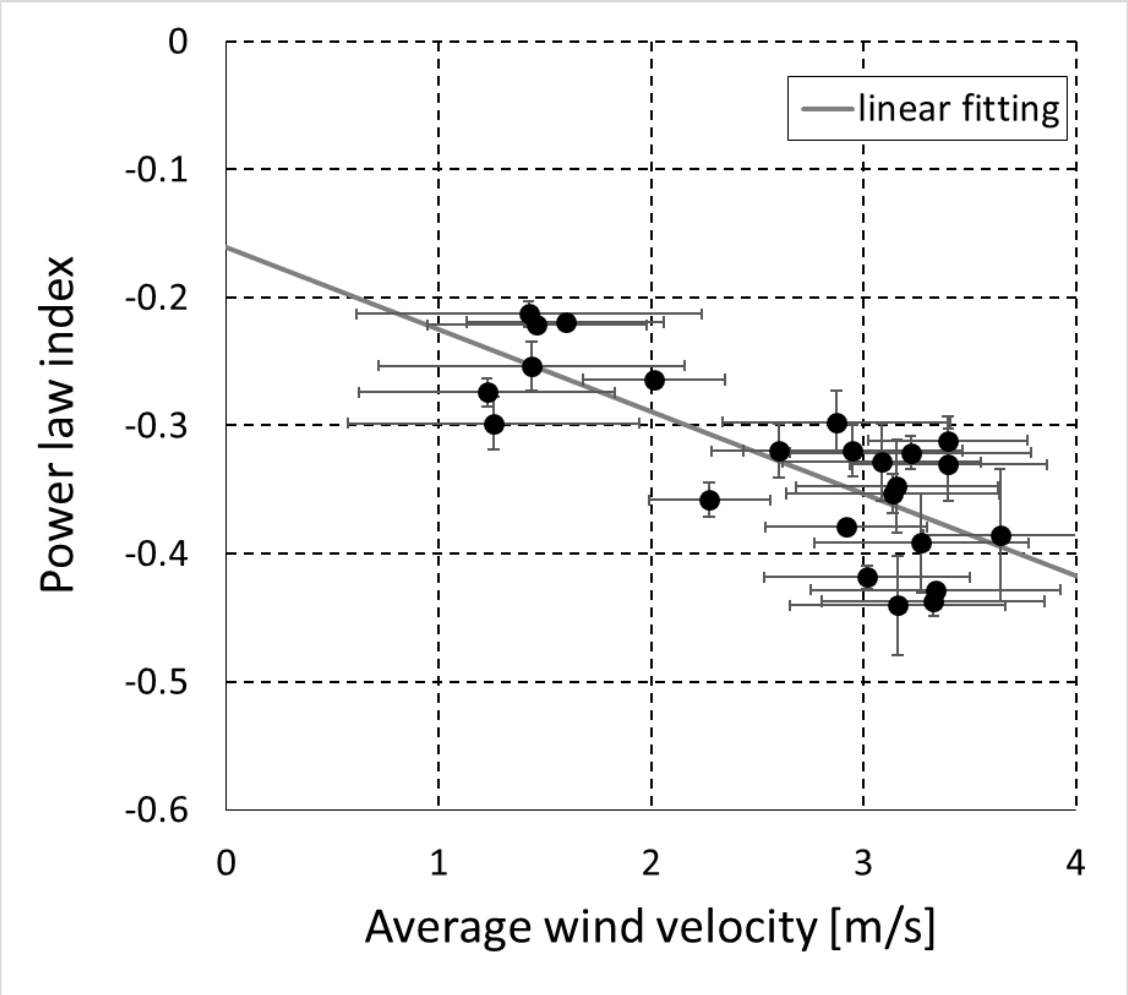

Figure 3-11 Power law indices as a function of the average wind velocities. A solid line is the result of a linear fitting. These parameters are listed in column (4) and (5) in Table 3-3.

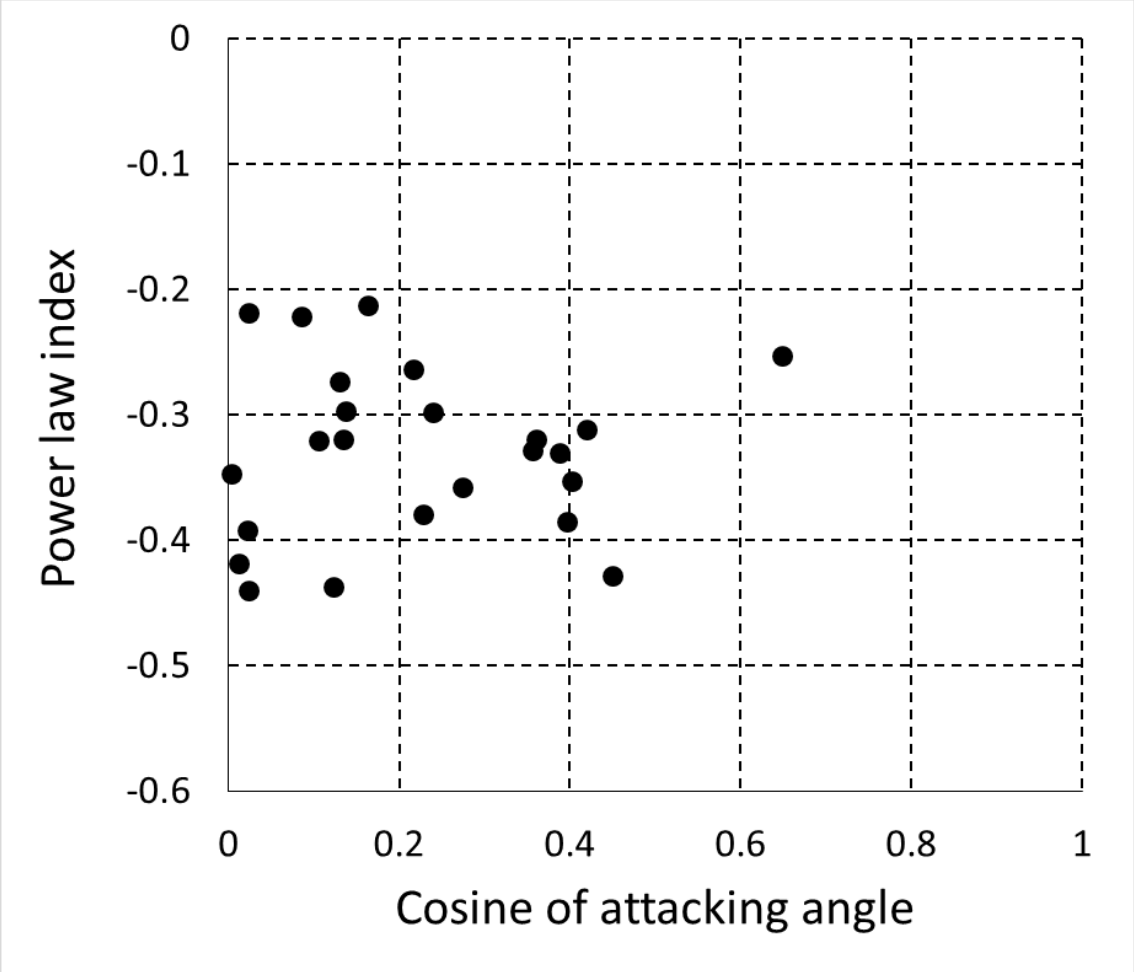

Figure 3-12 Power law indices as a function of the cosine of wind attacking angles. These parameters are listed in column (4) and (6) in Table 3-3.

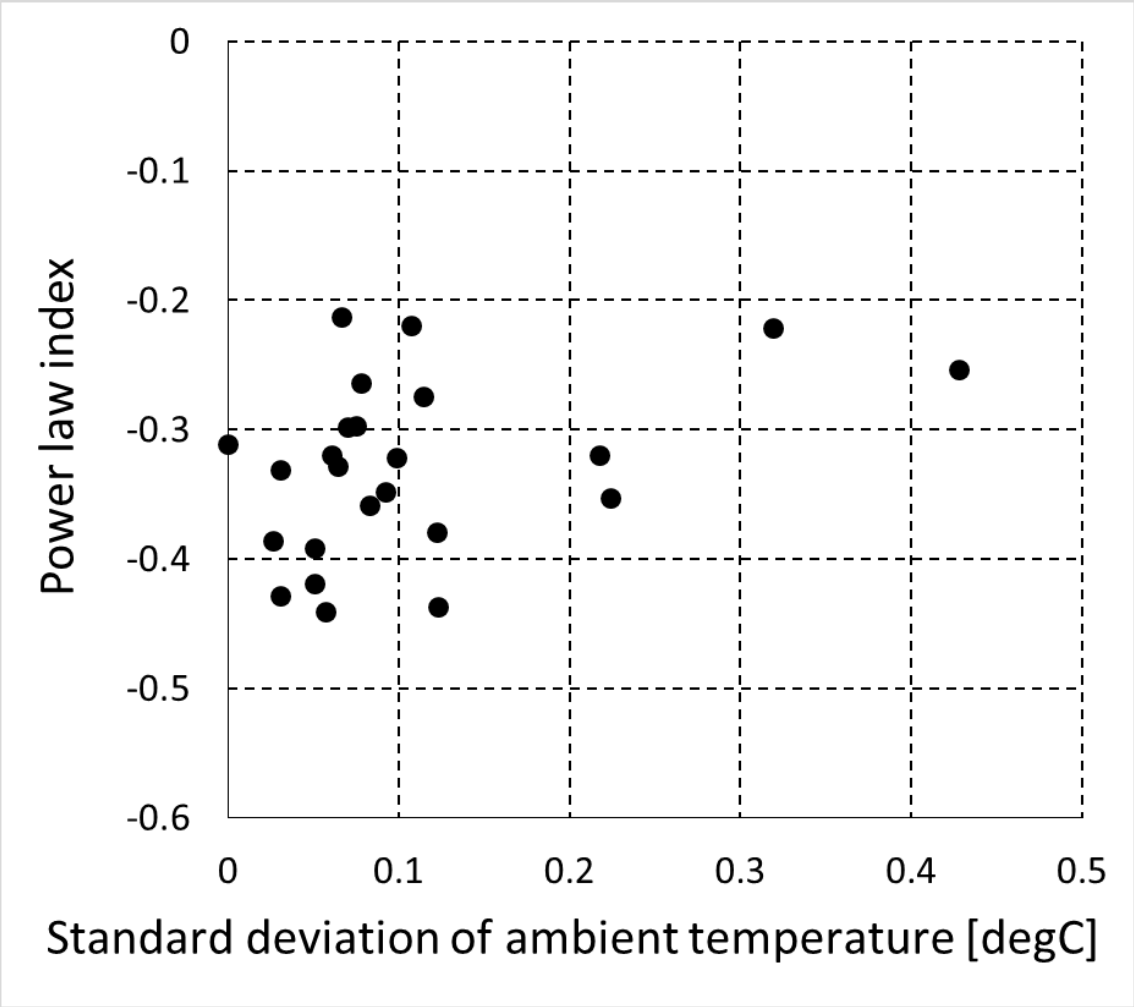

Figure 3-13 Power law indices as a function of the deviations of ambient temperature. These parameters are listed in column (4) and (7) in Table 3-3.

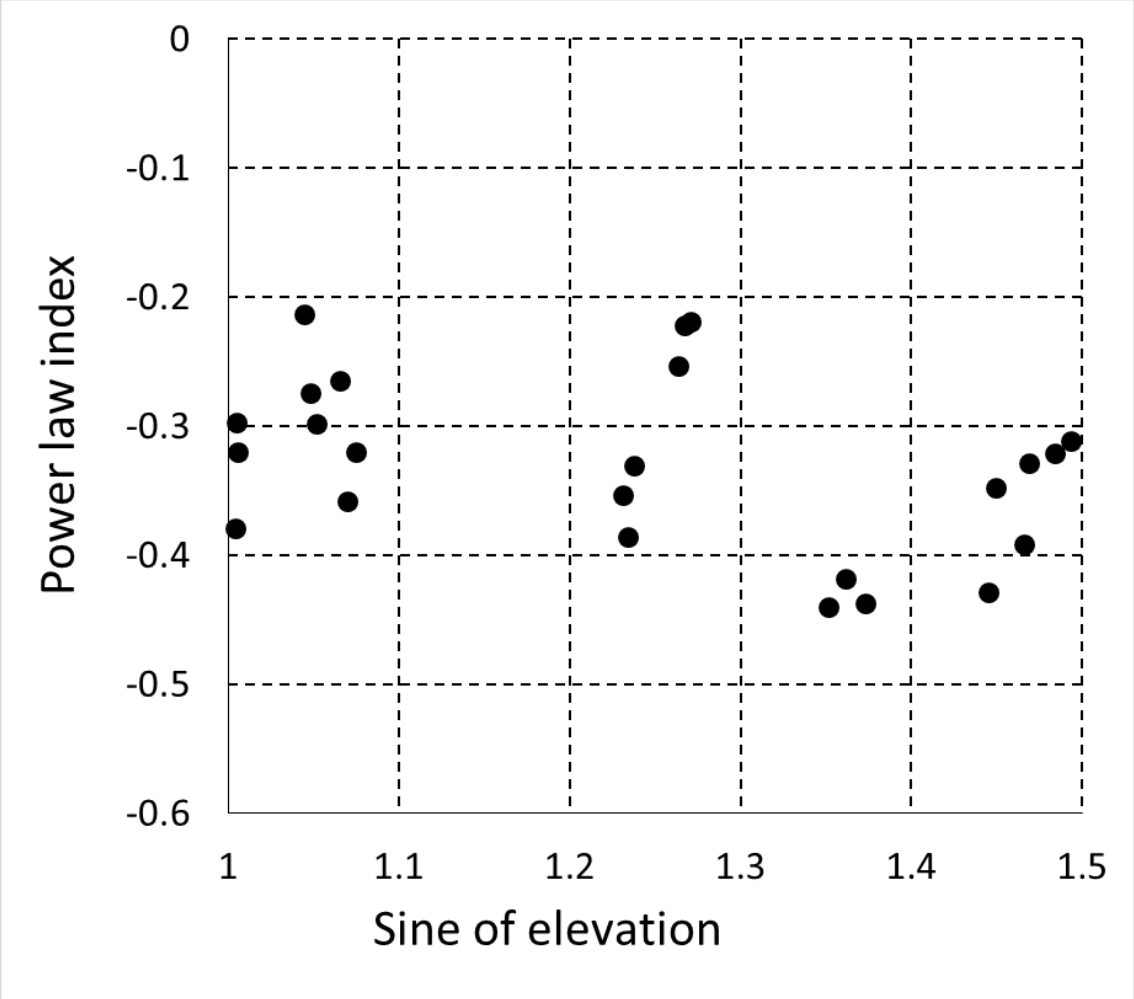

Figure 3-14 Power law indices as a function of the sine of El angle. These parameters are listed in column (4) and (7) in Table 3-3.

Table 3-5 Summary of power law indices and average wind velocity.

(1) Date	(2) Start (UT) [hh:mm]	(3) Power law index	(4) Average wind velocity [m/s]
2012/6/11	3:43	-0.36	3.17
2012/6/11	5:06	-0.35	2.90
2012/6/11	5:43	-0.38	3.39
2012/6/15	2:29	-0.24	1.30
2012/6/15	4:05	-0.37	3.23
2012/6/16	2:16	-0.26	1.52
2012/6/16	2:51	-0.31	2.28
2012/6/16	3:33	-0.37	3.29

The RMS of centroid positions with integration times of 1, 2, and 5 seconds and the two power law relationship are shown in Figure 3-15, Figure 3-16, Figure 3-17, and Figure 3-18. A dashed line indicates the time-dependence from Kolmogorov PSD [see equation (3-12)]. A solid line indicates the time-dependence of the average wind velocity during this measurement, as derived in the present study. It is evident that RMSs of centroid positions lie along the solid line rather than the dashed line. With a low average wind velocity (V_{wind} ~ 1 m/s), the solid line approaches the dashed line. (For example, see lower figures in Figure 3-16 and Figure 3-17).

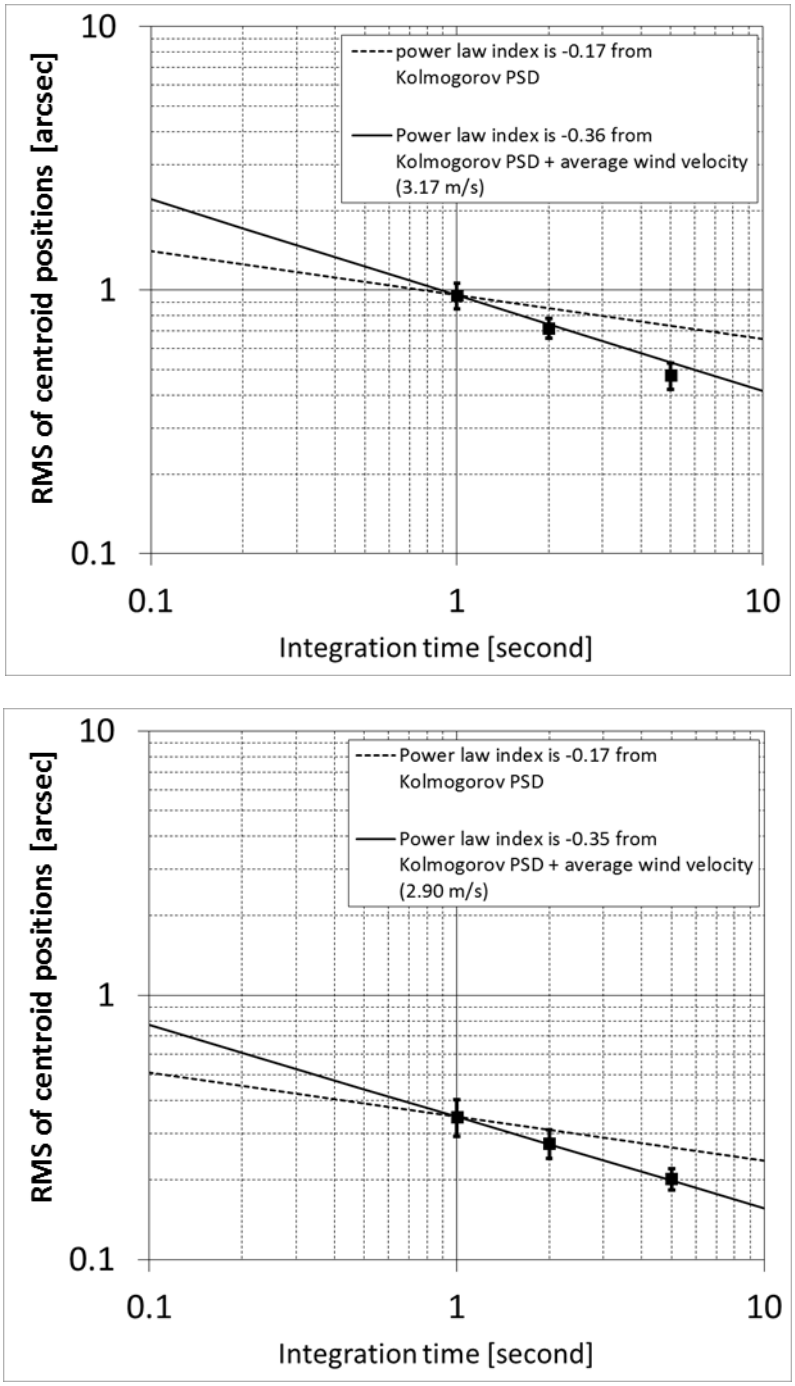

Figure 3-15 Comparison of two dependencies. The measurement results are RMSs of centroid positions with the integration times of 1, 2 and 5 seconds taken at UT3:43 - 3:48, June 11, 2012 (upper) and UT5:06 - 5:21, June 11, 2012 (lower). A dashed line indicates dependencies by equation (3-12). A solid line indicates dependencies by equation (3-15) with average wind velocity during this measurement [3.17 m/s (upper) and 2.90 m/s (lower)].

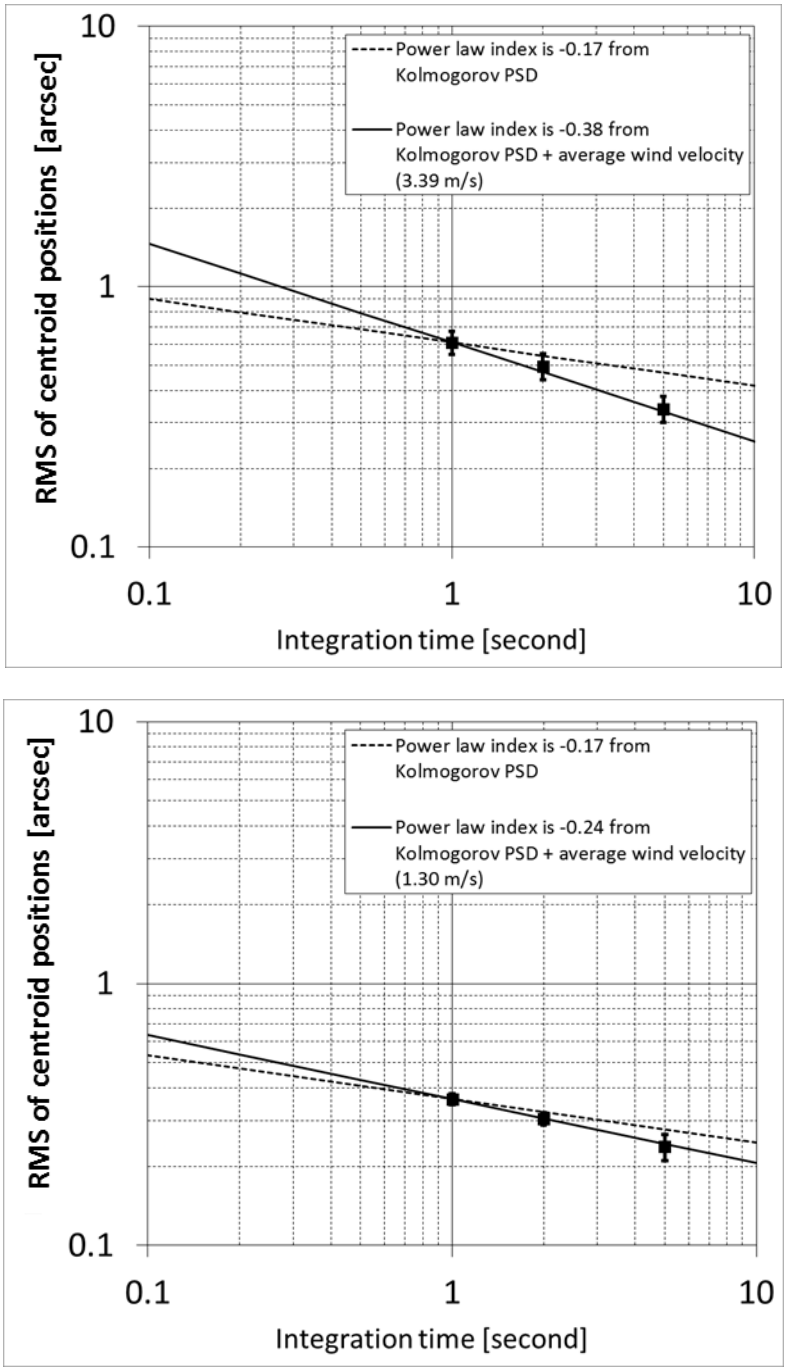

Figure 3-16 Comparison of two dependencies. The measurement results are RMSs of centroid positions with the integration times of 1, 2 and 5 seconds taken at UT5:43 - 5:58, June 11, 2012 (upper) and UT2:29 - 2:34, June 15, 2012 (lower). A dashed line indicates dependencies by equation (3-12). A solid line indicates dependencies by equation (3-15) with average wind velocity during this measurement [3.39 m/s (upper) and 1.30 m/s (lower)].

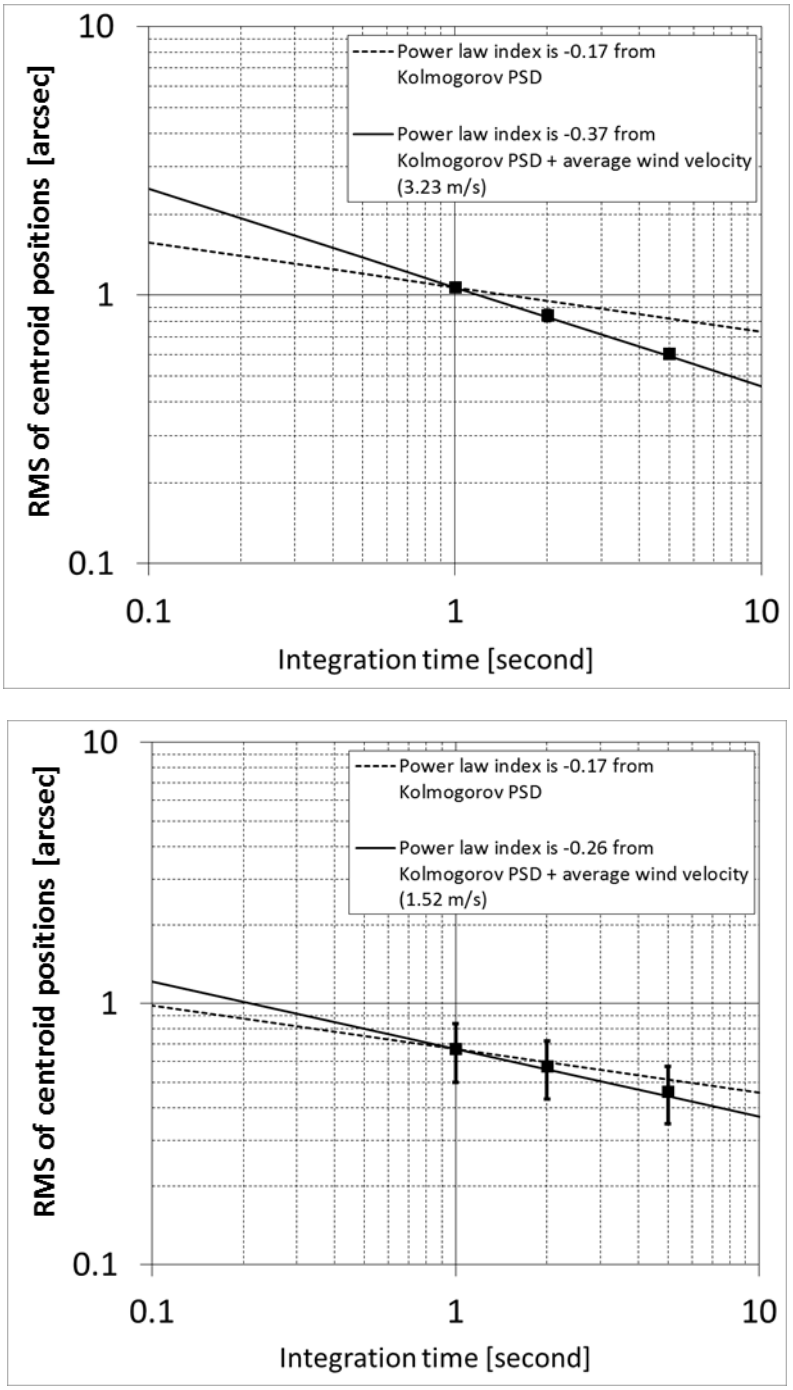

Figure 3-17 Comparison of two dependencies. The measurement results are RMSs of centroid positions with the integration times of 1, 2 and 5 seconds taken at UT4:05 - 4:20, June 15, 2012 (upper) and UT2:16 - 2:31, June 16, 2012 (lower). A dashed line indicates dependencies by equation (3-12). A solid line indicates dependencies by equation (3-15) with average wind velocity during this measurement [3.23 m/s (upper) and 1.52 m/s (lower)].

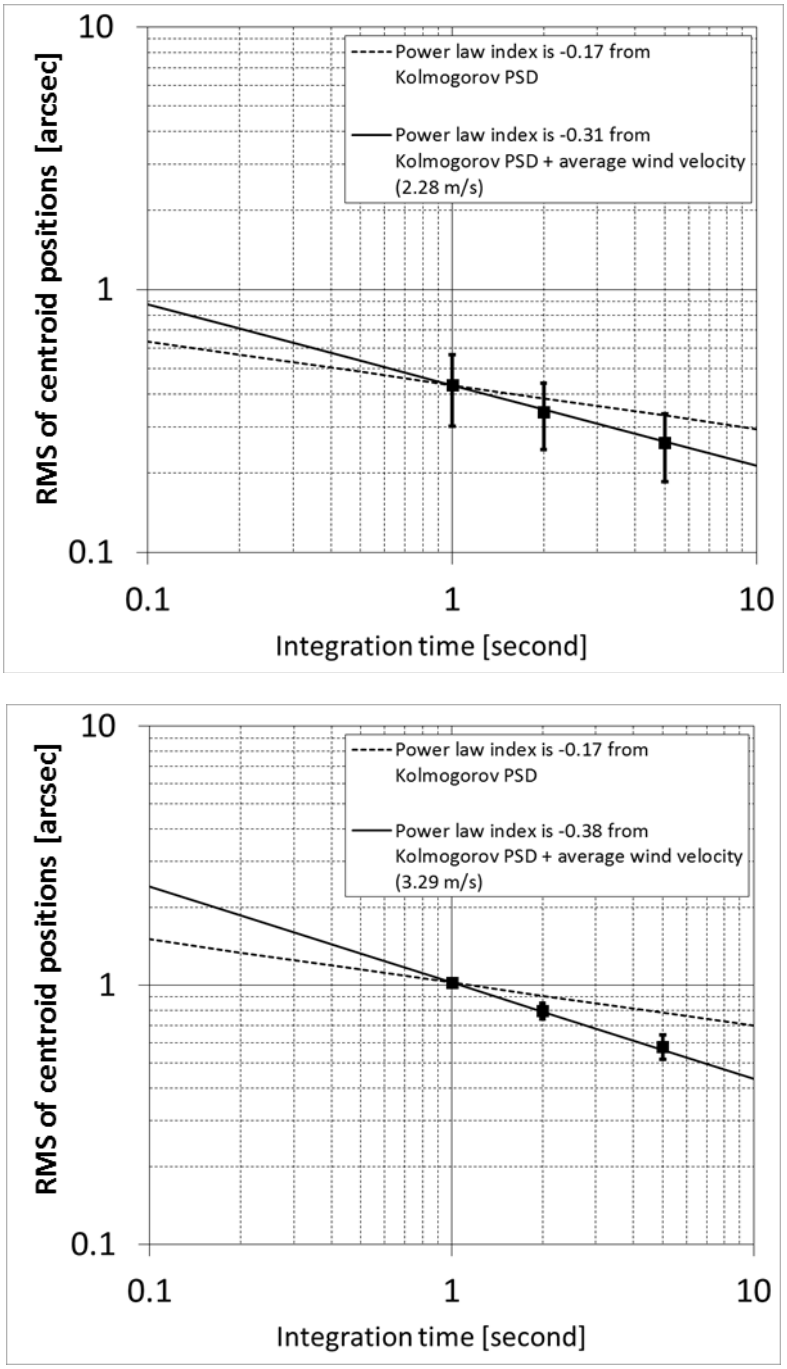

Figure 3-18 Comparison of two dependencies. The measurement results are RMSs of centroid positions with the integration times of 1, 2 and 5 seconds taken at UT2:51 - 3:06, June 16, 2012 (upper) and UT3:33 - 3:48, June 16, 2012 (lower). A dashed line indicates dependencies by equation (3-12). A solid line indicates dependencies by equation (3-15with average wind velocity during this measurement [2.28 m/s (upper) and 3.29 m/s (lower)].

3.3 Time-Dependence of Optical Seeing and Wind Velocity

Table 3-6 Comparison of parameters between uncorrected power law indices and corrected power law indices with average wind velocity. These parameters are common in Figure 3-19, Figure 3-20, and Figure 3-21.

Parameters	Uncorrected	Corrected with average wind velocity
Average	-0.33	0.02
Maximum	-0.21	0.08
Minimum	-0.44	-0.06
Standard deviation	0.07	0.04
Peak to peak	0.21	0.14

The absolute values of the average, maximum and minimum power law indices decrease significantly when corrected for the average wind velocity, and the absolute values of the standard deviation and the peak-to-peak also decrease when corrected for average wind velocity (see Table 3-6). From plots of the corrected power law indices with or without the average wind velocity, the scatter of the corrected power law index is smaller (Figure 3-19, Figure 3-20, and Figure 3-21). It appears that the average wind velocity determines the power law indices, which can be completely corrected by correcting for the average wind velocity. Thus, the contributions of attack angle to OPT and the ambient temperature and elevation to the power law index of the time-dependence of optical seeing are very small.

It is sufficiently accurate to say that the optical seeing at integration times from 1 to 5 seconds relates only the wind velocity [see equation (3-14)]. Finally, the new correction equation for optical seeing, including the wind velocity, is derived as follows,

$$d\theta_{\mathrm{s}} = d\theta_{\mathrm{s\ measure}} \times \frac{5^{-(0.16\pm0.05)-(0.06\pm0.02)\times V_{\mathrm{Wind}}}}{1^{-(0.16\pm0.05)-(0.06\pm0.02)\times V_{\mathrm{Wind}}}}, \qquad (3\text{-}15)$$

where $d\theta_{\mathrm{s}}$ is pointing error due to the effect of optical seeing on referencing pointing performance [see equation (2-1)] and $d\theta_{\mathrm{s\ measure}}$ is measured value of optical seeing.

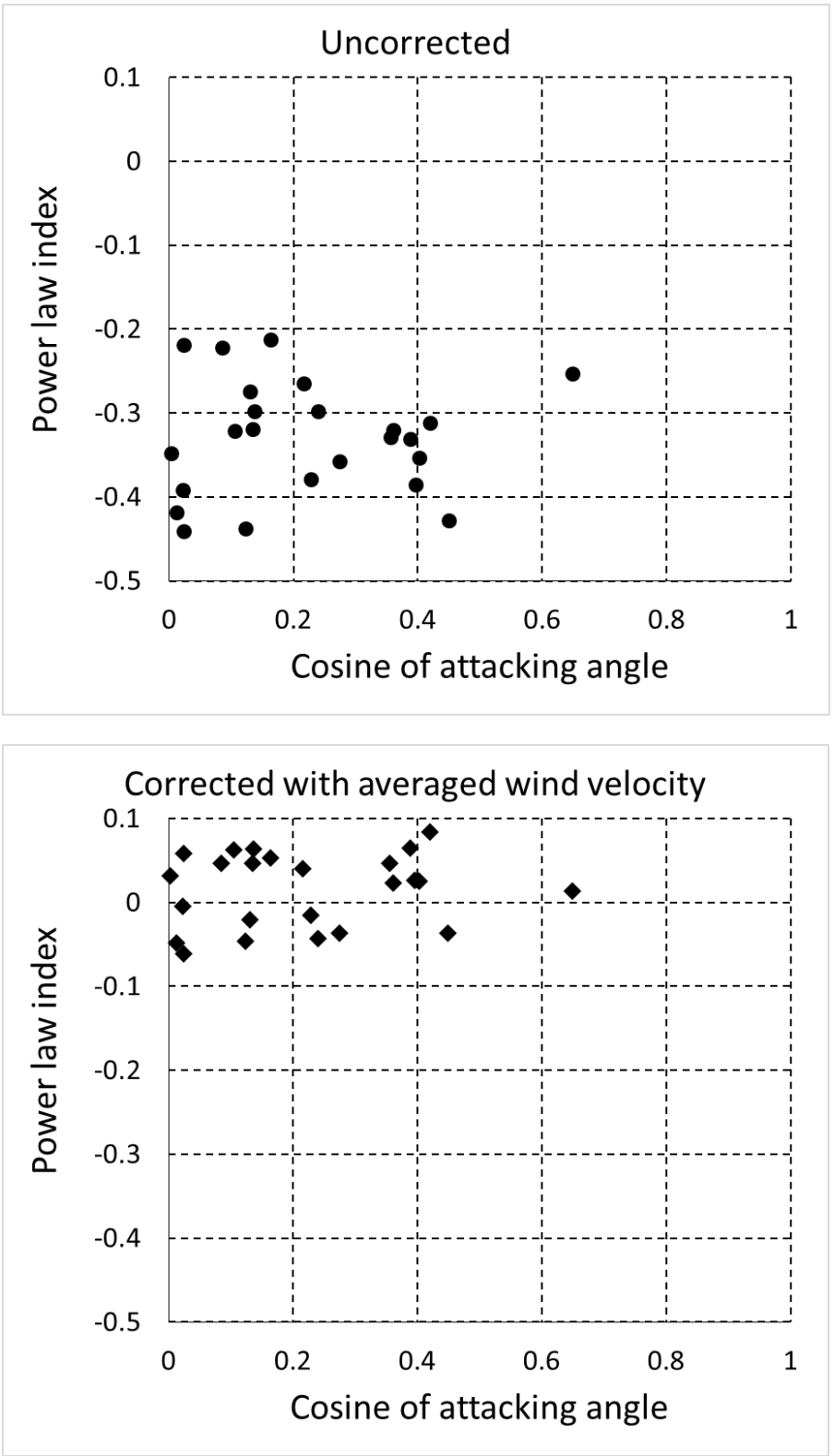

Figure 3-19 Plots of uncorrected power law indices (upper), and corrected power law indices with average wind velocity (lower). The power law indices as a function of the cosine of wind attacking angles.

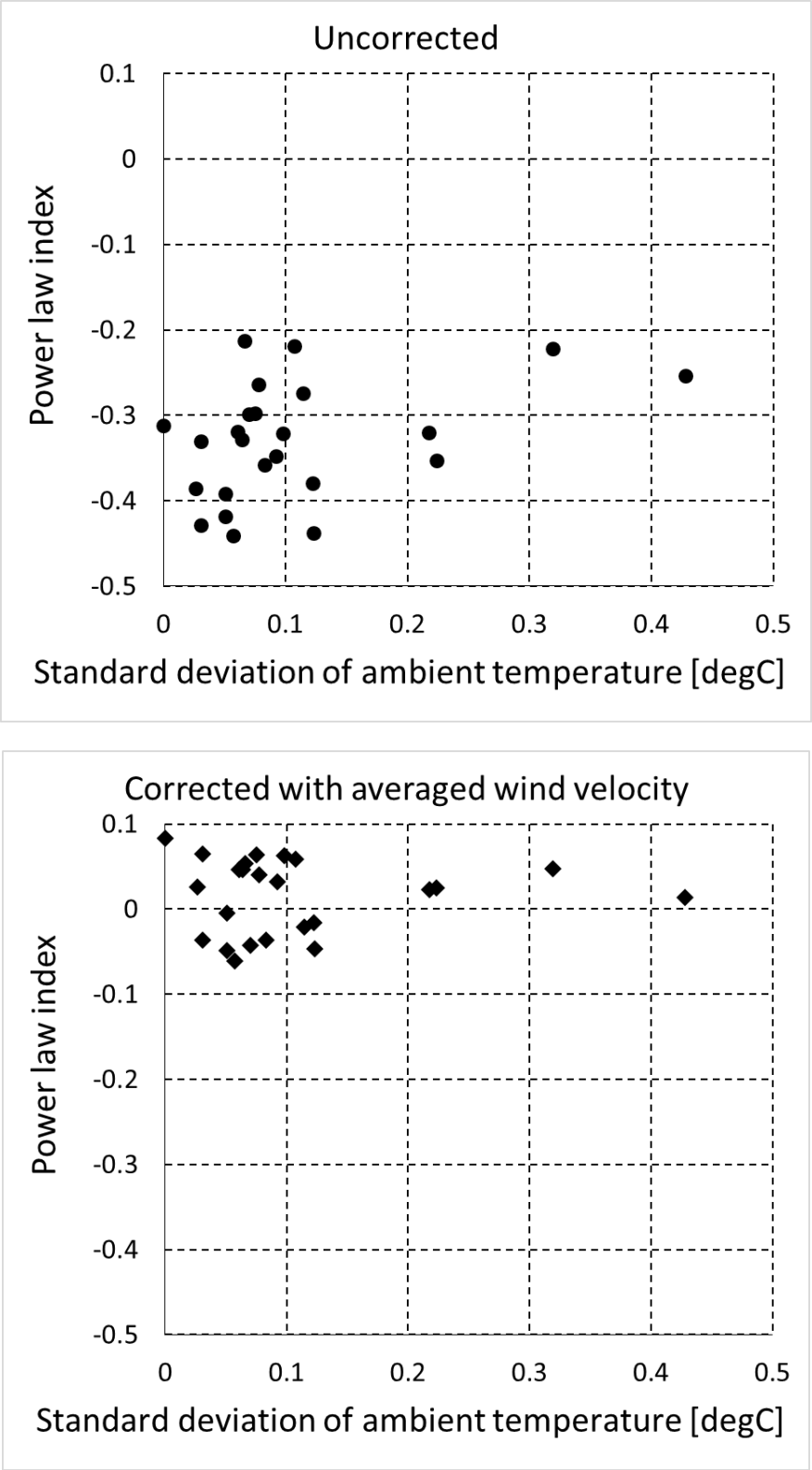

Figure 3-20 Plots of uncorrected power law indices (upper), and corrected power law indices with average wind velocity (lower). The power law indices as a function of the standard deviations of ambient temperature.

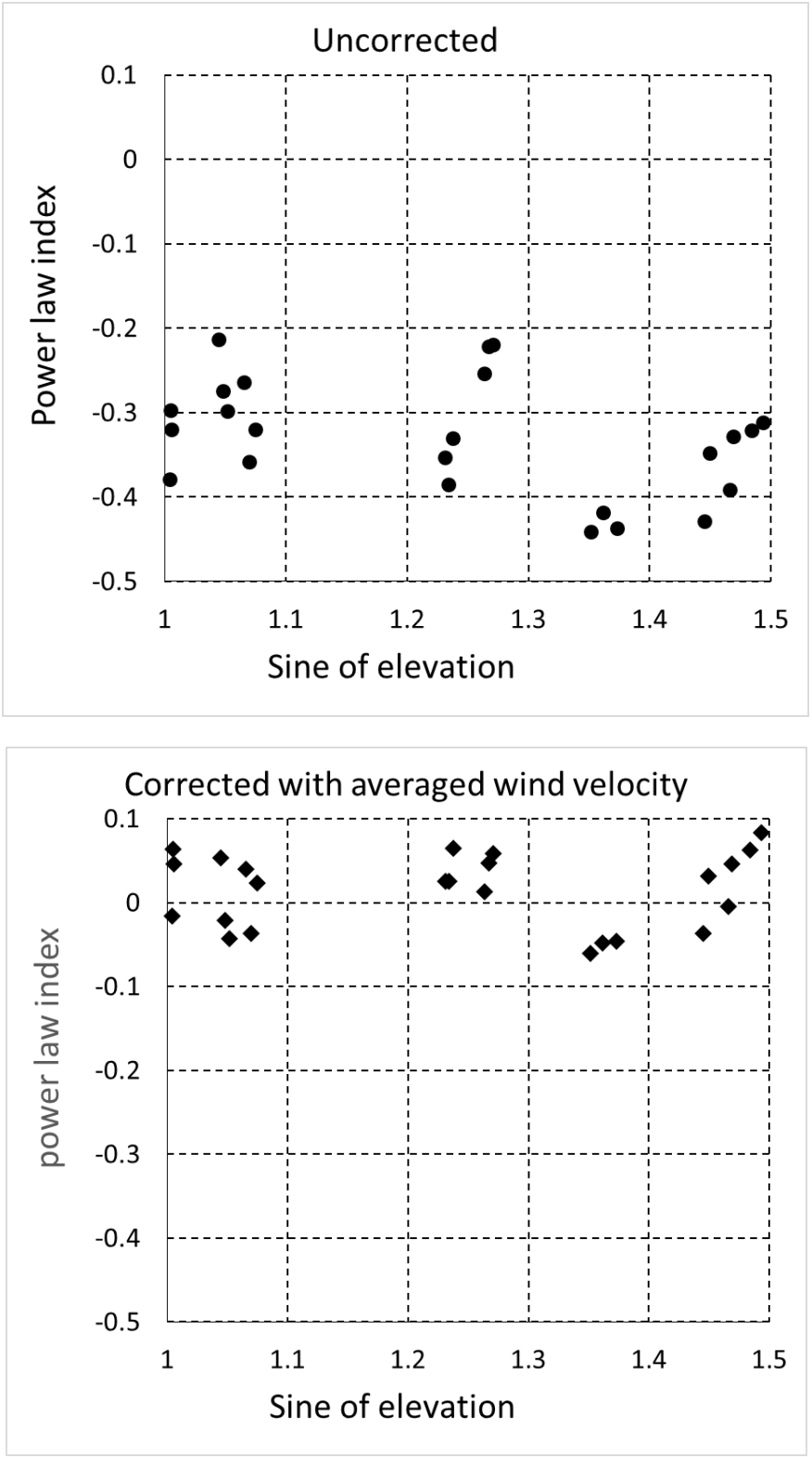

Figure 3-21 Plots of uncorrected power law indices (upper), and corrected power law indices with average wind velocity (lower). The power law indices as a function of the sine of El angle.

4 Investigations of Servo Error in Referencing Pointing Performance

The angles and rotational velocities of the Az and El axes are measured with the angular resolvers and the angular encoders. The antenna control unit (ACU) reads the output of the angular resolvers and the angular encoders. The specifications of the angular resolvers are listed in Table 4-1. The angular resolvers are mounted on the antenna base, which does not move even when driving the antenna. The coils in the angular resolvers generate a voltage proportional to the rotation angle. The angular resolvers measure the Az/El angles by measuring the voltage, and the resolvers-to-digital converters convert the quantity to a digital signal. Meanwhile, the angular encoders measure the angle and the rotational velocities by reading the steel scale mounted on the antenna base by using the sensors mounted on the moving part of the ACA antenna. The Az angular encoder has four sensors, and the El angular encoder has two (see Figure 4-2). In Saito et al. (2012), the angle was measured with the angular resolver, which verified the performance reported by Ukita et al. (2001). The ACU of the ACA antenna has both angular resolvers for measuring the angle itself and angular encoders for measuring the rotational velocity.

As mentioned in Section 2, the RMS of servo error is measured as the RMS of time-variable differences between readout angles measured by the angular resolver connected to the antenna control unit (ACU) and angles commanded by the antenna bus master. The ACU outputs the angle every 900econds (sampling frequency is 20.83 Hz). The angle measured by the angular resolver is affected by the instruments involved in antenna control. Therefore, the servo error includes a torque error due to incomplete suppression of external disturbances and a detection error in the angle resolvers and resolvers-to-digital converter, in addition to an error due to the antenna control by the ACU. If the instruments (For example, the angular encoder) encounter a problem, the reliability of the angle measured with the angular resolver becomes low. However, since the ACU is manufactured by the antenna vendor, the details of the ACU and the specifications of the angular encoders are not available to the public. Therefore, it is important that the ACU be checked by comparing the angle and the rotational velocity with the readout of the angular resolver and the angular encoder connected to the ACU.

In this study, the drive control function of the ACU was checked by measuring the angle as reported by the readout of the angular resolvers during constant velocity rotation. Two measurements were performed: i) In order to check readout angles from the angular resolvers, the time-variable differences between the readout of the angle and an ideal angle were measured over the entire driving range of the Az and El axes during

constant velocity rotation, ii) The RMSs of servo error were measured at various rotation velocities during constant velocity rotation to investigate the contribution of the RMS of servo error to the referencing pointing performance. Ukita et al. (2004) reported that RMS of servo error increases at higher rotational velocities, as seen from the result of the El RMS of servo error when rotating only in the El direction with the ALMA prototype antenna. As in Ukita et al. (2004), both the Az and El RMSs of servo error were measured with the angular resolvers in the present study. The measurement methods are described in Section 4.1. The measurement results are described in Section 4.2. An increase in the RMS of servo error at low rotational velocities (rotational velocity = 0.000005 to 0.00005 deg/s) is discussed in Section 4.3.

Table 4-1 Specifications of the angular resolvers of the ACA antenna.

Parameters	Specification
The angular resolvers	Tamagawa Seiki TS2189N1E1
Resolvers digital converter	Tamagawa Seiki TA3972N11
Angular resolution	25 bit/revolution (0.038 arcsec/LSB)
Angular measuring accuracy	≤ RMS 0.037 arcsec

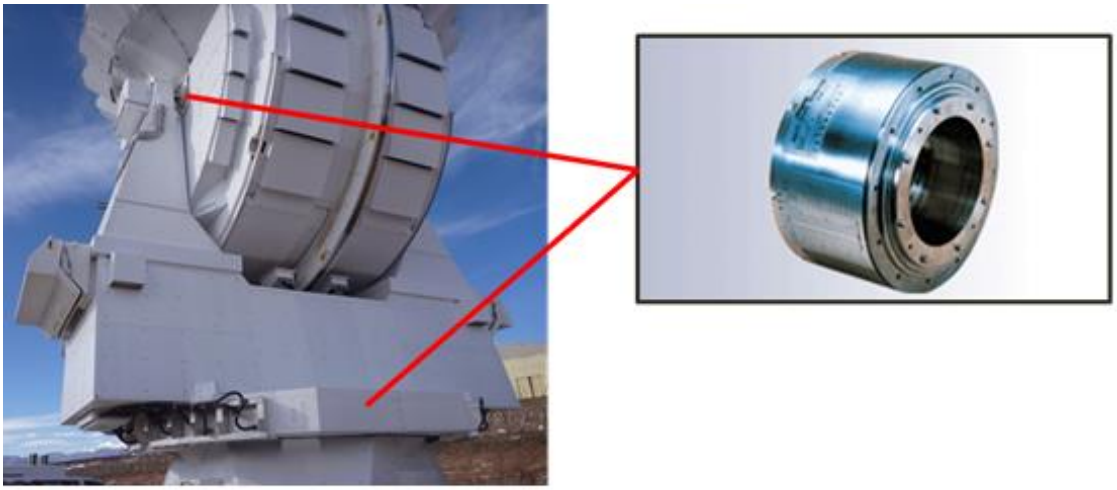

Figure 4-1 Location of the angular resolvers in the ACA antenna (left) and image of the angular resolvers (right).

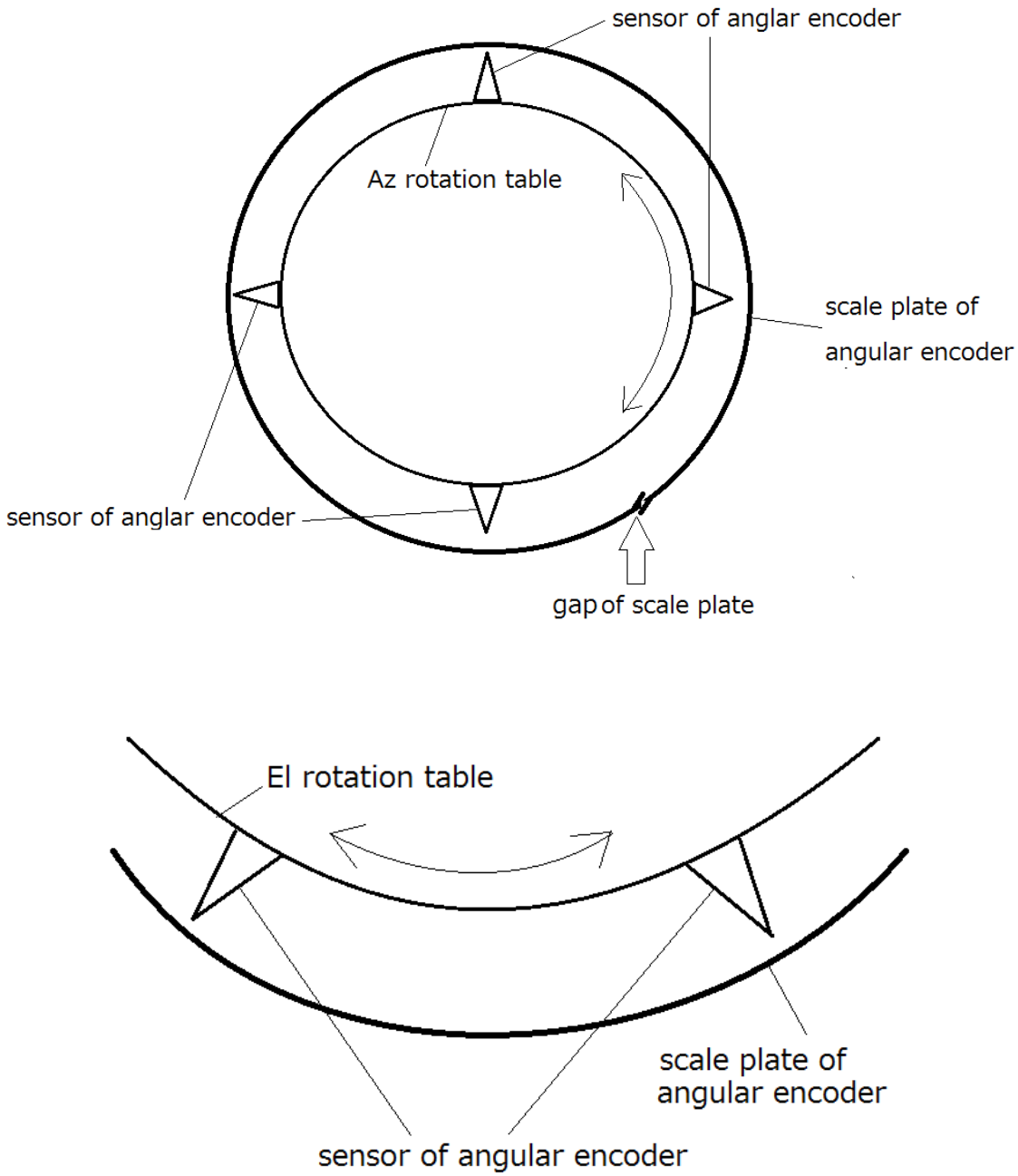

Figure 4-2 Conceptual diagram of the sensors of the angular encoders on the Az axis (upper) and the El axis (lower).

4.1 Measurement Methods for investigating Servo Error

Two measurement methods, ACU checking measurement and servo measurement, are described in this section. An example of the readout data from the ACU is shown in Appendix B.

The purpose of the ACU checking measurement is to check the readout of angles with the angular resolver connected to the ACU by measuring the time-variable differences between readout angles measured by the angular resolver and the ideal angles during constant velocity rotation. The ACA antenna is rotated on only one axis (Az axis or El axis) with a constant rotational velocity of 0.5 deg/s. The ideal angle indicates the predicted arrival angle of the perfect constant velocity rotation from the angle at the start time of the measurement (see Figure 4-3). The rotational range of the Az axis is -200 to 200 deg (0 deg is the North, 90 deg is the East and -90 deg is the West). The rotational range of the El axis is 2 to 88.9 deg (90 deg is a zenith). In this measurement, the time-variable differences between the readout of the angle and the ideal angle are measured from -180 to 180 deg on the Az axis and 8 to 83 deg on the El axis in order to avoid the effect of acceleration of the ACA antenna after the start of the measurement (see Figure 4-3).

The purpose of the servo measurement was to investigate the contribution of the RMS of servo error to the referencing pointing performance. The ACA antenna was rotated around either the Az or El axis with various constant rotational velocities in 210 seconds, and the RMSs of servo error were measured. The rotational velocities on the Az axis are 2, 1, 0.5, 0.2, 0.1, 0.05, 0.02, 0.01, 0.005, 0.002, 0.001, 0.0005, 0.0002, 0.0001, 0.00005, 0.00002, 0.00001, 0.000005, and 0.000002 deg/s. The rotational velocities on the El axis are 0.2, 0.1, 0.05, 0.02, 0.01, 0.005, 0.002, 0.001, 0.0005, 0.0002, 0.0001, 0.00005, 0.00002, 0.00001, 0.000005, and 0.000002 deg/s. In this measurement, the servo errors within five seconds after the start were not used, to avoid any effect of the acceleration of the ACA antenna.

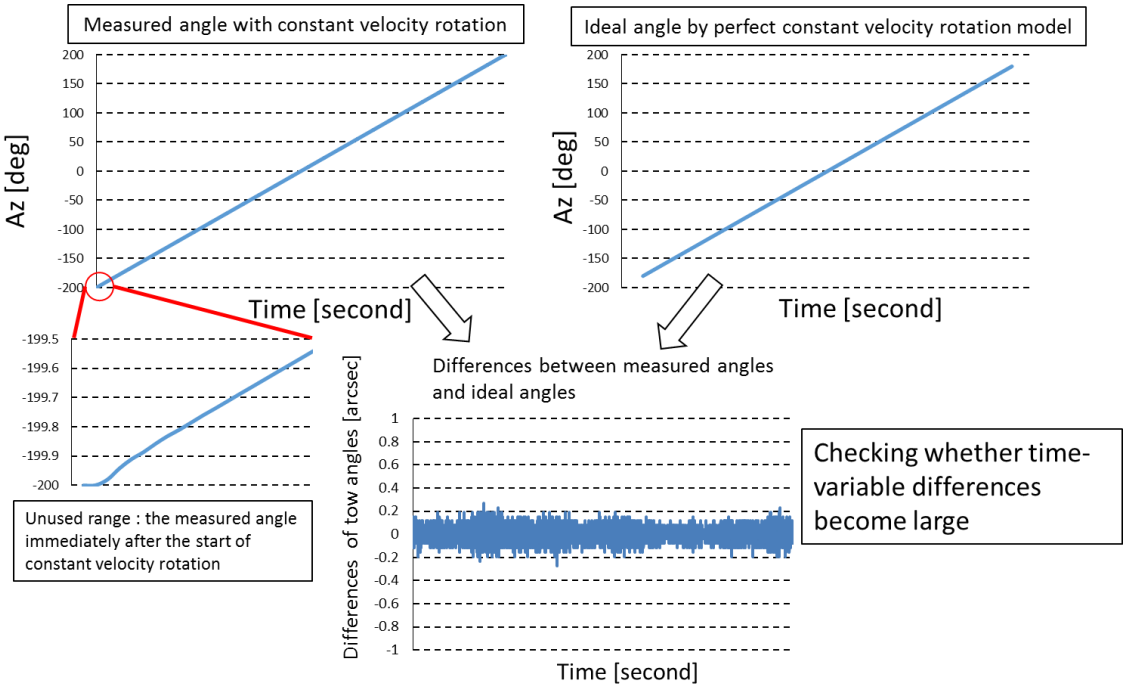

Figure 4-3 Conceptual diagram of the first measurement that checks whether time-variable differences between the readout of the angle and the ideal angle become large.

4.2 Measurement Results for investigating Servo Error

Table 4-2 Summary of the first measurement for checking the ACU when the Az axis rotated (upper) and the El axis rotated (lower).

(1)Date	(2)Start(UT)	(3)Fixed El angle	(4)Wind velocity	(5)RMS of differences			(6)Peak of differences	
				Az	El	Total	Az	El
	[hh:mm]	[deg]	[m/s]	[arcsec]	[arcsec]	[arcsec]	[arcsec]	[arcsec]
2011/12/2	23:51	10.6	3.50	0.09	0.05	0.10	0.36	0.19
2011/12/3	0:24	88.0	1.94	0.08	0.05	0.10	0.33	0.25
2011/12/9	20:14	88.0	3.74	0.08	0.05	0.10	-0.39	0.27

(1)Date	(2)Start(UT)	(3)Fixed Az angle	(4)Wind velocity	(5)RMS of differences			(6)Peak of differences	
				Az	El	Total	Az	El
	[hh:mm]	[deg]	[m/s]	[arcsec]	[arcsec]	[arcsec]	[arcsec]	[arcsec]
2011/12/3	5:42	-200	1.78	0.02	0.20	0.20	-0.09	-0.92
2011/12/9	22:05	60	8.39	0.03	0.17	0.18	-0.12	-0.69
2011/12/9	22:18	150	8.31	0.02	0.18	0.18	0.08	-0.66

The time-variable differences between readout angles with angular resolvers and the ideal angles are shown in Figure 4-4, and Figure 4-5. The summary of the first measurement is listed in Table 4-2. The ACA antenna was rotated around only one axis with a constant rotational velocity of 0.5 deg/s. It was confirmed that no excessive differences were seen over the entire range of angles measured when either the Az axis or the El axis was rotated. From three Az axis rotation measurements, all RMSs of servo error were similar, at approximately 0.1 arcsecs [see column (5) in Table 4-2]. From three measurements when the El axis rotated, all RMSs of servo error were also similar at about 0.18 arcsecs [see column (5) in Table 4-2], even in the presence of a strong wind of 8.3 m/s. Furthermore, it was confirmed that the absolute values of the peak time-variable differences were smaller than one arcsec [see column (6) in Table 4-2]. These results indicate no significant problem in the measurement of angles by the angular resolvers (e.g., the effect of the gap in the steel scale in the angular encoders).

Next, Figure 4-6 shows the RMSs of servo error as a function of rotation velocities from the second measurement. These results confirmed that the RMS of servo

error increases at high rotational velocities (>0.5deg/s when the Az axis rotated, >0.005 deg/s when the El axis rotated). A similar tendency was reported by Ukita et al. (2004) for rotation about the Az axis. The behavior of these RMSs of servo error is described below. The diurnal motion is 0.0042 deg/s, but the maximum rotational velocity of the ACA antenna on the Az axis reaches about 0.2 deg/s at an El angle of 88.9 deg during sidereal tracking. The rotational velocity of the ACA antenna on the Az axis [*V (antenna)*] is proportional to the velocity on the sky [*V (sky)*] and the cosine of the El angle, as given by

$$V(antenna) = V(sky)/cos(El). \qquad (4\text{-}1)$$

RMSs of servo error were better than 0.1 arcsecs at rotation velocities below 0.2 deg/s on the Az axis and 0.0042 deg/s on the El axis (see dashed line in Figure 4-6). These results indicate that the contribution of the RMS of servo error to referencing pointing performance is small.

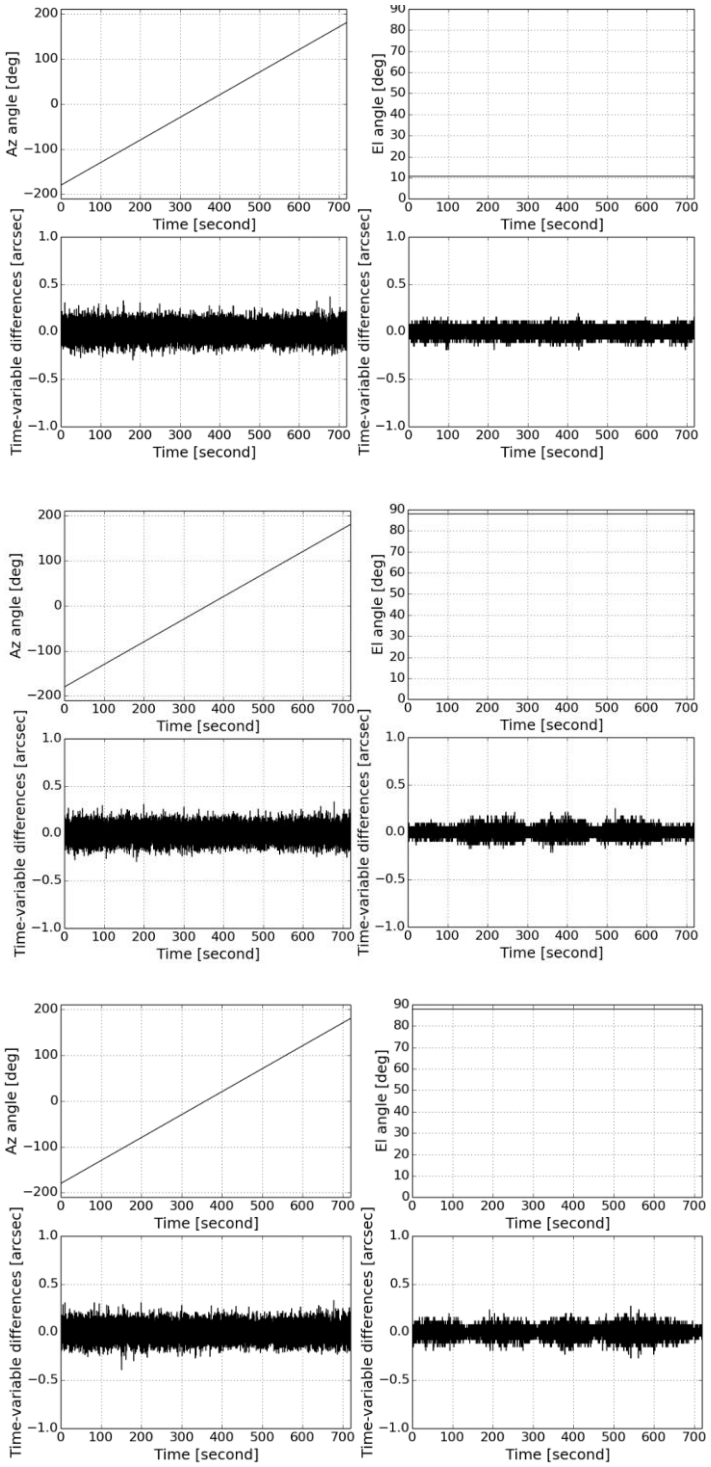

Figure 4-4 Measurement results of the readout of angle and the time-variable differences between the readout of angle and the ideal when the Az axis rotated that are taken at UT 22:51, December, 2, 2011 (upper), UT 0:24, December, 3, 2011 (middle), and UT 20:14, December, 8, 2011 (lower).

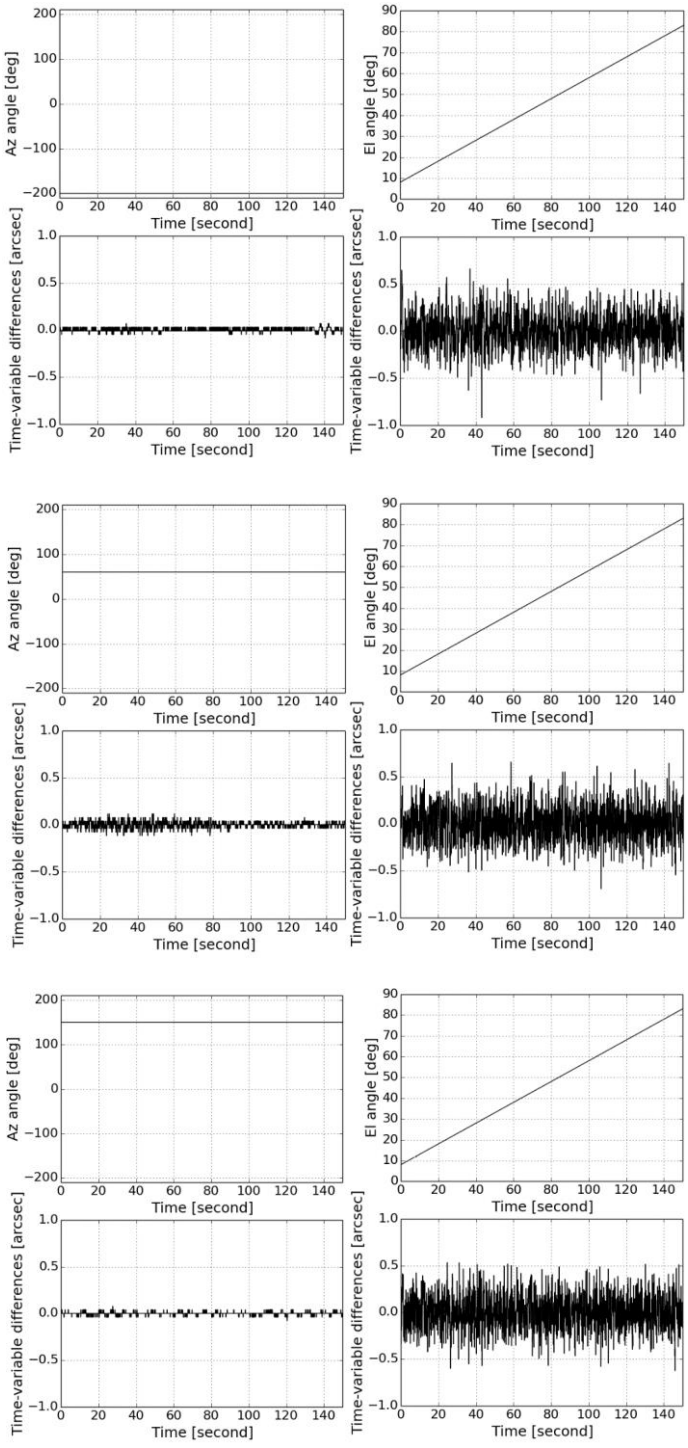

Figure 4-5 Measurement results of the readout of angle and the time-variable differences between the readout of angle and the ideal when the Az axis rotated that are taken at UT 5:42, December, 3, 2011 (upper), UT 22:05, December, 9, 2011 (middle), and UT 22:18, December, 9, 2011 (lower).

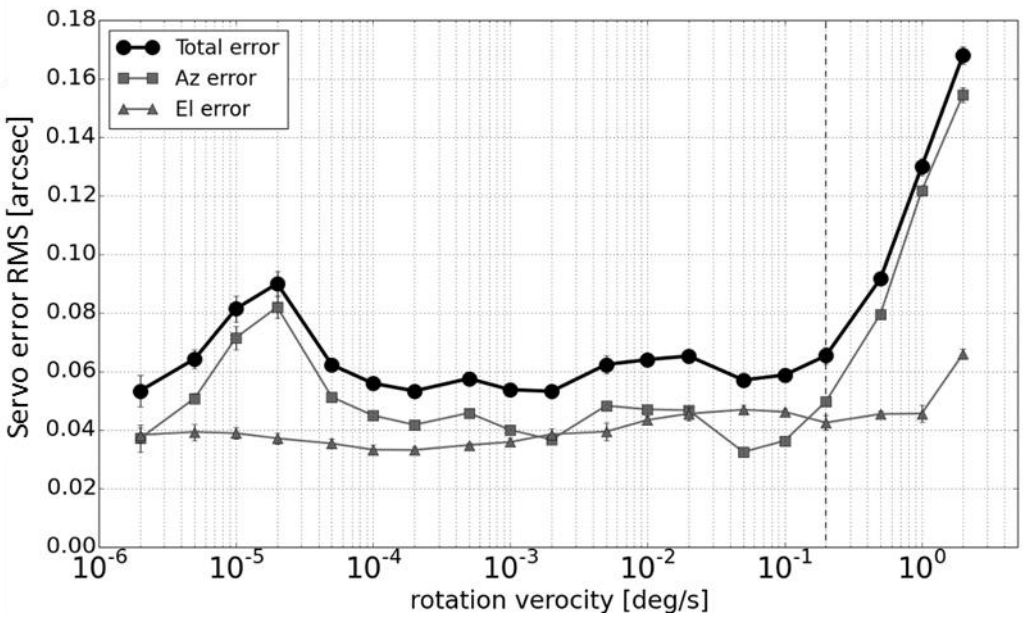

(a) RMS of servo error when Az axis rotated

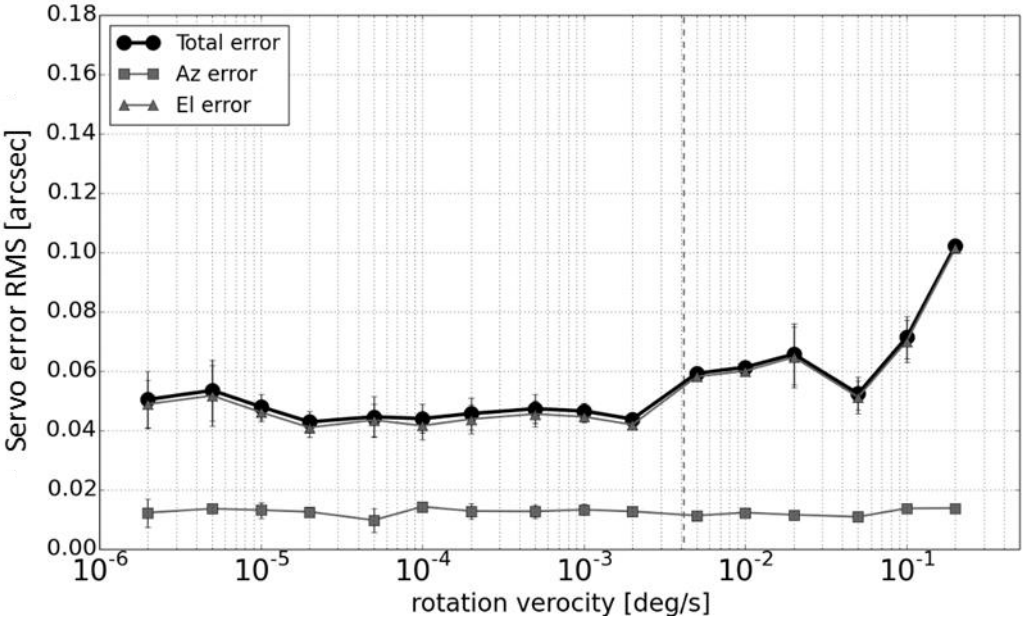

(b) RMS of servo error when El axis rotated

Figure 4-6 RMSs of servo error (Az axis: square, El axis: triangle, total: circle) as a function of rotation velocities taken at UT 1:14, December, 3, 2011 (Upper) and UT 21:11, December (lower), 8, 2011. A dashed line indicates maximum rotation velocities.

4.3 Characteristics of Servo Error at Low Rotation Velocities

RMSs of servo error at low rotation velocities are investigated in this section. From the measurement results of the RMS of servo error when the Az axis was rotated, the RMSs of servo error were about 0.6 arcsecs at rotational velocities of 0.2 to 0.00001 deg/s. However, the RMS of servo error increased to 0.9 arcsecs at low rotational velocities (rotational velocity of 0.000005 to 0.00005 deg/s) (see Figure 4-6). In order to investigate this several fold increase servo error, a Fourier transform was applied to the RMSs of servo error at all rotational velocities. The sampling time of the servo error is 0.048 seconds (sampling frequency is 20.83 Hz). The spectra from the Fourier transform are shown in Figure 4-7, Figure 4-8, and Figure 4-9, showing peaks of about 0.25 to 0.35 Hz at low rotational velocities (rotational velocity = 0.000005 to 0.00005 deg/s) (see Figure 4-6). These peaks differ from an Eigen-frequency of the ACA antenna (about 7 Hz), even considering the effect of aliasing. Furthermore, the frequencies of these peaks change with the rotation velocity. It is considered that these peaks do not originate in the Eigen frequencies of the instruments, and may be caused by oscillation in the control of the ACA antenna by the ACU. However, the RMSs of servo error are still better than 0.1 arcsecs at low rotation velocities. The contribution of the RMS of servo error to the referencing pointing performance is negligible.

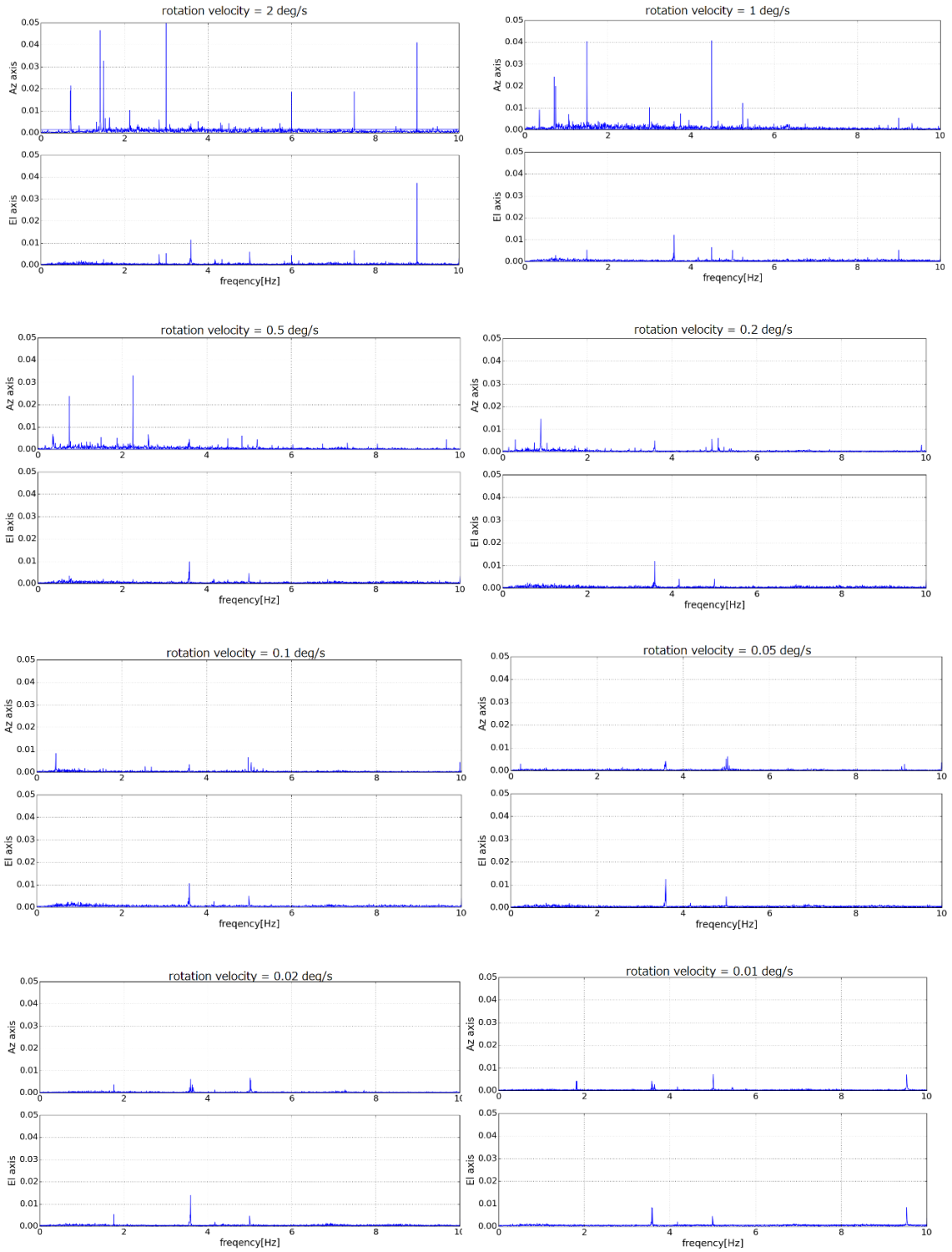

Figure 4-7 Spectra of servo error of Az and El axis by Fourier transform.

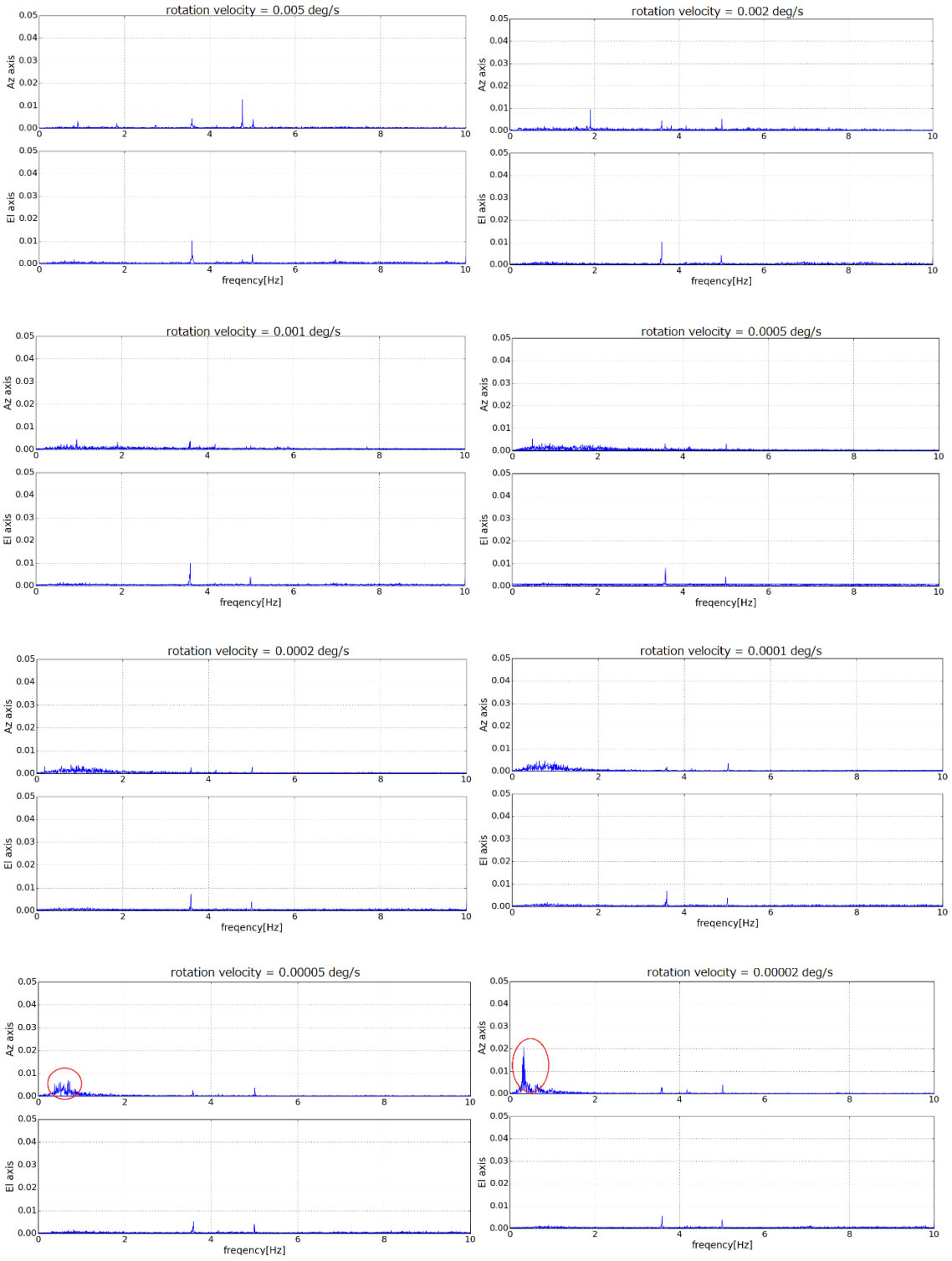

Figure 4-8 Spectra of the servo error of Az and El axis by Fourier transform. Red circles seem to be a factor of increase of servo error shown in Figure 4-6.

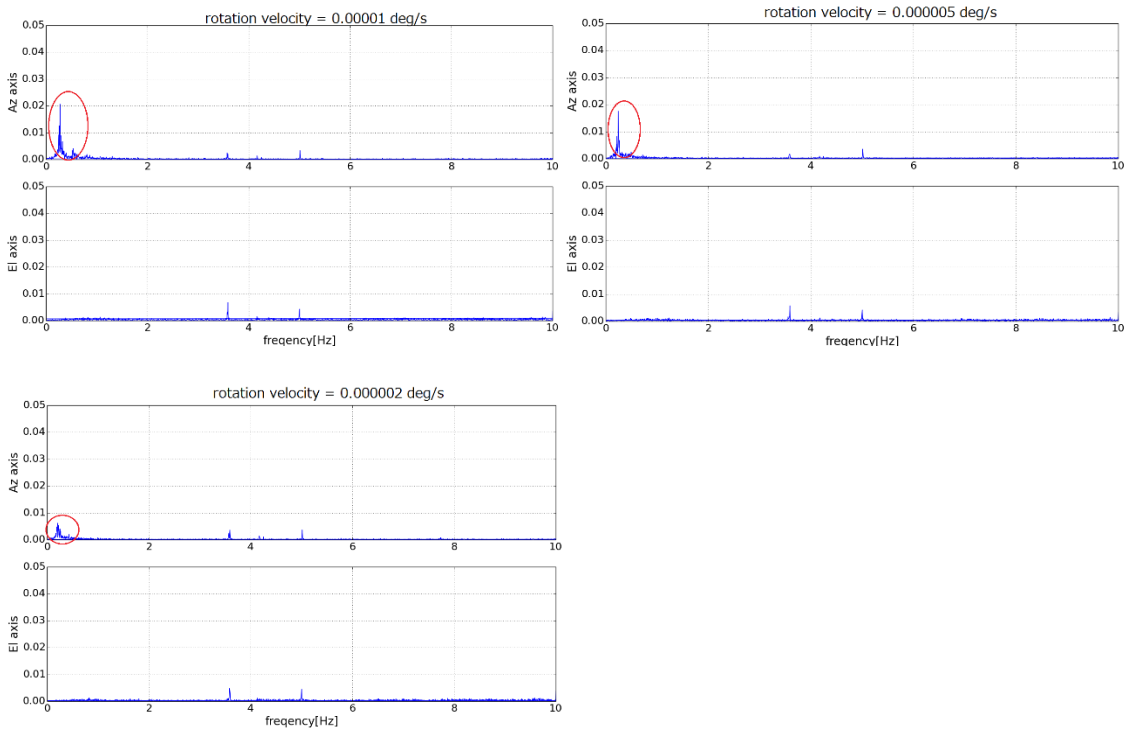

Figure 4-9 Spectra of the servo error of Az and El axis by Fourier transform. Red circles seem to be a factor of increase of servo error shown in Figure 4-6.

5 Az and El Effects on Optical Seeing due to Atmospheric Path Length

As described in Section 2, the measured pointing value includes the referencing pointing performance of the ACA antenna and the pointing error due to optical seeing conditions (hereinafter optical seeing). To estimate the referencing pointing performance of the ACA antenna, the optical seeing correction term must be included in the referencing pointing measurement. Since variations in the optical seeing account for a large portion of the referencing pointing measurement, it is important to estimate the optical seeing component of the results with high accuracy. To measure referencing pointing performance, 3 to 5 stars within a radius of 4 degrees are observed, to reproduce a typical observation in which antennas track a target source and occasionally switch to a calibrator source using fast switching. However, only one star is observed when measuring the optical seeing to avoid the pointing error caused by fast switching. The observing directions Az and El differ when measuring the referencing pointing performance and measuring optical seeing. The optical seeing contribution to referencing pointing performance must be properly calculated from the measurement of the optical seeing because it is determined by observations made in different directions. In Saito et al. (2012), it is assumed that the optical seeing does not depend on the Az angle and depends only on the El angle, due to the atmospheric path length. The assumed El dependence of the optical seeing ($d\theta_s$) is

$$d\theta_s \propto 1/[sin\,(El)]^{0.5}. \qquad (5\text{-}1)$$

The power law index of 0.5 is explained by the random walk of light as it passes through the atmosphere [27]. The light from a star is refracted in random directions by air parcels with different refractive indices, which are mainly caused by differences in temperature, pressure, or moisture content. This process can be mathematically modeled as a random walk. The refracted light distorts the image of the star in the Optical Pointing Telescope (OPT). The optical seeing is measured by the root mean square (RMS) of the centroid positions of a star in the image formed by the OPT. In the case of an n-step random walk through the atmosphere, the optical seeing is proportional to $\sqrt{n}$, which is the RMS of the centroid position of the star's image as formed by refracted light after such a random walk. This dependence can also be derived from the Kolmogorov model of turbulence (see Appendix A). In Saito et al. (2012), the difference between the optical seeing ($d\theta_s$) at different El angles is corrected by the following

equation.

$$d\theta_{\mathrm{s}} = d\theta_{\mathrm{s0}} \times \frac{[sin(El_{\mathrm{seeing}})]^{0.5}}{[sin(El_{\mathrm{pointing}})]^{0.5}} \qquad (5\text{-}2)$$

where $d\theta_{\mathrm{s0}}$ is the result of the raw measurement of the optical seeing, El_{seeing} is the El angle of the star when the optical seeing is measured, and El_{pointing} is the El angle of the star used in the measurement of the referencing pointing performance. Although this correction method is used for the verification of the referencing pointing of the ACA antenna, the El dependence and the Az dependence of the optical seeing have never been verified at the Operations Support Facility (OSF).

In this study, the El dependence and the Az dependence were verified by measuring the optical seeing at various El angles and Az angles with the OPT mounted on the ACA 7-m antenna at the OSF. The measurement method is described in Section 5.1. The measurements and what they reveal about El dependence are explained in Section 5.2, and the Az dependence is discussed in Section 5.3.

5.1 Measurement Method for Optical Seeing related to Atmospheric Path Length

The measurement method used in this study to determine the required the optical seeing correction is described. The optical seeing in different directions was measured by the RMS of centroid positions of stars in an image from the OPT (hereinafter RMS of centroid positions). The RMSs of centroid positions were measured for 120 stars from Az -200 to 200 degrees, and El 20 to 90 degrees (see Figure 5-1). In order to reduce the effect of changing conditions in the atmosphere, each star was tracked for only ten seconds. The total measurement time was 25 minutes. The OPT obtains images with an integration time of 1/30 seconds, and the centroid positions of images are integrated for one second. The RMSs of centroid positions are estimated by the RMS of five integrated centroid positions for the final five seconds of the ten-second tracking to avoid any effect of the pointing error caused by switching. Since the tracking time of each star is very short, the effect of the pointing error caused by tracking is very small. Therefore, the measured RMSs of centroid positions are attributed only to the optical seeing conditions. The measurements were performed at UT 1:53, June 11, 2012, and UT 7:22, June 11, 2012.

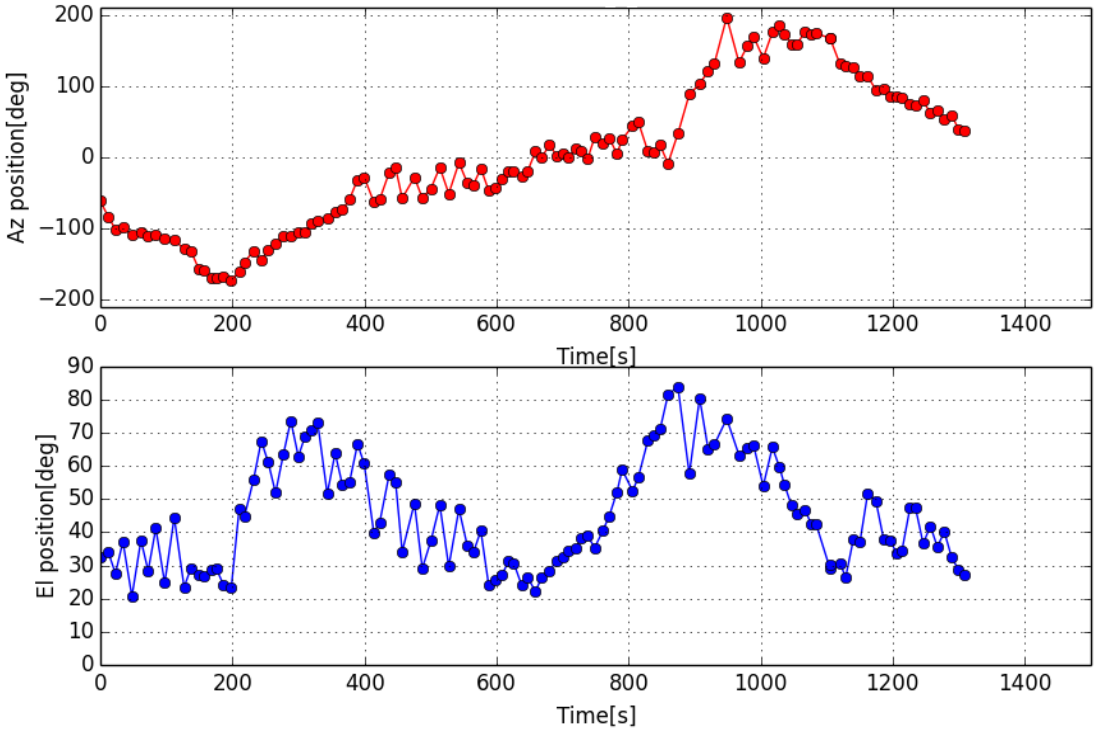

Figure 5-1 Az and El angles in the optical seeing measurement.

5.2 El Dependence of Optical Seeing on Atmospheric Path Length

The El-related dependence of the optical seeing (RMS of centroid positions) as measured is derived as follows. The RMSs of centroid positions and the sine of their El angles are shown in Figure 5-2. The El dependence of the RMS of centroid positions is calculated in the fitting by assuming $d\theta_s \propto sin\ (El)^{\alpha}$ (power law index α is a free parameter). The fitting result for the measurement taken at UT 1:53, June 11, 2012, is

$$d\theta_s \propto 1/[sin(El)]^{0.58\pm0.09}. \quad (5\text{-}3)$$

The fitting result for the measurement taken at UT 7:22, June 11, 2012, is

$$d\theta_s \propto 1/[sin(El)]^{0.48\pm0.07}. \quad (5\text{-}4)$$

The two measurement results of power law index of the optical seeing corresponding to theoretically predict of 0.5 [see equation (5-1)]. Consequently, the El dependence of $d\theta_s \propto sin\ (El)^{-0.5}$ is valid for verification of the referencing pointing measurement at the OSF.

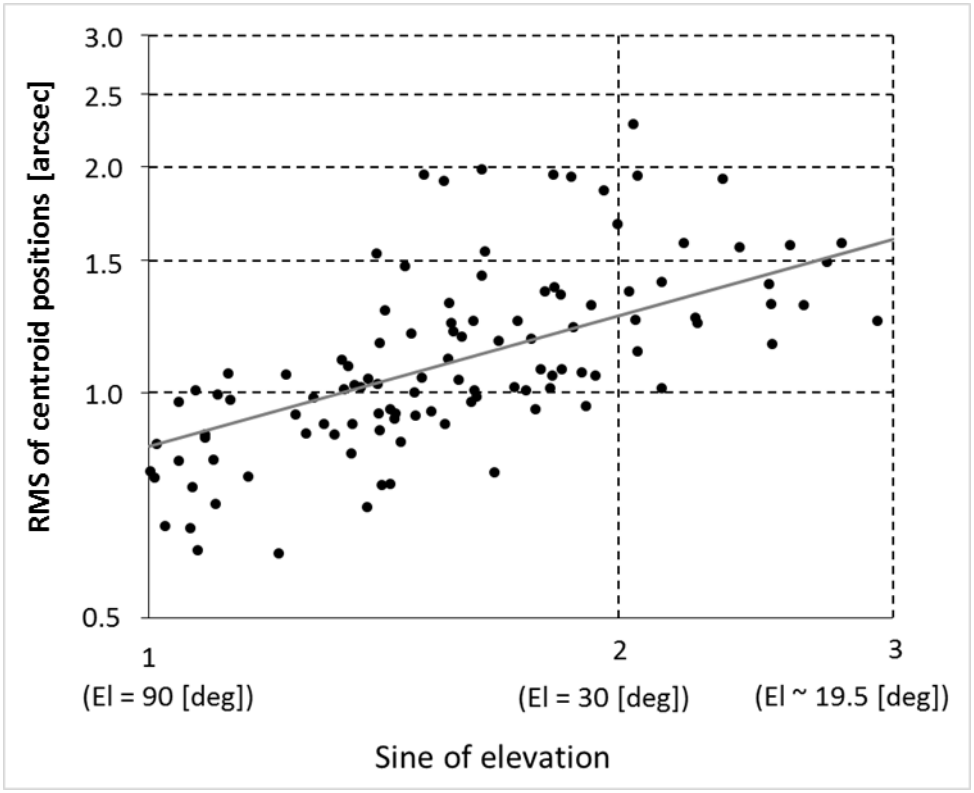

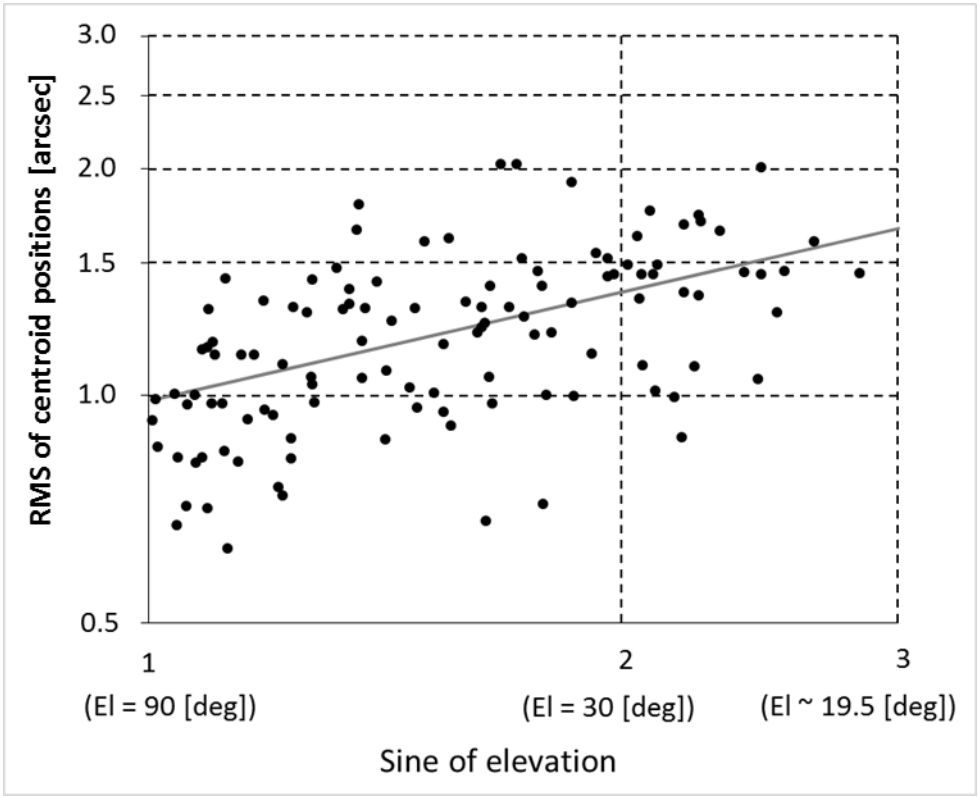

Figure 5-2 The RMSs of centroid positions with sin (El) taken at UT 1:53, June 11, 2012 (upper) and UT 7:22, June 11, 2012 (lower).

5.3 Az Dependence of Optical Seeing due to Atmospheric Path Length

Determining the Az dependence of the optical seeing correction for RMS of centroid positions from measurements is explained as follows. The RMSs of centroid positions with Az angles are shown in Figure 5-3. These two figures show the common characteristic of an apparent increase in their RMS of centroid positions in the Az angle region of -50 to 50 deg. However, these RMSs of centroid positions include El dependence, and this characteristic may be due to the low El angles of the measurements (20 to 30 deg) [see Figure 5-1]. Therefore, the RMSs of centroid positions must are corrected for the El dependence in order to quantitatively verify the Az dependence. A comparison of the parameters of the uncorrected RMSs of centroid positions and the RMSs of centroid positions corrected for the El angle are shown in Table 5-1, and Table 5-2. These tables show that no parameters are significantly changed by correction for El angle dependence. Plots of the uncorrected RMSs of centroid positions and the RMSs of centroid positions corrected for the El angle are shown in Figure 5-4, and Figure 5-5. In these figures, the El-angle-corrected RMSs of centroid positions, taken at UT 1:53, June 11, 2012 increase in the region of -50 to 50 deg, as in Figure 5-3. On the other hand, the El-angle-corrected RMSs of centroid positions taken at UT 7:22, June 11, 2012, do not increase in the region of -50 to 50 deg [see red circle in Figure 5-6]. The correction for El angle dependence makes the common characteristics of the two measurement results become less prominent. It is considered that the RMSs of centroid positions do not depend on the Az angle at the OSF.

Table 5-1 Comparison of parameters between uncorrected RMSs of centroid positions and corrected RMSs of centroid positions with elevation taken at UT 1:53, June 11, 2012.

Parameters	Uncorrected	Corrected with elevation
Average	1.15	0.89
Maximum	2.29	1.58
Minimum	0.61	0.55
Standard deviation	0.34	0.21
Peak to peak	1.68	1.03

Table 5-2 Comparison of parameters between uncorrected RMSs of centroid positions and corrected RMSs of centroid positions with elevation taken at UT 7:22, June 11, 2012.

Parameters	Uncorrected	Corrected with elevation
Average	1.22	0.96
Maximum	2.03	1.54
Minimum	0.63	0.53
Standard deviation	0.31	0.21
Peak to peak	1.40	1.02

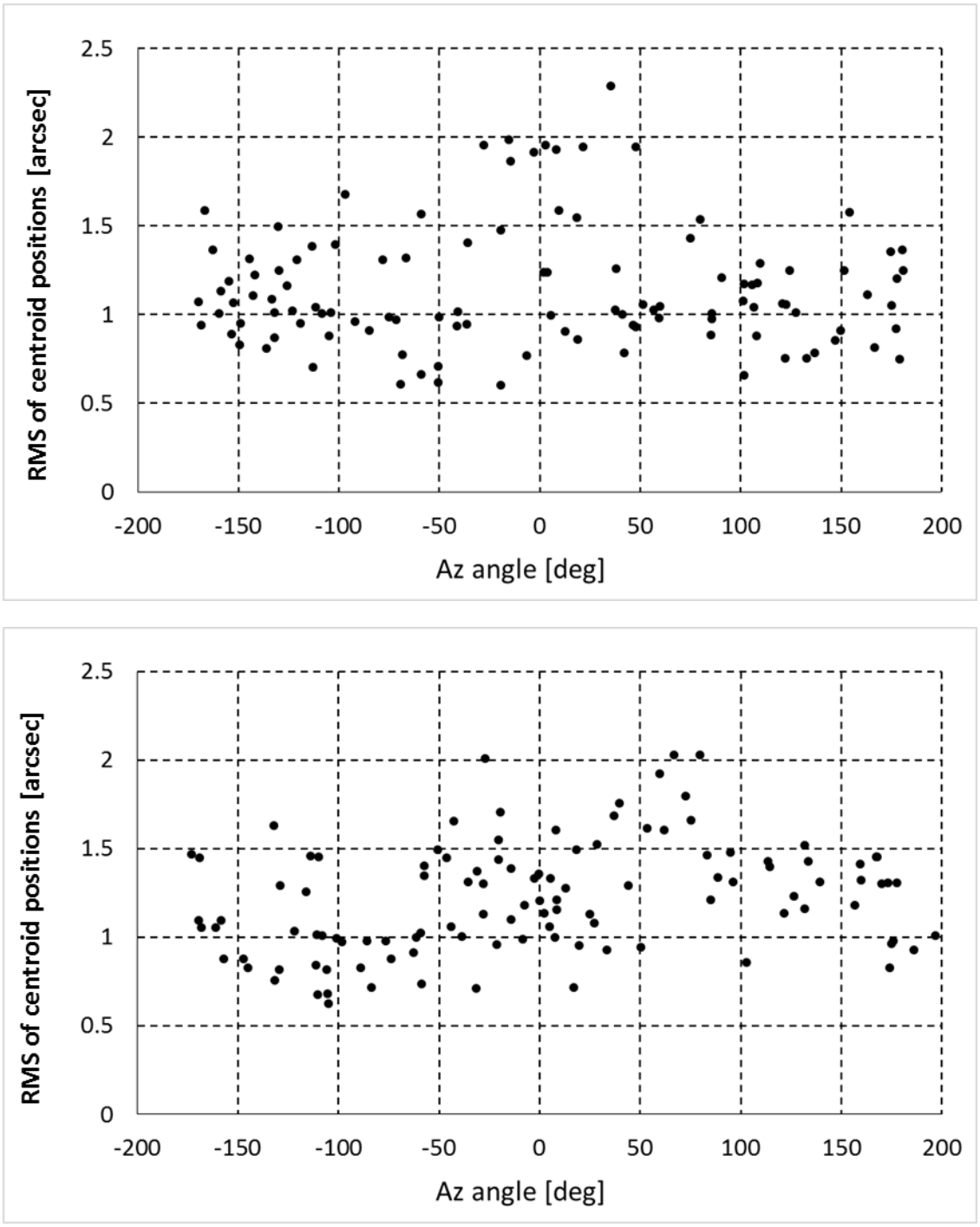

Figure 5-3 RMSs of centroid positions with Az angle taken at UT 1:53, June 11, 2012 (upper) and UT 7:22, June 11, 2012 (lower).

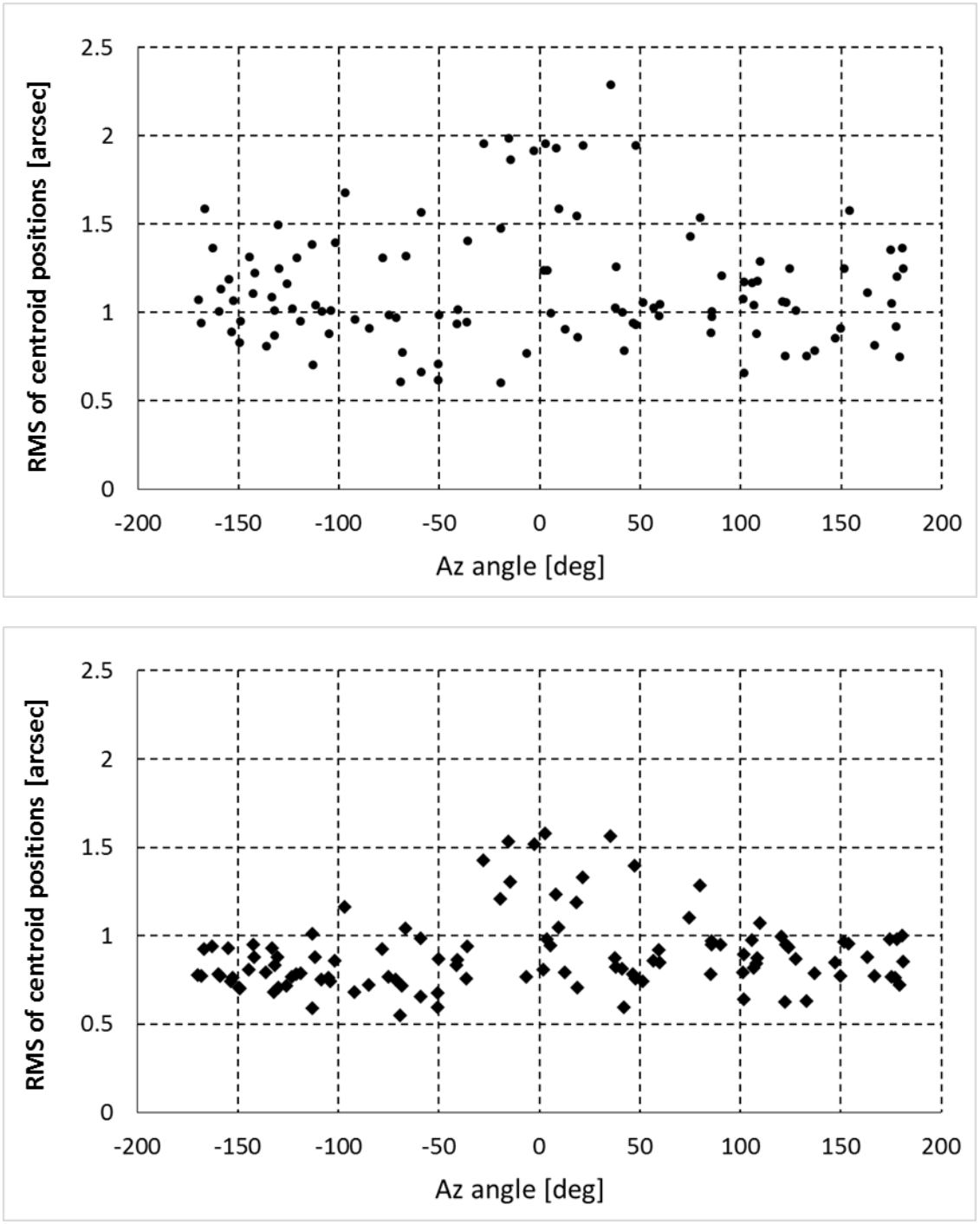

Figure 5-4 Plots of uncorrected RMS of centroid positions with Az angle (upper), and corrected RMS of centroid positions by El dependence with Az angle (lower). The RMSs of centroid positions with Az angle taken at UT 1:53, June 11, 2012.

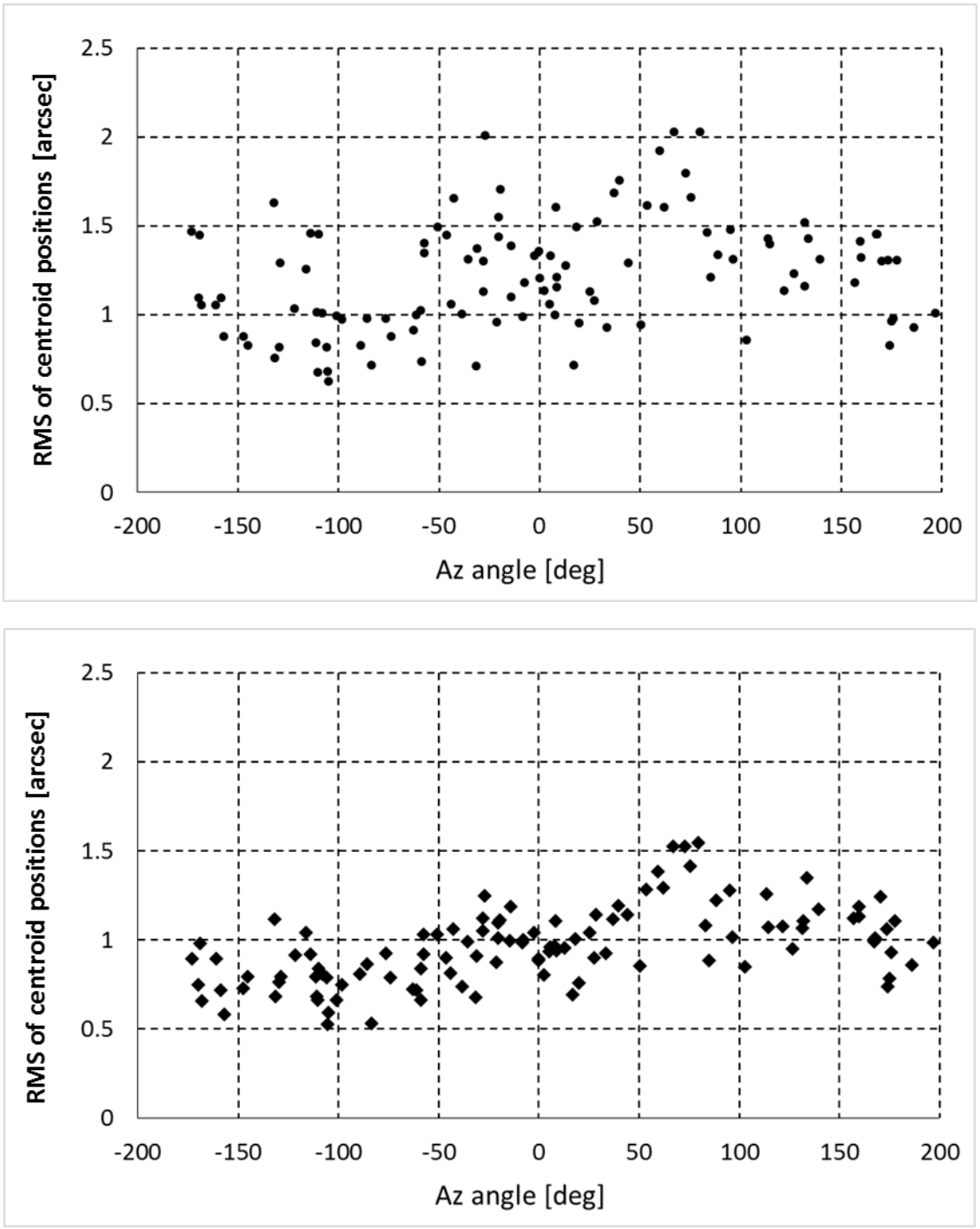

Figure 5-5 Plots of uncorrected RMS of centroid positions with Az angle (upper), and corrected RMS of centroid positions by El dependence with Az angle (lower). The RMSs of centroid positions with Az angle taken at UT 7:22, June 11, 2012.

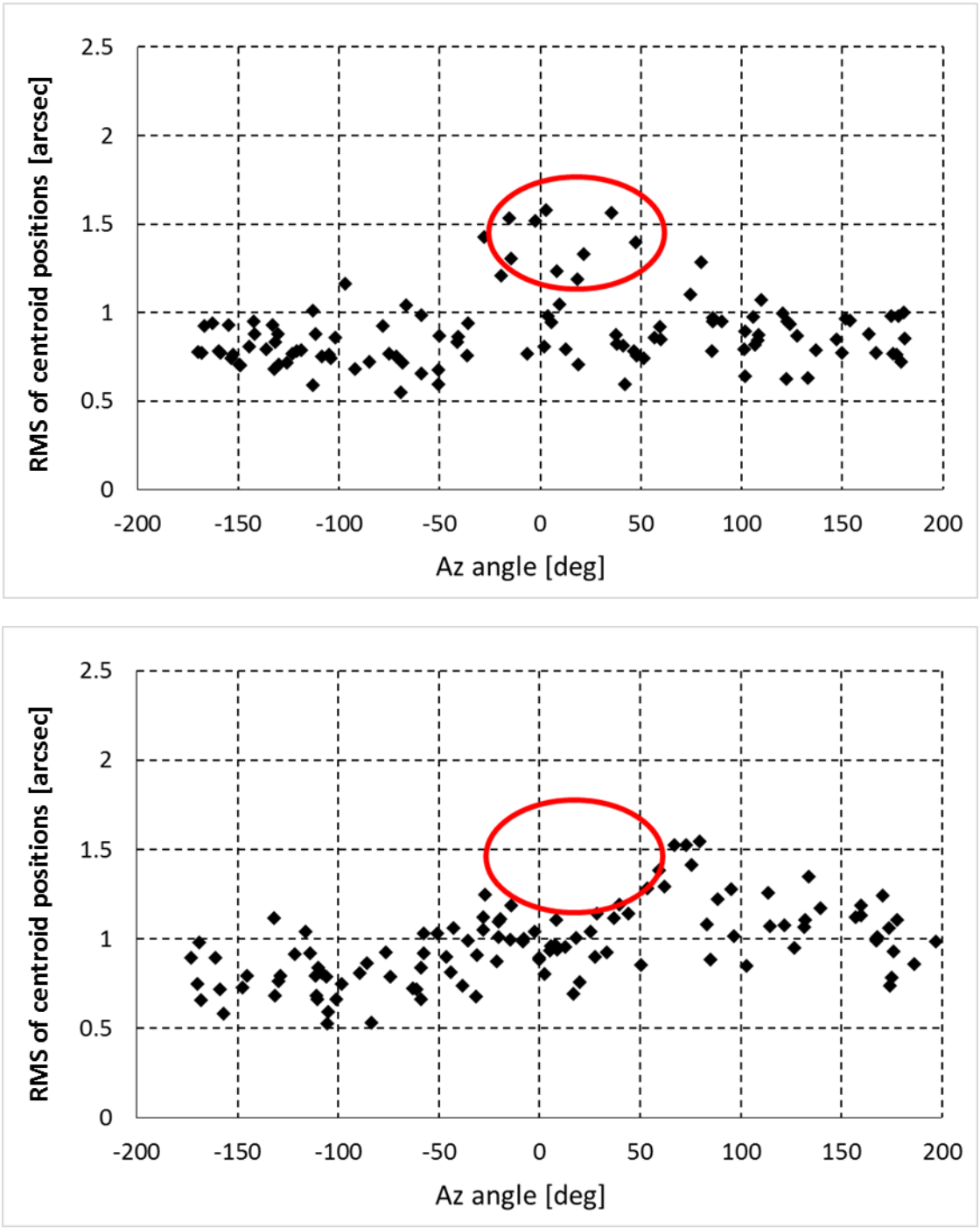

Figure 5-6 Comparison of plots of two measurement results. The corrected RMS of centroid positions by El dependence with Az angle taken at UT 1:53, June 11, 2012 (upper) and UT 7:22, June 11, 2012 (lower).

6 Pointing Performance during Settling Time after Fast Switching

The pointing performance during the settling time after fast switching from one source to another is very important. In actual astronomical observations, the ALMA antennas switch quickly between a target source and a calibrator source (typically within 4 degrees for ACA antennas) [17]. This fast switching is expected to be effective for calibrating the phase of atmospheric phase fluctuation [31]. The ALMA antenna must settle down to shorten the dead time after fast switching so as to allow the observation of a target source and a calibrator source as close to simultaneously as possible.

There are two technical specifications for the ACA 7-m antenna for the pointing performance that involve the settling time after fast switching under the primary operating conditions (Table 1-1). i) The instantaneous pointing offset must be settled down to better than 3.0 arcsecs within 1.9 seconds after a switching of 1.5 degrees on the sky [8]. This technical specification requires that a star enters the field of view of the ALMA antennas (6.6 arcsecs for 12-m antenna with an observing frequency of 950GHz) within 1.9 seconds after switching. ii) The pointing performance is required to be better than 0.6 arcsecs RMS in the period from 2.4 to 4.4 seconds after switching 1.5 degrees on the sky [8]. This technical specification requires that the pointing performance must be better than 0.6 arcsecs RMS (technical specification of the ALMA) within 4.4 seconds after switching.

In this study, the pointing performance in terms of the settling time after fast switching to three directions for the ALMA ACA 7-m antennas was verified. The measurement method is shown in Section 6.1. The measured results of the pointing performance with respect to settling time after fast switching for three directions are shown in Section 6.2. The verification of the directional characteristics of the pointing performance with respect to the settling time after fast switching to eight directions is shown in Section 6.3.

6.1 Measuring Pointing Performance during Settling Time after Fast Switching

The measurement of the pointing performance during the settling time after fast switching is explained. The ACA 7-m antenna is commanded to switch between two positions separated by 1.5 degrees on the sky cyclically every 10 seconds. The switching directions are 270 degrees (Az only), 0 degrees (El only), and 45 degrees (both Az and El) (see Figure 6-1). The measurement is performed at 18 positions in the sky: for Az 0 to 360 degrees in steps of 60 degrees, and for El 30 to 60 degrees in steps of 15 degrees. Measurements were taken 30 times for the three directions at each Az/El position.

The pointing performance during the settling time after fast switching is verified by the measured servo error, which is the time-variable difference between the readout angle and the commanded angle, as taken with the angular encoders and the angular resolvers, respectively. Since the ACA 7-m antenna is settled down after fast switching by its servo system, it is important that the pointing performance be verified by the servo error with the angular encoders as the first step of pointing verification. The first technical specification of the pointing performance during the settling time after fast switching is verified by measuring the peak difference between the readout angle and the commanded angle (hereinafter: peak servo error) in the interval from 1.9 to 2.4 seconds after switching. The second technical specification of the pointing performance during the settling time after fast switching is verified by measuring the root mean square (RMS) of the difference between the readout angle and the commanded angle (hereinafter: RMS servo error) in the interval from 2.4 to 4.4 seconds after switching. Examples of time series plots of measured servo error with the angular resolvers are shown in Figure 6-2.

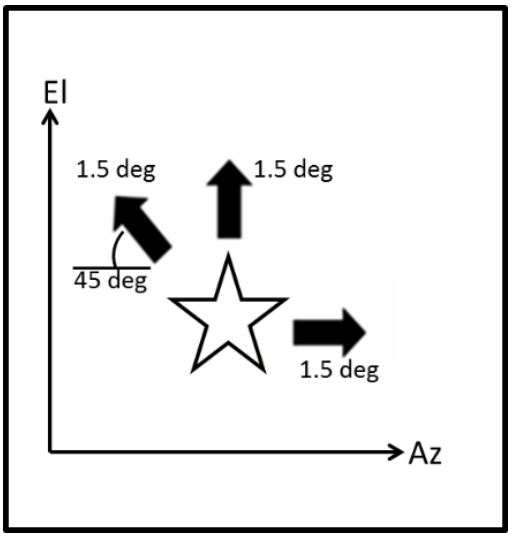

Figure 6-1 Switching directions of the measurements.

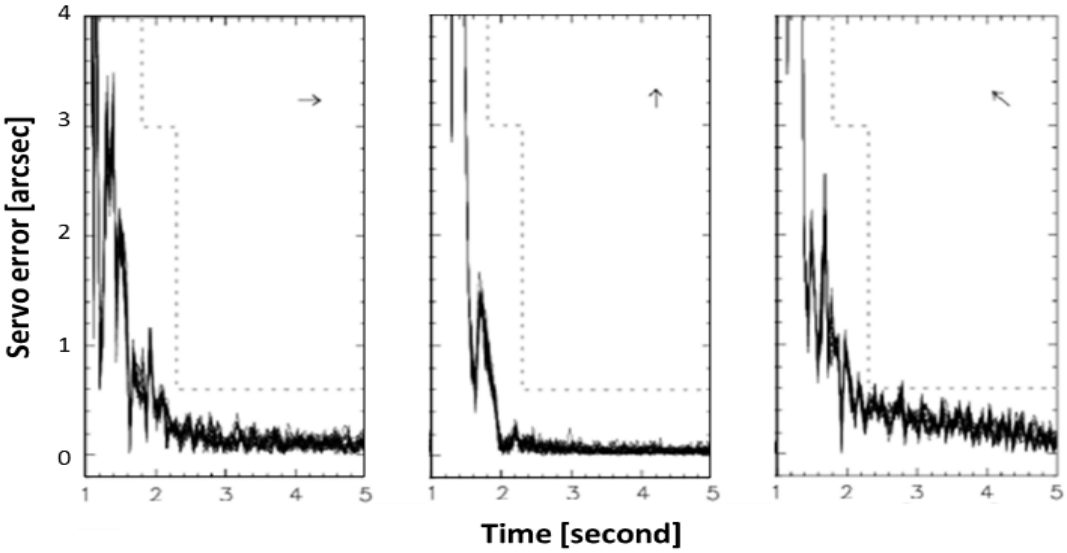

(a) Switching to 270 deg (Az only)

(b) Switching to 0 deg (El only)

(c) Switching to 45 deg (both Az and El)

Figure 6-2 Examples of the measured servo errors from 30 runs of fast switching in different directions. Fast switching directions are indicated as arrows: (a) pure Az, (b) pure El, and (c) both Az and El. Dashed lines represent technical specifications of fast switching for the ACA 7-m antenna.

6.2 Measurement of Pointing Performance during Settling Time after Fast Switching

The measurement of the pointing performance during the settling time after fast switching was performed with the ACA 7-m antenna No. 12. Figure 6-3 shows a histogram of the peak servo errors in the interval from 1.9 to 2.4 seconds after switching. All the peak servo errors settle down to 3.0 arcsecs at 1.9 seconds after switching. Figure 6-4 shows a histogram of times soon after switching in which the peak servo error did not exceed 3.0 arcsecs. In all measurements, the peak servo errors are less than 3.0 arcsecs just 1.9 seconds after switching. These histograms clearly show that the ACA 7-m antenna No. 12 settled down to 3.0 arcsecs in 1.9 to 2.4 seconds after switching in all measurements performed.

Figure 6-5 shows a histogram of the RMS servo errors in the period from 2.4 to 4.4 seconds after fast switching. All the RMS servo errors are much better than the technical specification of 0.6 arcsecs RMS in the period from 2.4 to 4.4 seconds. These verification tests confirmed that the pointing performance during the settling time after fast switching of the ACA 7-m antenna No. 12 meet the technical specification of the ALMA.

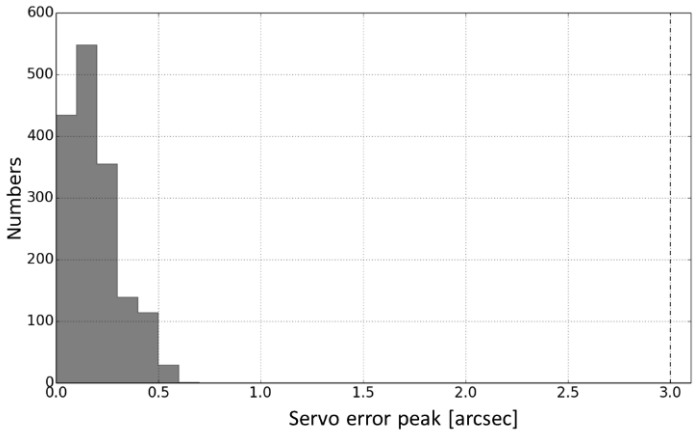

Figure 6-3 Histogram of peak servo error in 1.9 seconds after starting switch of the ACA 7-m antenna No. 12.

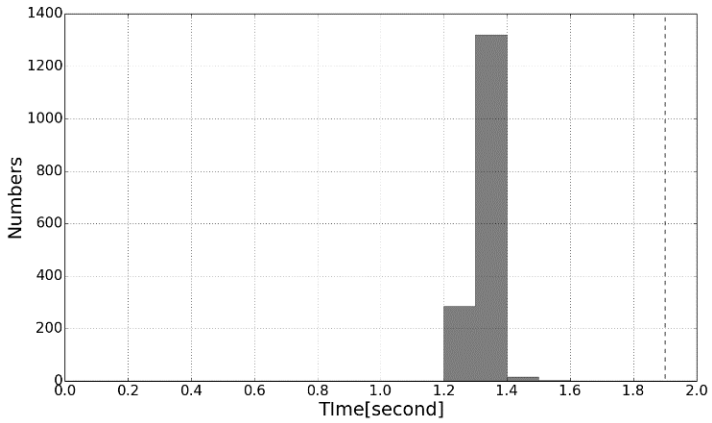

Figure 6-4 Histogram of times for peak servo error not exceeding 3 arcsecs from after start fast switching of the ACA 7-m antenna No. 12.

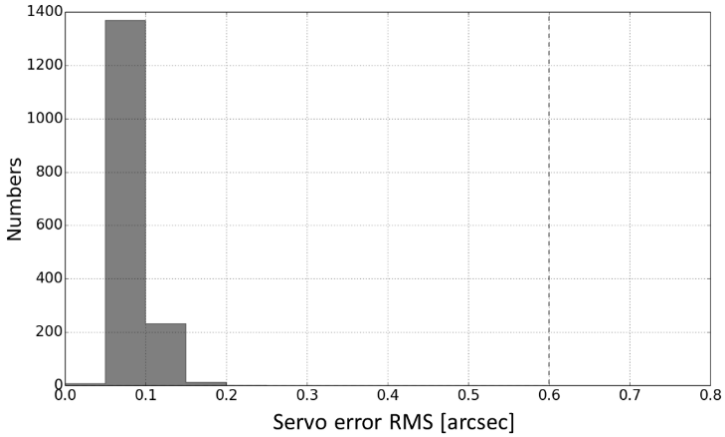

Figure 6-5 Histogram of the RMS servo errors in the period from 2.4 to 4.4 seconds after start fast switching of the ACA 7-m antenna No. 12.

6.3 Directional Dependence of Pointing Performance during Settling Time after Fast Switching

Table 6-1 Peak servo error and the RMS servo error or eight directions around star.

Angle [deg]	Peak servo error in 1.9 seconds after switching [arcsec]	RMS servo errors in the a period from 2.4 and 4.4 seconds after switching [arcsec]
0 (positive El)	0.37	0.046
45	0.53	0.064
90 (positive Az)	0.36	0.049
135	0.65	0.052
180 (negative El)	0.53	0.051
225	0.41	0.061
270 (negative Az)	0.50	0.056
315	0.44	0.045

The directional characteristics of the pointing performance during the settling time after fast switching must also be examined by switching to various directions. In actual astronomical observations, the ACA antenna keeps track of a star. The pointing errors caused by switching to directions along the sidereal motion and against the sidereal motion may differ. The pointing error caused by switching to a direction against the sidereal motion may become large because the vibration of the antenna caused by switching to a direction against the sidereal motion is larger than that from switching to a direction along the sidereal motion. In order to verify the directional characteristics of the pointing performance during the settling time after fast switching, the pointing performance should be measured in eight directions around a star (0, 45, 90, 135, 180, 225, 270 and 315 degrees). This verification test was performed with ACA 7-m antenna No. 12 in the night of June 17, 2012.

Figure 6-6 shows the measurements of the servo errors in 30 runs after switching to eight directions around a star. Table 6-1 lists the peak servo errors in the interval from 1.9 to 2.4 seconds after switching and the RMS servo errors in the period from 2.4 to 4.4 seconds after fast switching at each directions. It was confirmed that these results meet the technical specifications for the pointing performance during the settling time after switching. Furthermore, the values of the peak servo errors and the RMS servo errors are much smaller than the technical specifications, indicating that the effect of the direction of changes is negligible. This confirms that there are no

directional biases in the ALMA ACA antennas. Since the directional variations are very small, they may be invisible at the accuracy limit of the current measurement method. Some directional bias might be seen by improving the accuracy of the measurement method. However, the measurement results met the technical specifications of the ALMA perfectly. Pointing performance superior to that observed is not critical for the ALMA ACA antenna. Therefore, the directional characteristics are not further pursued in this study.

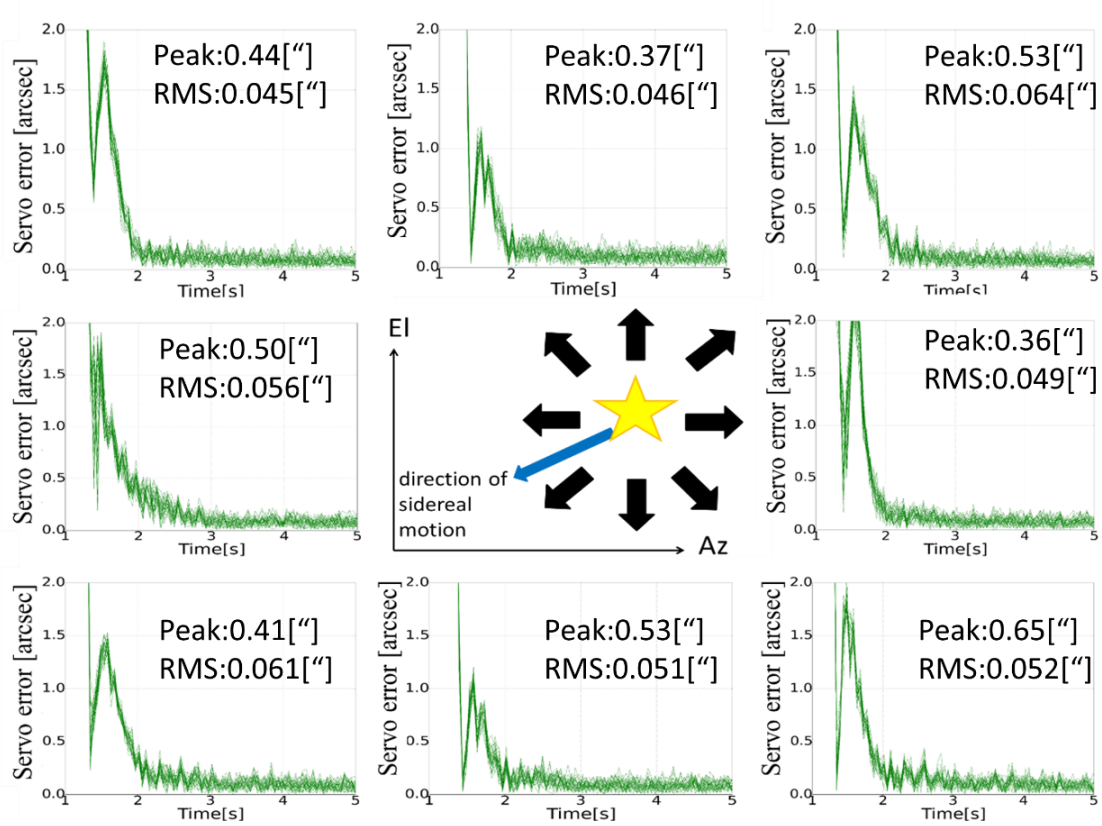

Figure 6-6 Results of measured servo errors from 30 runs of eight fast switching directions taken on June 17, 2012.

7 Referencing Pointing Performance of ALMA ACA antennas in This Study

In this study, the referencing pointing performance of the ACA antenna is calculated according to method by Saito et al. (2012) [see equation (2-1)] and the new correction method of the optical seeing [see equation (3-15)]. This method is represented by the following equation:

$$d\theta_{\mathrm{main}} = sqrt({d\theta_0}^2 - 2 \times \left(d\theta_{\mathrm{s\ measure}} \times \frac{5^{-0.16-0.06\times V_{\mathrm{wind}}}}{1^{-0.16-0.06\times V_{\mathrm{wind}}}} \times \frac{\left[sin\left(El_{\mathrm{seeing}}\right)\right]^{0.5}}{\left[sin\left(El_{\mathrm{pointing}}\right)\right]^{0.5}} \right)^2 - 2 \times d\theta_{\mathrm{tw}}(OSF)^2 + d\theta_{\mathrm{tw}}(AOS)^2 + {d\theta_{\mathrm{mr}}}^2 + {d\theta_{\mathrm{sr}}}^2 + {d\theta_{\mathrm{se}}}^2) \quad (7\text{-}1)$$

where $d\theta_0$ is the measured pointing value with OPT (the integration time of five second), $d\theta_{\mathrm{s\ measure}}$ is the measurement result of the pointing error due to optical seeing (hereinafter optical seeing) (the integration time of one second), V_{wind} is the average wind velocity in the measurement of the referencing pointing, El_{seeing} is the El angle at the star of the measurement of the optical seeing, and El_{pointing} is the El angle of the star in the measurement of the referencing pointing performance, $d\theta_{\mathrm{tw}}$ *(OSF)* is the pointing jitter due to wind load at the OSF, $d\theta_{\mathrm{se}}$ is the RMS of servo error, $d\theta_{\mathrm{tw}}$ *(AOS)* is the pointing jitter due to wind load at the AOS, $d\theta_{\mathrm{mr}}$ is the pointing error due to the main reflector thermal metrology system, and $d\theta_{\mathrm{sr}}$ is the pointing error due to the sub reflector. The pointing jitter due to wind load (9.5 m/s) at the AOS, the pointing error due to the main reflector thermal metrology system, and the pointing error due to the sub reflector are estimated as 0.32, 0.21, and 0.05 arcsecs, respectively, using the simulation provided by the antenna vendor. The verification results of the referencing pointing performance of the ACA antennas along with the above verification method are described in Section 7.1. The validation of the new correction method derived in this study [see equation (3-15)] is described in Section 7.2. The physical interpretation of the new relation between the optical seeing and the wind velocity [see equation (3-14)] are described in Section 7.3.

7.1 Referencing Pointing Performance of ACA antennas with New Correction Method of Optical Seeing

Table 7-1 Referencing pointing performances of all the ACA antennas

Antenna	No.	Referencing pointing performance [arcsec]	
		This study	Saito et al.(2012)
7m antenna	1	0.556	0.531
	2	0.614	0.550
	3	0.601	0.555
	4	0.631	0.578
	5	0.628	0.559
	6	0.519	0.459
	7	0.526	0.470
	8	0.502	0.485
	9	0.536	0.522
	10	0.496	0.475
	11	0.578	0.500
	12	0.634	0.579
12m antenna	1	0.598	0.582
	2	0.629	0.597
	3	0.643	0.600
	4	0.653	0.588

The verification results of the referencing pointing performance in this study and from Saito et al. (2012) are listed in Table 7-1. From the results of this research, three ACA 12-m antennas (No. 2, No. 3 and No. 4) and five ACA 7-m antennas (No. 2, No. 3 No. 4, No. 5, and No. 12) exceed the technical specification of the referencing pointing performance of ALMA (0.6 arcsecs) (see Table 7-1). The referencing pointing performance of each ACA antenna is estimated as the root sum square (RSS) of the average and the standard deviation of the referencing pointing performance calculated at each measurement [see the bottom line in Table 7-2]. The parameters of measurements of all ACA antennas from this research and Saito et al. (2012) are listed in Table 7-2, Table 7-3, Table 7-4, Table 7-5, Table 7-6, Table 7-7, Table 7-8, Table 7-9, Table 7-10, Table 7-11, Table 7-12, Table 7-13, Table 7-14, Table 7-15, Table 7-16, and Table 7-17.

Table 7-2 Summary of measurement results of the referencing pointing performance of ACA 7-m antenna No. 1.

Saito et al.(2012)								This study		
(1)Date	(2)Start (UT)	(3)V_{wind}[1] [m/s]	(4)$d\theta_0$[2] [arcsec]	(5)$d\theta_s$[3] [arcsec]	(6)$d\theta_{se}$[4] [arcsec]	(7)$d\theta_{tw}(OSF)$[5] [arcsec]	(8)$d\theta_{main}$[6] [arcsec]	(9)Power law index[7]	(10)$d\theta_s$[8] [arcsec]	(11)$d\theta_{main}$[9] [arcsec]
2011/04/05	3:41	2.40	0.51	0.36	0.06	0.03	0.39	-0.31	0.30	0.48
2011/04/05	4:09	2.46	0.38	0.30	0.04	0.03	0.38	-0.32	0.25	0.40
2011/04/05	5:33	2.42	0.68	0.26	0.14	0.03	0.70	-0.32	0.21	0.73
2011/04/05	5:51	2.31	0.41	0.19	0.05	0.03	0.49	-0.31	0.16	0.51
2011/04/05	6:09	2.44	0.59	0.22	0.08	0.03	0.63	-0.32	0.19	0.66
2011/04/05	7:05	3.09	0.37	0.19	0.05	0.05	0.47	-0.36	0.14	0.50
2011/04/05	7:30	3.06	0.53	0.21	0.06	0.04	0.59	-0.36	0.16	0.62
2011/04/08	2:05	2.01	0.47	0.17	0.08	0.02	0.56	-0.29	0.15	0.57
2011/04/08	2:28	2.54	0.36	0.15	0.06	0.03	0.48	-0.32	0.12	0.49
2011/04/08	2:50	2.62	0.31	0.21	0.07	0.03	0.39	-0.33	0.17	0.43
2011/04/08	3:11	2.70	0.47	0.26	0.08	0.03	0.48	-0.33	0.21	0.52
2011/04/08	3:32	2.58	0.54	0.26	0.06	0.03	0.54	-0.33	0.21	0.58
2011/04/08	4:22	2.24	0.43	0.20	0.05	0.02	0.48	-0.30	0.17	0.51
2011/04/08	4:41	2.23	0.91	0.26	0.07	0.02	0.91	-0.30	0.22	0.93
2011/04/08	5:00	2.29	0.30	0.22	0.05	0.02	0.37	-0.31	0.19	0.39
2011/04/09	1:01	1.55	0.32	0.21	0.07	0.01	0.39	-0.26	0.19	0.41
2011/04/09	1:19	2.09	0.30	0.18	0.06	0.02	0.41	-0.29	0.15	0.43
2011/04/09	1:38	1.77	0.50	0.24	0.07	0.01	0.54	-0.27	0.21	0.56
2011/04/09	1:56	2.46	0.54	0.20	0.06	0.03	0.60	-0.32	0.16	0.62
2011/04/09	2:16	2.32	0.45	0.20	0.05	0.03	0.52	-0.31	0.17	0.54
2011/04/09	2:35	1.99	0.44	0.20	0.07	0.02	0.52	-0.29	0.17	0.54
2011/04/09	2:54	1.99	0.52	0.19	0.05	0.02	0.58	-0.29	0.17	0.60
2011/04/09	3:13	1.56	0.51	0.21	0.09	0.01	0.57	-0.26	0.19	0.58
2011/04/12	4:00	2.24	0.34	0.22	0.05	0.02	0.40	-0.30	0.19	0.44
						Average	0.516			0.543
						Standard deviation	0.123			0.119
RSS of average and standard deviation ($\sqrt{\text{average}^2 + \text{standard deviation}^2}$)							**0.531**			**0.556**

[1] Measured average wind velocity in Saito et al. (2012)

[2] Measured pointing value in Saito et al. (2012)

[3] Pointing error due to optical seeing in Saito et al. (2012)

[4] RMS of servo error in Saito et al. (2012)

[5] Pointing jitter due to wind load at the OSF in Saito et al. (2012)

[6] Estimated referencing pointing performance in Saito et al. (2012)

[7] Power law index estimated by the equation (3-14) wind measured average wind velocity

[8] Pointing error due to optical seeing of this study

[9] Estimated referencing pointing performance of this study

Table 7-3 Summary of measurement results of the referencing pointing performance of ACA 7-m antenna No. 2.

Saito et al.(2012)								This study		
(1)Date	(2)Start (UT)	(3)V_{wind} [m/s]	(4)$d\theta_0$ [arcsec]	(5)$d\theta_s$ [arcsec]	(6)$d\theta_{se}$ [arcsec]	(7)$d\theta_{tw}$*(OSF)* [arcsec]	(8)$d\theta_{main}$ [arcsec]	(9)Power law index	(10)$d\theta_s$ [arcsec]	(11)$d\theta_{main}$ [arcsec]
2011/04/29	3:04	3.24	0.75	0.29	0.09	0.05	0.74	-0.37	0.22	0.79
2011/04/29	3:23	3.81	0.56	0.32	0.08	0.07	0.50	-0.41	0.23	0.59
2011/04/29	4:42	3.51	0.62	0.35	0.08	0.06	0.54	-0.39	0.26	0.63
2011/04/29	5:02	3.48	0.45	0.29	0.08	0.06	0.43	-0.38	0.22	0.51
2011/04/30	1:10	3.21	0.78	0.28	0.08	0.05	0.78	-0.37	0.21	0.82
2011/05/01	1:03	2.14	0.86	0.21	0.07	0.02	0.90	-0.30	0.18	0.91
2011/05/01	1:21	2.94	0.34	0.21	0.07	0.04	0.42	-0.35	0.17	0.46
2011/05/01	1:40	4.03	0.38	0.23	0.08	0.08	0.42	-0.42	0.16	0.48
2011/05/01	3:46	3.60	0.73	0.37	0.08	0.06	0.63	-0.39	0.28	0.73
2011/05/01	4:05	3.91	0.55	0.33	0.08	0.07	0.47	-0.41	0.24	0.58
2011/05/01	4:24	4.41	0.49	0.40	0.11	0.09	0.38	-0.44	0.27	0.49
2011/05/01	4:42	4.59	0.48	0.48	0.09	0.10	0.37	-0.46	0.32	0.37
2011/05/01	5:01	4.64	0.76	0.50	0.07	0.10	0.45	-0.46	0.33	0.70
2011/05/01	5:19	3.83	0.28	0.41	0.12	0.07	0.39	-0.41	0.29	0.39
2011/05/01	6:39	4.47	0.39	0.48	0.08	0.09	0.37	-0.45	0.32	0.37
2011/05/01	6:58	4.24	0.74	0.31	0.19	0.08	0.72	-0.43	0.21	0.79
2011/05/01	7:17	4.16	0.67	0.30	0.16	0.08	0.66	-0.43	0.21	0.72
2011/05/01	7:38	3.46	0.61	0.39	0.07	0.06	0.46	-0.38	0.29	0.59
2011/05/02	23:47	2.41	0.29	0.23	0.08	0.03	0.39	-0.32	0.19	0.41
2011/05/03	1:03	2.98	0.33	0.35	0.11	0.04	0.40	-0.35	0.28	0.40
2011/05/03	1:24	2.63	0.82	0.36	0.07	0.03	0.75	-0.33	0.29	0.81
2011/05/03	2:46	3.66	0.63	0.33	0.07	0.06	0.57	-0.40	0.24	0.65
2011/05/03	3:06	3.61	0.33	0.25	0.08	0.06	0.38	-0.39	0.18	0.44
2011/05/03	3:54	3.64	0.43	0.23	0.24	0.06	0.53	-0.39	0.17	0.57
						Average	0.528			0.592
						Standard deviation	0.156			0.163
RSS of average and standard deviation ($\sqrt{\text{average}^2 + \text{standard deviation}^2}$)							**0.550**			**0.614**

Table 7-4 Summary of measurement results of the referencing pointing performance of ACA 7-m antenna No. 3.

Saito et al.(2012)								This study		
(1)Date	(2)Start (UT)	(3)V_{wind} [m/s]	(4)$d\theta_0$ [arcsec]	(5)$d\theta_s$ [arcsec]	(6)$d\theta_{se}$ [arcsec]	(7)$d\theta_{tw}$*(OSF)* [arcsec]	(8)$d\theta_{main}$ [arcsec]	(9)Power law index	(10)$d\theta_s$ [arcsec]	(11)$d\theta_{main}$ [arcsec]
2011/05/15	1:54	2.96	0.57	0.27	0.08	0.04	0.58	-0.35	0.21	0.62
2011/05/15	2:21	2.31	0.54	0.23	0.07	0.03	0.58	-0.31	0.19	0.61
2011/05/15	2:40	2.85	0.58	0.31	0.08	0.04	0.54	-0.34	0.25	0.61
2011/05/15	2:59	2.41	0.76	0.27	0.06	0.03	0.76	-0.32	0.23	0.79
2011/05/17	6:12	2.54	0.40	0.35	0.05	0.03	0.39	-0.32	0.29	0.39
2011/05/17	6:32	2.87	0.46	0.31	0.06	0.04	0.41	-0.34	0.25	0.49
2011/05/17	6:51	2.63	0.43	0.39	0.06	0.03	0.39	-0.33	0.32	0.39
2011/05/18	9:18	1.94	0.44	0.20	0.05	0.02	0.52	-0.29	0.17	0.53
2011/05/18	9:38	2.08	0.42	0.27	0.05	0.02	0.43	-0.29	0.23	0.47
2011/05/19	6:54	3.16	0.57	0.40	0.06	0.05	0.39	-0.36	0.31	0.53
2011/05/19	7:14	3.21	0.87	0.34	0.06	0.05	0.82	-0.37	0.26	0.88
2011/05/19	7:34	2.99	0.82	0.34	0.06	0.04	0.77	-0.35	0.27	0.82
2011/05/19	8:51	2.33	0.61	0.39	0.05	0.03	0.46	-0.31	0.33	0.55
2011/05/20	8:01	2.99	0.68	0.39	0.06	0.04	0.56	-0.35	0.30	0.66
2011/05/20	8:20	2.94	0.40	0.24	0.05	0.04	0.44	-0.35	0.19	0.49
2011/05/20	8:41	2.98	0.60	0.30	0.07	0.04	0.57	-0.35	0.24	0.63
2011/05/20	9:05	2.99	0.79	0.27	0.06	0.04	0.79	-0.35	0.21	0.83
2011/05/23	1:32	2.24	0.48	0.19	0.06	0.02	0.55	-0.30	0.16	0.57
2011/05/23	1:51	2.24	0.62	0.20	0.07	0.02	0.68	-0.30	0.17	0.69
2011/05/23	2:11	2.37	0.35	0.19	0.06	0.03	0.45	-0.31	0.16	0.47
2011/05/23	2:34	2.05	0.46	0.18	0.09	0.02	0.55	-0.29	0.15	0.57
2011/05/23	2:53	2.35	0.46	0.18	0.07	0.03	0.55	-0.31	0.15	0.56
2011/05/23	3:13	2.97	0.58	0.39	0.07	0.04	0.43	-0.35	0.30	0.55
2011/05/23	5:18	2.90	0.55	0.35	0.07	0.04	0.45	-0.35	0.28	0.55
2011/05/23	5:57	2.88	0.38	0.43	0.08	0.04	0.39	-0.35	0.34	0.39
						Average	0.538			0.586
						Standard deviation	0.134			0.135
RSS of average and standard deviation ($\sqrt{\text{average}^2 + \text{standard deviation}^2}$)							**0.555**			**0.601**

Table 7-5 Summary of measurement results of the referencing pointing performance of ACA 7-m antenna No. 4.

Saito et al.(2012)								This study		
(1)Date	(2)Start (UT)	(3)V_{wind} [m/s]	(4)$d\theta_0$ [arcsec]	(5)$d\theta_s$ [arcsec]	(6)$d\theta_{se}$ [arcsec]	(7)$d\theta_{tw}$*(OSF)* [arcsec]	(8)$d\theta_{main}$ [arcsec]	(9)Power law index	(10)$d\theta_s$ [arcsec]	(11)$d\theta_{main}$ [arcsec]
2011/07/10	5:01	2.51	0.72	0.31	0.07	0.03	0.69	-0.32	0.26	0.74
2011/07/10	5:20	2.39	1.22	0.37	0.08	0.03	1.17	-0.31	0.31	1.20
2011/07/10	5:42	3.26	0.71	0.34	0.06	0.05	0.65	-0.37	0.26	0.72
2011/07/11	5:50	4.02	0.65	0.29	0.06	0.08	0.63	-0.42	0.20	0.69
2011/07/11	6:10	4.23	0.52	0.25	0.07	0.08	0.53	-0.43	0.18	0.59
2011/07/11	6:35	3.90	0.45	0.23	0.06	0.07	0.49	-0.41	0.16	0.54
2011/07/13	0:49	2.45	0.43	0.20	0.08	0.03	0.51	-0.32	0.17	0.53
2011/07/13	1:08	2.48	0.47	0.25	0.07	0.03	0.49	-0.32	0.21	0.53
2011/07/13	1:26	2.88	0.41	0.30	0.06	0.04	0.39	-0.35	0.24	0.45
2011/07/13	1:45	2.66	0.33	0.32	0.07	0.03	0.39	-0.33	0.26	0.39
2011/07/13	2:09	2.85	1.20	0.39	0.07	0.04	1.14	-0.34	0.31	1.18
2011/07/13	2:28	2.82	0.63	0.38	0.07	0.04	0.52	-0.34	0.30	0.61
2011/07/13	2:48	2.77	0.37	0.35	0.07	0.04	0.39	-0.34	0.28	0.39
2011/07/13	3:31	3.09	0.36	0.44	0.09	0.04	0.39	-0.36	0.34	0.39
2011/07/13	3:53	3.28	0.47	0.40	0.06	0.05	0.38	-0.37	0.31	0.43
2011/07/13	4:14	3.15	0.64	0.43	0.07	0.05	0.43	-0.36	0.33	0.58
2011/07/13	4:34	3.69	0.53	0.37	0.06	0.06	0.38	-0.40	0.27	0.53
2011/07/13	4:53	3.62	0.61	0.40	0.06	0.06	0.44	-0.39	0.29	0.59
2011/07/13	5:12	3.47	0.52	0.41	0.05	0.06	0.38	-0.38	0.30	0.48
2011/07/13	5:36	3.07	0.49	0.37	0.09	0.04	0.39	-0.36	0.29	0.47
2011/07/13	6:32	3.07	0.44	0.40	0.08	0.04	0.39	-0.36	0.31	0.39
2011/07/13	6:50	2.66	0.49	0.44	0.07	0.03	0.39	-0.33	0.36	0.39
2011/07/13	7:09	2.22	0.78	0.31	0.06	0.02	0.75	-0.30	0.27	0.79
2011/07/13	7:28	2.47	0.50	0.38	0.08	0.03	0.39	-0.32	0.32	0.45
2011/07/13	7:53	2.08	0.75	0.34	0.07	0.02	0.70	-0.29	0.29	0.74
2011/07/13	8:13	2.35	0.68	0.39	0.07	0.03	0.56	-0.31	0.32	0.64
						Average	0.537			0.593
						Standard deviation	0.214			0.214
RSS of average and standard deviation ($\sqrt{\text{average}^2 + \text{standard deviation}^2}$)							**0.578**			**0.631**

Table 7-6 Summary of measurement results of the referencing pointing performance of ACA 7-m antenna No. 5.

Saito et al.(2012)								This study		
(1)Date	(2)Start (UT)	(3)V_{wind} [m/s]	(4)$d\theta_0$ [arcsec]	(5)$d\theta_s$ [arcsec]	(6)$d\theta_{se}$ [arcsec]	(7)$d\theta_{tw}$*(OSF)* [arcsec]	(8)$d\theta_{main}$ [arcsec]	(9)Power law index	(10)$d\theta_s$ [arcsec]	(11)$d\theta_{main}$ [arcsec]
2011/07/16	23:51	2.70	0.74	0.28	0.05	0.03	0.74	-0.33	0.23	0.77
2011/07/17	0:10	3.20	0.43	0.28	0.05	0.05	0.42	-0.37	0.21	0.49
2011/07/17	0:28	2.87	0.41	0.33	0.05	0.05	0.38	-0.34	0.26	0.42
2011/07/17	0:47	2.36	0.55	0.58	0.06	0.03	0.39	-0.31	0.48	0.39
2011/07/17	1:10	2.20	0.86	0.53	0.05	0.02	0.57	-0.30	0.45	0.70
2011/07/17	1:28	2.27	0.80	0.46	0.06	0.02	0.61	-0.31	0.39	0.70
2011/07/17	2:16	1.33	0.43	0.41	0.07	0.01	0.39	-0.25	0.38	0.39
2011/07/17	2:35	1.66	0.52	0.48	0.07	0.01	0.39	-0.27	0.43	0.39
2011/07/17	2:53	2.27	0.82	0.36	0.05	0.02	0.75	-0.31	0.30	0.80
2011/07/17	3:11	1.88	0.65	0.37	0.05	0.02	0.55	-0.28	0.32	0.60
2011/07/17	3:34	2.30	0.49	0.35	0.05	0.03	0.39	-0.31	0.29	0.47
2011/07/17	4:25	2.15	0.45	0.37	0.05	0.02	0.39	-0.30	0.32	0.39
2011/07/17	4:43	2.42	0.47	0.36	0.05	0.03	0.39	-0.32	0.30	0.44
2011/07/17	5:02	3.43	1.45	0.41	0.06	0.06	1.38	-0.38	0.31	1.44
2011/07/17	5:24	2.69	0.56	0.37	0.06	0.03	0.44	-0.33	0.30	0.53
2011/07/17	5:43	2.23	0.69	0.36	0.05	0.02	0.61	-0.30	0.30	0.66
2011/07/17	6:01	2.44	0.39	0.41	0.05	0.03	0.39	-0.32	0.34	0.39
2011/07/17	6:19	2.45	0.32	0.31	0.05	0.03	0.39	-0.32	0.26	0.39
2011/07/17	7:04	0.84	0.68	0.35	0.07	0.00	0.61	-0.21	0.34	0.62
2011/07/17	7:27	0.94	0.73	0.34	0.05	0.00	0.67	-0.22	0.33	0.68
2011/07/17	8:05	1.60	0.72	0.41	0.05	0.01	0.58	-0.26	0.37	0.63
2011/07/17	8:23	3.52	1.15	0.42	0.05	0.06	1.06	-0.39	0.31	1.13
2011/07/19	0:31	2.81	0.66	0.39	0.05	0.04	0.53	-0.34	0.31	0.62
2011/07/19	0:51	2.92	0.82	0.61	0.05	0.04	0.39	-0.35	0.48	0.60
2011/07/19	1:11	4.45	0.59	0.61	0.06	0.09	0.37	-0.45	0.41	0.37
2011/07/19	1:34	4.08	1.12	0.79	0.05	0.08	0.38	-0.42	0.55	0.88
2011/07/19	2:23	4.85	0.64	0.78	0.06	0.11	0.36	-0.47	0.50	0.36
2011/07/19	2:42	4.41	0.40	0.63	0.05	0.09	0.37	-0.44	0.43	0.37
2011/07/19	3:09	4.54	0.45	0.71	0.07	0.10	0.37	-0.45	0.47	0.37
2011/07/19	3:27	4.25	0.54	0.76	0.06	0.09	0.37	-0.43	0.52	0.37
2011/07/19	4:15	4.78	0.52	0.75	0.05	0.11	0.36	-0.47	0.49	0.36
2011/07/19	4:37	2.54	1.07	0.74	0.06	0.03	0.45	-0.32	0.61	0.75
2011/07/19	4:55	1.82	1.34	0.84	0.06	0.02	0.73	-0.28	0.74	0.92
2011/07/19	5:14	1.98	0.74	0.33	0.06	0.02	0.69	-0.29	0.29	0.73
2011/07/19	5:37	2.48	0.62	0.28	0.05	0.03	0.61	-0.32	0.23	0.65
2011/07/19	5:56	3.11	0.36	0.27	0.06	0.05	0.38	-0.36	0.21	0.44
2011/07/19	6:14	3.09	0.47	0.33	0.05	0.05	0.38	-0.36	0.26	0.49
2011/07/19	6:33	2.16	0.59	0.40	0.05	0.02	0.42	-0.30	0.34	0.52
2011/07/19	7:19	2.06	0.35	0.32	0.05	0.02	0.39	-0.29	0.28	0.39
2011/07/19	7:38	1.92	0.58	0.37	0.06	0.02	0.46	-0.28	0.32	0.53
2011/07/19	7:56	2.23	0.85	0.38	0.06	0.02	0.77	-0.30	0.32	0.82
						Average	0.518			0.584
						Standard deviation	0.210			0.231
RSS of average and standard deviation ($\sqrt{\text{average}^2 + \text{standard deviation}^2}$)							**0.559**			**0.628**

Table 7-7 Summary of measurement results of the referencing pointing performance of ACA 7-m antenna No. 6.

Saito et al.(2012)								This study		
(1)Date	(2)Start (UT)	(3)V_{wind} [m/s]	(4)$d\theta_0$ [arcsec]	(5)$d\theta_s$ [arcsec]	(6)$d\theta_{se}$ [arcsec]	(7)$d\theta_{tw}$*(OSF)* [arcsec]	(8)$d\theta_{main}$ [arcsec]	(9)Power law index	(10)$d\theta_s$ [arcsec]	(11)$d\theta_{main}$ [arcsec]
2011/09/02	7:01	1.41	0.53	0.28	0.03	0.01	0.52	-0.25	0.26	0.55
2011/09/02	7:21	1.59	0.40	0.28	0.03	0.01	0.39	-0.26	0.25	0.43
2011/09/02	7:39	1.75	0.28	0.33	0.03	0.01	0.39	-0.27	0.29	0.39
2011/09/03	1:08	2.50	0.35	0.32	0.04	0.03	0.39	-0.32	0.26	0.39
2011/09/03	1:32	2.75	0.42	0.32	0.05	0.04	0.39	-0.34	0.26	0.44
2011/09/03	1:52	2.08	0.60	0.42	0.04	0.02	0.40	-0.29	0.36	0.50
2011/09/03	2:16	2.68	0.66	0.43	0.10	0.03	0.47	-0.33	0.35	0.59
2011/09/03	3:35	4.96	0.64	0.31	0.04	0.12	0.58	-0.48	0.20	0.67
2011/09/03	3:54	4.80	0.54	0.33	0.08	0.11	0.45	-0.47	0.21	0.58
2011/09/03	4:14	2.99	0.46	0.33	0.03	0.04	0.38	-0.35	0.26	0.47
2011/09/03	4:39	2.53	0.33	0.32	0.03	0.03	0.38	-0.32	0.26	0.38
2011/09/03	5:17	3.14	0.55	0.33	0.05	0.05	0.48	-0.36	0.25	0.57
2011/09/03	6:40	2.01	0.34	0.46	0.04	0.02	0.39	-0.29	0.40	0.39
2011/09/03	7:00	1.70	0.43	0.45	0.04	0.01	0.39	-0.27	0.40	0.39
2011/09/03	7:19	2.02	0.41	0.51	0.04	0.02	0.39	-0.29	0.44	0.39
2011/09/04	1:50	2.08	0.39	0.33	0.05	0.02	0.39	-0.29	0.28	0.39
2011/09/04	2:09	3.50	0.72	0.36	0.04	0.06	0.63	-0.39	0.27	0.72
2011/09/04	2:28	2.36	0.39	0.32	0.03	0.03	0.38	-0.31	0.27	0.40
2011/09/04	2:52	2.35	0.42	0.36	0.34	0.03	0.51	-0.31	0.30	0.51
2011/09/04	3:12	1.86	0.45	0.33	0.04	0.02	0.39	-0.28	0.29	0.43
2011/09/04	4:31	2.47	0.46	0.38	0.04	0.03	0.39	-0.32	0.31	0.40
2011/09/04	4:54	3.74	0.49	0.36	0.04	0.07	0.38	-0.40	0.26	0.49
2011/09/04	5:15	4.38	0.61	0.30	0.08	0.09	0.58	-0.44	0.20	0.65
2011/09/04	5:41	4.24	0.76	0.38	0.28	0.08	0.71	-0.43	0.26	0.81
2011/09/04	7:07	4.19	0.34	0.40	0.04	0.08	0.37	-0.43	0.28	0.37
2011/09/04	7:27	4.85	0.69	0.51	0.05	0.11	0.36	-0.47	0.33	0.62
2011/09/04	7:52	4.80	0.42	0.40	0.04	0.11	0.36	-0.47	0.26	0.41
2011/09/04	8:12	3.89	0.48	0.40	0.05	0.07	0.38	-0.41	0.29	0.46
2011/09/04	8:31	2.82	0.82	0.39	0.35	0.04	0.80	-0.34	0.31	0.86
2011/09/04	8:58	3.01	0.28	0.38	0.05	0.04	0.38	-0.35	0.30	0.38
						Average	0.446			0.501
						Standard deviation	0.111			0.135
RSS of average and standard deviation ($\sqrt{\text{average}^2 + \text{standard deviation}^2}$)							**0.459**			**0.519**

Table 7-8 Summary of measurement results of the referencing pointing performance of ACA 7-m antenna No. 7.

Saito et al.(2012)								This study		
(1)Date	(2)Start (UT)	(3)V_{wind} [m/s]	(4)$d\theta_0$ [arcsec]	(5)$d\theta_s$ [arcsec]	(6)$d\theta_{se}$ [arcsec]	(7)$d\theta_{tw}$*(OSF)* [arcsec]	(8)$d\theta_{main}$ [arcsec]	(9)Power law index	(10)$d\theta_s$ [arcsec]	(11)$d\theta_{main}$ [arcsec]
2011/10/08	0:20	4.83	0.54	0.29	0.08	0.11	0.50	-0.47	0.19	0.59
2011/10/08	0:39	5.23	0.41	0.24	0.08	0.13	0.42	-0.50	0.15	0.50
2011/10/08	1:27	3.19	0.51	0.24	0.08	0.05	0.54	-0.37	0.18	0.59
2011/10/08	2:32	1.02	0.44	0.31	0.08	0.00	0.40	-0.23	0.30	0.41
2011/10/08	2:51	0.85	0.62	0.30	0.08	0.00	0.60	-0.22	0.29	0.61
2011/10/08	3:40	1.60	0.76	0.30	0.07	0.01	0.74	-0.26	0.27	0.76
2011/10/08	3:59	2.09	0.34	0.36	0.08	0.02	0.39	-0.29	0.31	0.39
2011/10/08	4:47	2.26	0.52	0.36	0.08	0.02	0.41	-0.31	0.30	0.49
2011/10/08	5:06	2.21	0.31	0.49	0.07	0.02	0.39	-0.30	0.42	0.39
2011/10/08	5:53	2.17	0.60	0.49	0.07	0.02	0.39	-0.30	0.42	0.41
2011/10/08	6:11	2.42	0.52	0.58	0.07	0.03	0.39	-0.32	0.48	0.39
2011/10/08	6:59	2.32	0.64	0.58	0.07	0.03	0.39	-0.31	0.49	0.39
2011/10/08	7:18	3.02	0.49	0.39	0.07	0.04	0.39	-0.35	0.30	0.45
2011/10/08	8:06	3.07	0.56	0.39	0.07	0.04	0.40	-0.36	0.30	0.53
2011/10/08	8:24	2.64	0.47	0.43	0.06	0.03	0.39	-0.33	0.35	0.39
2011/10/10	4:04	1.65	0.45	0.23	0.08	0.01	0.50	-0.27	0.21	0.52
2011/10/10	4:22	1.84	0.70	0.47	0.07	0.02	0.45	-0.28	0.41	0.55
2011/10/10	5:11	3.22	0.44	0.47	0.08	0.05	0.39	-0.37	0.36	0.39
2011/10/10	5:29	4.15	0.74	0.44	0.07	0.08	0.55	-0.43	0.31	0.71
2011/10/10	6:17	3.17	0.87	0.44	0.07	0.05	0.72	-0.36	0.34	0.82
2011/10/10	6:35	2.75	0.50	0.52	0.07	0.04	0.39	-0.34	0.42	0.39
2011/10/10	7:23	6.27	0.48	0.52	0.07	0.19	0.29	-0.56	0.29	0.29
2011/10/10	7:42	5.93	0.44	0.28	0.08	0.17	0.31	-0.54	0.16	0.49
2011/10/10	8:29	4.29	0.38	0.28	0.06	0.09	0.37	-0.44	0.19	0.46
2011/10/10	8:47	4.81	0.35	0.23	0.07	0.11	0.36	-0.47	0.15	0.46
2011/10/18	2:33	1.94	0.59	0.38	0.08	0.02	0.46	-0.29	0.33	0.53
2011/10/18	3:45	2.55	0.57	0.28	0.08	0.03	0.57	-0.32	0.23	0.61
2011/10/18	4:04	2.54	0.64	0.26	0.07	0.03	0.65	-0.32	0.21	0.69
2011/10/18	5:35	3.42	0.63	0.39	0.07	0.06	0.49	-0.38	0.29	0.61
						Average	0.456			0.510
						Standard deviation	0.114			0.128
RSS of average and standard deviation ($\sqrt{\text{average}^2 + \text{standard deviation}^2}$)							**0.470**			**0.526**

Table 7-9 Summary of measurement results of the referencing pointing performance of ACA 7-m antenna No. 8.

Saito et al.(2012)								This study		
(1)Date	(2)Start (UT)	(3)V_{wind} [m/s]	(4)$d\theta_0$ [arcsec]	(5)$d\theta_s$ [arcsec]	(6)$d\theta_{se}$ [arcsec]	(7)$d\theta_{tw}$*(OSF)* [arcsec]	(8)$d\theta_{main}$ [arcsec]	(9)Power law index	(10)$d\theta_s$ [arcsec]	(11)$d\theta_{main}$ [arcsec]
2011/12/6	2:46	1.89	0.40	0.28	0.05	0.02	0.39	-0.28	0.25	0.44
2011/12/6	3:04	1.29	0.69	0.24	0.05	0.01	0.72	-0.24	0.22	0.73
2011/12/6	3:23	1.64	0.44	0.28	0.06	0.01	0.44	-0.27	0.25	0.47
2011/12/6	3:43	1.46	0.53	0.29	0.05	0.01	0.51	-0.25	0.27	0.54
2011/12/6	5:06	1.32	0.51	0.25	0.05	0.01	0.54	-0.25	0.23	0.55
2011/12/6	5:25	1.00	0.41	0.26	0.05	0.00	0.43	-0.22	0.25	0.44
2011/12/6	5:44	1.03	0.44	0.20	0.05	0.01	0.51	-0.23	0.19	0.52
2011/12/6	6:03	1.01	0.51	0.21	0.06	0.00	0.57	-0.23	0.20	0.58
2011/12/6	6:26	0.95	0.27	0.19	0.05	0.00	0.39	-0.22	0.18	0.40
2011/12/6	6:45	1.28	0.28	0.16	0.05	0.01	0.42	-0.24	0.15	0.43
2011/12/7	1:02	1.71	0.38	0.30	0.05	0.01	0.39	-0.27	0.27	0.39
2011/12/7	1:20	0.72	0.45	0.29	0.05	0.00	0.43	-0.21	0.29	0.44
2011/12/7	1:40	0.55	0.46	0.19	0.06	0.00	0.54	-0.20	0.19	0.54
2011/12/7	1:59	1.71	0.43	0.18	0.05	0.01	0.52	-0.27	0.16	0.53
2011/12/7	3:23	1.80	0.31	0.29	0.05	0.02	0.39	-0.28	0.26	0.39
2011/12/7	3:42	1.22	0.63	0.26	0.05	0.01	0.64	-0.24	0.24	0.65
2011/12/7	4:00	1.35	0.31	0.30	0.05	0.01	0.39	-0.25	0.28	0.39
2011/12/7	4:19	2.06	0.44	0.35	0.05	0.02	0.39	-0.29	0.30	0.40
2011/12/7	5:38	1.71	0.27	0.29	0.05	0.01	0.39	-0.27	0.26	0.39
2011/12/7	5:58	1.98	0.38	0.30	0.05	0.02	0.39	-0.29	0.26	0.40
2011/12/7	6:18	2.30	0.52	0.39	0.05	0.03	0.39	-0.31	0.33	0.45
2011/12/7	6:42	2.31	0.66	0.35	0.06	0.03	0.58	-0.31	0.29	0.64
2011/12/7	7:00	2.26	0.52	0.37	0.05	0.02	0.39	-0.31	0.31	0.48
2011/12/7	7:19	2.67	0.44	0.34	0.05	0.03	0.39	-0.33	0.27	0.44
2011/12/8	2:38	1.21	0.52	0.19	0.05	0.01	0.59	-0.24	0.18	0.60
2011/12/8	3:03	0.83	0.35	0.18	0.04	0.00	0.46	-0.21	0.18	0.46
2011/12/8	4:47	1.09	0.64	0.20	0.05	0.01	0.69	-0.23	0.19	0.70
2011/12/8	5:06	1.60	0.39	0.24	0.05	0.01	0.43	-0.26	0.22	0.46
2011/12/8	5:25	1.08	0.43	0.26	0.05	0.01	0.45	-0.23	0.25	0.46
						Average	0.474			0.493
						Standard deviation	0.099			0.097
RSS of average and standard deviation ($\sqrt{\text{average}^2 + \text{standard deviation}^2}$)							**0.485**			**0.502**

Table 7-10 Summary of measurement results of the referencing pointing performance of ACA 7-m antenna No. 9.

Saito et al.(2012)								This study		
(1)Date	(2)Start (UT)	(3)V_{wind} [m/s]	(4)$d\theta_0$ [arcsec]	(5)$d\theta_s$ [arcsec]	(6)$d\theta_{se}$ [arcsec]	(7)$d\theta_{tw}$*(OSF)* [arcsec]	(8)$d\theta_{main}$ [arcsec]	(9)Power law index	(10)$d\theta_s$ [arcsec]	(11)$d\theta_{main}$ [arcsec]
2012/01/21	5:25	1.52	0.51	0.16	0.07	0.01	0.60	-0.26	0.15	0.61
2012/01/21	5:45	1.63	0.58	0.23	0.08	0.01	0.62	-0.27	0.21	0.64
2012/01/21	7:06	2.74	0.35	0.19	0.08	0.04	0.45	-0.34	0.15	0.48
2012/01/21	7:25	3.20	0.41	0.20	0.07	0.05	0.49	-0.37	0.15	0.52
2012/01/23	1:46	1.11	0.57	0.25	0.07	0.01	0.59	-0.23	0.24	0.60
2012/01/23	2:05	1.00	0.82	0.20	0.08	0.00	0.87	-0.22	0.19	0.87
2012/01/23	2:24	1.33	0.32	0.16	0.07	0.01	0.45	-0.25	0.15	0.46
2012/01/23	7:13	2.29	0.35	0.20	0.06	0.02	0.44	-0.31	0.17	0.47
2012/01/23	7:32	2.23	0.32	0.26	0.08	0.02	0.39	-0.30	0.22	0.40
2012/01/23	7:52	1.73	0.43	0.18	0.07	0.01	0.52	-0.27	0.16	0.54
2012/01/23	9:14	1.77	0.30	0.19	0.08	0.01	0.42	-0.27	0.17	0.43
2012/01/24	1:13	1.56	0.52	0.18	0.04	0.01	0.60	-0.26	0.16	0.61
2012/01/24	1:32	0.57	0.49	0.18	0.06	0.00	0.57	-0.20	0.18	0.57
2012/01/24	1:52	0.97	0.59	0.27	0.07	0.00	0.60	-0.22	0.26	0.61
2012/01/24	3:14	1.40	0.30	0.23	0.07	0.01	0.39	-0.25	0.21	0.39
2012/01/24	3:33	1.14	0.57	0.23	0.05	0.01	0.61	-0.23	0.22	0.62
2012/01/24	3:53	0.99	0.50	0.30	0.09	0.00	0.48	-0.22	0.29	0.49
2012/01/24	4:12	1.23	0.31	0.27	0.08	0.01	0.39	-0.24	0.25	0.39
2012/01/24	5:36	2.18	0.44	0.26	0.07	0.02	0.46	-0.30	0.22	0.50
2012/01/24	5:57	1.79	0.46	0.32	0.09	0.02	0.40	-0.28	0.28	0.46
2012/01/24	6:18	1.28	0.34	0.25	0.04	0.01	0.39	-0.24	0.23	0.40
2012/01/24	6:37	1.36	0.36	0.30	0.08	0.01	0.39	-0.25	0.28	0.39
2012/01/24	8:00	1.08	0.40	0.30	0.08	0.01	0.39	-0.23	0.29	0.39
2012/01/24	8:19	1.33	0.62	0.29	0.08	0.01	0.61	-0.25	0.27	0.63
2012/01/24	8:43	1.58	0.61	0.41	0.09	0.01	0.44	-0.26	0.37	0.50
2012/01/24	9:03	1.73	0.36	0.37	0.08	0.01	0.39	-0.27	0.33	0.39
2012/01/25	1:53	1.61	0.68	0.37	0.07	0.01	0.59	-0.26	0.33	0.63
2012/01/25	2:12	1.86	0.44	0.36	0.08	0.02	0.39	-0.28	0.32	0.39
2012/01/25	2:31	1.10	0.47	0.32	0.08	0.01	0.41	-0.23	0.30	0.44
2012/01/25	4:34	0.85	0.27	0.16	0.05	0.00	0.42	-0.22	0.16	0.42
2012/01/25	6:24	1.22	0.56	0.27	0.69	0.01	0.89	-0.24	0.35	0.90
						Average	0.505			0.520
						Standard deviation	0.131			0.130
RSS of average and standard deviation ($\sqrt{\text{average}^2 + \text{standard deviation}^2}$)							**0.522**			**0.536**

Table 7-11 Summary of measurement results of the referencing pointing performance of ACA 7-m antenna No. 10.

Saito et al.(2012)								This study		
(1)Date	(2)Start (UT)	(3)V_{wind} [m/s]	(4)$d\theta_0$ [arcsec]	(5)$d\theta_s$ [arcsec]	(6)$d\theta_{se}$ [arcsec]	(7)$d\theta_{tw}$*(OSF)* [arcsec]	(8)$d\theta_{main}$ [arcsec]	(9)Power law index	(10)$d\theta_s$ [arcsec]	(11)$d\theta_{main}$ [arcsec]
2012/02/27	6:23	2.96	0.44	0.30	0.05	0.04	0.40	-0.35	0.24	0.48
2012/02/27	6:50	3.98	0.52	0.33	0.05	0.07	0.44	-0.42	0.23	0.55
2012/02/27	8:08	2.24	0.39	0.40	0.05	0.02	0.39	-0.30	0.34	0.39
2012/02/27	8:27	2.50	0.46	0.39	0.05	0.03	0.39	-0.32	0.32	0.39
2012/02/28	1:05	1.09	0.53	0.28	0.05	0.01	0.52	-0.23	0.27	0.54
2012/02/28	1:23	0.73	0.43	0.23	0.04	0.00	0.48	-0.21	0.23	0.48
2012/02/28	1:43	1.17	0.26	0.25	0.05	0.01	0.39	-0.24	0.24	0.39
2012/02/28	3:01	0.94	0.67	0.27	0.06	0.00	0.67	-0.22	0.26	0.68
2012/02/28	3:21	1.54	0.41	0.21	0.05	0.01	0.48	-0.26	0.19	0.50
2012/02/28	3:40	0.87	0.43	0.28	0.05	0.00	0.42	-0.22	0.27	0.43
2012/02/28	5:00	0.91	0.39	0.22	0.05	0.00	0.46	-0.22	0.21	0.46
2012/02/28	5:19	0.87	0.37	0.27	0.06	0.00	0.39	-0.22	0.26	0.39
2012/02/28	5:38	1.03	0.69	0.29	0.05	0.01	0.68	-0.23	0.28	0.69
2012/02/28	6:57	1.34	0.66	0.28	0.05	0.01	0.66	-0.25	0.26	0.67
2012/02/28	7:16	1.33	0.58	0.24	0.05	0.01	0.61	-0.25	0.22	0.62
2012/02/28	7:35	2.50	0.34	0.25	0.05	0.03	0.39	-0.32	0.21	0.43
2012/03/08	5:02	1.18	0.61	0.67	0.05	0.01	0.39	-0.24	0.63	0.39
2012/03/09	3:55	2.12	0.61	0.36	0.05	0.02	0.51	-0.30	0.31	0.58
2012/03/09	5:54	1.45	0.72	0.35	0.05	0.01	0.65	-0.25	0.32	0.68
2012/03/09	6:13	1.46	0.46	0.31	0.06	0.01	0.41	-0.25	0.28	0.45
2012/03/09	6:32	2.80	0.46	0.52	0.05	0.04	0.39	-0.34	0.41	0.39
2012/03/10	5:01	0.91	0.42	0.29	0.05	0.00	0.40	-0.22	0.28	0.41
2012/03/10	5:20	1.38	0.49	0.29	0.05	0.01	0.47	-0.25	0.27	0.50
2012/03/10	5:39	2.20	0.43	0.32	0.05	0.02	0.39	-0.30	0.27	0.43
2012/03/10	6:56	3.04	0.28	0.31	0.05	0.04	0.39	-0.36	0.24	0.39
2012/03/10	7:15	2.82	0.33	0.43	0.05	0.04	0.38	-0.34	0.34	0.38
2012/03/10	7:34	2.80	0.31	0.31	0.05	0.04	0.39	-0.34	0.25	0.39
						Average	0.464			0.484
						Standard deviation	0.102			0.106
RSS of average and standard deviation ($\sqrt{\text{average}^2 + \text{standard deviation}^2}$)							**0.475**			**0.496**

Table 7-12 Summary of measurement results of the referencing pointing performance of ACA 7-m antenna No. 11.

Saito et al.(2012)								This study		
(1)Date	(2)Start (UT)	(3)V_{wind} [m/s]	(4)$d\theta_0$ [arcsec]	(5)$d\theta_s$ [arcsec]	(6)$d\theta_{se}$ [arcsec]	(7)$d\theta_{tw}$*(OSF)* [arcsec]	(8)$d\theta_{main}$ [arcsec]	(9)Power law index	(10)$d\theta_s$ [arcsec]	(11)$d\theta_{main}$ [arcsec]
2012/6/28	2:27	2.95	0.50	0.40	0.09	0.04	0.39	-0.35	0.31	0.45
2012/6/28	2:46	2.66	0.59	0.38	0.08	0.03	0.46	-0.33	0.31	0.56
2012/6/28	4:12	3.10	0.55	0.47	0.09	0.05	0.39	-0.36	0.36	0.44
2012/6/28	4:32	2.76	0.63	0.41	0.09	0.04	0.46	-0.34	0.33	0.58
2012/6/28	4:50	3.19	0.46	0.30	0.10	0.05	0.43	-0.37	0.23	0.51
2012/6/28	6:25	4.10	0.42	0.30	0.11	0.08	0.38	-0.42	0.21	0.49
2012/6/28	6:44	3.07	0.42	0.30	0.10	0.05	0.39	-0.36	0.23	0.47
2012/6/28	7:03	3.08	0.68	0.32	0.10	0.05	0.64	-0.36	0.25	0.70
2012/6/28	23:57	2.00	0.46	0.18	0.10	0.02	0.55	-0.29	0.16	0.57
2012/6/29	0:15	2.85	0.74	0.44	0.12	0.04	0.57	-0.34	0.35	0.68
2012/6/29	1:55	3.02	0.71	0.42	0.10	0.04	0.55	-0.35	0.33	0.67
2012/6/29	2:14	3.46	0.76	0.42	0.09	0.06	0.61	-0.38	0.31	0.73
2012/6/29	5:59	4.12	0.51	0.44	0.08	0.08	0.38	-0.43	0.31	0.46
2012/6/29	6:19	3.62	0.52	0.36	0.10	0.06	0.40	-0.39	0.26	0.53
2012/6/29	6:39	3.53	0.46	0.36	0.13	0.06	0.40	-0.39	0.27	0.48
2012/6/29	8:14	3.01	0.69	0.40	0.11	0.04	0.56	-0.35	0.31	0.66
2012/6/29	8:36	2.87	0.38	0.40	0.09	0.04	0.39	-0.34	0.32	0.39
2012/6/30	0:13	1.89	0.43	0.23	0.08	0.02	0.48	-0.28	0.20	0.51
2012/6/30	0:32	2.09	0.44	0.21	0.09	0.02	0.51	-0.29	0.18	0.53
2012/7/1	2:08	3.47	0.84	0.33	0.10	0.06	0.80	-0.38	0.25	0.86
2012/7/1	2:27	3.67	0.61	0.32	0.10	0.06	0.56	-0.40	0.23	0.64
2012/7/1	2:45	2.84	0.54	0.40	0.10	0.04	0.40	-0.34	0.32	0.50
2012/7/1	4:08	2.88	0.77	0.45	0.09	0.04	0.58	-0.35	0.36	0.70
2012/7/1	4:28	3.10	0.44	0.35	0.07	0.05	0.39	-0.36	0.27	0.44
2012/7/1	4:47	2.97	0.37	0.37	0.09	0.04	0.39	-0.35	0.29	0.39
2012/7/1	6:45	2.93	0.55	0.33	0.08	0.04	0.49	-0.35	0.26	0.57
2012/7/1	7:07	2.61	0.73	0.29	0.10	0.03	0.72	-0.33	0.24	0.76
2012/7/1	8:49	3.12	0.32	0.26	0.06	0.05	0.39	-0.36	0.20	0.41
2012/7/3	0:38	3.74	0.62	0.49	0.09	0.07	0.38	-0.40	0.35	0.53
2012/7/3	4:20	3.73	0.72	0.48	0.08	0.07	0.45	-0.40	0.35	0.65
2012/7/3	6:06	4.00	0.62	0.31	0.11	0.08	0.58	-0.42	0.22	0.66
						Average	0.487			0.565
						Standard deviation	0.111			0.118
RSS of average and standard deviation ($\sqrt{\text{average}^2 + \text{standard deviation}^2}$)							**0.500**			**0.578**

Table 7-13 Summary of measurement results of the referencing pointing performance of ACA 7-m antenna No. 12.

Saito et al.(2012)								This study		
(1)Date	(2)Start (UT)	(3)V_{wind} [m/s]	(4)$d\theta_0$ [arcsec]	(5)$d\theta_s$ [arcsec]	(6)$d\theta_{se}$ [arcsec]	(7)$d\theta_{tw}$*(OSF)* [arcsec]	(8)$d\theta_{main}$ [arcsec]	(9)Power law index	(10)$d\theta_s$ [arcsec]	(11)$d\theta_{main}$ [arcsec]
2012/5/19	5:36	2.68	0.69	0.39	0.07	0.03	0.57	-0.33	0.32	0.66
2012/5/19	5:55	2.58	0.68	0.40	0.07	0.03	0.54	-0.33	0.33	0.63
2012/5/19	6:13	2.72	0.63	0.47	0.06	0.03	0.39	-0.34	0.38	0.51
2012/5/19	7:36	2.92	0.63	0.37	0.07	0.04	0.52	-0.35	0.29	0.61
2012/5/19	7:55	3.39	0.76	0.40	0.07	0.05	0.64	-0.38	0.30	0.74
2012/5/19	8:14	3.34	0.31	0.17	0.07	0.05	0.43	-0.37	0.13	0.46
2012/5/19	8:38	2.71	0.67	0.17	0.07	0.03	0.74	-0.33	0.14	0.75
2012/5/19	9:17	3.19	0.43	0.26	0.06	0.05	0.44	-0.37	0.20	0.50
2012/5/19	9:40	3.21	0.56	0.24	0.07	0.05	0.59	-0.37	0.18	0.63
2012/5/20	0:47	3.00	0.47	0.18	0.07	0.04	0.55	-0.35	0.14	0.58
2012/5/20	1:05	2.48	0.86	0.32	0.06	0.03	0.83	-0.32	0.26	0.87
2012/5/20	1:25	2.21	0.45	0.30	0.06	0.02	0.42	-0.30	0.25	0.47
2012/5/20	2:44	4.90	0.93	0.24	0.06	0.11	0.94	-0.48	0.15	0.97
2012/5/20	3:04	4.53	0.86	0.35	0.07	0.10	0.79	-0.45	0.23	0.87
2012/5/20	3:24	4.03	0.42	0.32	0.09	0.08	0.38	-0.42	0.22	0.47
2012/5/20	4:49	3.71	0.61	0.29	0.06	0.07	0.59	-0.40	0.21	0.65
2012/5/20	5:08	3.94	0.62	0.25	0.07	0.07	0.64	-0.41	0.18	0.68
2012/5/20	5:27	3.38	0.57	0.31	0.07	0.05	0.53	-0.38	0.23	0.60
2012/5/20	7:27	4.51	0.52	0.27	0.07	0.10	0.51	-0.45	0.18	0.58
2012/5/20	7:49	3.23	0.74	0.24	0.08	0.05	0.76	-0.37	0.18	0.79
2012/5/20	8:08	2.32	0.60	0.19	0.09	0.03	0.67	-0.31	0.16	0.68
2012/5/20	8:31	3.13	0.35	0.20	0.07	0.05	0.44	-0.36	0.15	0.47
2012/5/20	8:51	3.54	0.45	0.18	0.08	0.06	0.53	-0.39	0.13	0.56
2012/5/20	9:10	3.58	0.59	0.33	0.07	0.06	0.53	-0.39	0.24	0.61
2012/5/21	1:56	3.18	0.49	0.25	0.07	0.05	0.51	-0.36	0.19	0.56
2012/5/21	2:18	1.56	0.53	0.29	0.06	0.01	0.52	-0.26	0.26	0.54
2012/5/21	4:02	3.82	0.33	0.28	0.08	0.07	0.38	-0.41	0.20	0.42
2012/5/21	4:22	3.38	0.32	0.29	0.07	0.05	0.39	-0.38	0.22	0.40
2012/5/21	6:49	3.67	0.50	0.32	0.07	0.06	0.44	-0.40	0.23	0.54
2012/5/21	7:11	2.92	0.74	0.37	0.06	0.04	0.65	-0.35	0.29	0.73
						Average	0.562			0.618
						Standard deviation	0.143			0.140
RSS of average and standard deviation ($\sqrt{\text{average}^2 + \text{standard deviation}^2}$)							**0.579**			**0.634**

Table 7-14 Summary of measurement results of the referencing pointing performance of ACA 12-m antenna No. 1.

Saito et al.(2012)								This study		
(1)Date	(2)Start (UT)	(3)V_{wind} [m/s]	(4)$d\theta_0$ [arcsec]	(5)$d\theta_s$ [arcsec]	(6)$d\theta_{se}$ [arcsec]	(7)$d\theta_{tw}$*(OSF)* [arcsec]	(8)$d\theta_{main}$ [arcsec]	(9)Power law index	(10)$d\theta_s$ [arcsec]	(11)$d\theta_{main}$ [arcsec]
2010/1/21	2:25	1.15	0.61	0.29	0.06	0.00	0.61	-0.23	0.27	0.63
2010/1/21	4:58	1.07	0.46	0.18	0.09	0.00	0.57	-0.23	0.17	0.57
2010/1/21	6:38	1.13	0.35	0.25	0.07	0.00	0.39	-0.23	0.24	0.43
2010/1/21	7:02	0.86	0.44	0.28	0.07	0.00	0.46	-0.22	0.27	0.46
2010/1/21	7:21	1.56	0.34	0.26	0.06	0.01	0.39	-0.26	0.24	0.42
2010/1/21	7:39	1.15	0.60	0.27	0.06	0.00	0.62	-0.23	0.26	0.63
2010/1/21	7:58	2.28	0.44	0.27	0.07	0.02	0.47	-0.31	0.23	0.51
2010/1/21	8:39	2.45	0.44	0.17	0.09	0.02	0.56	-0.32	0.14	0.57
2010/1/22	1:10	3.13	0.41	0.17	0.08	0.03	0.53	-0.36	0.13	0.55
2010/1/22	1:53	2.64	0.54	0.19	0.07	0.02	0.62	-0.33	0.15	0.64
2010/1/22	2:13	2.19	0.66	0.20	0.06	0.02	0.72	-0.30	0.17	0.74
2010/1/22	2:32	2.55	0.47	0.15	0.11	0.02	0.59	-0.32	0.12	0.61
2010/1/22	2:54	1.78	0.47	0.15	0.08	0.01	0.59	-0.27	0.13	0.60
2010/1/22	3:54	0.92	0.57	0.18	0.07	0.00	0.66	-0.22	0.17	0.66
2010/1/22	6:16	0.98	0.39	0.19	0.08	0.00	0.50	-0.22	0.18	0.51
2010/1/22	6:34	1.32	0.60	0.19	0.12	0.01	0.68	-0.25	0.18	0.69
2010/1/22	6:53	2.95	0.56	0.21	0.07	0.03	0.63	-0.35	0.16	0.65
2010/1/23	2:02	2.80	0.54	0.19	0.08	0.03	0.62	-0.34	0.15	0.65
2010/1/23	2:20	2.21	0.44	0.20	0.06	0.02	0.53	-0.30	0.17	0.55
2010/1/23	3:46	2.39	0.37	0.19	0.12	0.02	0.49	-0.31	0.16	0.52
2010/1/23	5:12	3.32	0.54	0.28	0.07	0.04	0.55	-0.37	0.21	0.61
2010/1/24	1:00	1.78	0.57	0.17	0.06	0.01	0.66	-0.27	0.15	0.67
2010/1/24	3:29	1.09	0.54	0.17	0.07	0.00	0.64	-0.23	0.16	0.64
2010/1/24	3:48	1.00	0.63	0.20	0.09	0.00	0.70	-0.22	0.19	0.71
						Average	0.575			0.592
						Standard deviation	0.091			0.086
RSS of average and standard deviation ($\sqrt{\text{average}^2 + \text{standard deviation}^2}$)							**0.582**			**0.598**

Table 7-15 Summary of measurement results of the referencing pointing performance of ACA 12-m antenna No. 2.

Saito et al.(2012)								This study		
(1)Date	(2)Start (UT)	(3)V_{wind} [m/s]	(4)$d\theta_0$ [arcsec]	(5)$d\theta_s$ [arcsec]	(6)$d\theta_{se}$ [arcsec]	(7)$d\theta_{tw}$*(OSF)* [arcsec]	(8)$d\theta_{main}$ [arcsec]	(9)Power law index	(10)$d\theta_s$ [arcsec]	(11)$d\theta_{main}$ [arcsec]
2009/10/29	7:12	3.60	0.66	0.37	0.08	0.04	0.58	-0.39	0.27	0.68
2009/11/3	2:33	1.41	0.50	0.15	0.18	0.01	0.64	-0.25	0.14	0.64
2009/11/3	5:11	4.31	0.51	0.29	0.07	0.06	0.51	-0.44	0.20	0.59
2009/11/3	7:01	2.24	0.54	0.16	0.12	0.02	0.65	-0.30	0.14	0.66
2009/11/26	8:06	1.04	0.54	0.12	0.14	0.00	0.67	-0.23	0.11	0.67
2009/11/27	7:34	3.21	0.46	0.41	0.12	0.03	0.40	-0.37	0.31	0.44
2009/11/28	2:06	0.74	0.45	0.30	0.07	0.00	0.44	-0.21	0.30	0.45
2009/11/28	4:47	1.23	0.86	0.26	0.11	0.01	0.88	-0.24	0.24	0.89
2009/11/28	5:08	2.14	0.64	0.23	0.17	0.02	0.71	-0.30	0.20	0.73
2009/11/28	5:32	3.37	0.60	0.23	0.08	0.04	0.65	-0.38	0.17	0.69
2009/11/28	5:53	2.96	0.51	0.29	0.06	0.03	0.51	-0.35	0.23	0.57
2009/11/28	7:31	3.59	0.45	0.23	0.11	0.04	0.52	-0.39	0.17	0.57
2009/11/29	0:29	2.32	0.44	0.19	0.12	0.02	0.55	-0.31	0.16	0.57
2009/11/29	3:23	2.72	0.37	0.23	0.09	0.02	0.45	-0.34	0.19	0.49
2009/11/29	3:45	2.81	0.75	0.22	0.09	0.03	0.80	-0.34	0.18	0.82
2009/11/29	4:13	3.01	0.50	0.21	0.09	0.03	0.58	-0.35	0.16	0.61
2009/11/29	5:37	2.21	0.44	0.21	0.13	0.02	0.54	-0.30	0.18	0.56
2009/12/1	7:16	3.69	0.34	0.24	0.10	0.05	0.39	-0.40	0.17	0.48
2009/12/2	5:15	2.94	0.56	0.21	0.12	0.03	0.64	-0.35	0.17	0.66
2009/12/2	6:33	3.39	0.48	0.18	0.10	0.04	0.58	-0.38	0.14	0.61
2009/12/2	8:28	3.81	0.53	0.16	0.14	0.05	0.64	-0.41	0.12	0.66
2009/12/3	4:29	2.67	0.85	0.23	0.12	0.02	0.89	-0.33	0.19	0.91
2009/12/3	4:47	2.67	0.52	0.23	0.18	0.02	0.60	-0.33	0.19	0.63
2009/12/3	7:05	2.87	0.50	0.32	0.10	0.03	0.47	-0.34	0.25	0.54
2009/12/3	7:24	2.16	0.59	0.36	0.17	0.02	0.53	-0.30	0.31	0.60
2009/12/3	7:43	2.81	0.30	0.33	0.11	0.03	0.40	-0.34	0.26	0.40
2009/12/4	23:59	2.81	0.48	0.28	0.15	0.03	0.51	-0.34	0.22	0.56
						Average	0.582			0.617
						Standard deviation	0.132			0.124
RSS of average and standard deviation ($\sqrt{\text{average}^2 + \text{standard deviation}^2}$)							**0.597**			**0.629**

Table 7-16 Summary of measurement results of the referencing pointing performance of ACA 12-m antenna No. 3.

Saito et al.(2012)								This study		
(1)Date	(2)Start (UT)	(3)V_{wind} [m/s]	(4)$d\theta_0$ [arcsec]	(5)$d\theta_s$ [arcsec]	(6)$d\theta_{se}$ [arcsec]	(7)$d\theta_{tw}$*(OSF)* [arcsec]	(8)$d\theta_{main}$ [arcsec]	(9)Power law index	(10)$d\theta_s$ [arcsec]	(11)$d\theta_{main}$ [arcsec]
2010/9/24	2:12	1.68	0.75	0.32	0.10	0.01	0.73	-0.27	0.29	0.76
2010/9/24	2:30	1.85	0.66	0.32	0.09	0.01	0.64	-0.28	0.28	0.67
2010/9/24	4:18	1.62	0.71	0.37	0.19	0.01	0.66	-0.26	0.33	0.70
2010/9/25	0:01	1.05	0.57	0.33	0.08	0.00	0.53	-0.23	0.32	0.55
2010/9/25	0:20	1.41	0.59	0.37	0.09	0.01	0.50	-0.25	0.34	0.54
2010/9/25	0:38	0.98	0.55	0.35	0.09	0.00	0.48	-0.22	0.34	0.50
2010/9/28	0:26	3.90	0.45	0.33	0.10	0.05	0.39	-0.41	0.24	0.51
2010/9/28	1:25	1.79	0.47	0.33	0.08	0.01	0.42	-0.28	0.29	0.47
2010/9/28	2:29	1.56	0.65	0.34	0.18	0.01	0.62	-0.26	0.31	0.66
2010/9/28	3:07	1.57	0.82	0.34	0.08	0.01	0.78	-0.26	0.31	0.81
2010/9/29	0:08	4.24	0.79	0.44	0.10	0.06	0.64	-0.43	0.30	0.78
2010/9/29	0:26	3.56	0.78	0.46	0.10	0.04	0.60	-0.39	0.34	0.74
2010/9/29	0:44	1.89	0.70	0.53	0.13	0.01	0.41	-0.28	0.46	0.49
2010/9/29	1:04	2.02	0.81	0.39	0.09	0.01	0.72	-0.29	0.34	0.78
2010/9/29	2:10	0.93	0.84	0.47	0.09	0.00	0.66	-0.22	0.45	0.68
2010/9/29	2:29	0.95	0.92	0.48	0.10	0.00	0.75	-0.22	0.46	0.77
2010/9/29	2:48	1.19	0.61	0.43	0.12	0.00	0.43	-0.24	0.41	0.48
2010/9/30	1:43	0.69	0.51	0.28	0.07	0.00	0.52	-0.21	0.28	0.53
2010/9/30	2:02	2.49	0.53	0.28	0.08	0.02	0.54	-0.32	0.23	0.59
2010/9/30	2:30	2.45	0.68	0.25	0.10	0.02	0.72	-0.32	0.21	0.74
2010/10/1	0:15	0.72	0.57	0.25	0.09	0.00	0.61	-0.21	0.25	0.61
2010/10/1	1:43	1.37	0.53	0.25	0.10	0.01	0.58	-0.25	0.23	0.59
2010/10/1	2:05	1.75	0.65	0.26	0.10	0.01	0.68	-0.27	0.23	0.70
2010/10/1	3:06	1.77	0.48	0.26	0.08	0.01	0.52	-0.27	0.23	0.54
						Average	0.589			0.633
						Standard deviation	0.115			0.112
RSS of average and standard deviation ($\sqrt{\text{average}^2 + \text{standard deviation}^2}$)							**0.600**			**0.643**

Table 7-17 Summary of measurement results of the referencing pointing performance of ACA 12-m antenna No. 4.

Saito et al.(2012)								This study		
(1)Date	(2)Start (UT)	(3)V_{wind} [m/s]	(4)$d\theta_0$ [arcsec]	(5)$d\theta_s$ [arcsec]	(6)$d\theta_{se}$ [arcsec]	(7)$d\theta_{tw}$*(OSF)* [arcsec]	(8)$d\theta_{main}$ [arcsec]	(9)Power law index	(10)$d\theta_s$ [arcsec]	(11)$d\theta_{main}$ [arcsec]
2012/4/10	4:29	2.64	0.61	0.33	0.07	0.02	0.57	-0.33	0.27	0.63
2012/4/10	4:48	2.66	0.62	0.34	0.08	0.02	0.57	-0.33	0.28	0.64
2012/4/10	6:32	2.69	0.87	0.32	0.08	0.02	0.85	-0.33	0.26	0.89
2012/4/10	7:10	2.59	0.65	0.28	0.08	0.02	0.66	-0.33	0.23	0.70
2012/4/10	8:32	3.28	0.55	0.22	0.07	0.04	0.61	-0.37	0.17	0.64
2012/4/10	8:52	2.54	0.63	0.25	0.08	0.02	0.67	-0.32	0.20	0.70
2012/4/10	9:11	1.90	0.55	0.27	0.08	0.01	0.57	-0.28	0.24	0.60
2012/4/10	9:30	2.09	0.67	0.28	0.08	0.01	0.68	-0.29	0.24	0.71
2012/4/10	9:54	2.55	0.66	0.30	0.06	0.02	0.65	-0.32	0.25	0.70
2012/4/10	10:12	3.00	0.54	0.28	0.08	0.03	0.55	-0.35	0.22	0.61
2012/4/12	0:02	2.01	0.67	0.17	0.08	0.01	0.75	-0.29	0.15	0.76
2012/4/12	0:39	2.19	0.52	0.25	0.08	0.02	0.56	-0.30	0.21	0.59
2012/4/13	23:23	4.11	0.59	0.27	0.07	0.06	0.61	-0.42	0.19	0.67
2012/4/14	0:01	4.16	0.40	0.34	0.09	0.06	0.39	-0.43	0.24	0.46
2012/4/14	0:19	4.48	0.47	0.29	0.08	0.07	0.47	-0.45	0.19	0.56
2012/4/14	2:39	4.10	0.63	0.17	0.08	0.06	0.71	-0.42	0.12	0.73
2012/4/14	2:57	2.96	0.81	0.16	0.07	0.03	0.88	-0.35	0.13	0.89
2012/4/14	3:15	1.69	0.35	0.26	0.07	0.01	0.39	-0.27	0.23	0.43
2012/4/14	3:34	1.66	0.32	0.30	0.08	0.01	0.39	-0.27	0.27	0.39
2012/4/14	23:24	2.91	0.74	0.25	0.07	0.03	0.77	-0.35	0.20	0.80
2012/4/14	23:42	2.52	0.57	0.22	0.07	0.02	0.63	-0.32	0.18	0.66
2012/4/15	0:19	1.85	0.43	0.29	0.08	0.01	0.43	-0.28	0.26	0.48
2012/4/15	23:43	4.29	0.52	0.30	0.08	0.06	0.51	-0.44	0.21	0.59
2012/4/16	0:02	3.85	0.41	0.29	0.08	0.05	0.41	-0.41	0.21	0.50
2012/4/16	0:21	3.26	0.68	0.50	0.09	0.04	0.39	-0.37	0.38	0.59
2012/4/16	0:44	2.82	0.55	0.59	0.11	0.03	0.40	-0.34	0.47	0.40
2012/4/16	1:02	3.59	0.70	0.45	0.09	0.04	0.50	-0.39	0.33	0.66
2012/4/16	1:20	3.30	1.01	0.59	0.08	0.04	0.70	-0.37	0.45	0.89
2012/4/16	2:34	1.83	0.70	0.33	0.07	0.01	0.67	-0.28	0.29	0.70
2012/4/16	2:53	3.25	0.60	0.44	0.09	0.04	0.39	-0.37	0.34	0.55
2012/4/16	3:11	3.57	0.51	0.38	0.08	0.04	0.39	-0.39	0.28	0.52
2012/4/16	3:33	3.65	0.69	0.45	0.08	0.04	0.49	-0.39	0.33	0.65
2012/4/16	3:51	2.79	0.67	0.41	0.06	0.03	0.53	-0.34	0.33	0.64
2012/4/21	5:42	3.30	0.58	0.41	0.08	0.04	0.39	-0.37	0.31	0.56
2012/4/21	7:38	2.52	0.88	0.39	0.09	0.02	0.80	-0.32	0.32	0.86
2012/4/21	7:57	3.63	0.66	0.37	0.09	0.04	0.58	-0.39	0.27	0.68
						Average	0.570			0.640
						Standard deviation	0.143			0.130
RSS of average and standard deviation ($\sqrt{\text{average}^2 + \text{standard deviation}^2}$)							**0.588**			**0.653**

7.2 Validation of New Correction Method of Optical Seeing

Table 7-18 Example of comparison between the measured pointing value ($d\theta_0^2$) and the random component [$2\times (d\theta_s^2 + d\theta_{tw}(OSF)^2)$] [see equation (7-2)] from the parameters of the ACA 7-m antenna No.1 [see line (1), (2), and (3) in Table 7-2].

		Saito et al. (2012)					This study	
(1)Date	(2)Start (UT)	(3)$d\theta_0$	(4)$d\theta_0^2$	(5)$d\theta_s$	(6)$d\theta_{tw}(OSF)$	(7)$2\times(d\theta_s^2+d\theta_{tw}(OSF)^2)$	(8)$d\theta_s$	(9)$2\times(d\theta_s^2+d\theta_{tw}(OSF)^2)$
2011/04/05	3:41	0.51	0.26	0.36	0.05	0.25	0.30	0.17
2011/04/05	4:09	0.38	0.14	0.30	0.07	0.17	0.25	0.11
2011/04/05	5:33	0.68	0.46	0.26	0.06	0.13	0.21	0.09
:	:	:	:	:	:	:	:	:

The validation of the time-dependence of the optical seeing derived from this study is described in this section. In Saito et al. (2012), there are 134 negative residuals in 458 datasets (about 29% of all measurements). There are negative residual values between the measured pointing value ($d\theta_0$) from the fluctuating components that change randomly day by day [$d\theta_s$ and $d\theta_{tw}$ (OSF)] (hereinafter random fluctuating components). The negative values occur as follows [see line (2) in Table 7-18],

$$d\theta_0{}^2 - 2\times d\theta_s{}^2 - 2\times d\theta_{tw}(OSF)^2 < 0, \qquad (7\text{-}2)$$

In this case, the residuals of the measured pointing value ($d\theta_0$) from the random fluctuating components [$(d\theta_s^2 + d\theta_{tw}(OSF)^2$] are assumed to be zero.

$$d\theta_0{}^2 - 2\times d\theta_s{}^2 - 2\times d\theta_{tw}(OSF)^2 = 0, \qquad (7\text{-}3)$$

and the referencing pointing performance of the ACA antenna is calculated by following equation instead of the equation (7-1),

$$d\theta_{main} = sqrt[d\theta_{tw}(AOS)^2 + d\theta_{mr}{}^2 + d\theta_{sr}{}^2 + d\theta_{se}{}^2]. \qquad (7\text{-}4)$$

Table 7-19 Comparison of the number of negative residual measured pointing values in all measurement result each ACA 12-m antenna and 7-m antenna between this study and Saito et al. (2012).

Antenna	No.	The number of measurement	The number of negative residuals	
			This study	Saito et al.(2012)
7m antenna	1	24	0	2
	2	24	3	7
	3	25	3	3
	4	26	5	11
	5	41	12	19
	6	30	10	19
	7	29	8	13
	8	29	3	9
	9	31	6	8
	10	27	8	11
	11	31	2	12
	12	30	0	4
12m antenna	1	24	0	2
	2	27	1	3
	3	24	0	2
	4	36	2	9
Total		458	63	134

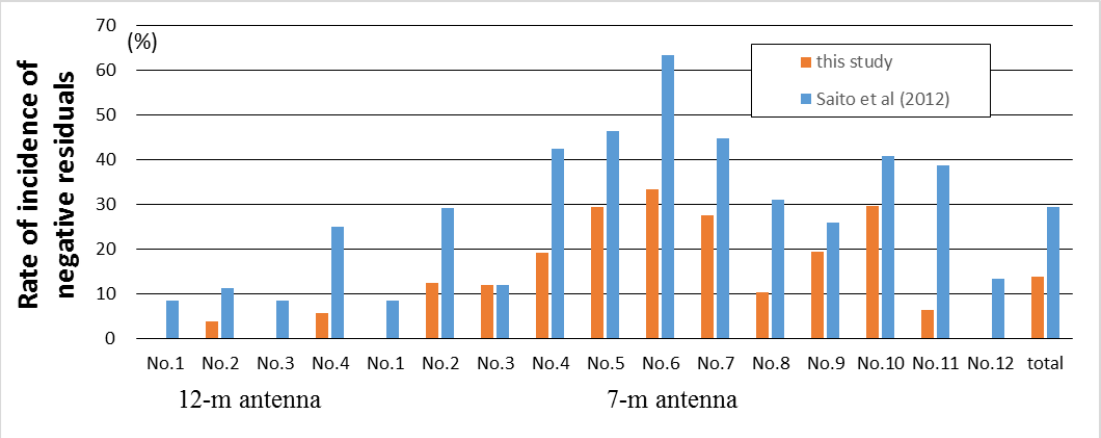

Figure 7-1 Rate of incidence of a negative residuals of all measurements for the ACA antennas.

As mentioned in Section 3, the negative residuals may be caused by an overestimation of the optical seeing by correction method with the time-dependence from Kolmogorov PSD as equation (3-12). In this study, the number of negative residuals is improved from 134 in 458 datasets (about 29%) to be 63 datasets (about 14%) (see Table 7-19, Figure 7-1) when the optical seeing is corrected by the new correction method [see equation (3-15)]. This result indicates that the new correction method of the optical seeing derived from this study may be valid for the verification of the referencing pointing performance of the ACA antennas.

There are two possible interpretations of the negative residuals. One possible interpretation is that the contribution of different weather conditions (For example, wind velocity, opacity) between the referencing pointing measurement and the optical seeing measurement (see Section 2). The optical seeing component in the measured pointing value and the measured optical seeing may be different from in wind and atmospheric opacity conditions. The effect of different wind condition between the referencing pointing measurement and the optical seeing measurement is described below. As mentioned in Section 2, the pointing jitter due to wind load at the OSF is estimated by the difference in wind velocity between the OSF and the AOS as follows [see equation (2-2)],

$$\begin{aligned} d\theta_{\mathrm{tw}}[V(measure)] &= d\theta_{\mathrm{tw}}(AOS) \times [V(measure)/V(AOS)]^2/[\mathrm{P(AOS)/P(OSF)}] \\ &= 0.32 \times [V(measure)/9.5]^2/0.75 \\ &= 0.00472760849492151 \times V(measure)^2 \\ &\approx 0.005 \times V(measure)^2, \qquad (7\text{-}5) \end{aligned}$$

where $d\theta_{\mathrm{tw}}$ *(AOS)* is the pointing jitter due to wind load at the AOS, *V (measure)* is wind velocity during the measurement of the pointing performance at the OSF, *V(AOS)* is the maximum wind velocity, 9.5 m/s, for nighttime under the primary operating condition at the AOS (see Table 1-1), and P (AOS)/ P(OSF) = 0.75 is the atmospheric pressure ratio at the AOS to the OSF. The residual between the measured pointing value and the optical seeing assumes that it is caused only by the difference between the wind velocity at the referencing pointing measurement [*V (pointing)*] and wind velocity at the optical seeing measurement [*V (seeing)*]. In this case, the residual by wind velocity discrepancy [$d_{\mathrm{residual}}(V)$] relates to *V (pointing)* and *V (seeing)* as follows,

$$
\begin{aligned}
d\theta_0{}^2 - 2 \times d\theta_s{}^2 &= d_{\mathrm{residual}}(V) \\
&= 2 \times \{ d\theta_{\mathrm{tw}}[V(pointing)]^2 - d\theta_{\mathrm{tw}}[V(seeing)]^2 \} \\
&\approx 2 \times 0.00002235 \times [V(pointing)^4 - V(seeing)^4] \\
&\approx 0.00004 \times [V(pointing)^4 - V(seeing)^4]. \qquad (7\text{-}6)
\end{aligned}
$$

If the residual depends only the difference in wind velocity between two measurements, the wind velocity at the optical seeing measurement is smaller than the wind velocity for the referencing pointing measurement [*V(seeing)* > *V(pointing)*], and thus, one obtain a negative residual ($d_{\mathrm{residual}}(V) < 0$). In the case of the negative residual caused by wind velocity difference, the relation between the wind velocity for the referencing pointing measurement *V (pointing)* and wind velocity for the optical seeing measurement *V (seeing)* is shown in Figure 7-2. The maximum, average, and minimum of the absolute value of the negative residual caused by a difference in wind velocity [$d_{\mathrm{residual}}(V)$] are -0.426, -0.092, and -0.007 arcsecs, respectively. In Figure 7-2, in order for the difference in wind velocity to cause a residual of -0.092 arcsecs, the wind velocity for the optical seeing measurement must always be at least 6.6 m/s. This is independent of the wind velocity for the referencing pointing measurement. This wind condition is not realistic at the OSF because all measured wind velocities at the referencing pointing measurement at the OSF are less than 6.6 m/s in Saito et al. (2012). In addition, in order for difference in wind velocity to become -0.007 arcsecs, the wind velocity for the optical seeing measurement must always be at least 3.5 m/s; independent of the wind velocity at the referencing pointing measurement. The number of the measurements in Saito et al. (2012), that the recorded a wind velocity faster than 3.5 m/s, are seen on 82 in 458 datasets (about 18% of all measurements). Therefore, it is considered that the contribution to negative residual from the differences in wind conditions between two measurements is very small.

Another possible interpretation involves the contribution of the factor of 2 in the random fluctuating components in equation (2-1). As mentioned in Section 2, the measured pointing value with the OPT is estimated by the RMS of all relative positions between the reference position (the first measured centroid position) in Saito et al. (2012). In order to estimate the referencing pointing performance of the ACA, the random fluctuating components must be subtracted from the measured pointing value. The reference position (the first measured centroid position) has an offset from the true average of the random fluctuating components (see Figure 2-5), and this offset must also be subtracted from the measured pointing value. However, the random fluctuating components in any time are unknowable value and is not easy to be derived.

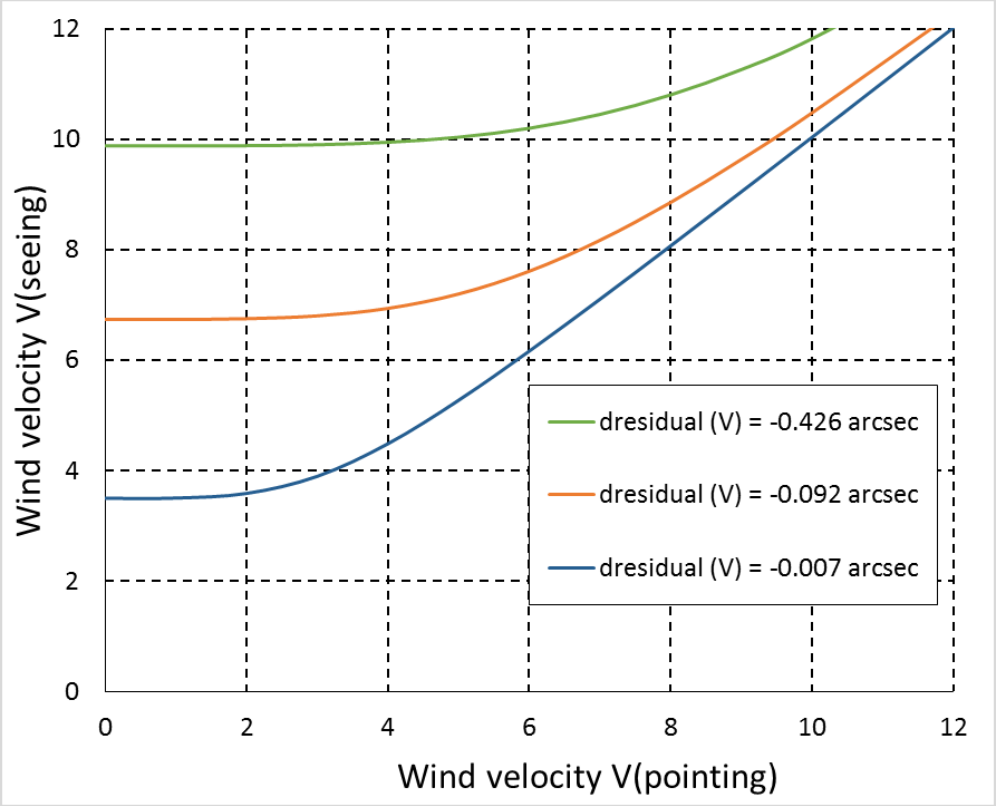

Figure 7-2 Relation between the wind velocity at the referencing pointing measurement *V (pointing)* and wind velocity at the optical seeing measurement *V (seeing)* in the case of the negative residual by wind velocity difference [$d_{\mathrm{residual}}(V) < 0$]. -0.426, -0.092, and -0.007 is maximum, average, minimum of an absolute value of negative residuals by wind velocity difference [$d_{\mathrm{residual}}(V)$] in this study.

Therefore, the offset between the position and true average of the random fluctuating components (d_{offset}) cannot be measured. In Saito et al. (2012), the random fluctuating components is substituted for this offset. The measurement of the referencing pointing is performed more than 24 times for each of the ACA antennas. It is assumed that the average value of the offset of all measurements is comparable to the standard deviation of the random fluctuating components in Saito et al. (2012). Consequently, the random fluctuating components must be subtracted twice from the measured pointing value as follows,

$$d\theta_0{}^2 - d_{\mathrm{offset}}{}^2 - d\theta_{\mathrm{s}}{}^2 - d\theta_{\mathrm{tw}}(OSF)^2 = d\theta_0{}^2 - 2 \times d\theta_{\mathrm{s}}{}^2 - 2 \times d\theta_{\mathrm{tw}}(OSF)^2 \quad (7\text{-}7)$$

where d_{offset} is the offset between the reference position. In Saito et al. (2012), it is assumed that $d\theta_{\mathrm{s}}{}^2 + d\theta_{\mathrm{tw}}(OSF)^2 \sim d_{\mathrm{offset}}{}^2$, making this value a true average of the random fluctuating components. However, in the case of a smaller offset, the calculation with equation (7-7) may underestimate the residual, and the residual may become negative (see Figure 7-3). This is the case shown in Figure 7-3, where the residual between the measured pointing value and the random fluctuating components becomes negative [see equation (7-2)]. In this study, the measured pointing value without offset [$d\theta_0$ *(no offset)*] is proposed. Here, the measured pointing value without offset is calculated from the reference position as the average of all centroid positions (see Figure 7-4). In the measured pointing value, the systematic pointing error due to the ACA antenna is smaller than the random fluctuating components. The average of all centroid positions and the true average of the random fluctuating components are regarded as approximately equal values as follows,

$$d\theta_0(no\ offset)^2 \approx d\theta_0{}^2 - d_{\mathrm{offset}}{}^2. \qquad (7\text{-}8)$$

Figure 7-5 shows the comparison between the random fluctuating components and the offset which is differences between first measured centroid position and average of all measured centroid positions. In Figure 7-5, it can be seen the offset between the first measured centroid position and average of all measured centroid positions relates to the measured pointing value rather than the random fluctuating components. It can be concluded that equation (7-8) is more valid for the verification of the ACA antenna, when compared to the equation derived from the assumption in Saito et al. (2012) ($d\theta_{\mathrm{s}}{}^2 + d\theta_{\mathrm{tw}}(OSF)^2 \sim d_{\mathrm{offset}}{}^2$). The residuals of the ACA 7-m antennas No.1 to No.4 are calculated using four calculation methods: i) Calculation with equation (7-2) according

to Saito et al. (2012), ii) Calculation with the new correction method of the optical seeing [see equation (3-15)] as follows,

$$\text{residual} = {d\theta_0}^2 - 2 \times \left(d\theta_{\text{s measure}} \times \frac{5^{-0.16-0.06\times V_{\text{wind}}}}{1^{-0.16-0.06\times V_{\text{wind}}}} \times \frac{\left[sin(El_{\text{seeing}})\right]^{0.5}}{\left[sin(El_{\text{pointing}})\right]^{0.5}} \right)^2 - 2 \times d\theta_{\text{tw}}(OSF)^2, \quad (7\text{-}10)$$

iii) Calculation with the measured pointing value without offset as follows,

$$\text{residual} = d\theta_0(no\ offset)^2 - \left(d\theta_{\text{s measure}} \times \frac{5^{-0.2}}{1^{-0.2}} \times \frac{\left[sin(El_{\text{seeing}})\right]^{0.5}}{\left[sin(El_{\text{pointing}})\right]^{0.5}} \right)^2 - d\theta_{\text{tw}}(OSF)^2, \quad (7\text{-}11)$$

and iv) Calculation with both new correction method using the optical seeing and measured pointing value without offset as follows,

$$\text{residual} = d\theta_0(no\ offset)^2 - \left(d\theta_{\text{s measure}} \times \frac{5^{-0.16-0.06\times V_{\text{wind}}}}{1^{-0.16-0.06\times V_{\text{wind}}}} \times \frac{\left[sin(El_{\text{seeing}})\right]^{0.5}}{\left[sin(El_{\text{pointing}})\right]^{0.5}} \right)^2 - d\theta_{\text{tw}}(OSF)^2. \quad (7\text{-}12)$$

The number of negative residuals for the ACA 7-m antennas No.1 to No.4 from the above four calculation methods are (i) 24 in 99 datasets, (ii) 11 in 99 datasets, (iii) 17 in 99 datasets, and (iv) 2 in 99 datasets, respectively (see Table 7-20). It was confirmed that the contributions to negative residuals from both the new correction method of the optical seeing and the measured pointing value without offset are large. Finally, a large part of the factors of the negative residuals is resolved in this study.

The referencing pointing performance with the measured pointing value without offset [$d\theta_{\text{main}}$ *(no offset)*] is, instead of equation (2-1), represented by

$$d\theta_{\text{main}}(no\ offset) = sqrt\{d\theta_0(no\ offset)^2 - \left(d\theta_{\text{s measure}} \times \frac{5^{-0.16-0.06\times V_{\text{wind}}}}{1^{-0.16-0.06\times V_{\text{wind}}}} \times \frac{\left[sin(El_{\text{seeing}})\right]^{0.5}}{\left[sin(El_{\text{pointing}})\right]^{0.5}} \right)^2 - d\theta_{\text{tw}}(OSF)^2 + d\theta_{\text{tw}}(AOS)^2 + {d\theta_{\text{mr}}}^2 + {d\theta_{\text{sr}}}^2 + {d\theta_{\text{se}}}^2)\}. \quad (7\text{-}13)$$

It is confirmed that the referencing pointing performance of the ACA 7-m antennas No.1 to No.4 with the new correction method of the optical seeing and the measured pointing value without offset meet the technical specification of the ALMA (referencing pointing performance of 0.6 arcsecs) (see Table 7-21).

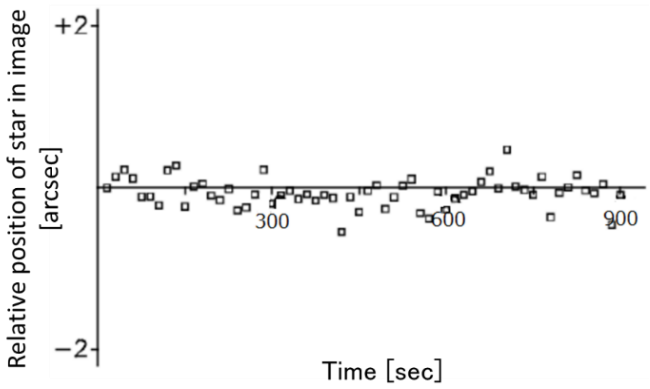

Figure 7-3 Example of measured centroid positions with a small offset. The residual between the measured pointing value and the random fluctuating components becomes negative in this case.

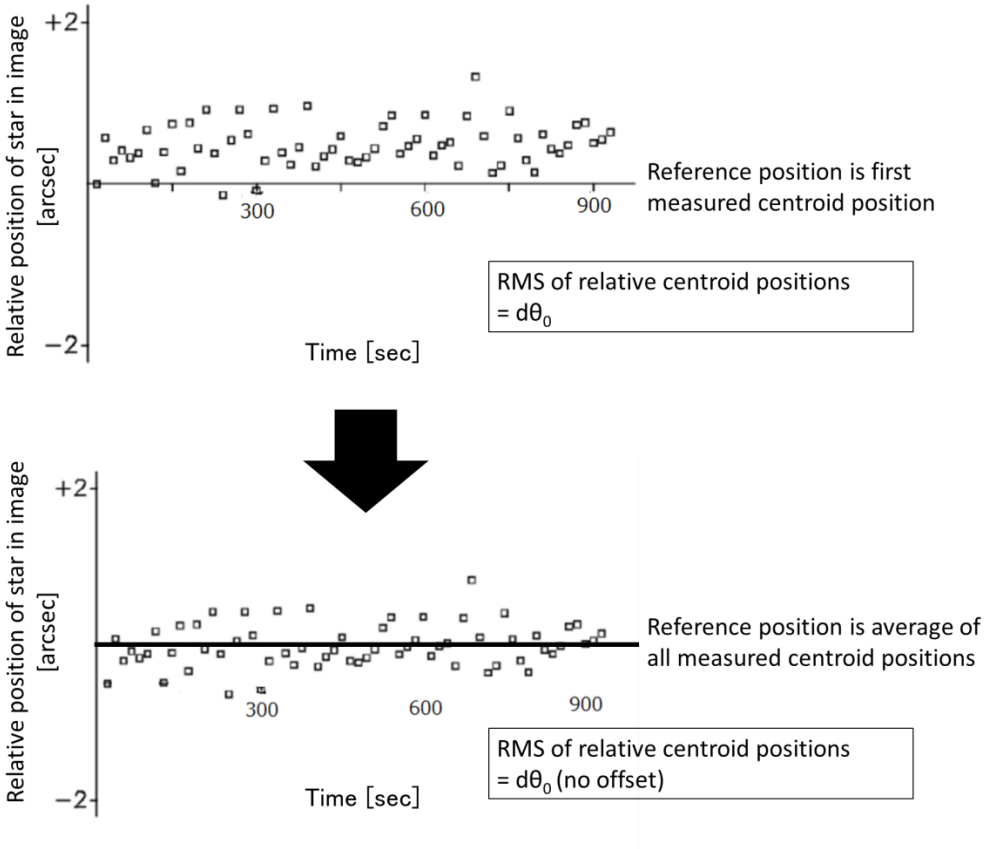

Figure 7-4 Conceptual diagram of calculation of the measured pointing value without offset between first measured centroid position and average of random fluctuating components [$d\theta_0$ (no offset)].

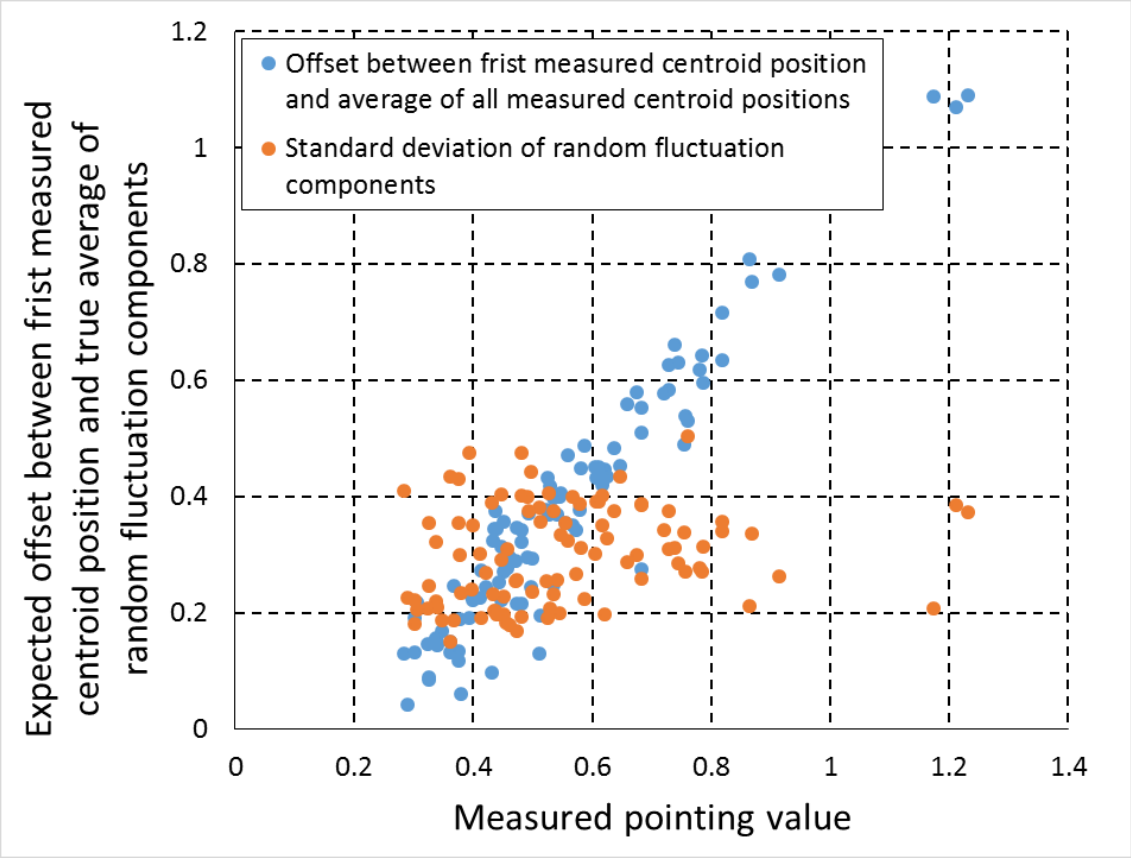

Figure 7-5 Expected offset values between first measured centroid position and true average of random fluctuating components. This offset is expected as the offset which is differences between first measured centroid position and average of all measured centroid positions in this study. This offset is expected as the standard deviation of random fluctuating components in Saito et al. (2012).

Table 7-20 The number of negative residual measured pointing values of the of the ACA 7-m antennas No.1 to No.4 with four calculation methods; i) calculation with equation (7-2) according to Saito et al. (2012), ii) calculation with the new correction method of the optical seeing [see equation (7-10)], iii) calculation with the measured pointing value without offset [see equation (7-11)], iv) calculation with both new correction method of the optical seeing and measured pointing value without offset [see equation (7-12)].

Antenna	No.	The number of measurement	The number of negative residuals			
			Saito et al.(2012)	This study		
			(i)	(ii)	(iii)	(iv)
7m	1	24	3	0	0	0
antenna	2	24	7	3	6	1
	3	25	3	3	2	0
	4	26	11	5	9	1
total		99	24	11	17	2

Table 7-21 Referencing pointing performances of the ACA 7-m antennas No. 1, No. 2, No. 3, and No. 4.

Antenna	No.	Referencing pointing performance [arcsec]	
		This study[10]	Saito et al.(2012)
7m antenna	1	0.485	0.530
	2	0.490	0.550
	3	0.504	0.555
	4	0.500	0.578

[10] Referencing pointing performance calculated with both the new correction method of the optical seeing and the measured pointing value without offset [see equation 7-13]

7.3 Physical Interpretation of New Relation between Optical Seeing and Wind Velocity

The physical interpretation of the new relations between the optical seeing and the wind velocity derived in Section 3 [see equation (3-12) and equation (3-14)] is discussed. If an outer scale of the phase structure function [Dφ(r)] of the Kolmogorov model of turbulence is larger than the observation scale (d_{obs}), it can become an aperture size of the telescope (d_{apeture}) (Section 3.1) and the observed optical seeing (RMS of centroid positions) will be dominated by the aperture size. However, an astronomical telescope observes light emitted from a star, which passes through turbulence in the atmosphere. This turbulence behaves as a frozen flow according to the Taylor's hypothesis [29]. In the case that the condition does not change time the observation scale of the telescope corresponds to the aperture of the telescope, 100 mm in this study. In this case, the observation result of the optical seeing with the OPT is described by the Kolmogorov model of turbulence, and the RMS of centroid positions is suggested to follow time-dependence of the Kolmogorov model of turbulence [see equation (3-4)] as mentioned above. When $V_{\mathrm{wind}} \times t >> d_{\mathrm{apeture}}$ or $d_{\mathrm{apeture}} << L$, as mentioned in equation (3-12), the observation scale of the telescope (d_{obs}) corresponds to the product of the wind velocity (V_{wind}) and the integration time (t) of the telescope (see Figure 7-6) as follows.

$$d_{\mathrm{obs}} = V_{\mathrm{wind}} \times t. \qquad (7\text{-}14)$$

In the case of the observation scale being smaller than the outer scale of eddy in turbulence ($L > d_{\mathrm{obs}}$) by low wind velocity and/or short integration time, the telescope observes a single turbulent eddy with the outer scale of L, and the observation result of the optical seeing with the OPT is also described with the Kolmogorov model of turbulence as mentioned above. Therefore, the RMSs of centroid positions obey the power law relationship as equation (3-4). On the other hand, in the case of the observation scale being larger than the outer scale of eddy in turbulence ($L < d_{\mathrm{obs}}$) by high wind velocity and/or long integration time, the observation scale may include multiple eddies. The RMSs of centroid positions from the multiple eddies case (σ_{m}) may be smaller than RMSs of centroid positions in a single eddy case (σ_0). For simplification, it is assumed that the telescope observes two independent eddies in turbulence that generate the same RMS of centroid positions. The RMS of centroid positions from the one eddy and the other eddy is σ_1 and σ_2, respectively. The measured RMS of centroid

positions (σ_m) through these two eddies in turbulence is considered as the standard error of σ_1 and σ_2 as follows,

$$\sigma_m = \frac{\sqrt{\sigma_1^2+\sigma_2^2}}{2} \qquad (7\text{-}15)$$

In the case of $\sigma_1=\sigma_2=\sigma_0$,

$$\sigma_m = \frac{\sqrt{\sigma_1^2+\sigma_2^2}}{2} = \frac{\sqrt{2}\sigma_0}{2} = \frac{\sigma_0}{\sqrt{2}} < \sigma_0 \qquad (7\text{-}16)$$

Therefore, the RMSs of centroid positions in the multiple eddies cases (σ_m) are smaller than the RMSs of centroid positions in single eddy case (σ_0). In the case that the integration time is longer and longer, the observation scale becomes larger and larger, and the amount of eddy included in the observation scale increases. If the observation scale includes *n* eddies, the measured RMS of centroid positions (σ) is

$$\sigma = \frac{\sqrt{\sum \sigma_n^2}}{n} \qquad (7\text{-}17)$$

The RMS of centroid positions decreases with increasing n over a long integration time. In this case, the power law index will be larger than -0.17, that is the index of time-dependence derived with the Kolmogorov model of turbulence [see equation (3-4)]. In summary, in the case of observation scale smaller than the outer scale of eddy in turbulence ($L > d_{obs}= V_{wind} \times t$), the RMS of centroid positions obeys the power law relationship of time-dependence from the Kolmogorov model of turbulence. On the other hand, in the case of observation scale larger than the outer scale of eddy in turbulence ($L< d_{obs}= V_{wind} \times t$), the RMS of centroid positions decreases steeper than the power law relationship from Kolmogorov PSD [see (Figure 7-6)].

The turnover arises on a border between the two cases. The integration time of turnover (t_{turn}) is estimated from the wind velocity (V_{wind}) and the observation scale equal to the outer scale ($d_{obs} = L$) as follows,

$$t_{turn} \cong \frac{L}{V_{wind}} \qquad (7\text{-}18)$$

If the outer scale is constant, the integration time of an arising turnover is determined solely by wind velocity. In the case of the high wind velocity, the turnover arises at

short integration time side. On the other hand, in the case of the low wind velocity, the turnover arises at long integration time side. This result is likely to the measurement results of the RMSs of centroid positions in this study as shown in Figure 3-7, Figure 3-8, Figure 3-9, and Figure 3-10. From these measurement results, the turnover is likely to arise at the integration time of about one second (see Figure 3-7, Figure 3-8, Figure 3-9, and Figure 3-10). The value of the RMS of centroid positions at the integration time of five seconds is changed by the turnover integration time. The power law index can be considered as the difference between the RMS of centroid positions at the integration time of one second and five seconds. Therefore, the power law index of the RMS of centroid positions in the integration time of 1 to 5 seconds depends on wind velocity (see Figure 7-7). Finally, the relation of the optical seeing with the wind velocity [see equation (3-14)] can have a physical meaning. On the other hand, the wind attacking angle, the ambient temperature, and the opacity do not relate to the power law index because these three parameters do not change the observation scale at long integration time.

In this study, furthermore, the outer scale of the Kolmogorov model of turbulence at the OSF is discussed below. The outer scale (L) can be estimated from the wind velocity and integration time arising turnover [see equation (7-18)]. In the case of the wind velocity of about 3 m/s, the turnover arises at the integration time of about one second in this study. Therefore, the outer scale of the OSF is estimated at about 3 m. This outer scale agrees with that reported in the previous research [32].

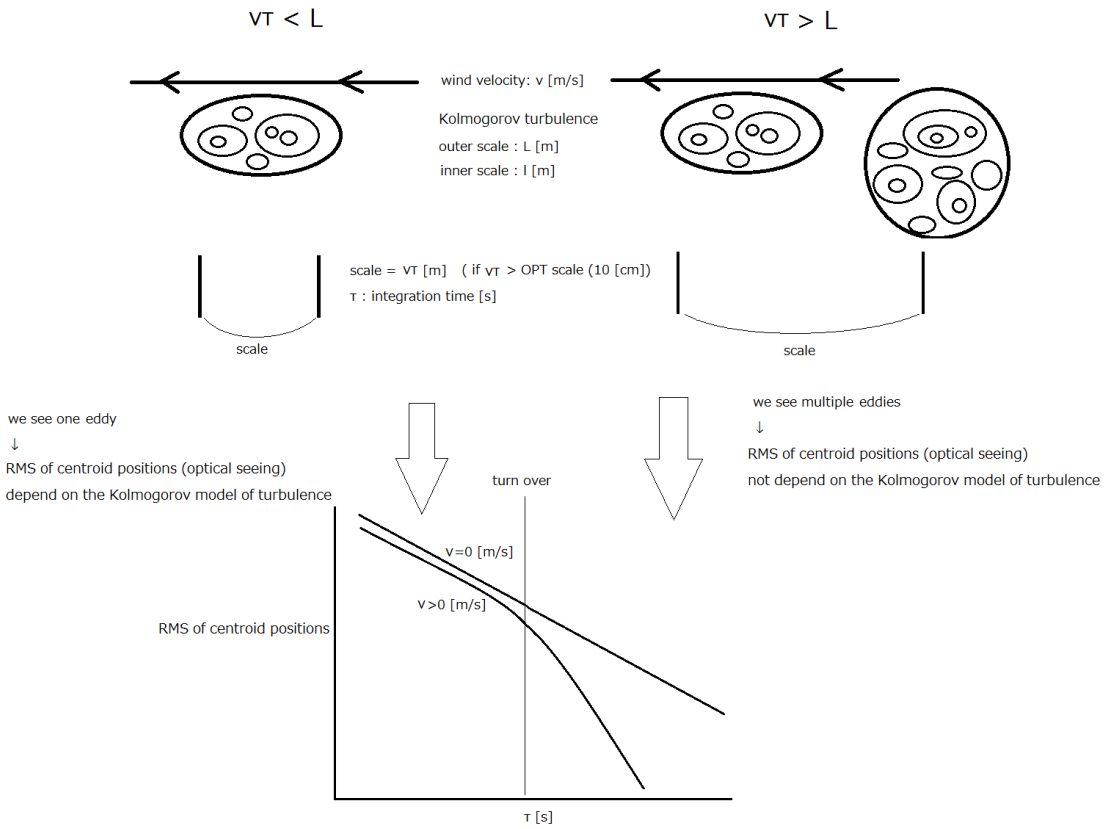

Figure 7-6 Conceptual diagram of the relation between the RMS of centroid positions and the integration time by changing the observing scale of the OPT.

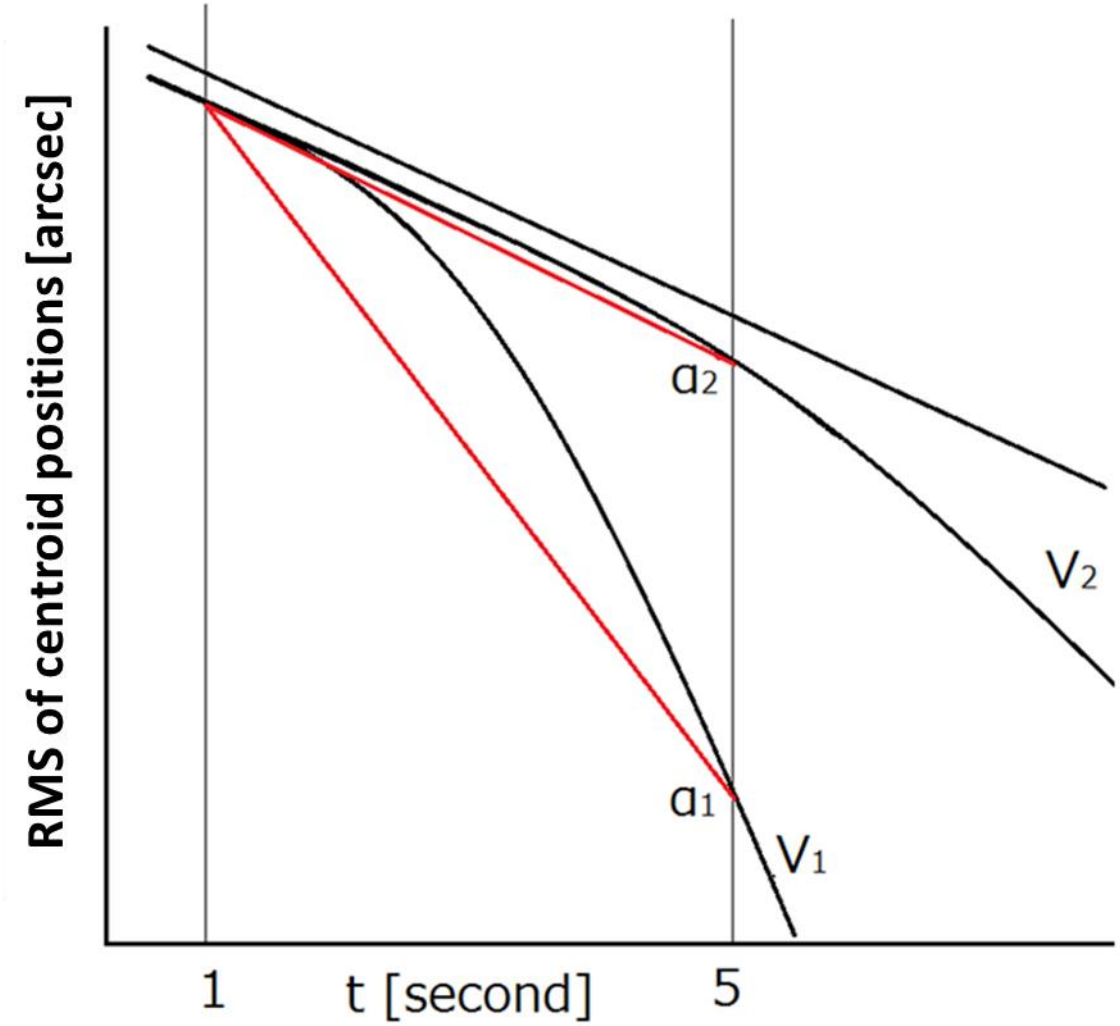

Figure 7-7 Conceptual diagram of changing power law indices with the integration time arising turnover by various wind velocities (V_1, and V_2, V_1>V_2).

8 Conclusion

8.1 Conclusion and Summary

This study reports the detailed verification measurement method of various components, including the referencing pointing performance of the ALMA ACA antennas. Additionally, the physical interpretation of the referencing pointing performance is reported.

In Section 1, some key scientific and system requirements for the ALMA ACA antenna are introduced. The pointing errors, which is the angular deviation of the peaks of the antenna response from the actual target locations, give a gain loss (e.g. gain loss is 50% when 1/2 of HPBW) in the observation sensitivity and then a decline in the image fidelity. The ALMA ACA antenna requires a high referencing pointing performance, which shall not exceed 0.6 arcsecs under the primary ALMA operating conditions. The referencing pointing performance is the accuracy of the relative positions of the star from the reference position (first measured position of the star) during the observation. The referencing pointing performance of the ALMA ACA antenna has been verified with an optical pointing telescope (OPT). To measure the referencing pointing performance of the ALMA ACA antenna, the undesirable effects, for example, troposphere, must be subtracted from the measured pointing values.

In Section 2, the measurement method of the referencing pointing performance in the previous research of Saito et al. (2012) is introduced. The referencing pointing performance of the ALMA ACA antenna is measured by the root mean square (RMS) of the differences between the first centroid position (as a reference position) and next time-variation centroid positions of the star in the images from the OPT that was mounted in the backup structure of the ALMA ACA antennas. To verify the referencing pointing performance of the ALMA ACA antenna, the unexpected components due to the optical seeing and wind load at the Operations Support Facility (OSF) must be estimated and then subtracted from the measured pointing values with the OPT. Additionally, the components due to sub reflector, the main reflector metrology system, the wind load at the Array Operation Site (AOS), and the servo error must be added to the measured pointing values. The measurement of the referencing pointing performance reproduces a typical observation of the ALMA.

In Section 3, the derivation of the new correction method of the optical seeing is described. The contribution to the measured pointing values of the optical seeing is significant in the case of the short integration time of the OPT. Therefore, the optical

seeing component was measured with the OPT under the several integration times, in which added one second shorter than that the referencing pointing measurement (five seconds). In Saito et al. (2012), the optical seeing was corrected with the relation of time-dependence from Kolmogorov power spectrum density (PSD) shown in Ukita et al. (2008). Ukita et al. (2004), however, did not derive it in theory. In this study, the time-dependence of the optical seeing with the Kolmogorov model of turbulence was derived in theory, finaly giving us $t^{-0.17}$. On the other hand, it is known that the correction method by the time-dependence from Kolmogorov PSD overestimates the corrected optical seeing at the integration time of five seconds. In this study, to resolve this issue, the time-dependence from Kolmogorov PSD, specifically in the integration time of 1 to 5 seconds, with some weather parameters (wind velocity, wind attacking angle, ambient temperature, and opacity) had been investigated by using multiple regression analysis. The results of this multiple regression analysis indicate that the wind velocity is more strongly correlated with the time-dependence of Kolmogorov PSD. Finally, the new correction method of the optical seeing, including the wind velocity was derived.

In Section 4, the investigation of the servo error is described. The servo error is measured as the time-variable differences between the readout angles measured by the angular resolver connected to the antenna control unit (ACU) and the angles commanded by the antenna bus master. In this study, two measurements were performed: the ACU checking measurement and the servo measurement. The purpose of the ACU checking measurement was to check the readout of the angles with the angular resolver connected to the ACU. This was carried out by measuring the time-variable differences between the readout angles, which were measured by the angular resolver and the ideal angles during constant velocity rotation. The results of ACU checking measurement indicate no significant problem in the measurement of angles by the angular resolvers. The purpose of the servo measurement was to investigate the contribution of the RMS of servo error to the referencing pointing performance. The RMS of the servo error were measured with various constant rotational velocities (Az 2 to 0.000002 deg/s, El 0.2 to 0.000002 deg/s) in 210 seconds. The results of the servo measurement show that the RMSs of the servo error were less than 0.1 arcsecs. Additionally, it was found that the contribution of the RMS of the servo error to the referencing pointing performance (0.6 arcsecs) was small, although the RMS of servo error increased to 0.9 arcsecs at low rotational velocities (rotational velocity of 0.000005 to 0.00005 deg/s).

In Section 5, the investigation of Az and El dependencies on the optical seeing

of the OSF is described. As a result of the measurements of the optical seeing at over 100 directions in the sky, it was revealed that the El dependence of optical seeing corresponding to theoretically predicted dependence as sin (El) $^{-0.5}$ was derived from the Kolmogorov model of turbulence. Furthermore, the correction for the El angle dependence makes the common characteristics of the two measurement results become less prominent. It was considered that the RMSs of centroid positions did not depend on the Az angle at the OSF.

In Section 6, investigating the pointing performance during the settling time after fast switching with the angular resolver is described. The verification tests confirmed that the pointing performance during the settling time after the fast switching of the ALMA ACA 7-m antenna No. 12 met the technical specification of the ALMA antenna. Furthermore, it is confirmed that there were no directional biases in the ALMA ACA antennas.

In section 7, the referencing pointing performance of the ALMA ACA antenna in this study and validation of the new correction method of the optical seeing for the ALMA ACA antenna are described. According to Saito et al. (2012), the residuals between the measured value and the random fluctuating components, which randomly change from the measurement date (for example, the optical seeing) had been estimated, then the 134 in 458 datasets (about 29%) in all measurements became negative. By using the new correction method, the negative residuals were improved as 63 in 458 (about 14%). As mentioned in Section 3, the new relationship between the optical seeing and the wind velocity, $t^{-0.17}$, was also derived in theory from the Kolmogorov model of turbulence under that the observation scale of the OPT is smaller than the outer scale of eddy in the turbulence. In addition, the OPT measurement results showed the relation of $t^{-(0.16\pm0.05)-(0.06\pm0.02)\times V_{\mathrm{wind}}}$ at a wind velocity (V_{wind}). When V_{wind} is too small, the relation can be replaced as of $t^{-(0.16\pm0.05)}$. This good matching between the theory and measurement result indicates that the new optical seeing correction method was valid for verifying the referencing pointing performance of the ALMA ACA antennas. As a result of the investigation of the 63 negative residuals, it was found that the residuals become negative by the uncertainty of the offset between the first measured centroid position (as a reference position) and the true average of the random fluctuating components. In this study, the random fluctuating components were dominant in the pointing measurements results, and then it was concluded that the average of all centroid positions and the true average of the random fluctuating components were regarded as approximately equal values. Consequently, a large part of the negative residuals were resolved in this study. Furthermore, with the new correction

method of the optical seeing and by using the measured pointing values without the offset from the reference position, it was confirmed that the referencing pointing performance of the ALMA ACA antennas No. 1, No. 2, No. 3, and No. 4 meet the technical specification of the ALMA (referencing pointing performance of 0.6 arcsecs) and also the negative residuals were reduced to a few %..

Finally, it is concluded that the referencing pointing performance of the ALMA ACA antenna was verified with a higher reliability than that which was shown in previous research of this study.

8.2 Future Works

Three future works of extending this study are described in this section. The first one is to cover a wider range of weather condition. In this study, the relation between the optical seeing and the wind velocity is derived when the wind velocity is in the range of 1 to 4 m/s. However, the maximum wind velocity in the measurement of the referencing pointing by Saito et al. (2012) reached 6.3 m/s taken at UT 7:23 to 7:38, October 10, 2011, with the ACA 7-m antenna No. 7 [see the line (22) in Table 7-8]. In order to check the new relation at high wind velocity, the measurement of the optical seeing should be performed under the condition of high wind velocity (4 to 6.3 m/s). In the case of very high wind velocity, the pointing jitter due to wind load at the OSF becomes significant (For example, the pointing jitter due to wind load becomes 0.32 arcsec with wind velocity of about 8 m/s at the OSF). Ambient wide range thermal load is also to be covered by measuring the ambient temperature in the evening to investigate the effect of solar radiation in the daytime. The second future work is to investigate the turnover in short integration times (1/20 to 1/10 seconds) (see Figure 3-7, Figure 3-8, Figure 3-9, and Figure 3-10). In case of short integration times, $V_{\mathrm{wind}} \times t$ is smaller than d_{apeture} and the observation scale is only dominated by d_{apeture} as mentioned in equation (3-12) ($d_{\mathrm{obs}} = d_{\mathrm{apeture}}$). Therefore, the optical seeing and integration time are no correlation and the optical seeing may become flat in very short integration times. The third future work is to investigate the turnover in long integration times (10 to 50 seconds). In the case of the long integration time, a turnover arises in the optical seeing relation, and the RMS of centroid positions is close to the power law relationship from Kolmogorov PSD [see equation (3-12)] (see Figure 3-10). It is important to cover wind range the measurement of the RMS of centroid positions to investigate this turnover. One possible interpretation is randomization of the turbulences in the large observing scale at long integration time. In the case of long integration time, the observing scale becomes very large. The large observing scale may include a lot of turbulences. The light passing through the Kolmogorov model of turbulence is refracted randomly by a lot of eddies smaller than outer scale in the turbulence, and the RMS of centroid positions from the refracted light indicates the power law relationship. The RMS of centroid positions measured at the large observing scale may also indicate the power law relationship by the light refracted randomly by a lot of turbulence.

8.3 Suggestions

The two suggestions for the future referencing pointing verification from the results of this study are described. The first suggestion is to investigate the servo error at the first step of the pointing verification. The second suggestion is to characterize the optical seeing as a function of integration time with OPT. Since the optical seeing accounts for a large portion of the measured pointing value, it is important to estimate the component of the optical seeing with high accuracy. The optical seeing may relate to the environmental conditions (For example, the wind) that change in a short time scale. It is important to investigate the relation between the optical seeing and the environmental conditions.

Acknowledgments

I am grateful to the many people who have contributed, directly and indirectly, to this dissertation and my research life.

First, I am deeply grateful to Prof. Satoru Iguchi, my main supervisor, for his passionate guidance, helpful advice, many suggestions, and psychological support. My deep thanks also go to Dr. Masao Saito, my sub-supervisor, for many comments and suggestions. He has supported the research, the journey, and daily life in Santiago and the ALMA OSF in Chile. I would like to thank Prof. Noriyuki Kawaguchi, Dr. Satomi Shimojo, and Dr. Yoshiaki Hagiwara, my sub-supervisors, for helpful advice on research and coursework.

I am indebted to Dr. Koichiro Nakanishi, my collaborator in the study of pointing performance, for many suggestions on the writing of a dissertation. I would like to thank Hiro Saito, Takahiro Naoi, and Yasuhiro Kato for their essential support with measuring the pointing performance in Chile. I want to thank Norikazu Mizuno, Junji Inatani, Hajime Ezawa, and all members of the ALMA antenna team, for their support in the measurement efforts in the ALMA OSF, Kengo Tachihara for lending a high performance machine, and George Kosugi for comments about optical seeing.

I would like to thank Kenichi Tatematus and Daisuke Iono for many insightful suggestions and much helpful advice on the writing of this dissertation. I want to thank Sachiko Okumura and Yasutaka Kurono for their guidance on using the interferometer and the ALMA antennas.

I am indebted to Keiichi Asada, Juan-Carlos Algaba-Marcos, Masanori Nakamura, my collaborators in research on active galactic nuclei in the ACADEMIA SINICA Institute of Astronomy and Astrophysics, for their guidance and suggestions about scientific research, as well as about daily life in Taipei. I want to thank Paul Ho, Satoki Matsushita, Makoto Inoue, and the entire staff of ASIAA for the trip to ASIAA, and all participants in the ASIAA Summer Student Program 2012 and all graduate students of ASIAA for their kind help and cooperation in Taipei.

I would like to thank Shinichiro Asayama for his reliable support in the ALMA OSF and help with recreation in a foreign country, Takeshi Okuda for his support in ASTE and San Pedro de Atacama, Shinya Komugi, Tsuyoshi Sawada, and Joaquin Collao for the trip and support in the ALMA OSF, Tetsuo Hasegawa, Ryusuke Ogasawara, Takahiro Yamaguchi, Kurazo Chiba, Ryohei Kawabe, Lars Nyman, the staff of the Joint ALMA Office, and the staff of the NAOJ Chile Observatory for the trip, their support, and help with daily life in Santiago Chile.

I would like to thank Tetsuhiro Minamidani, Yusuke Miyamoto, Atsushi Nishimura, Hiroyuki Kaneko, and the staff of Nobeyama for their support at the Nobeyama Radio Observatory.

I am indebted to Kazuhiro Hada for many research suggestions for potential investigations of active galactic nuclei, support in writing a graduation thesis, and much helpful advice on deciding on the courses to take. I would like to thank Kyoko Onishi for discussion and cooperation on presentation, Oh Daehyeon, Yuriko Saito, Sumire Tatehora, Katuya Hashizume, Min Cheul Hong, and all graduate students of SOKENDAI for their support and cooperation in class.

I would like to thank Kosuke Fujii, Kazuhiro Kiyokane, Chihomi Hara, Shin Koyamatsu, and all graduate students at the NAOJ Chile observatory for discussions, support in seminars, and daily life in Mitaka.

Finally, I want to deeply acknowledge my family, Nozomi Mouri, Haruki, Takako, Yoshikazu, Mutsumi, and Keiichi for their constant support and understanding of my extended study period.

塩島のおばあちゃん、今まで本当にありがとう。

References

[1] Hills, R. E., Kurz, R. J., Peck, A. B., “ALMA: status report on construction and early results from commissioning”, Proc. SPIE 7733, 773317-773317-10, Jul, 2010.

[2] Wootten, A., Thompson, A. R., “The Atacama Large Millimeter/Submillimeter Array,” Proc. IEEE vol.97, no.8, pp.1463-1471, Apr, 2009.

[3] Iguchi, S., et al.., "The Atacama Compact Array (the ACA)," Publ. Astron. Soc. Japan, vol. 61, no.1, pp.1-12, Sep, 2009.

[4] Hills, R. E., Beasley, A. J., “The Atacama Large Millimeter/submillimeter Array”, Proc. SPIE 7012, 70120N-70120N-8, Jul, 2008.

[5] Ksienski.A.A., “Multiplicative processing antenna system for radar applications”, The Radio and Electrons Engr., Vol.29, pp.53-67, Jan, 1965.

[6] Safak, M., “Limitations on Reflector Antenna Gain by Random Surface Errors, Pointing Errors, and the Angle - of- Arrival Jitter”, IEEE Trans. Ant. Propagate Vol.38, no.1, pp.117-121, Jan, 1999.

[7] Tsutsumi, T, et al.., "Wide-Field Imaging of ALMA with the Atacama Compact Array: Imaging Simulations", ALMA Memo 488, Mar, 2004.

[8] Saito, M., et al.., "Atacama Compact Array antennas", Proc. SPIE 8444, 128, Mar, 2012.

[9] Holdaway, M, A., “Calculation of Anomalous Refraction on Chajnantor”, MMA Memo 186, Sep, 1997.

[10] Dent, W. A. and Hobbs, R. W., “31.4-GHz flux density measurements of variable radio source,” Astronomical Journal, Vol. 78, pp.163-163, Mar, 1973.

[11] Mangum, J, G, “An Optical Pointing System for the ALAM Prototype Antennas,” ALMA Memo 288, Feb, 2000.

[12] Swift, J., “BIMA Optical Pointing Project I. The STV Video Camera,” BIMA Memoranda 88, Mar, 2002.

[13] Cogdell, J, R, et al., “High resolution millimeter reflector antennas,” IEEE Trans. Ant. Propagat., Vol.AP-18, pp.515-529, Jul, 1970.

[14] Assawaworrarit, S., Padin, S., “An Optical Pointing Telescope for Radio Astronomy,” PASP. 124, 242-246, Mar, 2012.

[15] John W. Hardy” Adaptive Optics for Astronomical Telescopes” New York: Oxford University Press, 1998.

[16] F, Forbes., “Dome induced image motion,” SPIE. Vol.332, 186-192, Nov, 1982.

[17] Mangum, J, G, et al.., “Evaluation of the ALMA Prototype antennas,” PASP. 118. 1257m, Sep, 2006.

[18] Granino A. Korn “Advanced Dynamic-system Simulation: Model-replication Techniques and Monte Carlo Simulation” John Wiley & Sons, 2007.

[19] Henry, L, “Wind Engineering – A handbook for Structural Engineers,” Prentice Hall, Englewood Cliffs, New Jersey, 1991.

[20] Ukita, N, Ikenoue, B, and Saito, M “The Seeing error Measurements with an Optical Telescope on a Radio antenna,” Publications of the National Astronomical Observatory of Japan, vol.11, pp.1-11, Jan, 2008

[21] Ukita, N, et al.., “Design and performance of the ALMA-J prototype antenna,” Proc. SPIE 5489, 1085-1093, 2004

[22] Ukita, N, et al.., “A High-Precision Angle Encoders for a 10-m Submillimeter antenna” Publications of the National Astronomical Observatory of Japan (ISSN 0915-3640), vol. 6 no. 2, pp. 59-64, Oct,2001.

[23] Matsuzawa. A et al.., “Development of High-Accuracy Pointing Verification for ALMA Antenna,” Proc. SPIE 9145, 91451Z1, Jul, 2014

[24] Martin, H. M. “Image motion as a measure of seeing quality,” Astronomical Society of the Pacific, Publications, vol.99, pp.1360 – 1370, Dec, 1987

[25] Tokovinin, A. 2002, “From Differential Image Motion to Seeing”, PASP, 114, 1156-1166, June, 2002.

[26] Russell J. Donnelly, Katepalli R. Streenivasan, “Flow at Ultra-High Reynolds and Rayleigh Numbers: A Status Report” Springer Science & Business Media, 2012.

[27] Thompson, A. R., Moran, J. M., & Swenson, G. W., Jr., “Interferometry and Synthesis in Radio Astronomy, 2nd ed.” New York: John Wiley & Sons, 2001

[28] Fried, D. L. “Statistics of a Geometric Representation of Wavefront Distortion,” JOURNAL OF THE OPTICAL SOCIETY OF AMERICA, 55, 1427, Feb, 1965

[29] Taylor. G. I., “The spectrum of turbulence” Proc.R.Soc.A, 164, 476, 1938.

[30] Tyler, G, A. “Bandwidth considerations for tracking through turbulence,” Journal of the Optical Society of America A, vol.11, pp.358 – 367, Jan, 1994

[31] Holdaway, M, A., “Fast Switching Phase Correction Revisited for 64 12 m Antennas”, ALMA Memo 403, Dec, 2001.

[32] Glindemann, A et al.., “Adaptive Optics on Large Telescopes”, Experimental Astronomy, v. 10, Issue 1, p. 5-47, 2000.

[33] Pierre Y. Bely “The Design and Construction of Large Optical Telescope” Springer, 2006.

Appendix A Difference between Size and RMS of Centroid Motion of Star in Distorted Image by Optical Seeing

Generally, the optical seeing in optical astronomy means the Full Width at Half-Maximum (FWHM) of the disc of a star image that is distorted by refracted light passing through the atmosphere (hereinafter seeing disc) [27], [33]. The optical seeing in this study, however, indicates the RMS of centroid motion of the stellar image that is distorted by refracted light passing through the atmosphere (hereinafter RMS of centroid positions). In the case of long integration time, the seeing size becomes large as the size of the star in the integrated image become large. On the other hand, the RMS of centroid positions becomes small as the motion of the centroid positions (centroid motion) of the star in the integrated image (see Figure A-1).

The relation between the phase of the optical wave [$\varphi(x)$] and the optical path length $l(x)$ is

$$\phi(\vec{x}) = \frac{2\pi}{\lambda} l(\vec{x}). \qquad \text{(A-1)}$$

where λ is wavelength. The RMS of optical path length in the scale of r on the line of sight from the distorted wavefront by the turbulence is represented with the phase structure function [$D_\varphi(r)$] as follows (see Figure A-2).

$$\sqrt{\langle [l(\vec{x}+\vec{r}) - l(\vec{x})]^2 \rangle} = \frac{\lambda}{2\pi} \sqrt{\langle [\phi(\vec{x}+\vec{r}) - \phi(\vec{x})]^2 \rangle} = \frac{\lambda}{2\pi} \sqrt{D_\phi(\vec{r})} \qquad \text{(A-2)}$$

Therefore, the relation between the RMS of the wavefront tilt (σ) and the RMS of the optical path length is

$$tan\,\sigma = \frac{\lambda}{2\pi} \frac{\sqrt{D_\phi(\vec{r})}}{r} \sim \sigma \;\; (\sigma \ll 1). \qquad \text{(A-3)}$$

The equation (A-3) corresponds to the equation (3-3). If wavefront tilt fluctuates, the centroid position of the star in the image taken with the OPT also fluctuate. Therefore, it is considered that the RMS of the wavefront tilt is represented by the RMS of centroid positions (see Figure A-3).

The relation between the seeing disc (θ), wavelength (λ), and the fried

parameter (r_0) is [see equation (13.93) from Thompson, A. R "Interferometry and Synthesis in Radio Astronomy" (2001)].

$$\theta \propto \frac{\lambda}{r_0} \qquad \text{(A-4)}$$

On the other hand, the relation between the RMS of centroid positions (σ), wavelength (λ), and the fried parameter (r_0) is [see equation (3.59) from John W. Hardy" Adaptive Optics for Astronomical Telescopes" (1998)] [15]

$$\sigma \propto \frac{\lambda}{r_0{}^{\frac{5}{6}}} \qquad \text{(A-5)}$$

Also, the relation between the opacity of the atmosphere [*sin* (*El*)] and the fired parameter (r_0) with the Kolmogorov model of turbulence is [see equation (1.12) from Pierre Y. Bely "The Design and Construction of Large Optical Telescope" (2006)] [33]

$$r_0 \propto sin(El)^{\frac{3}{5}} \qquad \text{(A-6)}$$

Therefore, the relation between the RMS of centroid positions (σ) and the opacity of the atmosphere [*sin* (*El*)]) with the Kolmogorov model of turbulence is

$$\sigma \propto r_0{}^{-\frac{5}{6}} \propto \left[sin(El)^{\frac{3}{5}}\right]^{-\frac{5}{6}} \propto sin(El)^{-\frac{1}{2}} \qquad \text{(A-7)}$$

The equation (A-7) corresponds to the equation (5-1).

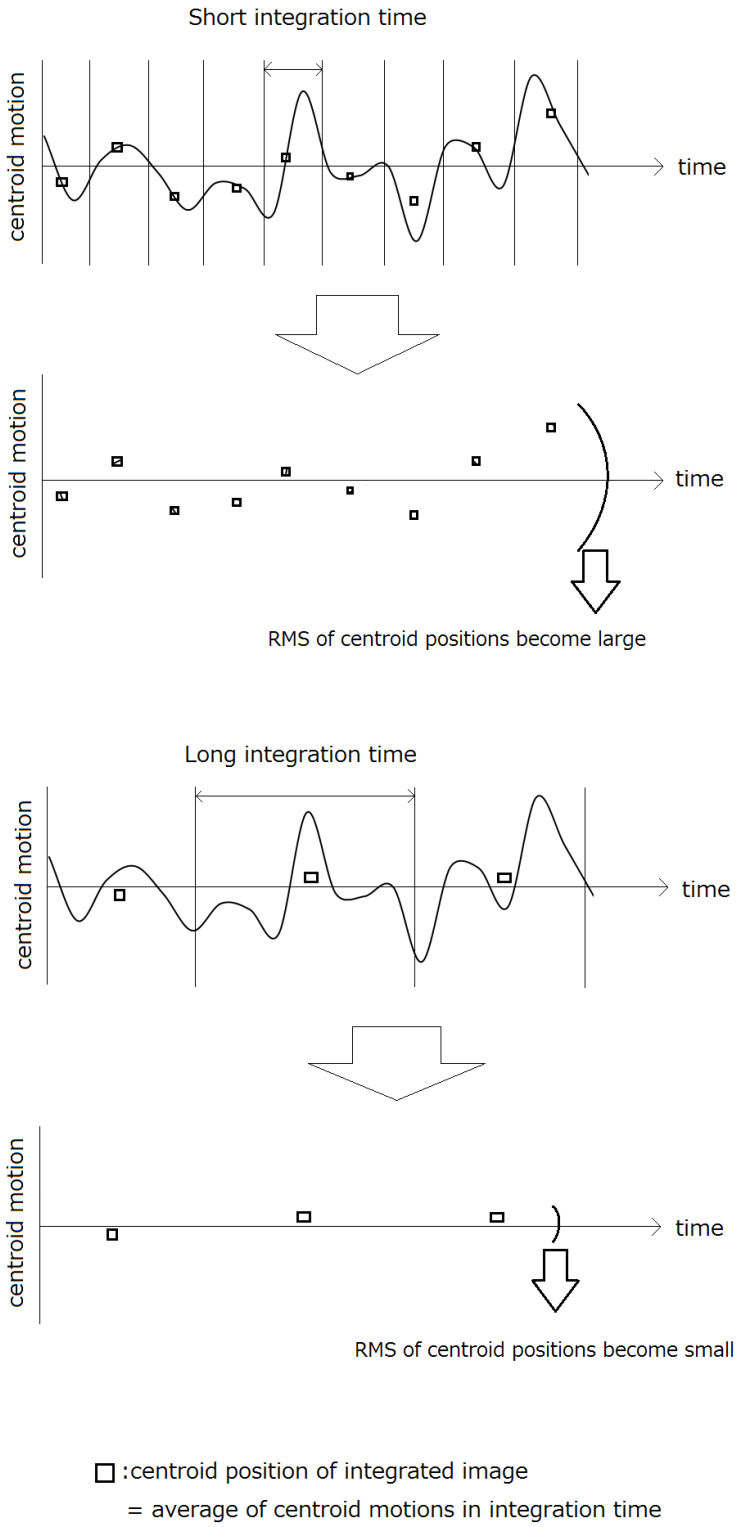

Figure A-1 Conceptual diagram of the relation between integration time and the RMS of centroid positions.

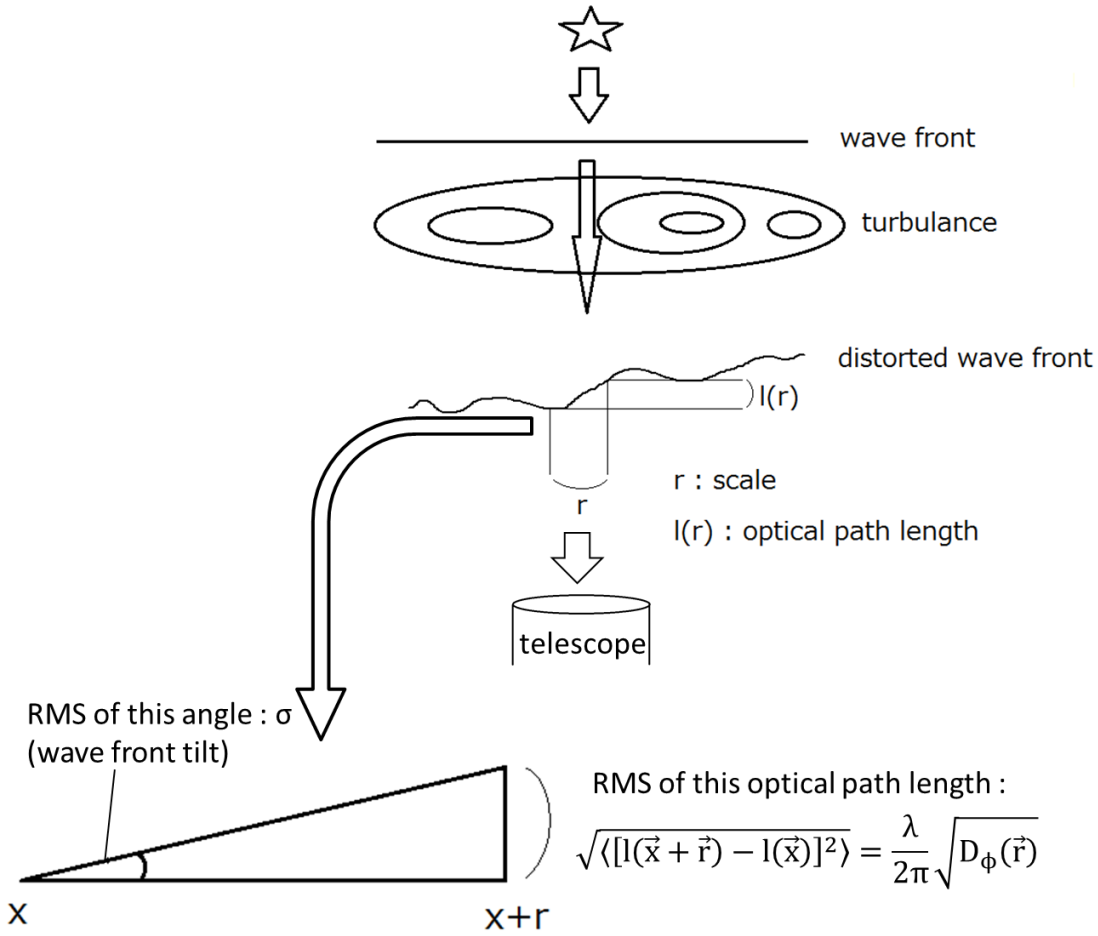

Figure A-2 Conceptual diagram of the RMS of optical path length in the scale of r on the line of sight from the distorted wavefront by the turbulence.

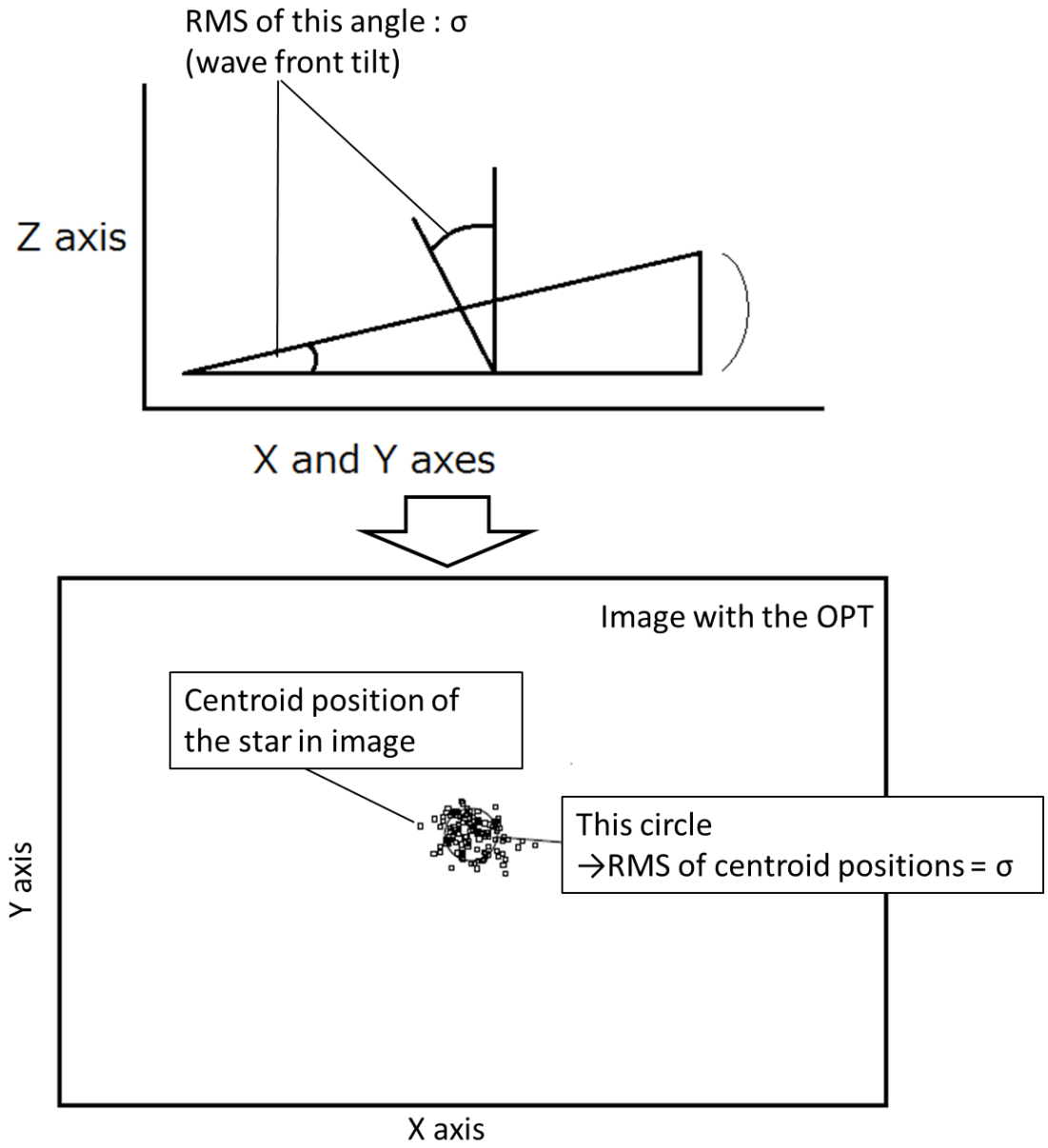

Figure A-3 Conceptual diagram of the relation between the wave front tilt and the RMS of centroid positions of the star in an image taken with the OPT.

Appendix B Example of Readout Data of Angles and Rotational Velocities of ACA Antenna

An example of readout data of an angle and a rotational velocity of the ACA antenna is contained in Table B-1. The readout data include the measured time [column (1)], the commanded Az angle [column (2)], the commanded El angle [column (3)], the rotational velocity in the Az axis [column (4)], the rotational velocity in the El axis [column (5)], the measured Az angle [column (8)], and the measured El angles [column (9)]. The angle and the rotational velocity are measured with the angular encoders and the angular resolvers as described in Section 4. These parameters are recorded every 0.048 seconds (sampling rate is about 20.83 Hz).

The servo error at a particular is measured by the difference between the measured angle [column (8) and column (9) in Table B-1] and the command angle 0.048 seconds before [column (2) and column (3) in Table B-1], because the commanded angle indicates the angle at which an antenna will arrive 0.048 seconds later (see Figure B-1).

Time	(2) Commanded Az angle	(3) Commanded El angle		(8) Measured Az angle	(9) Measured El angle
00.48.11.136	65.85405121	35.15897345	…	65.85405288	35.15897915
00.48.11.184	65.85391911	35.15914192	…	65.85391408	35.15913974

servo error = commanded angle – measured angle

Figure B-1 Calculation method of servo error from readout

```
Optical Pointing for ACA Script , long tracking
ant: CM12
script: AzElMidLog.py
CM12 None False
CAN Manager:"CM12", bus:2, node:0
CM12 (software name) : realname is 'CM12'
20120608t220706: start.
Time      commanded(Az,El)      commanded(Vaz,Vel)   mid-TE(Az,El)      on-TE(Az,El)      Metr(dAz,dEl,dPath)
epoch = 1355848602648O.0000 ms
22:07:07.440 154.84929739 57.80199990  0.0039145164 0.0016183779 154.84901190 57.80187249 154.84909773 57.80189395 0.00000000 0.00000000 340175
22:07:07.488 154.84948531 57.80207785  0.0039145164 0.0016183779 154.84921575 57.80196905 154.84930158 57.80197978 0.00000000 0.00000000 351892
22:07:07.536 154.84967323 57.80215563  0.0039145164 0.0016183779 154.84939814 57.80206561 154.84948397 57.80204415 0.00000000 0.00000000 311020
22:07:07.584 154.84986115 57.80223358  0.0039146841 0.0016183779 154.84958053 57.80211926 154.84968781 57.80216217 0.00000000 0.00000000 267512
22:07:07.632 154.85004907 57.80231154  0.0039146841 0.0016183779 154.84977365 57.80216217 154.84985948 57.80224800 0.00000000 0.00000000 262930
22:07:07.680 154.85023700 57.80238932  0.0039146841 0.0016183779 154.84994531 57.80224800 154.85002041 57.80233383 0.00000000 0.00000000 300667
22:07:07.728 154.85042492 57.80246727  0.0039146841 0.0016183779 154.85013843 57.80234456 154.85022426 57.80238748 0.00000000 0.00000000 350941
22:07:07.776 154.85061284 57.80254522  0.0039146841 0.0016183779 154.85034227 57.80245185 154.85041738 57.80244112 0.00000000 0.00000000 348581
22:07:07.824 154.85080060 57.80262318  0.0039146841 0.0016182102 154.85052466 57.80254841 154.85061049 57.80255914 0.00000000 0.00000000 299751
22:07:07.872 154.85098852 57.80270096  0.0039148517 0.0016182102 154.85070705 57.80260205 154.85081434 57.80264497 0.00000000 0.00000000 260700
22:07:07.920 154.85117627 57.80277891  0.0039148517 0.0016182102 154.85090017 57.80264497 154.85098600 57.80273080 0.00000000 0.00000000 261735
22:07:07.968 154.85136420 57.80285686  0.0039148517 0.0016182102 154.85107183 57.80273080 154.85115767 57.80280590 0.00000000 0.00000000 307979
22:07:08.016 154.85155212 57.80293465  0.0039148517 0.0016182102 154.85127568 57.80282736 154.85136151 57.80283809 0.00000000 0.00000000 347594
22:07:08.064 154.85174021 57.80301260  0.0039148517 0.0016182102 154.85147953 57.80291319 154.85155463 57.80289173 0.00000000 0.00000000 338554
22:07:08.112 154.85192813 57.80309055  0.0039148517 0.0016182102 154.85164046 57.80299902 154.85175848 57.80300975 0.00000000 0.00000000 291026
22:07:08.160 154.85211605 57.80316833  0.0039148517 0.0016182102 154.85183358 57.80304193 154.85195160 57.80311704 0.00000000 0.00000000 259823
22:07:08.208 154.85230397 57.80324629  0.0039150193 0.0016182102 154.85201597 57.80310631 154.85211253 57.80319214 0.00000000 0.00000000 271214
22:07:08.256 154.85249190 57.80332424  0.0039150193 0.0016182102 154.85219836 57.80319214 154.85229492 57.80327797 0.00000000 0.00000000 319318
22:07:08.304 154.85267982 57.80340202  0.0039150193 0.0016182102 154.85240221 57.80331016 154.85248804 57.80331016 0.00000000 0.00000000 355746
22:07:08.352 154.85286774 57.80347997  0.0039150193 0.0016182102 154.85258460 57.80339599 154.85268116 57.80338526 0.00000000 0.00000000 337201
22:07:08.400 154.85305566 57.80355792  0.0039150193 0.0016182102 154.85277772 57.80346036 154.85288501 57.80347109 0.00000000 0.00000000 290645
22:07:08.448 154.85324375 57.80363571  0.0039150193 0.0016182102 154.85294938 57.80351400 154.85305667 57.80357838 0.00000000 0.00000000 255547
22:07:08.496 154.85343168 57.80371366  0.0039150193 0.0016182102 154.85312104 57.80355692 154.85323906 57.80364275 0.00000000 0.00000000 276759
22:07:08.544 154.85361960 57.80379161  0.0039150193 0.0016180426 154.85332489 57.80365348 154.85343218 57.80371785 0.00000000 0.00000000 323151
22:07:08.592 154.85380752 57.80386940  0.0039150193 0.0016180426 154.85353947 57.80375004 154.85361457 57.80377150 0.00000000 0.00000000 350311
22:07:08.640 154.85399544 57.80394735  0.0039150193 0.0016180426 154.85372186 57.80384660 154.85381842 57.80383587 0.00000000 0.00000000 330244
```

Table B-1 Example of the readout data from the ACA antenna.

Appendix C Optical Pointing Telescope

The specifications and performance of the optical pointing telescope (OPT) and an image taken with the OPT are explained in this section. Table C-1 lists the specifications of the OPT. Figure C-1 shows an example of the image of a star taken with the CCD camera in the OPT. The size of the image is 640 pixels on the X axis and 480 pixels on the Y axis. The intensity of each pixel [Z axis in image (see Figure C-1)] was calculated by measuring the number of photons falling on each pixel. The OPT can obtain images with an integration time of up to 1/30 seconds (the sampling rate is 30 Hz). The image taken with the OPT has a high SNR (Signal to Noise Ratio) that is typically 80 to 100. The SNR is estimated as the ratio of a maximum intensity to the RMS noise of the image. The maximum image intensity is typically about 170, while the RMS noise is typically 1 to 2. The RMS noise is calculated from the RMS of intensities from the region without a star in the image (X = 0 to 640 pixels and Y = 380 to 480 pixels).

Pixel scales and rotation angles of the OPT mounted on each ACA antenna are listed in Table C-2. The pixel scale is the size of one pixel on the sky (unit is arcsec), while the rotation angle is that between the X, Y axis in the image and the Az, El axis in the sky. The coordinate transformation between the image (X_{OPT}, Y_{OPT} pixels) and the sky (X_{Az}, X_{El} arcsecs) is calculated thus:

$$X_{\mathrm{Az}} = X_{\mathrm{OPT}} \times C_{\mathrm{PS}} \times cos(\theta_{\mathrm{RA}}) - Y_{\mathrm{OPT}} \times C_{\mathrm{PS}} \times sin(\theta_{\mathrm{RA}}) \quad \text{(C-1)}$$

$$X_{\mathrm{El}} = X_{\mathrm{OPT}} \times C_{\mathrm{PS}} \times sin(\theta_{\mathrm{RA}}) + Y_{\mathrm{OPT}} \times C_{\mathrm{PS}} \times cos(\theta_{\mathrm{RA}}). \quad \text{(C-2)}$$

where C_{PS} is the pixel scale, and θ_{RA} is the rotation angle.

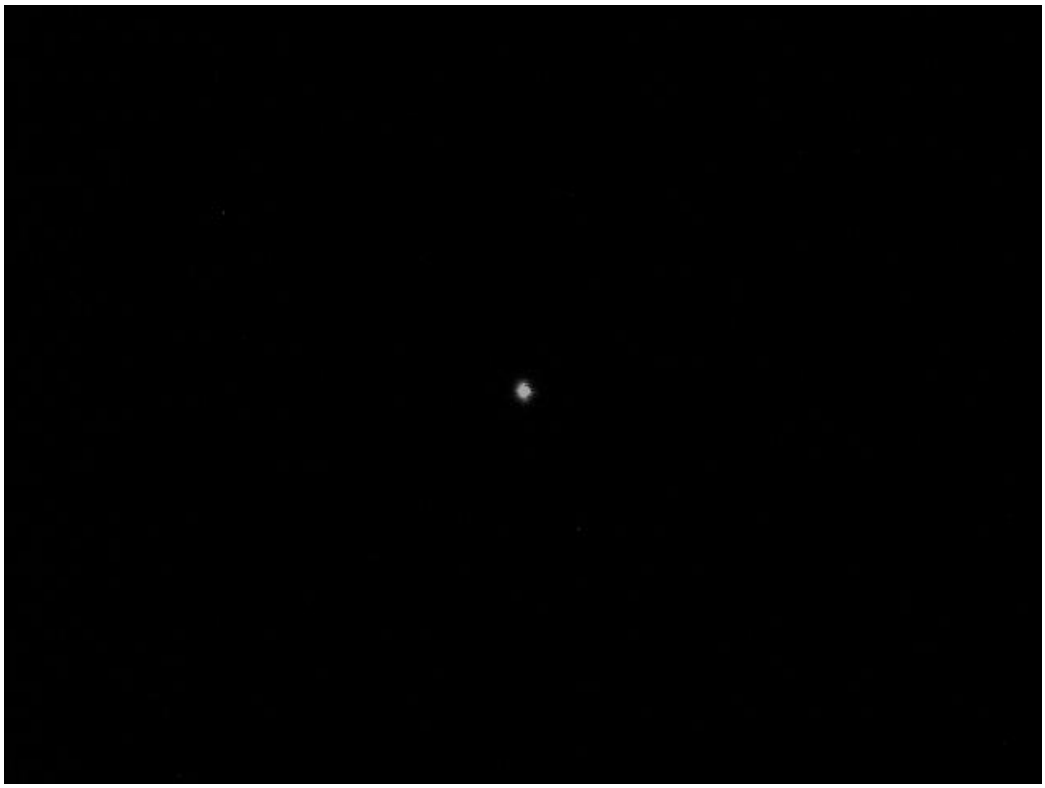

Figure C-1 Example of the image of a star taken with the CCD camera in the OPT.

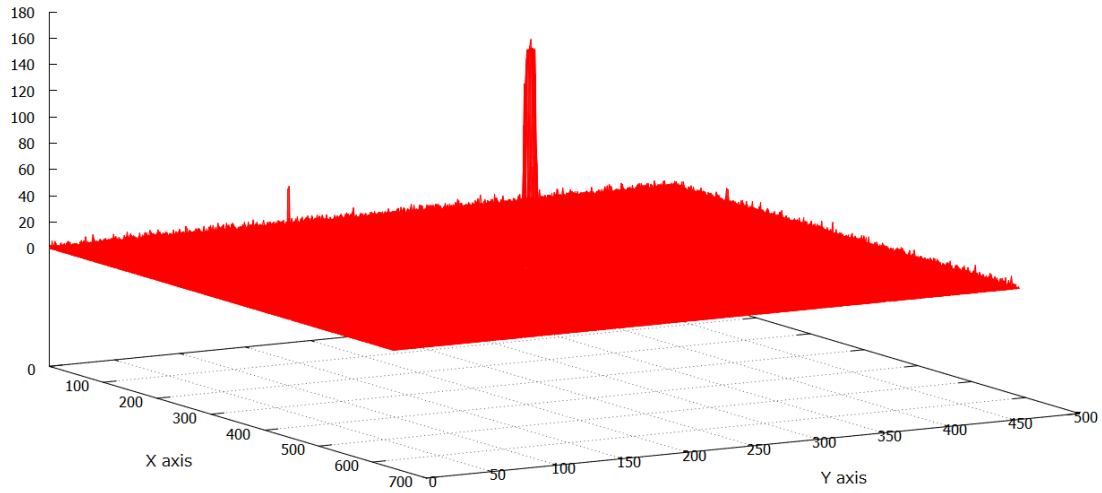

Figure C-2 Example of the three-dimensional plot of the image.

Table C-1 Specifications of the OPT.

Parameters	Specification
Diameter	102 [mm]
EFL	1840 [mm] (λ=660 [nm])
Wavelengths	640-1000[nm]
Filter	R64-C
Number of pixels	640×480
Sampling rate	30[Hz] (actual 20[Hz])

Table C-2 Pixel scales and rotation angles of the ACA antennas.

ACA antenna	No.	Pixel scale [arcsec]	Rotation angle [deg]
7m antenna	1	1.0947	20.4445
	2	1.1056	21.4322
	3	1.1383	24.3054
	4	1.1430	24.3452
	5	1.0993	20.7985
	6	1.1372	23.7234
	7	1.1030	21.1004
	8	1.1339	23.9594
	9	1.1003	18.8588
	10	1.1358	24.0431
	11	1.0966	20.3914
	12	1.1353	24.0184
12m antenna	1	1.0909	-16.9175
	2	1.0945	-20.2367
	3	1.1294	163.1961
	4	1.1341	21.0060

Appendix D Anemometer and Thermometer

An anemometer and a thermometer are mounted on a pole about 4 m high near the ACA antennas (see Figure D-1). The anemometer has the same height as the OPT.

Wind velocity and wind direction are measured with the USA-1 3D Ultrasonic Windsensor by EKO Instruments. The measuring range and the resolution of wind velocity are 0 to 60 m/s and 0.02 m/s, respectively. The measuring range and the resolution of wind direction are 0 to 359 deg (0 deg is north, 90 deg is east, 180 deg is south, and 270 deg is west) and 1 deg, respectively. The value measured by the anemometer is converted from analog to digital (AD conversion) with an LPC321316 by Interface, from an analog output range of 0 to 10 VDC.

The ambient temperature is measured with a PTU200 by VAISALA. The resolution of this thermometer is 0.1°C.

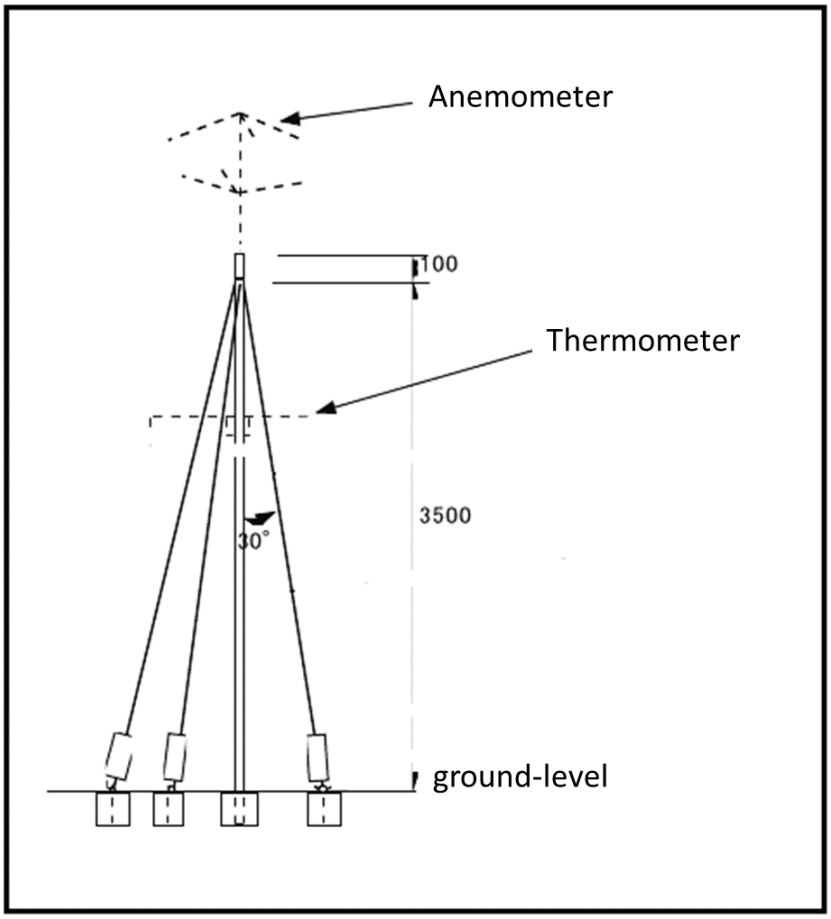

Figure D-1 Anemometer and the thermometer mounted on a pole.

Appendix E Estimation of Centroid Position of Star in Image obtained with Optical Pointing Telescope

The estimation of the centroid position of a star in an image is explained in this section. The centroid position can be considered to be the center of an intensity distribution of the star images in the whole image. The centroid position (X, Y) is calculated as follows.

$$X=\frac{\sum^{n} L_{x_n} \cdot x_n}{L_{tot}},\ Y=\frac{\sum^{n} L_{y_n} \cdot y_n}{L_{tot}}\ (1 \le x_n \le 640, 1 \le \cdot\, y_n \le 480), \quad \text{(E-1)}$$

where L_x is a summation of the intensities in the region from (x_n, 1) to (x_n, 480), x_n is a value of the x-coordinate, ranging from 0 to 640, L_y is the summation of the intensities of the region from (1, y_n) to (640, y_n), y_n is the value of the y-coordinate in the range from 0 to 480, and L_{tot} is the summation of the intensities in all pixels. Although the pixel scale of the image is about one arcsec, the centroid position can be determined from this equation with accuracy higher than 0.01 arcsecs.

The estimated centroid position may be affected by random noise and another star in the image. To remove the effect of the random noise, the intensities that are less than five times the RMS of random noise (5σ) are set to be zero. (see Figure E-1). To remove the effect of another star, the masking region is outside of ± 13 pixels from the maximum intensity position (x_{max}, y_{max}) (see Figure E-2). The star in the image is contained in a region from 25 × 25 pixels. When setting the masking, the centroid position (X, Y) is calculated as follows.

$$X=\frac{\sum^{n} L_{x_n} \cdot x_n}{L_{tot}},\ Y=\frac{\sum^{n} L_{y_n} \cdot y_n}{L_{tot}}\ (x_{max}-13 \le x_n \le x_{max}+13,\ y_{max}-13 \le \cdot\, y_n \le y_{max}+13), \quad \text{(E-2)}$$

where L_x is the sum of the intensities in the region from (x_n, y_{max} − 13) to (x_n, y_{max} + 13), x_n is the value of the x-coordinate in x_{max} − 13 to x_{max} + 13, L_y is the sum of the intensities in the region from (x_{max} − 13, y_n) to (x_{max} + 13, y_n), y_n is the value of the y-coordinate in y_{max} − 13 to y_{max} + 13, (x_{max}, y_{max}) is the location of the maximum intensity position.

To confirm the effectiveness of setting the threshold and masking, the following simulation is performed. Two ideal images are made; i) the image has only a perfect Gaussian source without noise, ii) the image has a perfect Gaussian source,

another source, and random noise (Figure E-4). Next, these three calculations are performed, i) the centroid position calculation without setting the threshold or masking, ii) the centroid position calculation with only the threshold set, iii) the centroid position calculation with both the threshold and the masking set. The calculated centroid positions of the two ideal images, using the three methods, are shown in Table E-1. The result of the simulation shows that the centroid position calculation with both the threshold and the masking set completely removes the effect of the random noise and the other source.

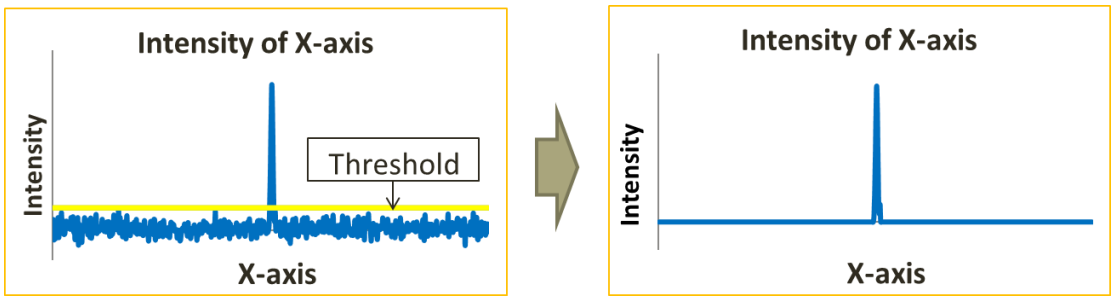

Figure E-1 Removal of the random noise by setting the threshold.

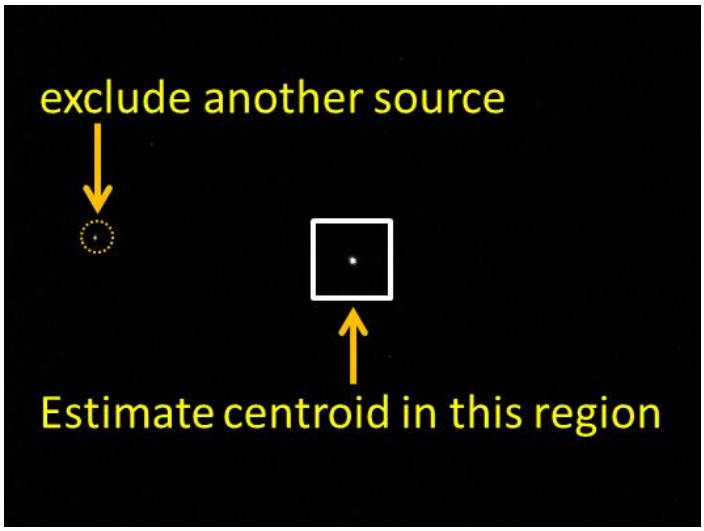

Figure E-2 Removal of the effect of another source by setting the masking.

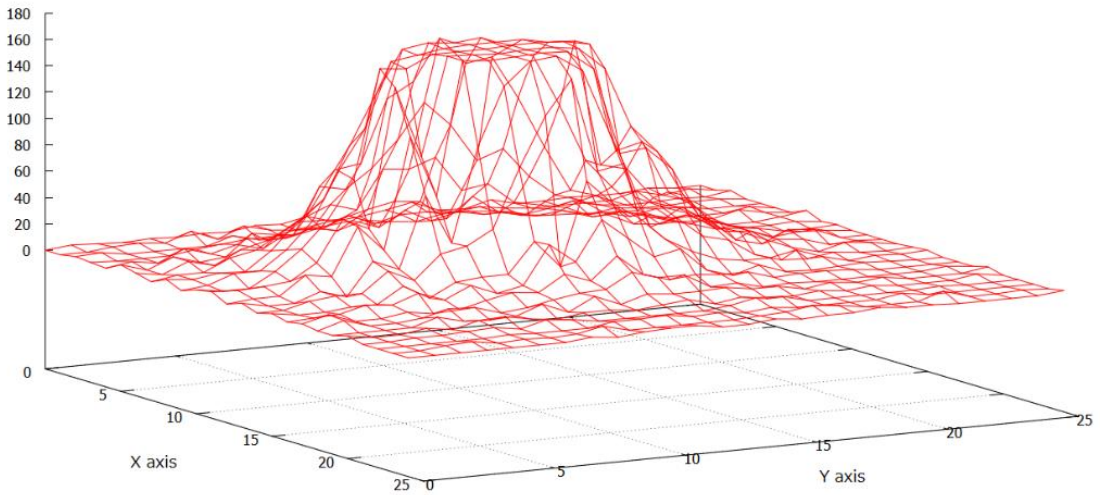

Figure E-3 Example of the three-dimensional plot of image within ±13 pixel around position of the maximum intensity position.

Figure E-4 Two ideal images used for the simulation. The image included only perfect Gaussian source without noise (left), and the image included perfect Gaussian source and another source and random noise (right).

Table E-1 Result of the simulation with three calculation methods to estimate the centroid position.

Script	Ideal image (no noise)		Ideal image (included noise)	
	X-centroid position	Y-centroid position	X-centroid position	Y-centroid position
i	320.00 [pixel]	240.00 [pixel]	352.02 [pixel]	250.67 [pixel]
ii	320.00 [pixel]	240.00 [pixel]	347.61 [pixel]	249.20 [pixel]
iii	320.00 [pixel]	240.00 [pixel]	320.00 [pixel]	240.00 [pixel]

Appendix F Performance of Optical Pointing Telescope

Table F-1 Minimum value of the RMSs of centroid positions at the integration time of five seconds (see Table 3 1).

(1) Date	(2) Start (UT) [hh:mm]	(3) End (UT) [hh:mm]		(4) RMS of centroid positions Integration time 1 second [arcsec]	2 second [arcsec]	5 second [arcsec]	(5) Power law index in 1 to 5 seconds
2012/6/11	5:06	5:21	1st 300 seconds	0.34	0.26	0.20	-0.32
			2nd 300 seconds	0.30	0.25	0.18	-0.3
			3rd 300 seconds	0.41	0.31	0.22	-0.38

The minimum value of the RMSs of centroid positions at the integration time of 5 seconds is 0.18 arcsecs taken at UT 5:06 to 5:21, June 11, 2011, with the ACA 7-m antenna No. 12 (see Table G-1). It confirmed that the measured centroid positions do not contain any problems such as data missing or sudden stop of measurements (see Figure G-2). Therefore, the OPT of the ACA antenna can measure the RMS of centroid positions at about 0.2 arcsecs with an integration time of five seconds in the best case.

Appendix G Derivation Method of Optical Seeing Component in Measured Pointing Value

In this study, to obtain the RMSs of centroid positions only attributed to the pointing error due to optical seeing (hereinafter optical seeing), the following procedure is conducted on the measured RMS of centroid positions. The measured RMS of centroid positions includes the pointing error due to the ACA antenna and the optical seeing. The pointing error due to the antenna includes the systematic component such as drift and fluctuating components. The systematic pointing drift component for 900 seconds is subtracted by the linear fitting (see Figure G-1). A Fourier transform applies to the centroid positions after subtracting the drift. Consequently, it is confirmed that No prominent feature is seen (see Figure G-2, Figure G-3, Figure G-4, and Figure G-5). On the other hand, the spectra of the servo error show several peaks which seem Eigen frequencies of the instruments. However, amplitude of the peaks in the spectra of the servo error is 1/100 smaller than that of the spectra of the centroid positions (see Figure G-6, Figure G-7, Figure G-8, and Figure G-9). Therefore, the fluctuating component of the pointing error due to the ACA antenna in the RMS of centroid positions is negligible. Consequently, it is confirmed that the RMS of centroid positions is only attributed to the optical seeing.

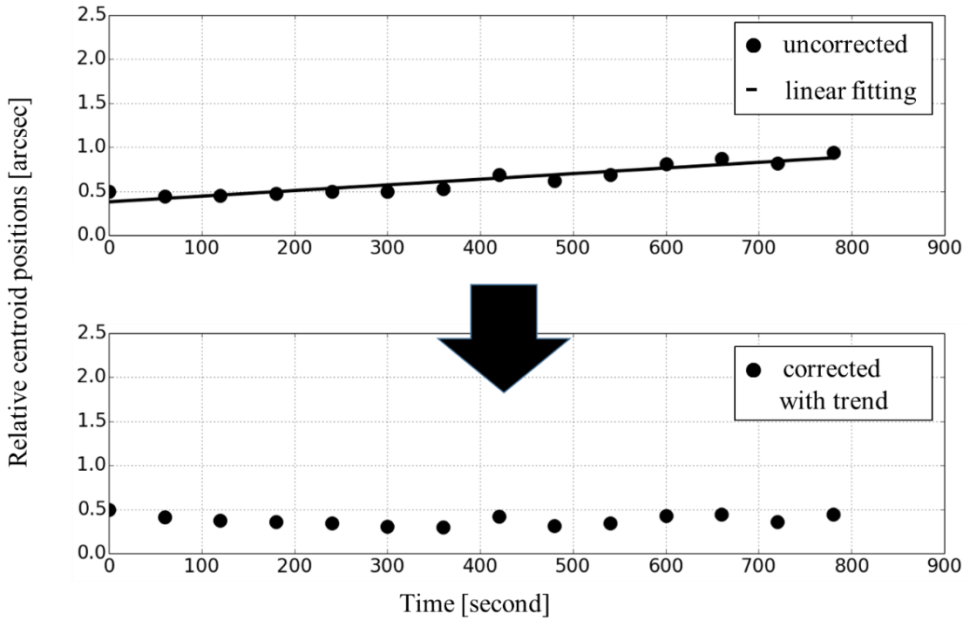

Figure G-1 Conceptual diagram of subtraction of drift from RMS of centroid positions in 900 seconds.

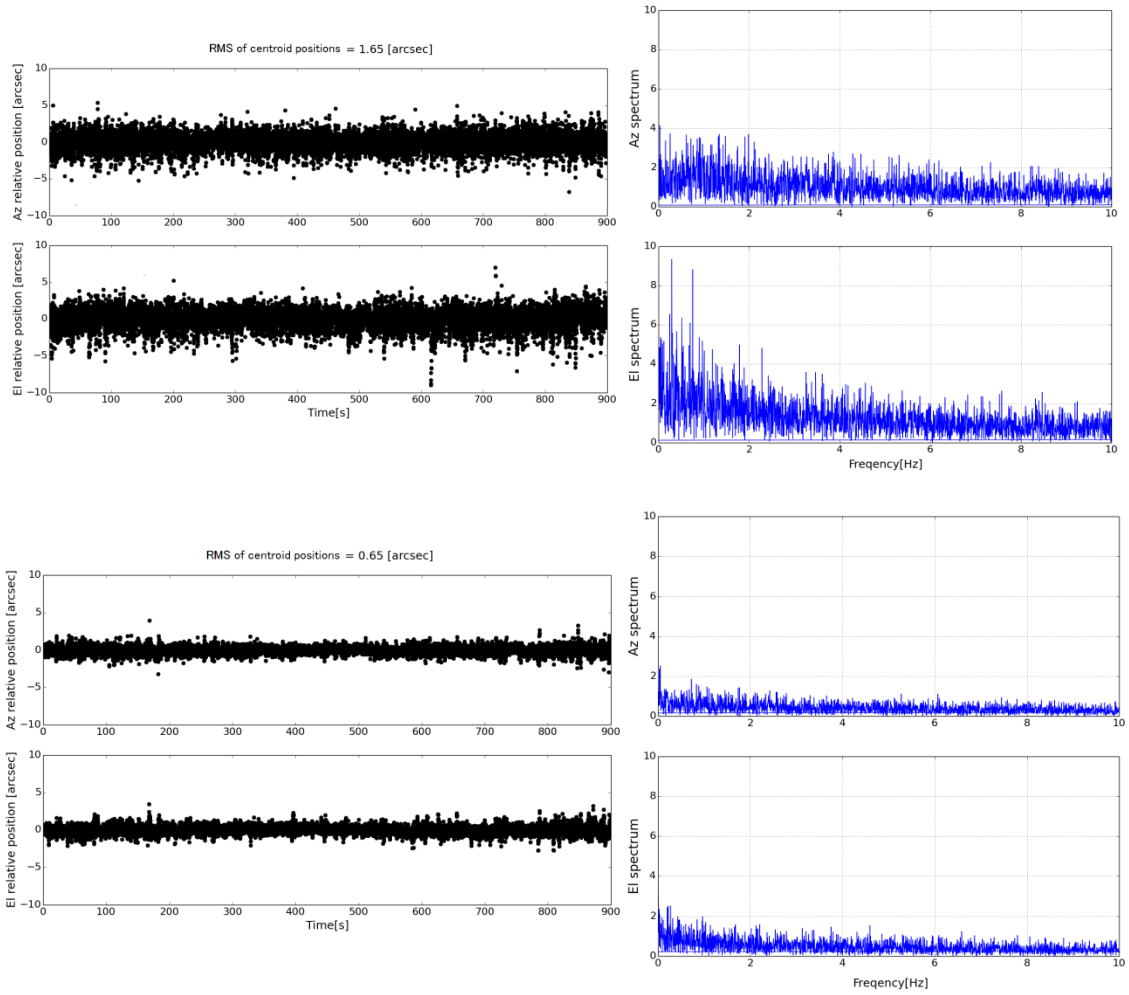

Figure G-2 Relative centroid positions of the Az axis and the El axis (left) and the spectra of relative centroid positions the Az axis and the El axis (right). These measurement results are taken at UT3:43 - 3:48, June 11, 2012 (upper) and UT5:06 - 5:21, June 11, 2012 (lower). The averaged wind velocities are 3.16 m/s (upper) and 2.90 m/s (lower). RMS of centroid positions is estimated as root sum square of RMS of centroid poisons in Az axis and El axis [RMS of centroid positions = $\sqrt{}$ (Az RMS of centroid positions) ^{2}+ (El RMS of centroid positions) ^{2}].

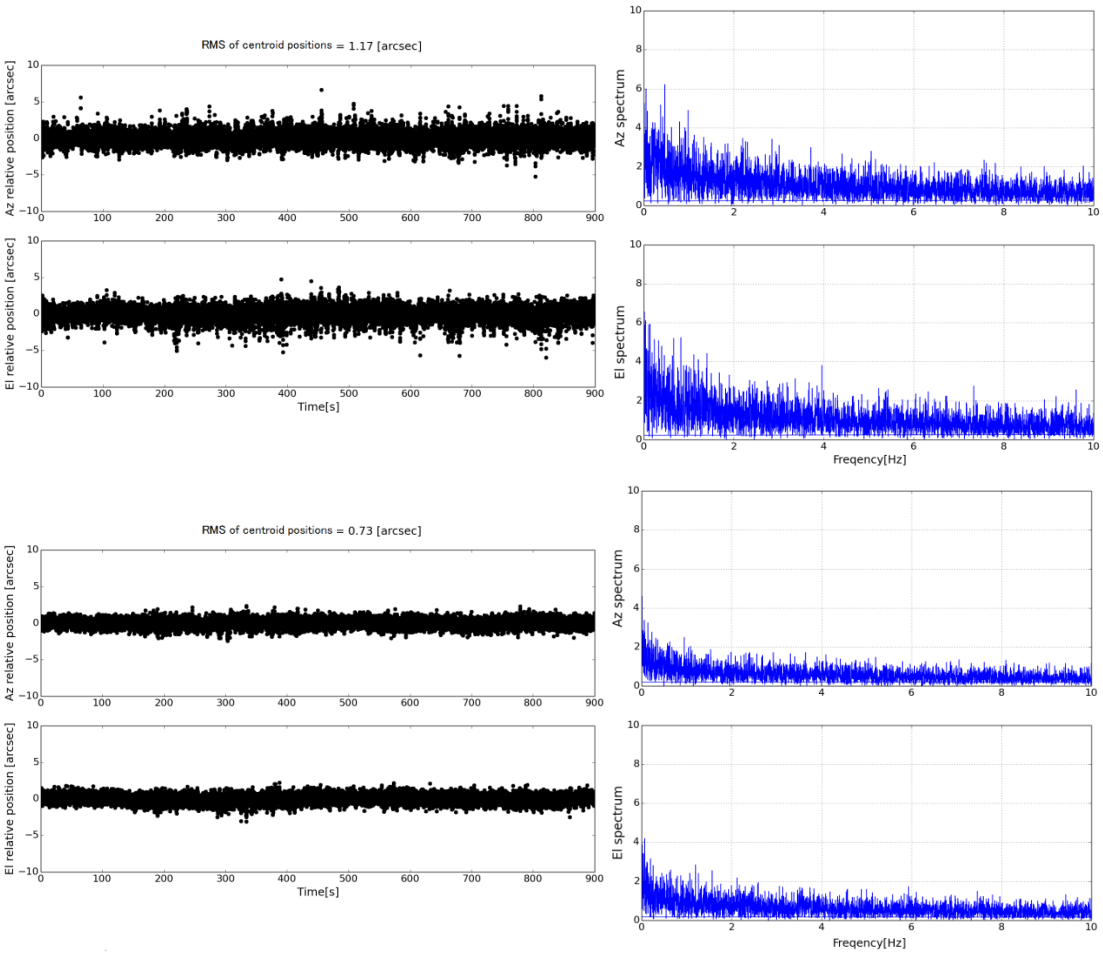

Figure G-3 Relative centroid positions of the Az axis and the El axis (left) and the spectra of relative centroid positions the Az axis and the El axis (right). These measurement results are taken at UT5:43 - 5:58, June 11, 2012 (upper) and UT2:29 - 2:34, June 15, 2012 (lower). The averaged wind velocities are 3.39 m/s (upper) and 1.30 m/s (lower). RMS of centroid positions is estimated as root sum square of RMS of centroid poisons in Az axis and El axis [RMS of centroid positions = √ (Az RMS of centroid positions) ^{2}+ (El RMS of centroid positions) ^{2}].

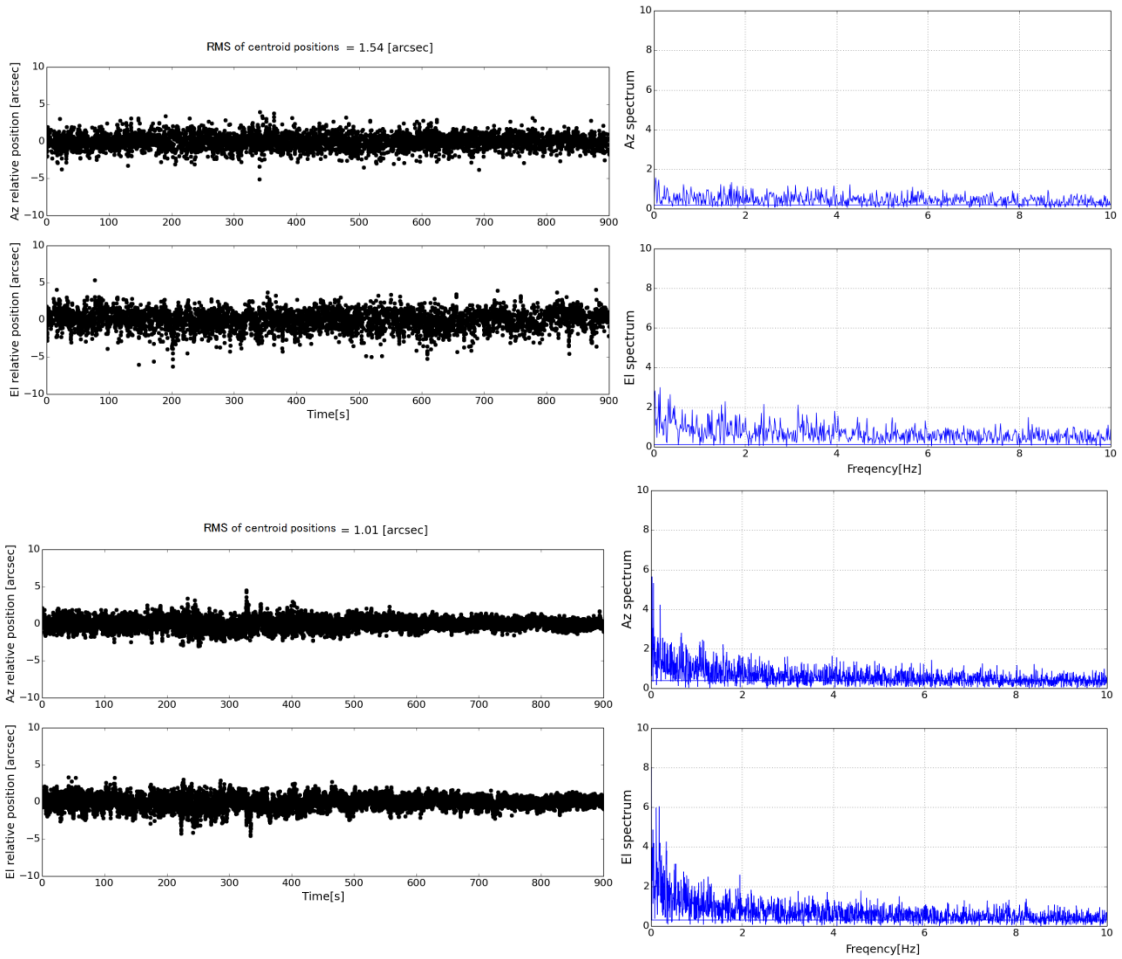

Figure G-4 Relative centroid positions of the Az axis and the El axis (left) and the spectra of relative centroid positions the Az axis and the El axis (right). These measurement results are taken at UT4:05 - 4:20, June 15, 2012 (upper) and UT2:16 - 2:31, June 16, 2012 (lower). The averaged wind velocities are 3.23 m/s (upper) and 1.52 m/s (lower). RMS of centroid positions is estimated as root sum square of RMS of centroid poisons in Az axis and El axis [RMS of centroid positions = $\sqrt{}$ (Az RMS of centroid positions) ^{2}+ (El RMS of centroid positions) ^{2}].

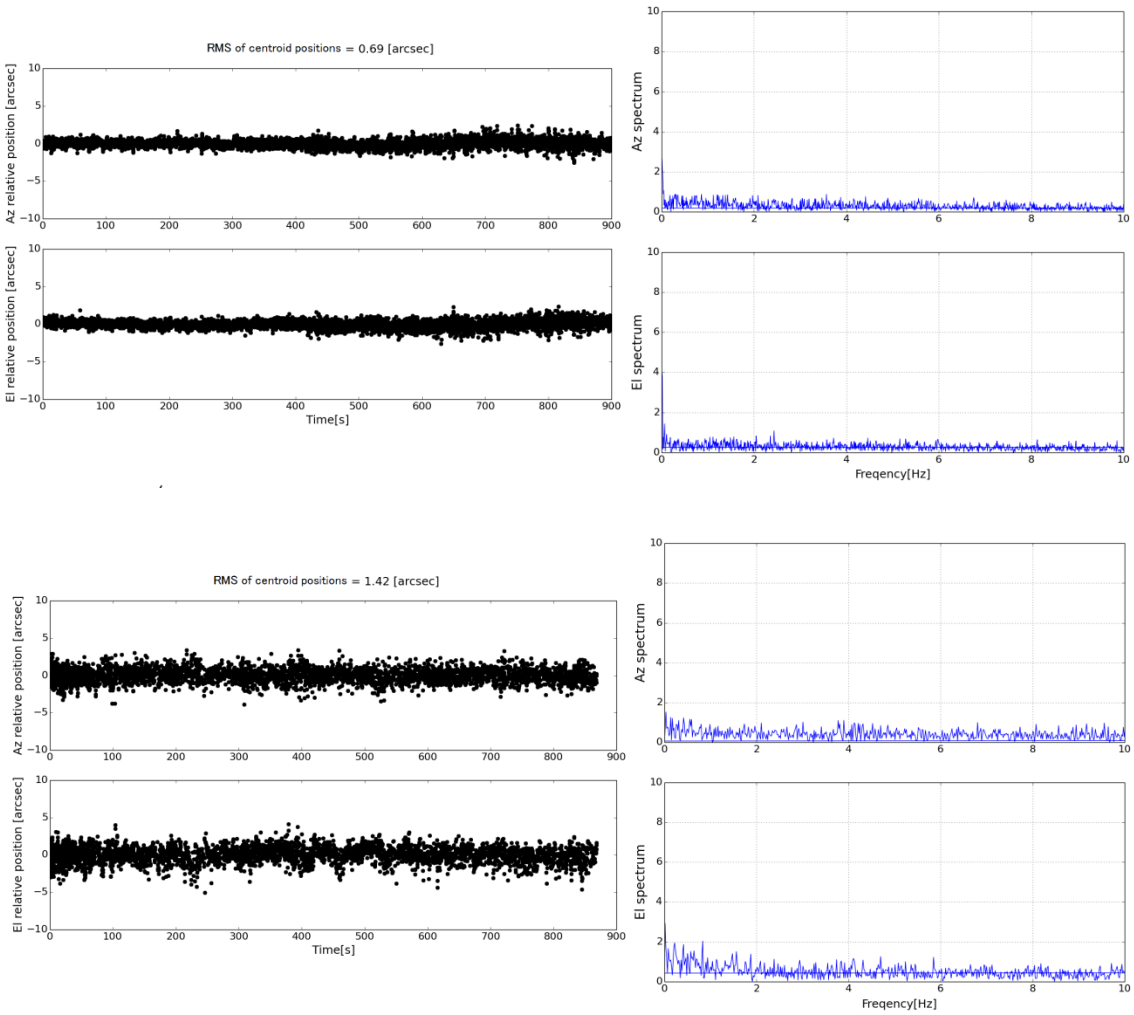

Figure G-5 Relative centroid positions of the Az axis and the El axis (left) and the spectra of relative centroid positions the Az axis and the El axis (right). These measurement results are taken at UT2:51 - 3:06, June 16, 2012 (upper) and UT3:33 - 3:48, June 16, 2012 (lower). The averaged wind velocities are 2.28 m/s (upper) and 3.29 m/s (lower). RMS of centroid positions is estimated as root sum square of RMS of centroid poisons in Az axis and El axis [RMS of centroid positions = √ (Az RMS of centroid positions) ^{2}+ (El RMS of centroid positions) ^{2}].

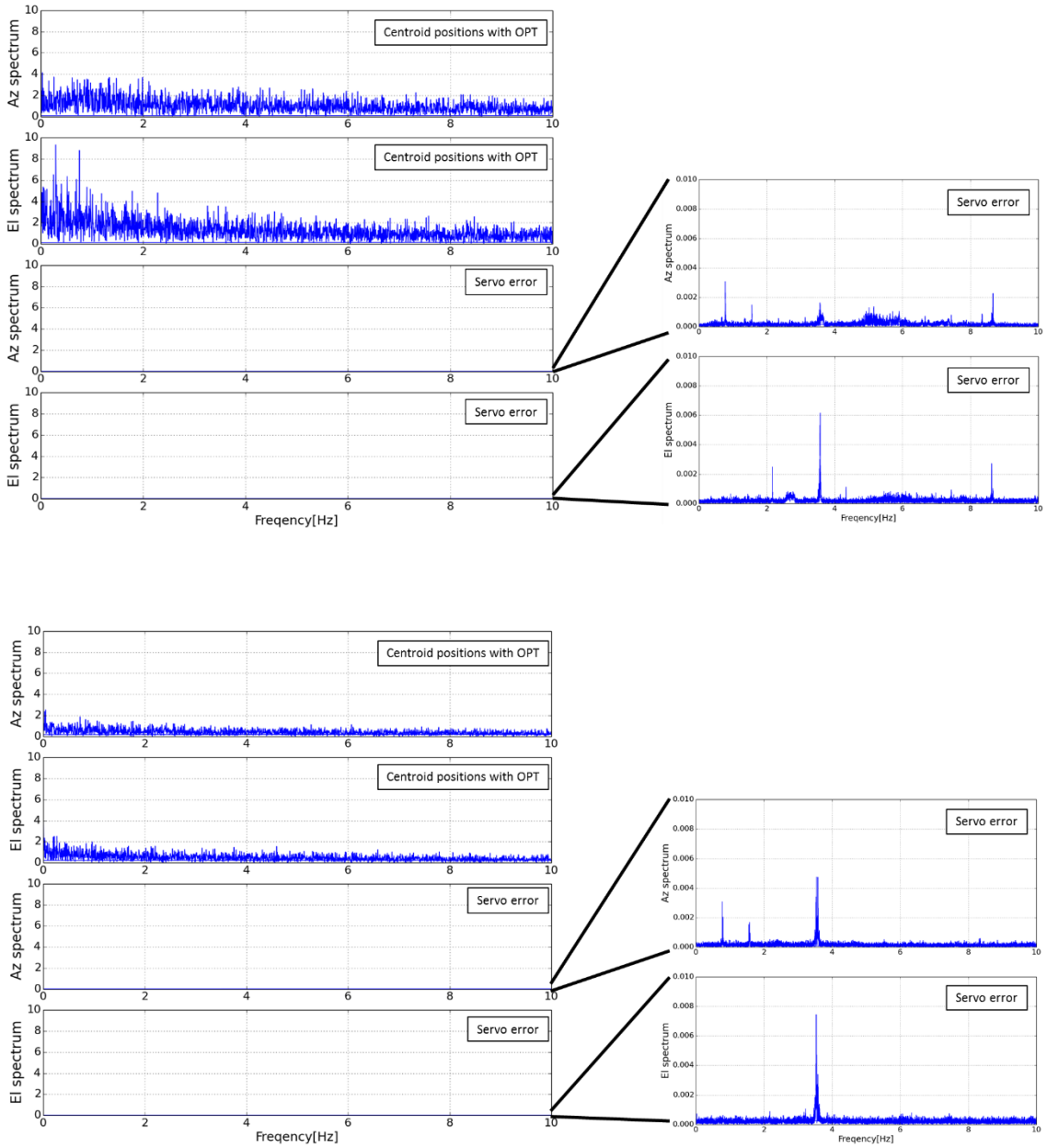

Figure G-6 Spectra of the relative centroid positions on the Az axis and the El axis, and spectra of the servo errors on the Az axis and the El axis. These measurement results are taken at UT3:43 - 3:48, June 11, 2012 (upper) and UT5:06 - 5:21, June 11, 2012 (lower). The averaged wind velocities are 3.16 m/s (upper) and 2.90 m/s (lower).

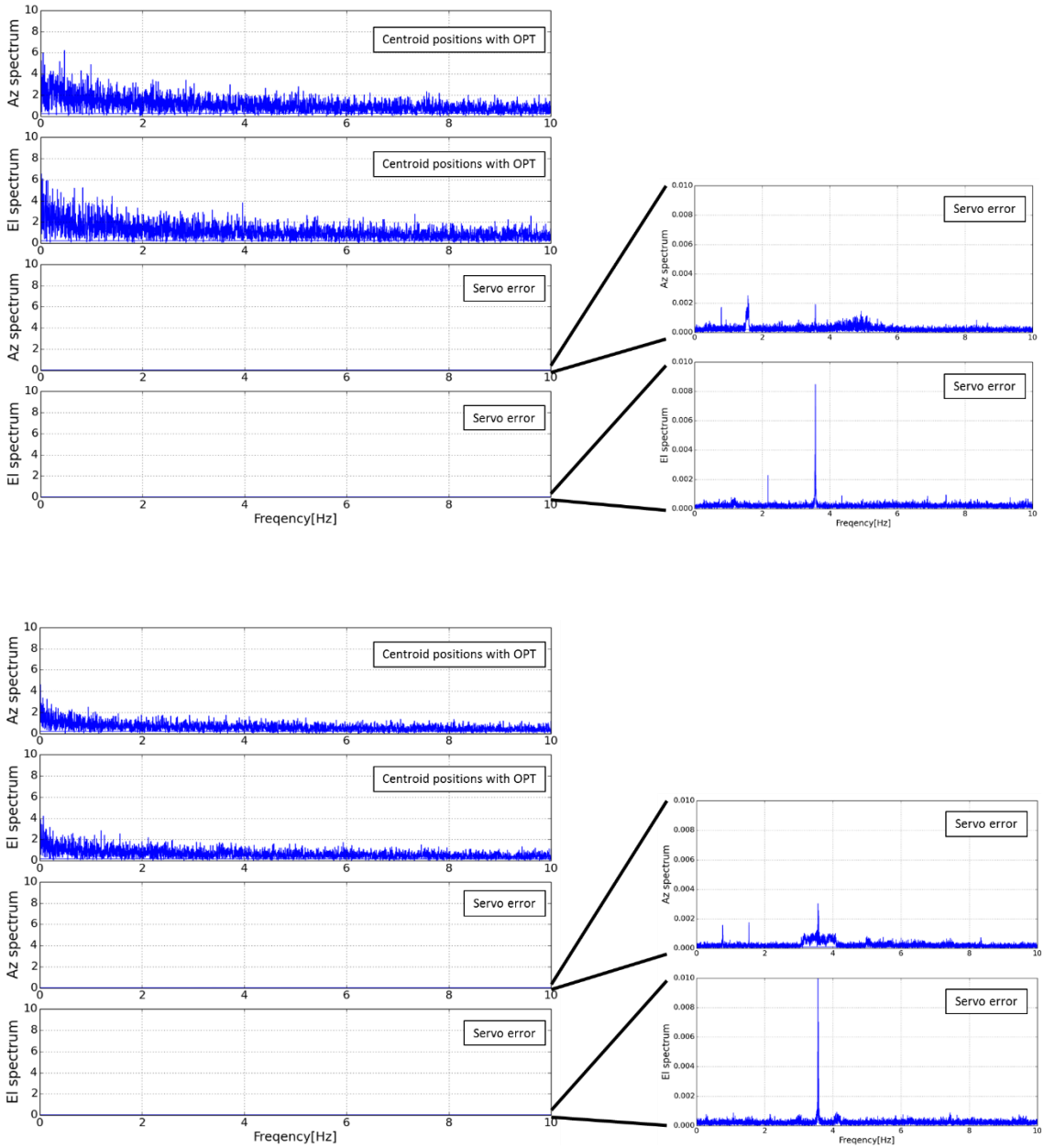

Figure G-7 Spectra of the relative centroid positions on the Az axis and the El axis, and spectra of the servo errors on the Az axis and the El axis. These measurement results are taken at UT5:43 - 5:58, June 11, 2012 (upper) and UT2:29 - 2:34, June 15, 2012 (lower). The averaged wind velocities are 3.39 m/s (upper) and 1.30 m/s (lower).

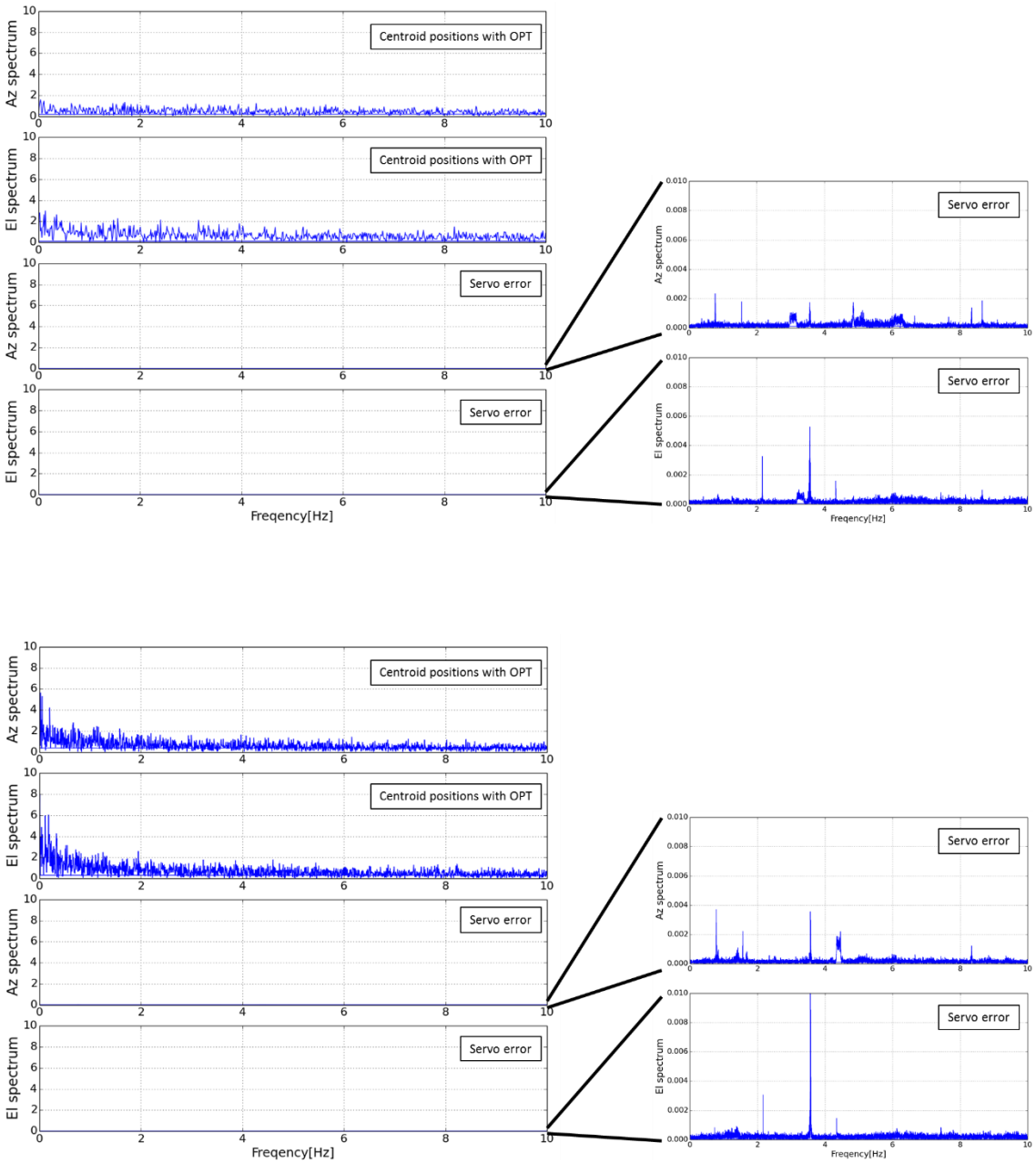

Figure G-8 Spectra of the relative centroid positions on the Az axis and the El axis, and spectra of the servo errors on the Az axis and the El axis. These measurement results are taken at UT4:05 - 4:20, June 15, 2012 (upper) and UT2:16 - 2:31, June 16, 2012 (lower). The averaged wind velocities are 3.23 m/s (upper) and 1.52 m/s (lower).

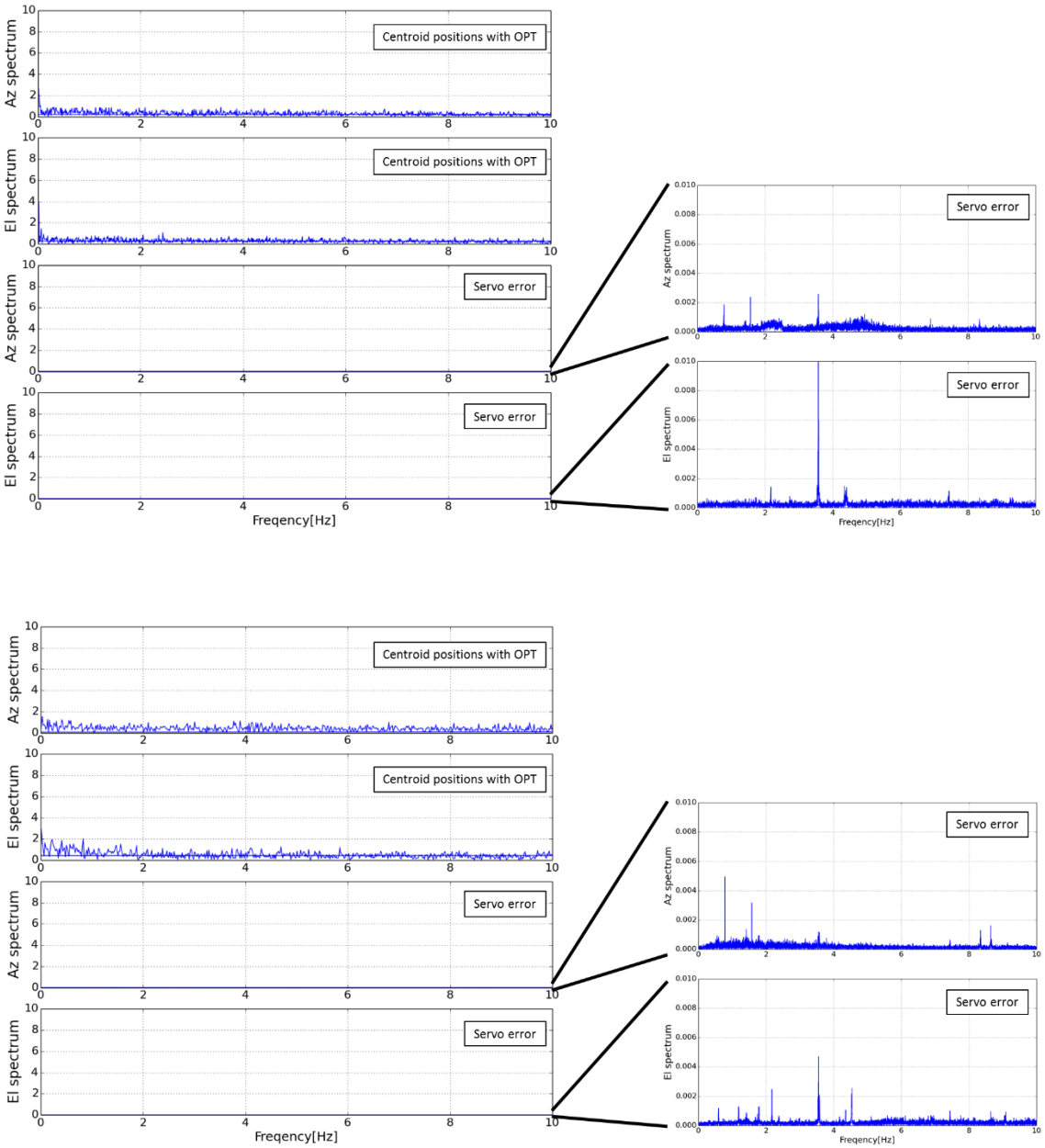

Figure G-9 Spectra of the relative centroid positions on the Az axis and the El axis, and spectra of the servo errors on the Az axis and the El axis. These measurement results are taken at UT2:51 - 3:06, June 16, 2012 (upper) and UT3:33 - 3:48, June 16, 2012 (lower). The averaged wind velocities are 2.28 m/s (upper) and 3.29 m/s (lower).

Appendix H Characteristic of Stars in Measurement of Referencing Pointing

As mentioned in Section 2, in Saito et al. (2012), three to five stars within 4 degrees on the sky are selected in the measurement of the referencing pointing to mimic a typical observation of the ALMA, which switches a target source and a calibrator source. In this study, one example is investigated if there are any systematic errors of the stars in the measured pointing value. The data were taken at UT 1:56 to 2:14, May 21, 2012, with the ACA 7-m antenna No. 12 in Saito et al. (2012). The centroid positions of each star are shown in Figure H-1. It is confirmed that any obvious systematic error of the stars in the measured pointing value is not seen in this case.

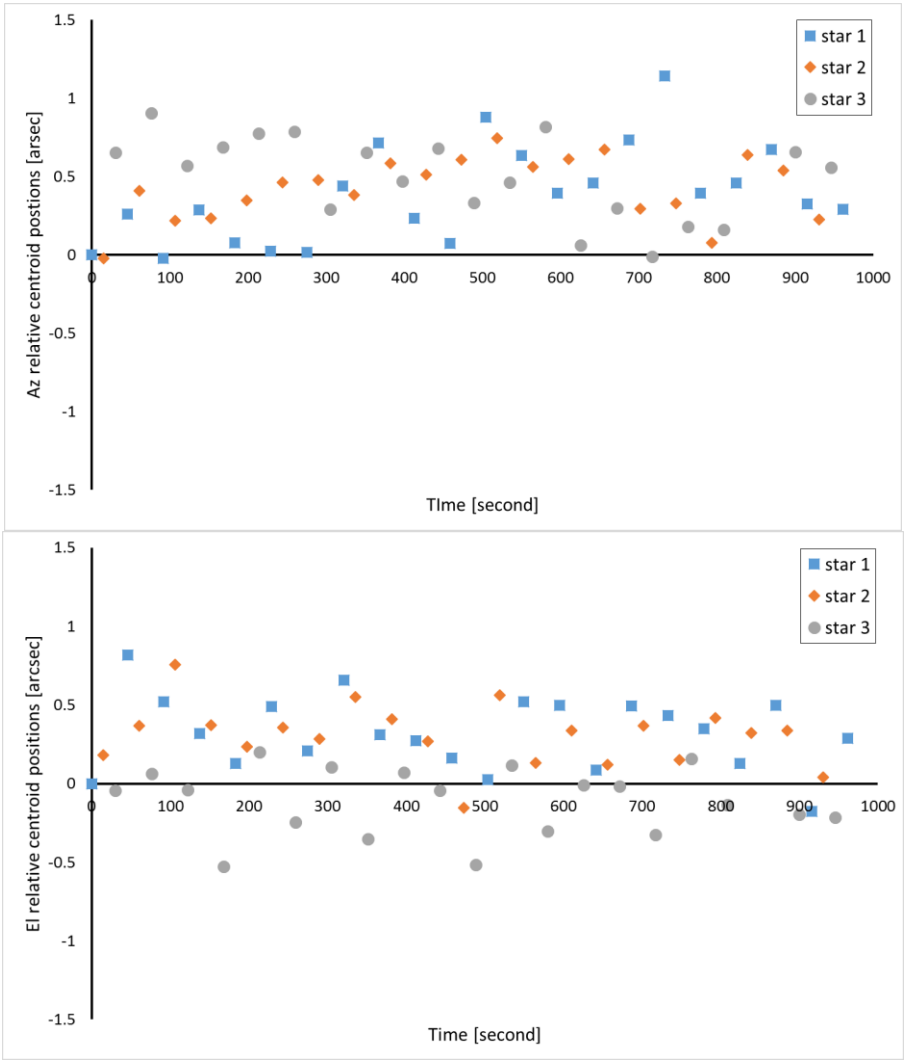

Figure H-1 Az centroid positions (upper) and El centroid positions (lower) of the every star. The reference position is measured by the star 1 (A turn of switching: Star 1→Star 2→Star 3→Star 1).